STUDY OF IMAGE ENHANCEMENT AND RESTORATION TECHNIQUES FOR UNDERWATER IMAGES

A Thesis Submitted
in Partial Fulfilment of the Requirements
for the Degree of

DOCTOR OF PHILOSOPHY

by

AMARENDRA KUMAR MISHRA
(Roll No. 2k18/Ph.D/EC/502)

Under the Supervision of
Prof. M. S. Choudhry and Dr. Manjeet Kumar
Delhi Technological University

Department of Electronics and Communication Engineering
DELHI TECHNOLOGICAL UNIVERSITY
(Formerly Delhi College of Engineering)
Shahbad Daulatpur, Main Bawana Road, New Delhi-110042, India

September, 2024

DELHI TECHNOLOGICAL UNIVERSITY

(Formerly Delhi College of Engineering)
Shahbad Daulatpur, Main Bawana Road, Delhi-42

CANDIDATE'S DECLARATION

I **Amarendra Kumar Mishra** hereby certify that the work which is being presented in the thesis entitled "**Study of Image Enhancement and Restoration Techniques for Underwater Images"** in partial fulfilment of the requirements for the award of the Degree of Doctor of Philosophy, submitted in the Department of Electronics and Communication Engineering, Delhi Technological University is an authentic record of my own work carried out during the period from January 2019 to September 2024 under the supervision of Pro. M. S. Choudhry and Dr. Manjeet Kumar.

The matter presented in the thesis has not been submitted by me for the award of any other degree of this or any other Institute.

Candidate's Signature

(Amarendra Kumar Mishra)
(Roll No. 2k18/Ph.D/EC/502)

DELHI TECHNOLOGICAL UNIVERSITY

(Formerly Delhi College of Engineering)
Shahbad Daulatpur, Main Bawana Road, Delhi-42

CERTIFICATE BY THE SUPERVISOR(s)

Certified that **Amarendra Kumar Mishra** (Enrollment no.: 2k19/Ph.D/EC/119/02) has carried out their search work presented in this thesis entitled "**Study of Image Enhancement and Restoration Techniques for Underwater Images"** for the award of **Doctor of Philosophy** from Department of Electronics and Communication Engineering, Delhi Technological University, Delhi, under our supervision. The thesis embodies results of original work, and studies are carried out by the student himself and the contents of the thesis do not form the basis for the award of any other degree to the candidate or to anybody else from this or any other University/Institution.

Signature

(Prof. M. S. Choudhry)
(Professor)
Department of Electronics
& Communication Engineering,
Delhi Technological University, Delhi

Signature

(Dr. Manjeet Kumar)
(Assistant Professor)
Department of Electronics
& Communication Engineering,
Delhi Technological University, Delhi

Date:

ABSTRACT

Underwater image processing serves several purposes across various domains such as marine biology for ecology, oceanography in environmental monitoring, underwater archaeology, search for rescue operations, underwater surveillance for security, underwater photography in filmmaking, commercial diving, and many more. In this thesis, we have investigated the problem of degraded underwater images. Over the decade, many efforts made to develop algorithms for enhancing degraded underwater images, but still it is a challenging task due to limited visibility, non-uniform illumination, and diminished contrast.

To start with, The most popular and prominent existing state-of-the-art methods have been reviewed. Based on the literature, it finds that the major challenges are imposed by underwater medium properties. At deeper depths, the one drawback of degraded underwater images is diminishing light attenuation visibility. Improvement in the clarity of degraded underwater images artificial lighting sources are employed to extend visibility, but they often create non-illumination patterns. Meanwhile, marine snow with small floating particles comes within the camera's range which causes forward and backward scattering of light energy in the image plane. This leads to a low-contrast and degraded appearance in the captured images. Furthermore, light undergoes attenuation as it propagates laterally, diminishing the amount of light energy reaching the camera and causing a loss of natural color.

In this thesis, our motivation lies in tackling challenges associated with underwater imaging, such as restricted visibility, non-uniform illumination, reduced contrast, noise removal, blurring of images, artifacts removal, structural preservation, and color restoration. The aim is to develop algorithms for enhancing and restoring underwater images, to overcome the limitations of existing state-of-the-art methods. Consequently, the main objective of underwater image enhancement is to eliminate the hazy veil and adjust color using a single underwater image. Image restoration involves several challenges such as noise removal, blurring of images, artifacts removal, structural preservation, and color restoration.

This thesis comprises of total six proposed methods in three chapters to address the above-mentioned problems. First, a novel underwater image enhancement method based on multiscale decomposition and brightness adjustment is presented in the third chapter. The

proposed method is constructed by decomposing the degraded underwater image into illumination and reflectance using the weighted least square filter. Further, gamma correction is applied to the base layer. The brightness adjustment is performed on the illumination component using the sigmoid function. The effectiveness of the proposed method is validated by comparison of it with state-of-the-art methods on multiple standard datasets such as underwater image enhancement benchmark (UIEB), real-world underwater image enhancement (RUIE), a dataset of real-world underwater video of artifacts (DRUVA) and underwater-45 (U45).

A novel method for image restoration is proposed in the third chapter of this thesis. It is based on illumination, reflectance, and white balance technique. In the first stage, we applied the white balance technique to the degraded underwater input image, and the obtained image is converted into *YCbCr* color space. In the second stage, the *Y-component* of the *YCbCr* color space has decomposed into illumination and reflectance. The reflectance is improved by contrast-limited adaptive histogram equalization (CLAHE) and the histogram definition of the illumination image is modified by creating a weighted histogram based on Bi-log transformation. The improved reflectance and illumination are combined to get an enhanced *Y-component* of *YCbCr* color space. Finally, the *Cr-component*, *Cb-component*, and restored *Y-component* are concatenated to get the restored image. The effectiveness of the proposed method is tested by comparing it with the existing state-of-the-art method on the UIEB dataset.

A new method is proposed for image enhancement using the blending technique in the fourth chapter. In the first stage of this method, color correction of the underwater degraded image has been done. In the second stage of this method, the white balance technique and contrast-limited adaptive histogram equalization are applied in parallel to the color-corrected image of the first stage. Then RGB output image corresponding to the white balance technique (Known as *input1*) and contrast-limited adaptive histogram equalization (Known as *input2*) are converted into *YCbCr* color space and finally decomposed into *Y-component*, *Cb-component*, and *Cr-component.* Next, the Laplacian, saliency, and saturation filtering are applied to the *Y*-component, and normalization is performed on the obtained image as the third stage of this method. Finally, the blending process is used to get an enhanced image. The proposed method is evaluated on the UIEB, RUIE, and U45 datasets in terms of parameters such as patch-based contrast quality index (PCQI), underwater image quality measure (UIQM), underwater color image quality evaluation

(UCIQE), peak signal to noise ratio (PSNR), absolute mean brightness enhancement (AMBE), contrast per pixel (CPP), discrete entropy (DE), modified measure of enhancement (MEME), and structure similarity index measure (SSIM).

Next, a novel method has been proposed for underwater image restoration based on color correction, and empirical mode decomposition in fourth chapter. In the first stage of this method, color correction is applied to degraded underwater images. Then color color-corrected image has been converted into *HSV* color space. The empirical mode decomposition is applied to all components (i.e., *H-component*, *S-component*, and *V-component*) of *HSV* color space. The weighted sum of the first four IMFs of all three components is used for the restoration of *HSV* color space. Finally, this *HSV* color space is converted into *RGB* color space. The proposed method is compared with existing state-of-the-art methods on publicly available datasets such as UIEB and U45. The effectiveness of the proposed method is evaluated in terms of the visual quality of the image and various parameters such as SSIM, CPP, measure of enhancement (EME), UCIQE, UIQM, PCQI, AMBE, PSNR, and DE.

Two different novel methods are used in the fifth chapter to address the problem of enhancement and restoration of underwater images and videos. The first proposed method deals with the problem of image enhancement, whereas the second proposed method is used for image enhancement and restoration.

The first method proposed in the fifth chapter for underwater image enhancement using principal component analysis based on the fusion of background light and transmission optimization. In the first stage, the background light (Known as I_1) is evaluated from input underwater images. Parallalley, the *RGB* color space has been converted into the international commission on illumination-luminance chrominance (*CIE-Lab*) color space. In the second stage, the transmission estimation has been done on the *L-component* of the *CIE-Lab* color space. Further, transmission optimization is applied to estimated transmission. Now, the *A-component*, *B-component*, and optimised transmission of *L-component* of *CIE-Lab* color space are multiplied to obtain an enhanced image (Known as I_2) in *CIE-Lab* color space. In the third stage, we evaluated the principal components of image I_1 (Known as P_{C_1}) and image I_2 (Known as P_{C_2}). Then, principal component P_{C_1} fused with the background light of the input image and principal component P_{C_2} fused with the enhanced image in *CIE-Lab* color space. The obtained images are added together, and

it is known as a fused image. In the final stage, the color correction is applied to the fused image and it is converted from *CIE-Lab* color space into *RGB* color space. The effectiveness of the proposed framework is tested on two standard datasets such as UIEB and RUIE by evaluating various parameters such as PSNR, SSIM, EME, DE, UIQM, and UCIQE. Finally, an ablation study has been conducted to validate the effectiveness of the proposed method.

In the initial stage of the second proposed method of the fifth chapter, applied the color correction on the input image. Then the color-corrected image is converted into *YCbCr* color space. In the second stage, the weighted list square (WLS) filter is applied on the *Y-component* of *YCbCr* color space for the multiscale decomposition (i.e., base layer, detail layer1, and detail layer2). Then, gamma correction is applied on the base layer and gradient-domain enhancement is carried out on detail layers. Parallelly, the color saturation and restoration are applied on the *Cb-component* and *Cr-component* of *YCbCr* color space. The enhanced *Y-component* is obtained by adding the gamma-corrected base layer and two details layers after applying the gradient domain enhancement. The image restoration is achieved by adding the modified *Cb-component* and *Cr-component* (*Cb-component* and *Cr-component* after applying color saturation and restoration) of *YCbCr* color space. Finally, image enhancement and restoration in *YCbCr* color space is achieved by multiplying the enhanced *Y-component* with the modified *Cb-component* and *Cr-component*. Then *YCbCr* is converted into *RGB* color space. The proposed method is evaluated on multiple datasets such as UIEB, UCCS, UIQS, and U45. The effectiveness of the method is tested by comparing it with existing state-of-the-art methods in terms of the visual quality of images and various parameters such as PSNR, SSIM, EME, DE, UIQM, and UCIQE. Additionally, the proposed method tested for other applications such as low-light images with the exclusively dark dataset and image database TID2013.

Finally, in this thesis, we summarize the conclusions inferred from our research work and highlight the potential future scope in the field of underwater imaging.

Publications Related to the Thesis

Journal Papers Published

1. Amarendra Kumar Mishra, Mahipal Singh Choudhry, and Manjeet Kumar. "Underwater image enhancement using multiscale decomposition and gamma correction." *Multimedia Tools and Applications* 82.10 (2023): 15715-15733, **SCIE, (IF: 3.6)** https://doi.org/10.1007/s11042-022-14008-2
2. Amarendra Kumar Mishra, Manjeet Kumar, and Mahipal Singh Choudhry. "Underwater image enhancement by using transmission optimization and background light estimation via principal component analysis fusion." *Signal, Image and Video Processing* (2024): 1-11, **SCIE, (IF: 2.3)** https://doi.org/10.1007/s11760-024-03047-x
3. Amarendra Kumar Mishra, Manjeet Kumar, and Mahipal Singh Choudhry. "Fusion of multiscale gradient domain enhancement and gamma correction for underwater image/video enhancement and restoration." *Optics and Lasers in Engineering* 178 (2024): 108154, **SCIE, (IF: 4.6)** https://doi.org/10.1016/j.optlaseng.2024.108154

Journal Paper Communicated

4. Amarendra Kumar Mishra, M S Choudhry, and Manjeet Kumar. "An Effective and Robust Underwater Image Enhancement Approach based on White Balance and Blending Technique " (*Optics and Lasers in Engineering* Journal) **(Under review).**

Conference Papers Published

5. Amarendra Kumar Mishra, Mahipal Singh Choudhry, and Manjeet Kumar. "Underwater image restoration using white balance and retinex algorithm." *2022 IEEE Conference on Interdisciplinary Approaches in Technology and Management for Social Innovation (IATMSI)*. **IEEE, 2022**. **doi:** 10.1109/IATMSI56455.2022.10119294.
6. Amarendra Kumar Mishra, Mahipal Singh Choudhry, and Manjeet Kumar. "Underwater image restoration using color correction and empirical mode decomposition." *2023 10th International Conference on Signal Processing and Integrated Networks (SPIN)*. **IEEE, 2023. doi:** 10.1109/SPIN57001.2023.10116627.

ACKNOWLEDGMENT

I am deeply grateful to Lord Shiva, whose guidance and power have allowed me to pursue this Ph.D. I thank the almighty for granting me the wisdom, health, and strength to undertake and complete this research. I pray for his continued blessings so that I may always serve him in all that he wills.

First and foremost, I would like to express my sincere gratitude to my supervisor, **Prof. M. S. Choudhry** and **Dr. Manjeet Kumar**, for their continuous support, patience, and guidance throughout my research. Their insightful feedback and encouragement were invaluable in completing this thesis.

My sincere regards *to* ***Prof. Prateek Sharma, Vice-Chancellor, Delhi Technological University*** for providing me with a platform for pursuing my PhD work. I express my gratitude to **Prof. Rajeshwari Pandey**, *DRC Chairman*, *Department of ECE*, **Prof. O. P. Verma**, *Head, Department of ECE*, and **Prof. S. Indu**, Dean, Student welfare, for their kind support and providing necessary facilities to undertake this research. I take this opportunity to thankfully acknowledge **Prof. Rajesh Rohilla**, *HOD (T&P), DTU,* and all my teachers.

I am grateful to Delhi Technological University for the financial support provided through the Scholarship, which made this research possible.

I wish to acknowledge the enjoyable company rendered by my friends, ***Rahul Bansal, Tej Singh, Gaurav Varshney, Reman Kumar, Rajiv Yadav, Prashant Rathi, Anurag Kumar, Arjun Kumawat, Owais Jamil***, ***Rahul Thakur****, Assistant Professor, Department of ECE, DTU, Munindra, Rahul Tiwari, Vishal Choudhry Ankit Yadav, Rahul Gupta, Amit Gautam,* and many others who offered me their time, help and support whenever needed.

Finally, I would like to express my deepest gratitude to my family. My parents (**Daya Shankar Mishra** and **Annapoorna Mishra**) are my life-coach; I feel proud of dedicating this PhD onto her lotus feet. I am grateful to my parents being an inspiration for me from childhood. They always taught me not to fear in any adverse situation and fight all odds with courage and patience.

Heartfelt and endless thanks to my sister and brother-in-law **Anju Mishra**, and **Durga Charan Mishra.** Endless thanks to my brother and sister-in-law **Sunil Mishra** and **Vandna Mishra.** My dear nephews **Aditya Mishra and Ayush Mishra** who always supported me at every stage of my life. They strengthen me by providing moral and emotional support. I am confident to be energized by their care, affection, and brilliant advice for the rest of my life.

I would like to express my deepest gratitude to my girlfriend, **Himani Pokhriyal**. Her unwavering support, patience, and encouragement have been invaluable to me throughout this journey. Her belief in me and her love provided the strength I needed to persevere, especially during the most challenging times. I am incredibly fortunate to have her by my side.

Thank you all for making this journey possible.

(Amarendra Kumar Mishra)

Dedication

This thesis is dedicated to mother, father, brother, and sister.

For their endless love, support, and encouragement

CONTENTS

CANDIDATE'S DECLARATION ..... **ii**

CERTIFICATE BY THE SUPERVISOR(s) ..... **iii**

ABSTRACT ..... **iv**

Publications Related to the Thesis ..... **viii**

ACKNOWLEDGMENT ..... **ix**

Dedication ..... **xi**

List of Tables ..... **xv**

List of Figures ..... **xvii**

List of Symbols and Abbreviations ..... **xxii**

Chapter 1 ..... **1**

Introduction of Underwater Image Enhancement and Restoration **1**

1.1 Background 1

1.2 Application of Underwater Image Enhancement and Restoration 2

1.3 Challenges of Underwater Optical Imaging 3

1.4 Motivation and Problem Statement 8

1.5 Performance Metrics 8

1.5.1 Full-Reference Assessment 8

1.5.2 Non-Reference Assessment 15

1.6 Contribution of this Thesis 20

1.7 Thesis Organization 22

Chapter 2 ..... **24**

Literature Review **24**

2.1 Introduction 24

2.2 Underwater Image Enhancement 24

2.3 Underwater Image Restoration 32

2.4 Research Gap 38

2.5 Research Objectives 39
2.6 Underwater Image and Video Dataset 40
2.6.1 Underwater Image Enhancement Benchmark Dataset 40
2.6.2 Real-World Underwater Image Enhancement Dataset 40
2.6.3 U45 Dataset 42
2.6.4 Dataset of Real-world Underwater Video of Artifacts 42
Chapter 3 43
Underwater Image Enhancement and Restoration Based on Multiscale Decomposition, Brightness Adjustment, and Retinex Algorithm. 43
3.1 Underwater Image Enhancement Based on Multiscale Decomposition 43
3.1.1 Introduction 43
3.1.2 Image Formation Optical Model 45
3.1.3 Proposed Method 46
3.1.4 Results and Discussion 54
3.2 Underwater Image Restoration Using White Balance and Retinex Algorithm 58
3.2.1 Methodology 58
3.2.2 Results and Discussion 61
3.3 Summary 65
Chapter 4 67
Underwater Image Enhancement and Restoration using White Balance, Contrast Enhancement, Empirical Mode Decomposition and Blending Techniques 67
4.1 Underwater Image Enhancement Based on White Balance and Blending Technique . 67
4.1.1 Introduction 67
4.1.2 Methodology 68
4.1.3 Results and Discussion 74
4.1.4 Discussion 79
4.2 Underwater Image Restoration Based on Color Correction and Empirical Mode Decomposition 94

4.2.1 Proposed Methodology 95
4.2.2 Results and Discussion 98
4.3 Summary 101
Chapter 5 103
Underwater Image and Video Enhancement and Restoration based on Fusion 103
5.1 Underwater Image Enhancement Based on Fusion of Background Light and Transmission Optimisation Via Principal Component Analysis 103
5.1.1 Proposed Methodology 104
5.1.2 Results and Discussion 108
5.2 Underwater Image/Video Enhancement and Restoration Based on Fusion of Gradient Domain Enhancement and Gamma Correction 114
5.2.1 Introduction 114
5.2.2 Methodology 115
5.2.3 Results and Discussion 119
5.3 Summary 134
Chapter 6 136
Conclusion and Future Scope 136
6.1 Conclusion 136
6.2 Future direction 137
REFERENCES 139
Author Biography 165

List of Tables

Table 3.1 Comparison of various parameters of 890 images with proposed method and existing state-of-the-art. 56
Table 3.2 Quantitative evaluation of proposed method and existing methods using UIQM parameter on U45 dataset..... 63
Table 3.3 Comparison of UCIQE with proposed method and existing state-of-the-art on U45 dataset. 64
Table 4.1 Comparison of patch-based contrast quality index of ten Images, taken randomly from the UIEB dataset, with the existing state-of-the-art and proposed methods. 80
Table 4.2 Comparison of underwater image quality measures of ten images taken randomly from the UIEB dataset with the existing state-of-the-art and proposed methods. 80
Table 4.3 Comparison of underwater color image quality evaluation of ten images taken randomly from the UIEB dataset with existing state-of-the-art and proposed methods..... 81
Table 4.4 Comparison of peak signal-to-noise ratio of ten images taken randomly from the UIEB dataset using existing state-of-the-art and proposed methods. 82
Table 4.5 Comparison of absolute mean brightness enhancement of ten images taken randomly from the UIEB dataset using existing state-of-the-art and proposed methods. 82
Table 4.6 Comparison of contrast per pixel of ten images taken randomly from the UIEB dataset using existing state-of-the-art and proposed methods. 83
Table 4.7 Comparison of discrete entropy of ten images taken randomly from the UIEB dataset with proposed method and existing state-of-the-art. 84
Table 4.8 Comparison of the modified measure of enhancement of ten images taken randomly from the UIEB dataset with the existing state-of-the-art and proposed methods. 84
Table 4.9 Comparison of structure similarity index measure of ten images taken randomly from the UIEB dataset with existing state-of-the-art and proposed methods. 85
Table 4.10 Average quantitative measurement of existing state-of-the-art and proposed methods on 890 underwater images taken from the UIEB dataset [143]. 85
Table 4.11 The UCIQE and UIQM of images have been compared with the existing and proposed method on the UIQS dataset..... 93
Table 4.12 The UCIQE and UIQM of images have been compared with the proposed method and existing state-of-the-art on the UCCS dataset. 93
Table 4.13 The UCIQE and UIQM of images have been compared with the proposed method and existing state-of-the-art on the U45 dataset. 94

Table 4.14 Comparative analysis of proposed method with existing state-of-the-art on the U45 dataset for SSIM matric. 99
Table 4.15 Comparative analysis of proposed method with existing state-of-the-art on the U45 dataset for PCQI matric. 99
Table 5.1 Comparative analysis of the proposed method in terms of PCQI, UCIQE, UIQM, SSIM, PSNR, and DE with existing state-of-the-art on the UIEB dataset. 109
Table 5.2 Summarises the quantitative findings from the ablation study of the proposed method conducted on the UCCS, UIQS, and UIEB ~~d~~atasets. 113
Table 5.3 Comparison of PSNR (in dB) value with the proposed method and existing state-of-the-art on the UIEB dataset. 124
Table 5.4 Comparison of SSIM value with the proposed method and existing state-of-the-art on the UIEB dataset. 125
Table 5.5 Comparison of DE value with the proposed and existing state-of-the-art methods on the UIEB dataset. 127
Table 5.6 Comparison of UIQM value with existing deep learning and proposed method on the U45 Dataset. 128
Table 5.7 Comparison of UCIQE parameter with existing deep learning methods and proposed method on fifteen images of different colors such as haze, blue, and green taken from U45 Dataset 129
Table 5.8 The comparative analysis of underwater video A12.mp4 with the proposed method and existing state-of-the-art on the underwater DRUVA video dataset in terms of execution time. 130

List of Figures

Fig. 1.1 Journal and conference publishing during 2012-2024 of underwater image enhancement and restoration.....2
Fig. 1.2 Different wavelengths of light are attenuated at different rates with respect to distance in water. The blue color travels the longest in the water due to its shortest wavelength. 5
Fig. 1.3 The light propagation mechanism for underwater. 6
Fig. 1.4 Challenges faced by underwater imaging. 7
Fig. 2.1 Classification of underwater image enhancement methods. 29
Fig. 2.2 Classification of underwater image restoration. 32
Fig. 2.3 (a) First-row image represents the UIEB dataset, (b) Second-row image is taken from the UCCS dataset, (c) Third-row image is taken from the UIQS dataset, and (d) Fourth-row image is taken from U45 dataset. 41
Fig. 3.1 Underwater optical image formation model (IFM) with forward and backward scattering. 44
Fig. 3.2 The proposed method based on multi-scale decomposition and brightness adjustment for underwater image enhancement. 47
Fig. 3.3 Intermediate process of underwater image enhancement (a) Input image (UIEB dataset), (b) Reflectance of the input image, (c) Illumination of the input image, (d) Output image. 49
Fig. 3.4 (a) Raw underwater image, (b) Brightness adjustment, and (c) Output of proposed method.....51
Fig. 3.5 Different stages of underwater image reflectance. 53
Fig. 3.6 Comparison of proposed method with existing state-of-the-art methods. (a) Input image, (b) Results of HPU, (c) Results of HUIE, (d) Results of MSRCR, (e) Results of MIL, (f) Results of HTU, (g) Results of MPORU, (h) Results of CBFU, (i) Results of UDCPGIF, (j) Results of UDCPSM, (k) Results of the proposed method. 55
Fig. 3.7 Work flow of the proposed method based on illumination and reflectance restoration for underwater image. 59
Fig. 3.8 Enhance results of various state-of-the-art and proposed methods, (a) Input image, (b) Result of WSCT, (c) Result of UIBL, (d) Result of UDCP, (e) Result of RED, (f) Result of FGAN, (g) Result of FE, (h) Result of CycleGAN, (i) Result of proposed method respectively. 62

Fig. 3.9 Quantitative comparision of UIQM parameter of the proposed with existing state-of-the-art methods for various images. 63
Fig. 3.10 Quantitative comparison of UCIQE parameter of proposed and existing state-of-the-art methods for various images. 64
Fig. 4.1 The proposed method involves processing a color-corrected image to produce two additional images: Input1 and Input2. Input1 is obtained by applying white balance technique, and Input2 is generated through CLAHE. These two images were input for the blending process to get the final restored image. 69
Fig. 4.2 (a) Degraded underwater images, (b) Color-corrected images, and (c) Enhanced images of the proposed method. 70
Fig. 4.3 (a) The input image, (b) The white balance image (input1), (c) The CLAHE image (input2), and (d) Enhanced images of the proposed method. 70
Fig. 4.4 (a) Degraded underwater image, (b) The Laplacian contrast weight for the input1, (c) The Laplacian contrast weight for the input2, and (d) The enhanced images of the proposed method 72
Fig. 4.5 (a) Degraded underwater image, (b) The saliency weight for the input1, (c) The saliency weight for the second input2, and (d) The enhanced images of the proposed method. 72
Fig. 4.6 (a) Input images, (b) The saturation weight for the input1, (c) The saturation weight for the input2, and (d) The enhanced images of the proposed method. 73
Fig. 4.7 (a) Degraded underwater images, (b) The normalized weight for the input1, (c) The normalized weight for the input2, and (d) The enhanced images of the proposed method. .. 74
Fig. 4.8 The visual quality of the proposed method compared with the existing state-of-the-art on the UIEB dataset. (a) The degraded image, followed by an enhanced image generated by (b) HLRP, (c) HUWIE, (d) MSRCR, (e) TEBCF, (f) UWIPHT, (g) CBFUWIE, (h) MIL, (i) MWM, (j) WCDUIE, (k) CBM, and (l) The proposed results, respectively. 75
Fig. 4.9 The visual quality of the proposed method compared with existing state-of-the-art on the UIQS dataset. (a) The degraded image, followed by an enhanced image generated by (b) HLRP, (c) HUWIE, (d) MSRCR, (e) TEBCF, (f) UWIPHT, (g) CBFUWIE, (h) MIL, (i) MWMGF, (j) WCDUIE, (k) CBM, and (l) The proposed results, respectively. 77
Fig. 4.10 The visual quality of the proposed method compared with existing state-of-the-art on the UCCS dataset. (a) The degraded image is followed by an enhanced image generated by (b) HLRP, (c) HUWIE, (d) MSRCR, (e) TEBCF, (f) UWIPHT, (g) CBFUWIE, (h) MIL, (i) MWMGF, (j) WCDUIE, (k) CBM, and (l) The proposed results, respectively. 78

Fig. 4.11 The visual quality of the proposed method compared with the existing state-of-the-art on the U45 dataset. (a) The degraded image followed by the enhanced image generated by (b) UIBLA, (c) UGAN, (d) UWCNN-SD, (e) WSCT, (f) CycleGAN, (g) FGAN, and (h) The method results, respectively. 79
Fig. 4.12 Comparative analysis of patch-based contrast quality index with the proposed method and existing state-of-the-art (SOTA) on the UIEB dataset. 86
Fig. 4.13 Comparative analysis of underwater image quality measures with the proposed method and existing state-of-the-art (SOTA) on the UIEB dataset. 87
Fig. 4.14 Comparative analysis of underwater color image quality evaluation metrics with the proposed method and existing state-of-the-art (SOTA) on the UIEB dataset. 87
Fig. 4.15 Comparative analysis of peak signal-to-noise ratio metric with the proposed method and existing state-of-the-art (SOTA) on the UIEB dataset. 88
Fig. 4.16 Comparative analysis of absolute mean brightness enhancement metric with the proposed method and existing state-of-the-art (SOTA) on the UIEB dataset. 89
Fig. 4.17 Comparative analysis of contrast per pixel metric with the proposed method and existing state-of-the-art (SOTA) on the UIEB dataset. 89
Fig. 4.18 Comparative analysis of discrete entropy metrics with the proposed method and existing state-of-the-art (SOTA) on the UIEB dataset. 90
Fig. 4.19 Comparative analysis of modified measures of enhancement metrics with the proposed method and existing state-of-the-art (SOTA) on the UIEB dataset. 91
Fig. 4.20 Comparative analysis of structure similarity index measure metric with proposed method and existing state-of-the-art (SOTA) on the UIEB dataset. 91
Fig. 4.21 Comparison of different metrics with existing state-of-the-art and proposed method on the UIEB dataset. 92
Fig. 4.22 Flow diagram of the proposed work based on color correction and empirical mode decomposition for underwater image. 95
Fig. 4.23 (a) The first column represents the input image; the rest are the output images of (b) MSRCR, (c) HUWIE, (d) RB, (e) RED, (f) WSCT, and (g) the proposed method, respectively. 98
Fig. 4.24 Comparative analysis of proposed method with existing state-of-the-art on U45 dataset for PCQI metric. 100
Fig. 4.25 Comparative analysis of the proposed method with existing state-of-the-art on the U45 dataset for SSIM metric. 100
Fig. 5.1 Framework of the proposed methodology (TOBPCA) for image enhancement 105

Fig. 5.2 Visual comparison of the proposed method with existing state-of-the-art methods such as (a) Degraded image, (b) Enhanced image of HLRP, (c) Enhanced image of MPORU, (d) Enhanced image of MSRCR, (e) Enhanced image of UHT, (f) Enhanced image of MIL, (g) Enhanced image of HUWIE, (h) Enhanced image of TEBCF, (i) Enhanced image of CBFUWIE, (j) Enhanced image of MWMGF, (k) Enhanced image of WCDUIE, and (l) Enhanced image of the proposed method over the UIEB dataset. 109
Fig. 5.3 Box plot of the performance metrics such as (a) UCIQE (b) PCQI (c) UIQM (d) SSIM (e) PSNR and (f) DE of the proposed method and existing state-of-the-art (SOTA) methods over UIEB datasets. 111
Fig. 5.4 Ablated results of each core component of the proposed method on UCCS, UIQS, and UIEB datasets. From top to bottom, the raw images (a) are derived from UCCS, UIQS, and UIEB datasets. The ablated results using (b) -w/o TO, (c) -w/o PCA, (d) -w/o CC, and (e) TOBPCA (full model). 112
Fig. 5.5 The proposed method is based on the fusion of gradient-domain enhancement and gamma correction. 116
Fig. 5.6 Enhanced results of the proposed method and existing state-of-the-art methods on the UIEB dataset. From left to right (a) Degraded underwater images, (b) Enhanced image of HPU, (c) Enhanced image of UDCPGF, (d) Enhanced image of MSRCR, (e) Enhanced image of WCDUIE, (f) Enhanced image of UWIPHT, (g) Enhanced the image of MPORU, (h) Enhanced image of HLRP, (i) Enhanced image of CBM, (j) Enhanced image of MIL, (k) Enhance the image of CBFUWIE, and (l) Enhanced image of proposed method. 121
Fig. 5.7 From left to right (a) Degraded haze underwater images, and enhanced results of (b) SESR, (c) UWCNN-SD, (d) UGAN, (e) WSCT, (f) CycleGAN, (g) FGAN, and (h) The proposed method respectively on the U45 dataset. 122
Fig. 5.8 From left to right (a) Degraded green underwater images, and enhanced results of (b) SESR, (c) UWCNN-SD, (d) UGAN, (e) WSCT, (f) CycleGAN, (g) FGAN, and (h) The proposed method respectively on the U45 dataset. 123
Fig. 5.9 From left to right (a) Degraded blue underwater images, and enhanced results of (b) SESR, (c) UWCNN-SD, (d) UGAN, (e) WSCT, (f) CycleGAN, (g) FGAN, and (h) The proposed method respectively on the U45 dataset. 123
Fig. 5.10 Quantitative comparison of the proposed method with existing state-of-the-art on the UIEB dataset for PSNR parameter. 125
Fig. 5.11 Quantitative comparison of the proposed method with existing state-of-the-art on the UIEB dataset for SSIM parameter. 126

Fig. 5.12 Quantitative comparison of the proposed method with existing state-of-the-art on the UIEB dataset for DE parameter. 127
Fig. 5.13 Enhanced results of the proposed method and existing state-of-the-art on the underwater video A12.mp4. (a) Raw underwater video A12.mp4 (from top to bottom are frame_0001, frame_0100, frame_0200, frame_0300, frame_0400, frame_0500, frame_0600, frame_0700, frame_0900, frame_1520 in this video). (b) Results of HPU, (c) Results of UDCPGF, (d) Results of MSRCR, (e) Results of WCDUIE, (f) Results of UWIPHT, (g) Results of MPORU, (h) Results of HLRP, (i) Results of CBM, (j) Results of MIL, (k) Results of CBFUWIE, (l) Results of the proposed method. Zoom in all images for better visibility. 131
Fig. 5.14 Comparative analysis of the proposed method with existing state-of-the-art on the TID 2013 dataset.....132
Fig. 5.15 Comparative analysis of the proposed method with existing state-of-the-art on low illumination images and underwater images.....133

List of Symbols and Abbreviations

Abbreviation	Description
AMBE	Absolute mean brightness enhancement
AMEE	Agaian measure of enhancement by entropy
BRISQUE	Blind/Referenceless image spatial quality evaluator
CBFUWIE	Color balance and fusion for underwater image enhancement
CBM	Contour bougie morphology
CDF	Cumulative density functions
CLAHE	Contrast-limited adaptive histogram equalization
CNN	Convolutional neural network
CPP	Contrast per pixel
CycleGAN	Cycle-consistent generative adversarial network
DCP	Dark channel prior
DE	Discrete entropy
DRUVA	Dataset of Real-world underwater video of artifacts
EMD	Empirical mode decomposition
EME	Measure of Enhancement
FGAN	Fusion generative adversarial network
FSIM	Feature similarity index measure
GAN	Generative adversarial network
GMSM	Gradient magnitude similarity mean
GMSD	Gradient magnitude similarity deviation
GUDCP	Generalized underwater dark channel prior
HE	Histogram equalization
HIS	Hue intensity saturation
HLRP	Hyper-laplacian reflectance prior
HSV	Hue saturation value
HUIE	Hybrid framework for underwater image enhancement
HUWIE	Hue preserving-based underwater image enhancement
ICM	Integrated color model
IFM	Image formation model
IMFs	Intrinsic mode functions
MEME	Modified measure of enhancement

MIL	Minimum information loss
MPORU	Multi-purpose oriented real-world underwater
MSRCR	Multiscale retinex with color restoration
MWMGF	Multi-weight and multi-granularity fusion
NIQMC	No-reference image quality metric for contrast distortion
PCA	Principal component analysis
PCQI	Patch-based contrast quality index
PDSCC	Pixel distribution shifting for color correction
PSNR	Peak signal-to-noise ratio
RGB	Red, green, blue
RUIE	Real-world underwater image enhancement
SESR	Simultaneous enhancement and super-resolution
SOTA	State of the art
SSIM	Structure similarity index measure
TEBCF	Texture enhancement blurriness and color fusion
TM	Transmission map
TOBPCA	Transmission optimisation and background light estimation via principal component analysis fusion
UCCS	Underwater color cast set
UCIQE	Underwater color image quality evaluation
UCM	Unsupervised color model
UDCP	Underwater dark channel prior
UDCPGIF	Underwater dark channel prior guided image filter
UDCPSM	Underwater dark channel prior soft matting
UGAN	Underwater generative adversarial network
UHTS	Underwater higher-level task-driven set
UHT	Underwater hybrid technique
UIConM	Underwater image contrast measure
UIBLA	Underwater image blurriness and light absorption
UICM	Underwater image color measure
UIEB	Underwater image enhancement benchmark dataset
UIQM	Underwater image quality measure
UIQS	Underwater image quality set

UISM	Underwater image sharpness measure
UWIPHT	Underwater image processing using hybrid technique
UWCNN-SD	underwater image convolutional neural network-structural decomposition
WB	White balance
WCDUIE	Wavelength compensation and dehazing of underwater image enhancement
WLS	Weighted least squares
WSCT	Weakly supervised color transform

Chapter 1

Introduction of Underwater Image Enhancement and Restoration

This chapter introduced the background of underwater image enhancement and restoration, the application of underwater image enhancement and restoration, and the challenges of underwater optical imaging. Furthermore, motivation and problem statement, performance metrics are categorized into full-reference and non-reference assessments, and thesis organization are discussed.

1.1 Background

Huge oceans cover a considerable amount of Earth's surface and substantially impact the planet's health. An essential area of oceanographic research is the exploration of these aquatic resources [1]. This scientific endeavor is incomplete without examining the flora and fauna of underwater environments. This is especially true for disciplines like archaeology [2], geology [3], undersea environment assessment [4], and the construction of major gas pipelines and communication networks that cross continental boundaries [5], which calls for accurate study of the underwater depth of ocean floor. Searches for historic shipwrecks are being conducted in ocean exploration [6]. As a result, underwater optical imaging has become an important, even though challenging, area of research. Let's see the historical background of underwater photography.

W. Thompson took the first underwater photograph in 1856 [7]. In England, Thompson pioneered by concealing a camera within a housing submerged in Weymouth Bay. The camera took a 10-minute exposure, triggered remotely from an anchored boat. Unfortunately, this initial endeavor resulted in the camera being flooded, but the film was nevertheless successfully recovered. Nowadays, underwater photography uses high-tech cameras that are frequently operated by scuba divers and has seen significant evolution.

Marine researchers have historically used sonar-based technology to find shallow-water fish, shipwrecks, and other objects. The implementation of tailored filtering algorithms was

nevertheless required because the images produced by sonar imaging systems frequently struggled with problems relating to visual clarity and pervasive noise [7]–[9]. Although sonar technology claims the benefits of long-range visibility and effective target identification [10], it becomes less effective when achieving high resolution for close ranges [11]. Notably, the noise in the sonar sub-band made it more difficult. Optical imaging systems have steadily gained popularity where high resolution at shorter distances is required. Optical imaging has several limitations despite its capacity to provide higher resolution because underwater conditions affect the image.

Fig. 1.1 denotes the yearly count of publications in journals and conferences spanning from 2012 to 2024 for underwater image enhancement and restoration. It is evident from Fig. 1.1 that there has been a notable surge in research activity regarding underwater image enhancement and restoration over the past decayed. This rise is mainly due to the need to develop technology and find new sources in the deep sea [12], [13].

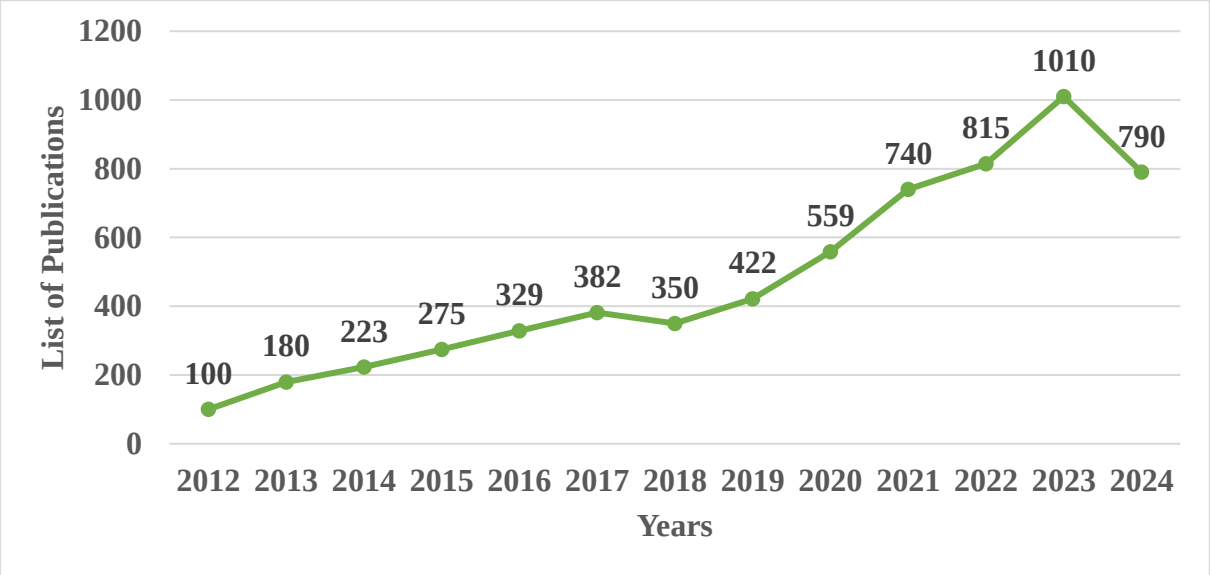

Fig. 1.1 Journal and conference publishing during 2012-2024 of underwater image enhancement and restoration.

1.2 Application of Underwater Image Enhancement and Restoration

Underwater image enhancement and restoration have various practical applications across several domains:

Marine biology and environment monitoring: Improved underwater imagery aids marine biologists in studying marine life, coral reefs, and ecosystems. Cleare images facilitate better species identification, population monitoring, and assessment of habitat health.

Underwater archaeology: Enhanced images can reveal submerged artefacts, shipwrecks, and archaeological sites more clearly, enabling archaeologists to study and preserve underwater cultural heritage.

Oceanography and geology: Enhanced underwater imagery assists in mapping and studying underwater geological features, such as seafloor topography, geological formations, and hydrothermal vents, contributing to a better understanding of Earth's oceans and processes.

Underwater inspection and maintenance: Enhanced images help in the inspection and maintenance of underwater structures, pipelines, and infrastructure, such as oil rigs, bridges, and underwater cables, ensuring their safety and integrity.

Defense and security: Clearer underwater imagery aids naval forces in underwater surveillance, mine detection, and reconnaissance missions, enhancing maritime security and defense capabilities.

Underwater robotics and exploration: Enhanced imagery supports underwater robotic systems in navigation, object detection, and exploration tasks, enabling autonomous and remotely operated vehicles to operate more effectively in challenging underwater environments.

Tourism and recreation: Enhanced underwater imagery enhances the visual appeal of underwater such as coral reefs and marine parks, attracting tourists and promoting underwater tourism and recreational activities like scuba diving and snorkeling.

Overall, underwater image enhancement and restoration play a crucial role in advancing various fields, from scientific research and environmental conservation to industrial applications and national security.

1.3 Challenges of Underwater Optical Imaging

Underwater photography is a popular form that captures images and other visual information of marine life and underwater environments. Taking an underwater image is more complicated than the outside because the water affects the light, color stability, and equipment, and there are safety concerns to consider.

A wide range of difficulties are present in underwater optical imaging. Cameras need specialized housing to be submerged beneath the water's surface. Another level of complication is added by the challenging job of operating the camera, either remotely or physically on-site. However, the distinctive characteristics of the underwater media present the most challenge.

The main factors affecting the results and appearance of underwater images are light absorption and scattering [14]–[18]. As the camera-to-object distance grows, the effect of light scattering becomes more severe, resulting in decreased contrast on the screen for underwater images. The complexity of underwater optical imaging is more challenging because the scattered light element is notable for its absence of essential scene information. The broad-spectrum attenuation coefficients in various color channels of underwater photographs have been extensively researched. The attenuation coefficient depends on factors like the original color composition and the distance between the camera and the object [19]. The scattering parameters are crucial for restoring a clear image. Still, their variability across locations of the same water body due to factors like turbidity, temperature, salinity, and turbulence necessitates accurate calibration.

The ambient light in clear and shallow aquatic habitats is often sufficient to produce high-quality images. However, adding an artificial light source is necessary to enable image capture for deep-sea underwater imaging. However, this additional lighting source poses a double obstacle. First, it causes a color cast to appear from the lighting source, which calls for an appropriate white-balance approach to fix the problem. Secondly, A bright central spot that gradually fades away radially from the image's center characterizes non-uniform illumination patterns that are frequently produced by artificial lighting sources. The underwater optical image technique is further complicated by light attenuation, which is caused by light absorption by water. This phenomenon overgrows as depth increases, affecting all the wavelengths differently [20]. The effect of wavelength variation concerning distance is shown in Fig. 1.2.

In the field of underwater optical imaging, a clear pattern appears: the shorter wavelengths associated with the blue spectrum travel the farthest, while the longer wavelengths, which include the reddish tones, experience the earliest attenuation [21], [22]. As depth increases, this phenomenon overgrows and affects all wavelengths differently. This decrease in color fidelity causes a shift towards greenish with the underwater environment's increasing spatial separation between the camera and the object. In coastal waters, organic particles like phytoplankton contribute to this phenomenon by absorbing mostly the shorter wavelengths, like blue, and

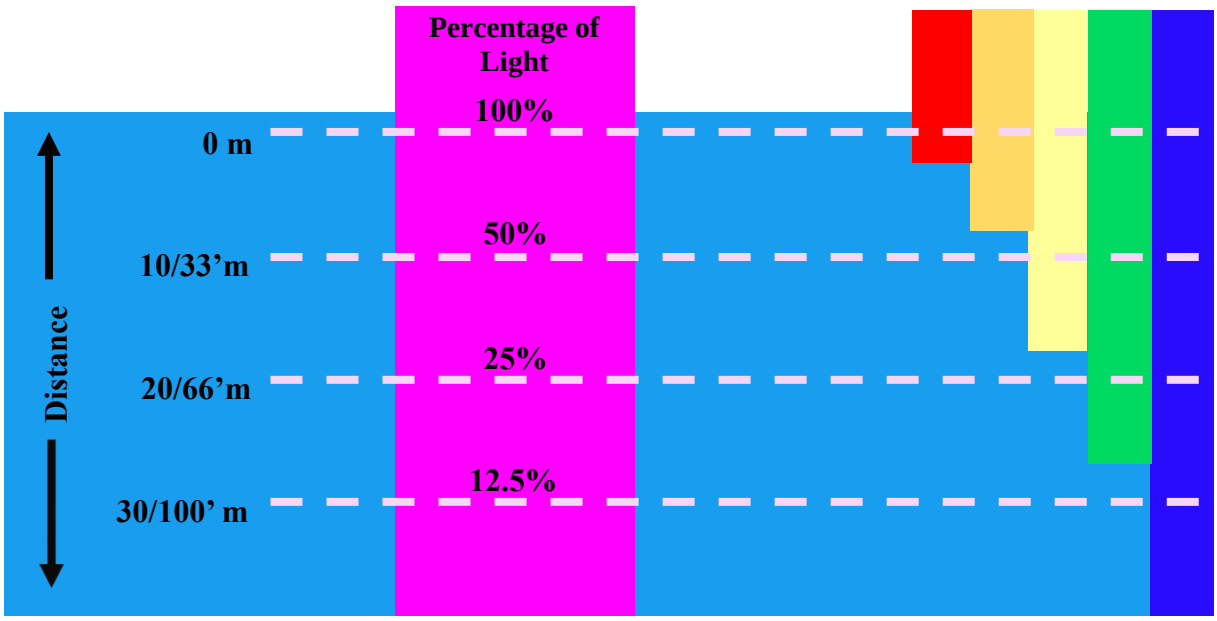

Fig. 1.2 Different wavelengths of light are attenuated at different rates with respect to distance in water. The blue color travels the longest in the water due to its shortest wavelength.

leaving behind an abundant greenish tinge (yellowish-green). This process is further clarified by the Rayleigh scattering theory, which emphasizes that scattering strength is inversely proportional to the fourth power wavelength. Consequently, shorter wavelengths of color scatter more noticeably than color with longer wavelengths. It is clear from the discussion that water absorbs color with long wavelengths while scattering those with short wavelengths in the visible light spectrum.

Dealing with scattering was difficult when we restored the dehaze image obtained from underwater environments. The direct, forward-scattering, and back-scattering components are the three parts of the total light reaching the camera, according to the Jaffe-McGlamery model for underwater imaging. The presence of organic and inorganic particles floating inside the water volume, which intersects the camera's field and the light source, is the primary cause of scattering. Increased level of turbidity notably influences the extent of the scattering phenomenon. Turbidity refers to the cloudiness or haziness of a fluid caused by suspended particles, which can increase scattering effects in the water column. The influence of scattering on the image is indistinguishably linked to the morphology and dimensions of these particles. The amount of scattering caused by particles underwater depends on their size and shape, which influences the visual quality of underwater images. There are two types of scattering, as shown in Fig. 1.3. The main challenge occurred underwater imaging as follows:

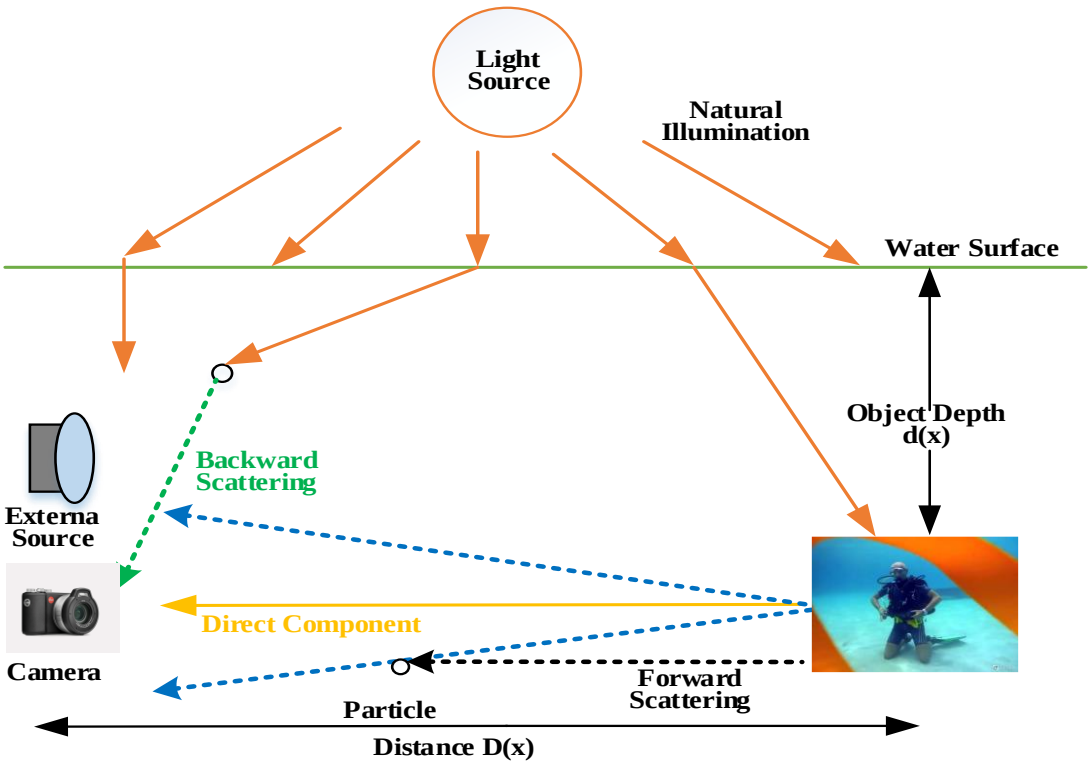

Fig. 1.3 The light propagation mechanism for underwater.

- When light travels through water, it interacts with particles suspended in the water. These particles scatter the light, causing it to bounce around in different directions. When a camera captures an underwater image, the light reaching the camera has been scattered multiple times by these particles. This scattering phenomenon is called forward scattering [23]. It occurs because the light is scattered toward the camera due to the mutual reflections of light between the particles along the path of the light. Essentially, the light bouncing between the particles contributes to the hazy or diffused appearance often observed in underwater photography. Its effects are noticeable, resulting in visual blurring, decreased contrast, and decreased color fidelity.
- Backward scattering [24], [25] is another phenomenon in underwater environments. Unlike forward scattering, which affects the clarity of images, backward scattering adds noise and can create what are known as marine snow patterns. When light particles travel toward an object in the water, some reflect toward the camera instead of reaching the object. These reflected light particles contribute to the formation of marine snow patterns. These patterns appear as specks or streaks in the image, reducing its clarity and adding unwanted elements. In essence, backward scattering introduces additional visual noise by redirecting light particles toward the camera before they reach the intended subject.

- The importance of forward scattering in causing image degradation has been underlined by Truco et al. [16], [17], [26]. They developed a filtering method based on the Jaffe-McGlamery image generation model to address this problem and lessen the effects of forward scattering.
- The amount of available light underwater varies depending on the time of day and weather conditions. When the sun is directly overhead, the water's surface reflects the least light. Stormy weather can also disrupt light conditions, especially when the water surface is uneven. Additionally, color absorption poses a significant challenge as specific wavelengths of light are absorbed underwater. Blue and green light, with their longer wavelengths, penetrate deeper into the water, resulting in underwater images predominantly displaying hues of blue and green.
- Absorption and scattering in underwater conditions result in blurred images, reduced contrast, and diminished image quality. This issue is exacerbated in highly turbid underwater environments or when powerful artificial light sources are used. Artificial lighting creates uneven illumination, causing reflections that obscure image details and produce bright spots. This can lead to misinterpretation of data.
- The biological matter's fluorescence and the large particle's presence further degrade underwater images. As demonstrated in Fig. 1.4, underwater image-enhancement and restoration techniques solve some challenges by integrating visual information into quantitative assessments. Underwater enhancement and restoration techniques can yield precise quantitative data with minimal human intervention, enhancing the reliability of visual inspection.

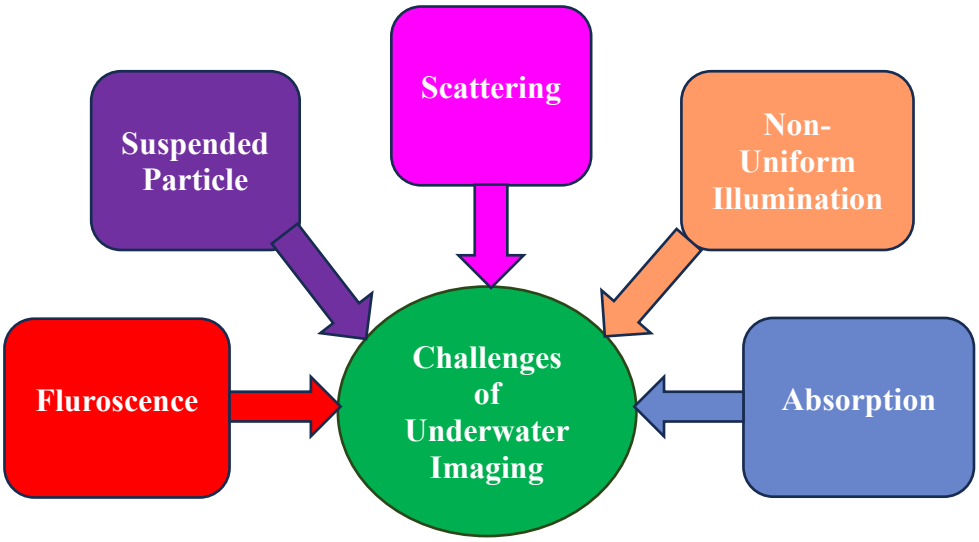

Fig. 1.4 Challenges faced by underwater imaging.

1.4 Motivation and Problem Statement

The fast progress of modern image enhancement and restoration technology has sparked widespread interest in improving degraded underwater images. Enhancing the contrast of individual foggy underwater images is challenging for complex applications (such as oceanography and marine biology, environmental monitoring, underwater archaeology, search and rescue, underwater inspections, aquaculture management, underwater exploration, underwater robotics, and many more). The underwater images often have poor visibility at deeper depths because of the attenuation in light transmission. When the artificial light source extends the underwater vision range, it can produce non-uniform illumination patterns in the captured images. This is another problem that requires a pre-processing of the underwater image. Marine snow and small floating particles in the camera's field lead to forward and backward scattering of light energy, resulting in low contrast and a hazy image appearance. Additionally, light loses its original color due to attenuation of transmission with lateral distance, which lowers the amount of light energy that reaches the camera. Therefore, using a single underwater image, the main objectives of underwater image enhancement are color correction and haze removal.

This thesis aims to develop underwater image enhancement and restoration techniques to overcome the limitations of existing state-of-the-art methods. These algorithms will address issues commonly encountered in underwater imaging, such as poor contrast, non-uniform illumination, color cast, and limited visibility.

1.5 Performance Metrics

The performance metrics are used to evaluate image enhancement and restoration techniques. It is broadly classified into reference and non-reference-based metrics. Reference-based metrics require access to a reference or ground truth image for comparison, while non-reference-based metrics assess image quality without relying on a reference image. Here are some examples of both types of metrics.

1.5.1 Full-Reference Assessment

A wide range of reference metrics and evaluation criteria are accessible for evaluating the quality of images. We want to analyze the precise features of image quality and determine which metric to employ based on the type of image we are working with. Here are some typical

reference metrics for assessing image quality.

1.5.1.1 Structure Similarity Index Measure

The structural similarity index measures the structural similarity between two images, often an original reference image and a deformed or altered image. SSIM is intended to record changes in structural information, brightness, contrast, and texture, which are significant elements in how well a person views an image.

Here are the key components and principles of the SSIM metric:

Luminance comparison: The luminance (brightness) similarity between the reference and distorted images is evaluated by SSIM. It considers how closely the overall brightness of the two photographs match.

Contrast comparison: By measuring how well contrast is preserved, SSIM evaluates how similar the contrast is between the images. This covers the variations in intensity between image sections.

Structure comparison: The metric analyses the structural similarity by comparing local patterns or textures in the images. It looks at how well fine details and edges are maintained.

Image size and position: To stabilize the division in the formula and prevent division by zero, SSIM incorporates a constant factor K.

The SSIM formulas can be expressed as follows:

$$SSIM(I,\tilde{I}) = \frac{(2\mu_I\mu_{\tilde{I}} + C_1)(2\sigma_{I\tilde{I}} + C_2)}{(\mu_I^2 + \mu_{\tilde{I}}^2 + C_1)(\sigma_I^2 + \sigma_{\tilde{I}}^2 + C_2)} \tag{1.1}$$

where μ_I and $\mu_{\tilde{I}}$ denotes the mean intensity of pixel values of reference and distorted image respectively defined as:

$$\mu_I = \frac{1}{M \times N}\sum_{i=0}^{M-1}\sum_{j=0}^{N-1} I(i,j) \tag{1.2}$$

and $\sigma_{I\tilde{I}}$ represents the covariance of pixel values between reference image ($I(i,j)$) and distorted image ($\tilde{I}(i,j)$) defined as:

$$\sigma_{I\tilde{I}} = \frac{1}{M \times N}\sum_{i=0}^{M-1}\sum_{j=0}^{N-1}(I(i,j) - \mu_I)(\tilde{I}(i,j) - \mu_{\tilde{I}}) \tag{1.3}$$

C_1 and C_2 are the positive constants, and it is used for indeterminant situations when $\mu_I^2 + \mu_{\tilde{I}}^2$ and $\sigma_I^2 + \sigma_{\tilde{I}}^2$ are very close to zero.

A perfect match between the two images is indicated by an SSIM value of 1, and higher SSIM

values for images represent more substantial structural similarity and better image quality. The SSIM value ranges from 0 to 1.

1.5.1.2 Peak Signal-to-Noise Ratio (PSNR)

Peak signal-to-noise ratio is an image quality that is frequently used in the fields of image processing and compression. It offers a quantitative evaluation of an image's quality when compared to an original or reference image that has been warped or compressed. The integrity of image reduction and restoration methods is frequently assessed using PSNR.

PSNR is calculated and interpreted as:

Mean square error (MSE): The mean squared error between the reference image (often denoted as *I*) and the deformed or compressed picture (typically denoted as $\tilde{I}$) is calculated as the first step in determining PSNR. MSE measures the average squared difference between the two image's pixel values and is calculated as follows:

$$MSE(I,\tilde{I}) = \frac{1}{M \times N}\sum_{i=0}^{M-1}\sum_{j=0}^{N-1}[I(i,j) - \tilde{I}(i,j)]^2 \tag{1.4}$$

where *M* and *N* denote the dimensions of the images.

Peak value: The peak value of the image is defined as 2^n. Where *n* is the number of bits used to represent the image. An 8-bit number represents the grayscale image. Therefore, the peak value for the grayscale image is 255. PSNR uses the image's peak pixel values to create a scale.

PSNR calculated by Eqn (1.5):

$$PSNR(I,\tilde{I}) = 10 \times log_{10}\left(\frac{(Peak\ value)^2}{MSE(I,\tilde{I})}\right) \tag{1.5}$$

The PSNR value is typically expressed in decibels (dB).

Interpretation of PSNR:

- Since greater PSNR values imply that the difference between the reference and distorted images is minimal compared to the peak value, they indicate higher image quality.
- Lower PSNR values imply more significant disparities between the reference and distorted images, which suggests lower image quality.
- PSNR has limitations and might not always match how people perceive image quality. It could miss tiny perceptual differences since it concentrates on overall differences.

Although PSNR is a commonly used metric, it's important to remember that it primarily measures pixel-wise fidelity and might not be the best option when evaluating image quality in situations where human perception plays a key role, such as in the evaluation of visually significant details, textures, or artifacts. In these circumstances, subjective evaluation by human observers or perceptual measures like the structural similarity index may offer more accurate image quality.

1.5.1.3 Contrast Per Pixel

As introduced by [27], the CPP metric measures the amount of contrast presents in an image. This metric calculates the contrast of each pixel by comparing it to the neighboring pixels in the image and then takes the average of these values. In other words, CPP measures the level of local contrast within an image. A higher CPP number indicates better contrast.
Mathematically, the contrast per pixel is defined as:

$$C = \frac{\sum_{i=0}^{N-1}\sum_{j=0}^{M-1}\left(\sum_{(i,j)\in R_3^{(i,j)}}\left|I(i,j)-\tilde{I}(i,j)\right|\right)}{M \times N} \tag{1.6}$$

Intuitively, this is the average difference in grey level between adjacent pixels. Here, M and N are the size of an image.

1.5.1.4 Measure of Enhancement

By dividing the image into non-overlapping blocks and calculating the average logarithmic maximum-to-minimum-intensity ratio, the EME can roughly estimate the typical contrast in an image. The input image is divided into sub-images of size $k_1 \times k_2$. The parameters are mathematically described as [27]

$$EME = \frac{1}{k_1 \times k_2}\sum_{i=1}^{k_1}\sum_{j=1}^{k2}\left(20 \times \ln\frac{I_{max,i,j}^{w}}{I_{min,i,j}^{w}+\varepsilon}\right) \tag{1.7}$$

where, $I_{max,i,j}^{w}$ and $I_{min,i,j}^{w}$ are the maximum and minimum intensities in a particular block $B(i,j)$, and ε is a small positive constant to avoid the indeterminant term.

1.5.1.5 Modified Measure of Enhancement

The enhancement measure primarily relies on range values, adjusting itself based on the maximum and minimum range, and may not always accurately assess enhancement in every situation. First, it is prone to noise as only the maximum and minimum intensities count for the

contrast in any blocks, but these blocks may have various statistical characteristics. Second, it does not mix the inter-block contrast. A modified measure of enhancement has been proposed based on the above analysis.

$I_{i,j}^{w}$ represents the intensity of the block with index (i,j) when an image is divided into $k_1 \times k_2$ blocks. MEME defined as

$$MEME = \alpha \times \frac{C_{I_{DC}}}{k_1 \times k_2} \times \frac{1}{k_1 \times k_2} \sum_{i=1}^{k_1} \sum_{j=1}^{k_2} C_{i,j}^{w} \tag{1.8}$$

In the context provided, the variable I_{DC} represents a thumbnail image of the original image (I). The size of the thumbnail image (I_{DC}), is exactly $k_1 \times k_2$, which is equivalent to the number of blocks. Each pixel within this thumbnail image is assigned a value equal to the mean of the corresponding block in the original image, which is represented as $mean$ ($I_{i,j}^{w}$). To enhance the resulting values and prevent them from being too small, a parameter α is introduced and set to 100 in this experiment. $C_{I_{DC}}$ and $C_{i,j}^{w}$ represents inter-block contrast and intra-block contrast, respectively. It is square root contrast and mathematically defined as

$$C = \sqrt{\frac{1}{M \times N} \sum_{i=1}^{M} \sum_{j=1}^{N} (I(i,j) - mean(I(i,j)))^2} \tag{1.9}$$

In the given context, the term $I(i,j)$ refers to an original image with dimensions $M \times N$. It's worth noting that in this context, a larger MEME value corresponds to a more pronounced enhancement in the resulting output image.

1.5.1.6 Feature Similarity Index Measure (FSIM)

The process of calculating the FSIM index involves two distinct phases. Initially, we compute a local similarity map, and subsequently, we aggregate and condense this similarity map into a single similarity score during the second stage. The FSIM measurement between $I(i,j)$ and $\tilde{I}(i,j)$ divide into two components, each corresponding to either phase congruency (PC) or gradient magnitude (GM). To begin with, we define the similarity measure between the original image and reference image using phase congruency which is represented as $S_{PC}(i,j)$**.** Mathematically it is defined as follows:

$$S_{PC}(i,j) = \frac{2 \times PC_1(i,j) \times PC_2(i,j) + Q_1}{PC_1^2(i,j) + PC_2^2(i,j) + Q_1} \tag{1.10}$$

where, Q_1 denotes a positive constant to increase the stability of $S_{PC}(i,j)$**,** and $PC_1(i,j)$,

$PC_2(i,j)$ denotes phase congruency of original image and reference image respectively. Similarly, the GM values $G_1(i,j)$ and $G_2(i,j)$ of $I(i,j)$, $\tilde{I}(i,j)$ respectively are compared, and the similarity measure is defined as follows:

$$S_G(i,j) = \frac{2 \times G_1(i,j) \times G_2(i,j) + Q_2}{G_1^2(i,j) + G_2^2(i,j) + Q_2} \tag{1.11}$$

where, Q_2 is a positive constant depending on the dynamic range of GM values. Both Q_1 and Q_2 are fixed for all the databases so that the proposed FSIM can be conveniently used. Then $S_{PC}(i,j)$ and $S_G(i,j)$ are combined to get the overall similarity $S_L(i,j)$ of $I(i,j)$ and $\tilde{I}(i,j)$. Mathematically, it is defined as follows:

$$S_L(i,j) = [S_{PC}(i,j)]^{\alpha}.[S_G(i,j)]^{\beta} \tag{1.12}$$

where α and β are parameters that are used to modify the relative weight of PC and GM attributes. Here $\alpha = 1$ and $\beta = 1$ for simplicity.

After obtaining the similarity measure, $S_L(i,j)$, at each position *(i,j)*, we can proceed to compute the overall similarity between $I(i,j)$ and $\tilde{I}(i,j)$. However, it's essential to acknowledge that different locations within an image contribute differently to the perception of the human visual system. For instance, edge locations carry more vital visual information compared to areas with smooth transitions. As the human visual cortex is particularly attuned to phase congruent structures [20], the PC value at a specific location can serve as an indicator of the likelihood that it represents a visually significant structural point.

In a straightforward sense, if either $I(i,j)$ or $\tilde{I}(i,j)$ exhibits a substantial PC value for a given location *i*, it suggests that this specific position *(i,j)* will exert a significant influence on the assessment of similarity by the human visual system when comparing $I(i,j)$ and $\tilde{I}(i,j)$. Consequently, we employ the $PC_m(i,j) = max\,[PC_1(i,j), PC_2(i,j)]$ to gauge the significance of $S_L(i,j)$, in the overall similarity evaluation between $I(i,j)$, and $\tilde{I}(i,j)$. Accordingly, the FSIM index between $I(i,j)$ and $\tilde{I}(i,j)$ is defined as follows:

$$FSIM = \frac{\sum_{(i,j)\in\delta} S_L(i,j).PC_m(i,j)}{\sum_{(i,j)\in\delta} PC_m(i,j)} \tag{1.13}$$

where δ means the whole image spatial domain.

1.5.1.7 Gradient Magnitude Similarity Deviation (GMSD)

It is a reference metrics assessment of the quality of images. Mathematically, it is defined as follows:

$$GMSD = \sqrt{\frac{1}{N}\sum_{i=1}^{N}(S_G(i,j) - GMM(i,j))^2} \tag{1.14}$$

where $S_G(i,j)$ stands for gradient magnitude similarity and is represented as calculated as:

$$S_G(i,j) = \frac{2 \times G_1(i,j) \times G_2(i,j) + Q_2}{G_1^2(i,j) + G_2^2(i,j) + Q_2} \tag{1.15}$$

$G_2(i,j)$ = gradient magnitude of a reference image ($\tilde{I}(i,j)$), and it is defined as follows:

$$G_2(i,j) = \sqrt{(\tilde{I}(i,j) * F_x)^2(i,j) + \left(\tilde{I}(i,j) * F_y\right)^2(i,j)} \tag{1.16}$$

$G_1(i,j)$ = gradient magnitude of distorted image ($I(i,j)$), and it is defined as follows:

$$G_1(i,j) = \sqrt{(I(i,j) * F_x)^2(i,j) + \left(I(i,j) * F_y\right)^2(i,j)} \tag{1.17}$$

where the symbol $*$ represents the convolution operation and F_x, F_y denotes the Prewitt filters along horizontal (x) and vertical (y) directions are defined as:

$$F_x = \begin{bmatrix} 1/3 & 0 & -1/3 \\ 1/3 & 0 & -1/3 \\ 1/3 & 0 & -1/3 \end{bmatrix}, \quad F_y = \begin{bmatrix} 1/3 & 1/3 & 1/3 \\ 0 & 0 & 0 \\ -1/3 & -1/3 & -1/3 \end{bmatrix}$$

GMM stands for gradient magnitude similarity mean, and it is defined as follows:

$$GMM = \frac{1}{N \times M}\sum_{i=0}^{N-1}\sum_{j=0}^{M-1} S_G(i,j) \tag{1.18}$$

where N and M represents the size of the image, it's important to note that a higher gradient magnitude similarity mean score is associated with improved image quality. In the context of image quality assessment, average pooling treats each pixel with equal significance when estimating the overall image quality. The gradient magnitude similarity deviation score indicates the degree of distortions in an image. A higher GMSD score essentially denotes a wider range of aberrations within the image, ultimately resulting in a lower image quality.

1.5.2 Non-Reference Assessment

No-reference measures, often referred to as non-reference image quality metrics, are used to evaluate an image's quality without needing a reference (original) image for comparison. These metrics examine several aspects and traits of the distorted or altered image to determine its quality. Here are some frequently used metrics for non-reference image quality:

1.5.2.1 Underwater Color Image Quality Evaluation

Underwater color image quality evaluation is a metric used to assess the quality of underwater color images. It considers factors specific to underwater environments, such as the absorption and scattering of light in water. To thoroughly determine how well an underwater image reproduces color and details, UCIQE considers several factors, including color correction, contrast, and sharpness. The objective is to determine how well, despite the difficulties caused by the optical characteristics of water, the photograph captures the genuine underwater scene. Essentially, UCIQE assists researchers and photographers in maintaining the high quality and accuracy of underwater images. For image I in the *CIE-Lab* color space, the underwater color image quality evaluation measure is defined as follows:

$$UCIQE = d_1 \times \sigma_c + d_2 \times con_1 + d_3 \times \mu_s \tag{1.19}$$

where, d_1, d_2, and d_3 are weighted coefficients. σ_c represent standard deviation of chroma, con_1 denote contrast of luminance and μ_s is the average of saturation. For underwater monitoring and survey color images with blurring, color cast, and marine snow distortions, the obtained coefficients are d_1 = 0.4680, d_2 = 0.2745, and d_3 = 0.2576.

1.5.2.2 Underwater Image Quality Measure (UIQM)

It has been shown that a linear superposition of absorbed and dispersed components can be used to model underwater images**.** Furthermore, it is well-recognized that color, sharpness, and contrast are degraded due to the absorption and scattering effects. As a result, it makes sense to create the overall underwater image quality metric using the linear superposition model. Next, the whole underwater image quality indicator is provided by

$$UIQM = q_1 \times UICM + q_2 \times UISM + q_3 \times UIConM \tag{1.20}$$

where the colorfulness, sharpness, and contrast measures are linearly combined. The value of parameters q_1, q_2, and q_3 are depends on the application. For example, the parameter q_1 has

more weight for color-correction applications, while in enhancing underwater image visibilities, the contrast term underwater image contrast measure ($UIConM$) and sharpness term underwater image sharpness measure ($UISM$) are more significant. The term UICM represents underwater image colorfulness measure; mathematically, it is defined as:

$$UICM = -0.0268\sqrt{v_{\alpha,RG}^2 + v_{\alpha,YB}^2} + 0.1586\sqrt{\delta_{\alpha,RG}^2 + \delta_{\alpha,YB}^2} \tag{1.21}$$

where, $v_{\alpha,RG}\ and\ v_{\alpha,YB}$ are asymmetric alpha-trimmed mean [28] of enhanced images for *RGB* color space and *YCbCr* color space respectively, δ^2 is second-order statistic variance of enhanced image.

UISM represents the measure of underwater image sharpness. Sharpness is an attribute related to the preservation of fine details and edges. For images captured underwater, severe blurring occurs due to the forward scattering [15]. This blurring effect causes degradation of image sharpness. The Sobel edge detector is initially applied to each RGB color component to measure the sharpness of edges. The grayscale edge map is then obtained by multiplying the resulting edge map by the original image. Only the margins of the original underwater image's pixels are kept when doing this. The enhancement measure estimation has been demonstrated to work well with images that exhibit nonperiodic patterns and have a uniform backdrop [29]**.** Consequently, the sharpness of edges is measured using the EME. The *UISM* is created as illustrated in a mathematical expression

$$UISM = \sum_{p=1}^{3} \lambda_p EME(grayscale\ edge_p) \tag{1.22}$$

$$EME = \frac{2}{m_1 n_1} \sum_{i=1}^{m_1} \sum_{j=1}^{n_1} log\left(\frac{I_{max}(i,j)}{I_{min}(i,j)}\right) \tag{1.23}$$

where the image is divided into $m_1 n_1$ blocks, $(I_{max}(i,j)/I_{min}(i,j))$ denotes the relative contrast ratio within each block and EME of each RGB color component are combined linearly with the coefficients λ_p where $\lambda_R = 0.299, \lambda_G = 0.587$, and $\lambda_B = 0.114$.

UIConM denoted as underwater image contrast measure; for underwater images, contrast degradation is caused by backward scattering. Here, the contrast is measured by applying the log(Agaian measure of enhancement by entropy (*AMEE*)) [30] on the intensity image, as shown in Eqn (1.24)

$$UIConM = \log\left(AMEE(Intensity)\right) \tag{1.24}$$

where,

$$\log(AMEE) = \frac{1}{m_1 n_1} \otimes \sum_{m=1}^{m_1} \sum_{n=1}^{n_1} \left(\frac{I_{max}(i,j) \Theta I_{min}(i,j)}{I_{max}(i,j) \oplus I_{min}(i,j)} \right) \times log \left(\frac{I_{max}(i,j) \Theta I_{min}(i,j)}{I_{max}(i,j) \oplus I_{min}(i,j)} \right) \quad (1.25)$$

Here, an image is divided into $m_1 n_1$ blocks, and $\otimes$, Θ, and $\oplus$ are the PLIP operation [30].

1.5.2.3 Patch-Based Contrast Quality Index

One type of image quality metric is the patch-based contrast quality index, which evaluates a picture's quality based on the contrast information in localized patches. Rather than considering the entire image, this metric is intended to capture the differences in contrast at a local level. The aim is to offer a more detailed assessment of contrast quality.

Here is the basic outline of how a patch-based contrast quality index is formulated:

Patch division: Divide the image into non-overlapping or overlapping patches. The size of these patches can be determined based on the characteristics of the images being analyzed.

Contrast measurement on patches: Compute a measure of contrast within each patch. This could involve calculating statistics such as standard deviation, range, or other contrast measures for the pixel values within the patch.

Quality assessment for each patch: Use the contrast information from each patch to assess the quality of that specific region. This step may involve comparing the local contrast characteristics to an ideal or reference distribution.

Aggregation across patches: Combine the local quality assessments from all patches to obtain an overall measure of image quality. This could be done by averaging, weighting, or using other aggregation methods.

Normalization or scaling: Normalize the computed quality index to a meaningful range between 0 and 1 for better interpretability. A specific formula for PCQI would depend on the exact contrast measurement used within the patches and the aggregation strategy. Different approaches can be taken based on the desired characteristics of the quality index. Mathematically, it is defined as:

$$PCQI(x,y) = q_i(x,y).q_c(x,y).q_s(x,y) \quad (1.26)$$

where $x \; and \; y$ are pairs of co-related patches in the original image I and test image $\tilde{I}$, respectively.

$$q_i(x,y) = e^{-\left(\frac{\left| {c_1}^I - {c_1}^{\tilde{I}} \right|}{\sqrt{N}L} \right)} \quad (1.27)$$

${c_1}^I = \sqrt{N}\mu_I$, N = number of pixels in image I and $\tilde{I}$, μ_I = mean value of the pixel of image I.

$$q_c(x,y) = \frac{4}{\pi} \cdot arctan\left(\left|\frac{c_2^{\tilde{I}}}{c_2^{I}}\right|\right) \tag{1.28}$$

Here nonlinear function $\frac{4}{\pi} \cdot arctan(\cdot)$ is introduced to control the saturation of the contrast changes. The value of $q_c(x,y)$ lies between 0 and 2.

$$q_s(x,y) = \frac{c_2^y + r^T v_2}{\left\| c_2^y . v_2 + r \right\|} \tag{1.29}$$

where y is the new patch and is defined as

$$\left.\begin{array}{c} y = c_1^y \cdot v_1 + c_2^y v_2 + r \\ c_1^y = \tilde{I}^T v_1 = \sqrt{N}\mu_{\tilde{I}} \\ c_2^y = \tilde{I}^T v_2 \end{array}\right\} \tag{1.30}$$

where the basis v_1 and v_2 points to a specific direction in the image signal space, and r denotes the residual image signal perpendicular to both v_1 and v_2 [31]. $\mu_{\tilde{I}}$ represents mean value of pixel of reference image ($\tilde{I}$).

1.5.2.4 No-Reference Image Quality Metric for Contrast Distortion (NIQMC)

When contrast levels are changed, it affects the image's visual quality and is referred to as contrast distortion in images. No-reference image quality metrics for contrast distortion evaluate the quality of an image without using a reference image as a comparison. These measures are especially helpful when evaluating images independently of a reference or in the absence of a reference image. Mathematically, it is defined as [32]

$$NIQMC = \frac{Q_L + \rho Q_G}{1 + \rho} \tag{1.31}$$

where ρ is a constant weight that regulates how important the local and global plans are in comparison. Here $\rho = -2.2$ has been taken. Q_L= Local quality measure and Q_G = Global quality measure.

$$Q_L = \max\{E_{l_1}, E_{l_2}, \dots \dots E_{l_5}\} \tag{1.32}$$

where, $E_{l_1}, E_{l_2}, \dots \dots, E_{l_5}$, entropy values of pixels.

$$Q_G = D_{JS}(h,u) \tag{1.33}$$

where $h,$ and u are histograms of pixel values. The higher local Q_L or lower value of Q_G represent more excellent contrast and better quality.

1.5.2.5 Blind/Referenceless Image Spatial Quality Evaluator (BRISQUE)

An algorithm for assessing the spatial quality of pictures that does not require a reference image for comparison is called a Blind/Referenceless image spatial quality evaluator (BRISQUE) [33]. In many applications, such as multimedia, computer vision, and image compression, evaluating the quality of an image is a crucial task.

Traditional image quality assessment methods often require a reference image (a high-quality version of the same image) to compare against the distorted image. However, obtaining a reference image may not be feasible or practical in many real-world scenarios. BRISQUE addresses this limitation by assessing image quality in a blind or Referenceless manner. Typically, BRISQUE takes an image and extracts natural scene statistics attributes. Some characteristics of natural photographs are captured by these statistical measures, which are called features. The algorithm then uses a trained model frequently built using machine learning methods to forecast the image quality based on these attributes. Typically, a collection of photos with known quality scores is used to train the model.

Applications for BRISQUE can be found in underwater image enhancement and restoration, video coding, and multimedia quality optimization, among other domains. They offer an automated method for assessing image quality without requiring a reference image, making them especially helpful when obtaining reference photos is impractical or unavailable.

1.5.2.6 Absolute Mean Brightness Enhancement

The absolute mean brightness enhancement is a metric used in image processing to quantify the difference in mean brightness between two images, i.e., distorted and enhanced images. It measures the average absolute difference in pixel intensities between the corresponding pixels in two images. Mathematically, the absolute mean brightness measure is calculated as follows:

$$AMBE = \frac{1}{N \times M} \sum_{i=0}^{N-1} \sum_{j=0}^{M-1} |I_1(i,j) + I_2(i,j)| \tag{1.34}$$

where M and N is the total number of pixels in the images. $I_1(i,j)$ and $I_2(i,j)$ are the pixel intensities at the i^{th} and j^{th} pixel in the two images being compared.

The AMBE provides a single scalar value representing the average absolute brightness difference across all pixels. A lower AMBE indicates a minor difference in mean brightness

between the images, suggesting they are more similar in overall brightness. Conversely, a higher AMBE indicates a significant difference in mean brightness.

AMBE is a simple and intuitive metric, but it may not capture certain aspects of image quality or perceptual differences that are important in specific applications. Therefore, it is often used in conjunction with other metrics to provide a more comprehensive assessment of image quality or to evaluate the performance of the image processing algorithm.

1.5.2.7 Discrete Entropy

In image processing, discrete entropy measures the amount of information or uncertainty associated with the pixel intensities in an image. Entropy is a concept borrowed from information theory used to quantify the randomness or disorder in a set of data [34]. For a discrete system like a digital image, the discrete entropy is often calculated using the histogram of pixel intensities. The histogram represents the frequency distribution of different pixel values in the image. The formula for discrete entropy (H) is given by:

$$H = \sum_{i=1}^{L} p(i) log_2\big(p(i)\big) \tag{1.35}$$

where L is the possible intensity levels (i.e., for an 8-bit image, $L = 256, p(i)$) is the probability mass function of the intensity level i, which is calculated as the normalized frequency of occurrence of intensity i in the image.

1.6 Contribution of this Thesis

Contributions of this thesis are as follows:

- ✓ We have proposed a method for underwater image enhancement based on multiscale decomposition, gamma correction, and brightness adjustment. The proposed method evaluated the underwater image enhancement benchmark dataset in terms of visual quality and various parameter estimation.
- ✓ The underwater image restoration framework is proposed based on white balance and retinex algorithm. The white balance is applied to degraded underwater images before color space transformation. The *Y-component* of *YCbCr* color space decomposed into reflectance and illumination and further enhancement has been done to that component.
- ✓ An image restoration method has been introduced for underwater images based on color correction and empirical mode decomposition. We have applied color correction to the underwater images in the proposed framework. The color-corrected image has been

converted into hue saturation value (*HSV)* color space from *RGB* color space. All three components of *HSV* color space, i.e., *H-component*, *S-component*, and *V-component,* are decomposed into four intrinsic mode functions. Each intrinsic mode function multiplies with some weight to adjust the pixel values of an image. Finally, concatenate the all-intrinsic mode function to restore the degraded image.

- ✓ A novel method for underwater image enhancement has been proposed based on the fusion of transmission optimization and background light estimation via principal component analysis. The degraded underwater image transforms into *CIE-Lab* color space from *RGB* color space. The transmission map of the *L-component* of the *CIE-Lab* color space is evaluated, and transmission optimization is performed. The optimized transmission and background light is fused through principal component analysis. Finally, color correction has been applied to the fused image. The effectiveness of the proposed method is tested on the standard dataset and compared with the existing state-of-the-art methods.
- ✓ Further, we continued our effort to explore the concept of image fusion. This proposed method fuses the multiscale gradient-domain enhancement and gamma correction to enhance and restore underwater images and videos. Before converting the *YCbCr* color space from *RGB* color space, we applied white balance to degraded underwater images for color correction. The *Y-component* of the base layer is decomposed into the base layer and details layer using a weighted list square filter. The sigmoid function and gamma correction are used to enhance the base layer and detail layer, respectively. The improved base layer and detail layer are fused. The proposed method has been tested on publicly available image and video datasets. We have compared the proposed framework's effectiveness with the existing state-of-the-art method based on the results obtained.
- ✓ We have proposed another novel method for the restoration of underwater images. This approach leverages both white balance and blending techniques to improve image quality. Firstly, the color correction is applied to degraded underwater images. The white balance and contrast limited adaptive histogram equalization (CLAHE) techniques have been used for the color-corrected image, with the corresponding output represented as *input1* and *input2*, respectively. *Input1* and *input2* are converted to *YCbCr* color space. The laplacian, saliency, and saturation have been applied to the *Y-component* of *YCbCr* color space for both *input1* and *input2*. The weight normalization is carried on the combination of Laplacian, saliency, and saturation. Finally, we

obtained the restored image through the blending process. The proposed method has been evaluated on three datasets, UIEB, RUIE, and U45, through subjective and objective assessment. In the subjective evaluation, the proposed method has been compared with the existing state-of-the-art methods regarding visual quality. On the other hand, an objective assessment has been performed on the proposed and existing methods. The proposed method is compared with the existing method in terms of various parameters.

1.7 Thesis Organization

The thesis consists of six chapters, which are organized as follows:

Chapter 1 introduces the brief background of underwater optical imaging and its applications. It also gives the motivation for this thesis, the challenge in underwater imaging, and the inherent problems faced in underwater imaging, and defines the problem statement. The underwater image enhancement and restoration field is relatively new and still developing. The various quantitative analysis metrics employed for comparing the proposed method with existing state-of-the-art methods are highlighted.

Chapter 2 is dedicated to the literature review, where the existing state-of-the-art methods for underwater image enhancement and restoration are reviewed by analyzing the various existing methods of underwater image enhancement and restoration to identify their strengths and limitations. Based on the limitations of existing state-of-the-art techniques, we found the available datasets used in this thesis for experimental validation of the proposed methods. Research gaps and established the objective of this study. Further, we discussed publicly available datasets.

Chapter 3 presents an effective underwater image enhancement method using multiscale decomposition, gamma correction, and empirical mode decomposition. The proposed framework decomposes the degraded underwater image into illumination and reflectance. Further, gamma correction is applied to one of the multiscale decomposition layers to obtain an enhanced image. The second method proposed for image restoration using white balance and retinex algorithm. The effectiveness of the proposed method is explained and validated through experiments on standard datasets and state-of-the-art comparison of obtained results.

Chapter 4 describes an effective underwater image enhancement and restoration method using white balance and the retinex algorithm. The algorithm combines two images obtained from

the original degraded image after applying white balance and CLAHE. The images are then converted into *YCbCr* color space from *RGB* color space. The *Y-component* of *YCbCr* color space images is then assigned weight maps based on laplace contrast, saliency, and saturation factors. These weight maps are normalized and combined using a blending process to address the issue of uneven illumination that can cause visual artifacts in images. Another method proposed to restore the degraded image is based on empirical mode decomposition. The proposed method is compared with the existing state-of-the-art methods on publicly available datasets. The effectiveness of the proposed method has been evaluated in terms of the image's visual quality and various parameters.

Chapter 5 focuses on the fusion of multiscale gradient-domain and gamma correction to enhance and restore underwater images and videos in detail. The WLS filter is used for the multiscale decomposition. Gamma correction is applied to the base layer, and gradient-domain enhancement is carried out on detail layers. The second solution discusses the contrast enhancement and visibility restoration of degraded underwater images using principal component analysis based on the fusion of background light and transmission optimization. The background light is evaluated for degraded underwater images and fused with optimized transmission using principal component analysis. The proposed framework tested for applications such as low light and storm images. Further, the effectiveness of the proposed framework has been tested on two standard datasets by ablation study and evaluation of various parameters in brief.

Finally, in **Chapter 6**, we summarize the conclusions inferred from our research work and highlight the potential future work in this area.

Chapter 2

Literature Review

This chapter explained the merits and demerits of existing state-of-the-art methods. We reviewed several methods of underwater image enhancement and restoration techniques. This helped us discover the research gaps in existing solutions in the area of underwater image enhancement and restoration. We also discussed the underwater image and video dataset for experimental comparison. Later, the research objective has been formulated based on these research gaps, which are addressed in this thesis. Finally, we have discussed the datasets used in this research.

2.1 Introduction

Early in the 1960s, Duntley made a significant contribution to underwater optics development by conducting ground-breaking research at the visibility laboratory of the Scripps Institute of Oceanography and the Massachusetts Institute of Technology [35]. This study developed the theoretical framework first developed by McGlamery to comprehend the optical characteristics of light propagation in water. Later, Jaffe built on McGlamery's work and created the underwater image formation model [17]. The Jaffe-McGlamery model was reduced by Truco and Antillon, who then utilized it to develop a self-tuning restoration method [16]. Additionally, Hou et al. [36] used the modular transfer function in the frequency domain and the point spread function in the spatial domain to add underwater optical features to the restoration procedure. Underwater image enhancement and restoration can be roughly divided into two different category. The first one makes use of traditional enhancement methods that rely on fictitious models of image generation. The second category focuses on restoration methods that make use of statistical priors or physical image generation models.

2.2 Underwater Image Enhancement

Several initiatives have been made to improve the visibility of underwater images, expanding on existing haze removal techniques [37]. Due to the multiplicative nature of underwater image generation and the inefficiency of linear enhancement techniques, these traditional methods

have some limitations [38]. Since it is frequently impractical to capture several underwater photographs of the same scene, the need for reference images and ground truth presents a substantial challenge in underwater image enhancement [39]. It's only sometimes possible to use methods like polarisation cameras for image capturing [40], [41]. As a result, we now concentrate on algorithmic methods for removing haze from individual underwater blurry images. To solve this problem, image enhancement methods have been employed [42]–[44]. Significantly, these techniques are independent of the requirement for in-depth physical modeling of the underwater environment.

In recent years, numerous methods have emerged for enhancing, restoring, detecting saliency, reducing noise, ensuring color constancy, correcting colors, and defogging to recover underwater images. While some older techniques, like contrast-limited adaptive histogram equalization [45], aim to reduce noise in underwater images, Deng [46] utilized a generalized unsharp masking algorithm to enhance contrast sharpness and mitigate halo effects. Another approach by Fu et al. [47] employs a probability method to simultaneously estimate illumination and reflectance, which is primarily effective for standard images. However, these traditional image enhancement methods are insufficient to compensate for the contrast degradation inherent in underwater images.

This research aims to correct color casts and enhance contrast by manipulating individual image pixels. Unlike the approach taken by Iqbal et al. [48], the goal here is to expand the saturation of the *RGB* color space. In contrast, Fu et al. [49] employed a two-step enhancement process, correcting colors and then enhancing contrast. Ancuti et al. [38] utilized complementary information from multiple images to further improve results. They integrated a multiscale fusion technique by blending color-corrected images with contrast to enhance the single input image. Ancuti et al. [50] introduced a fundamental color channel compensation (3C) pre-processing step to enhance image enhancement via color correction. The 3C algorithm notably enhances traditional restoration methods by reconstructing lost channels based on the opponent color channel.

Zhang et al. [51] enhanced the underwater image using multiscale retinex. Fu et al. [52] first corrected the color cast and then enhanced contrast using a retinex-based model. Dai et al. [53] addressed issues related to low-illuminated and underwater images by first utilizing different techniques on the incident light and subsequently improving the reflectance contrast.

Apart from retinex-based image enhancement methods, numerous methods for enhancing underwater images have been developed. While traditional image enhancement techniques like histogram equalization (HE), contrast-limited adaptive histogram equalization (CLAHE) [54], generalized unsharp masking [55], and probability-based methods [56] are adequate for standard images; they fall short in adaptively correcting the contrast loss in underwater images. It has been observed that conventional underwater image enhancement procedures often neglect the fact that the distance between the object and the camera influences contrast deterioration in underwater images. Recently, numerous single-image dehazing techniques have been introduced. Tan et al. [57] introduced a method based on the idea that clear images exhibit higher contrast than those diminished by adverse weather conditions. Colores et al. [58] developed an approach leveraging the local statistical uncorrelation between surface shading and transmission functions. He et al. [59] introduced the dark channel prior technique, which calculates the medium transmission by assuming that at least one color channel in a haze-free image has a low intensity. Ancuti et al. [60] employed a multiscale fusion technique to enhance the visual quality of images taken in misty conditions. Although these single-image denoising methods have proven effective for general photographs, they show limited improvement when applied to underwater images. The unique characteristics of underwater imaging and lighting conditions make the direct application of these methods less effective. The assumptions and previous applications of single-image denoising algorithms do not always hold in underwater environments.

Significant advancements have been made in underwater image enhancement methods in recent years. Sahu et al. [61] introduced an unsupervised color correction technique based on shade balancing and histogram stretching to improve underwater images. Bianco et al. [62] introduced a straightforward prior for estimating scene depth by leveraging the significant variation in attenuation among the three color channels in an underwater image, effectively reducing light scattering effects. The traditional dark channel prior technique also helps mitigate the impact of scattering haze. Additionally, reverse correction is applied to address color cast distortions based on the attenuation levels of different wavelengths. Using the fusion concept, Ancuti et al. [38] developed a novel technique to enhance the visual quality of underwater images and videos. Serikawa and Lu [63] addressed scattering and color fluctuation issues in underwater images by correcting attenuation mismatches along the propagation path. Galdran et al. [64] introduced a dark channel prior technique (DCP), which recovers colors associated with short wavelengths and restores lost contrast. Chani and Isa’s approach

significantly improves image divergence and minimizes under and over-enhanced areas. Zhao et al. [65] estimated the essential optical properties of water using background color and applied an underwater image formation model to enhance underwater images.

However, as mentioned earlier, many of the assumptions made in the procedures are only suitable for specific underwater conditions. Some current solutions rely on multiple images [39] or specialized hardware devices [66] to restore the quality of underwater images. Despite their effectiveness in enhancing underwater images, the above methods have disadvantage that might reduce their usefulness in practice.

The current advancements in underwater image enhancement have been primarily explored through various methodologies. As highlighted in references [34] and [9], some approaches rely on specialized hardware implementations for underwater image enhancement. For instance, diverging beam LIDAR imaging in turbid water system has been introduced for capturing images in challenging underwater conditions [67]. Due to its high cost and power consumption, the hardware system employed by this method poses practical limitations, rendering it unreliable for widespread application. Another approach involves polarisation-based techniques, where the camera's polarizing filter is rotated to capture multiple scene images, each with different polarization degrees. Schechner and Averbuch [40] utilize polarization induced by backward scattering light to estimate the transmission map. While the polarisation-based technique is effective for long-distance object retrieval, its suitability for capturing dynamic scenes in video format is limited.

The image enhancement techniques aim to replicate how light interacts with fog and underwater settings. Some methodologies enhance image quality in foggy outdoor scenes by recognizing parallels in light propagation between these environments. The methods, as documented in references [59], [68]–[71], focuses on boosting the inherent brightness of objects through the inversion of the visibility model. Yet, the Single image haze removal using dark channel prior [59] model was constructed with rigid presumptions, including uniform scattering processes and homogeneous atmospheric illumination, which may not universally apply in real-world scenarios. To mitigate these constraints, researchers have introduced techniques accommodating various lighting conditions [72]–[74]. However, the complexities in underwater imaging escalate notably due to the inverse correlation between scattering-induced loss and light wavelength.

Recently, several effective methods for enhancing underwater images using dark channels prior have been introduced, as noted in studies [59] and [75]. Originally, DCP was introduced for dehazing outdoor scenes, operating under the assumption that, in a natural scene, at least one-color component of an object's radiance is significantly low. This results in high minimal color values being characterized as regions with low transmission. Gautam et al. [76] applied DCP in their method to distinguish between foreground and background areas in underwater images. Drews et al. [77] utilized DCP to calculate the transmission of a single underwater image, assuming that the blue and green color channels are the primary sources of visual information beneath the water surface. The transmission derived from the underwater dark channel prior is more effective than that obtained through the traditional dark channel prior. Chiang et al. [78] suggested that underwater images could be enhanced through a combination of wavelength adjustment, dehazing, and incorporating the red channel, which aids in recovering the color associated with underwater short-wavelength light. Drews observed that red component become more vanishes as the camera distance increases. Lu et al. [79] use color lines to estimate transmission light to enhance underwater images. In a different approach [80], the authors calculate ambient light and transmission using a modified version of the DCP. They suggest applying a bilateral filter beforehand to eliminate highlighted areas. Additionally, Fattal uses a locally adaptive filter to refine the transmission for underwater images. Lu et al. [81] discuss the super-resolution techniques to enhance underwater images, though the resulting images do not always capture the textural variations in the scene. Li et al. [82] introduced a self-similarity-based super-resolution method to improve underwater image enhancement and address this limitation.

Recently, the standard techniques for underwater image enhancement such as color correction, histogram equalization/stretching, and linear mapping have developed [83]–[86]. However, the authors in [84] propose alternative methods to address specific challenges like unsupervised color correction, managing underwater noise, and employing a light attenuation model for image enhancement. The method described in [85] performs well in bright conditions but can produce halos and color distortions under low-light circumstances.

Numerous approaches have been introduced in the literature to improve the visibility of underwater images [83], [87], [88]. Image dehazing approaches are widely categorized into single and multiple image-based solutions. Multiple image-based methods employ images of similar scenes taken from various perceptions [89]. In [90], demonstrate effective color and

contrast enhancement using several images taken under poor weather conditions. However, this method is helpful for underwater image enhancement using simple additional information provided interactively by the user. When the reference image is unavailable, the images can be dehazed from single haze images. Based on the independent component analysis, Fattal et al. [91] proposed dehazing, an image enhancement technique. This conventional method is based on finding the lowest pixel intensity value among the three-color channels in a small region called a patch. The smallest pixel value should lie in the whole patch. The method [91] has evaluated the transmission map to enhance the underwater image using soft mapping filter which is quite complex. This problem is solved with the use of guided filter [92]. The guided filter is just a smoothing operator that preserves the edges, but it is not suitable for color correction of wavelength-dependent images.

The wavelength correction and image denoising approach provided the best results for underwater image enhancement [93]. Nevertheless, this method is based on pre-calculated extinction coefficient of medium. In a realistic scenario, it is different and depends on the structure of the water body, temperature, season, and other relevant factors. Consequently, this algorithm's potential for general use is constrained. The other two notable works in the haze removal field are dehazing based on contextual regularisation and boundary restriction [94] and dehazing based on color attenuation prior [68]. The underwater image enhancement techniques is categorized as shown in Fig. 2.1.

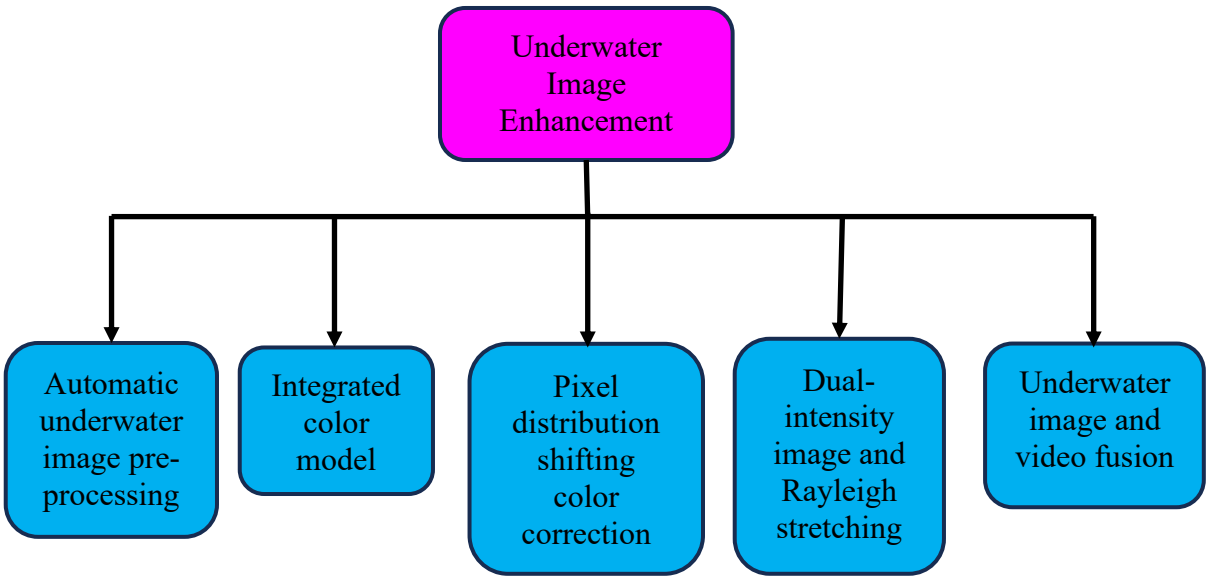

Fig. 2.1 Classification of underwater image enhancement methods.

Automatic underwater image pre-processing: A brand-new technique for enhancing turbid underwater images has been developed by Bazeille et al. [83] by utilizing frequency domain filtering and the *YCbCr* color space. A luminance (*Y*) component and two chrominance (*Cb*, *Cr*) components make the YCbCr model. This technique comprises various filter such as spectral analysis-based filter, homomorphic filter, and anisotropic filter. The program uses spectral analysis-based filtering to remove repeating wave patterns in the initial stage. A homomorphic filtering technique is used, followed by wavelet-based noise reduction, to address the problem of uneven lighting. The anisotropic filtering is applied on obtained image, which maintained the edge feature and smooths the processed image. Then intensity of the image is increased using contrast stretching. The improved image is then color normalized and returned to the *RGB* color space for consistent output. It's essential to remember that the resultant image may exhibit some color accuracy concerns due to conversion of image from *YCbCr* color space to *RGB* color space.

Integrated color model: Iqbal et al. [95] introduced an integrated color model (ICM) to improve underwater image quality dynamically. This model stretches the image's range using the complete *RGB* color space. Then, using the hue intensity saturation color space, contrast stretching is done to the generated image, focusing on the intensity and saturation parts. This method proved simple and effective, making it especially suitable for underwater pictures with slight haze. Concerning the Von Kries hypothesis, adjustments are performed to the red and green channels of the *RGB* color space to address color cast difficulties. The unsupervised color model (UCM) makes further contrast changes [48]. It's crucial to remember that this approach has contained significant noise. High picture noise is a problem because it affects pixels in the enhanced image and causes uneven enhancement, especially in darker areas with less information. The persistence of blue-green lighting in the processed images is another drawback. By applying stretching constraints to the murky underwater image's blue and red color channels, Ghani and Isa [96] could identify and fix the blue-green lighting problem.

Pixel distribution shifting color correction: A pixel distribution shifting for color correction (PDSCC) technique has been developed by Naim and Isa [97] to improve contrast in underwater images. The underlying image's pixel distribution is adjusted using a 3D rotational methodology. The PDSCC is an improved version of the traditional 3D rotational matrix. In essence, this methodology works as a color correction method where the authors alter the distribution of pixels in a color image. This correction is done to the white reference point to

make it achromatic. It's crucial to remember that this approach does not significantly enhance contrast. Another limitation of this method is its dependence on conventional color estimation, such as the grey world and white patch algorithms. Although these algorithms are not designed specifically for underwater circumstances, the authors have applied them to address some underwater images in their research publication.

Dual-intensity image and Rayleigh stretching: To solve the drawbacks of the ICM and UCM methods, Ghani and Isa [98] developed an algorithm based on the dark channel prior, image dehazing, and Rayleigh stretching technique. Their method uses a modified version of Von Krie's theory and consists of a two-step procedure: contrast correction and color correction. In this method [98], a global histogram stretching is implemented. This method performs histogram stretching based on the Rayleigh distribution for each segment after splitting the stretched histogram into two parts. An average rule is then applied to blend the two generated images. The hue saturation value (HSV) color model then processes the resulting image. This strategy aims to improve underwater image quality while overcoming the drawbacks of earlier techniques.

Underwater image and video fusion: Ancuti et al. [38] introduce a method for using fusion for underwater image and video enhancement. Through filtering, their method mixes many weighted images utilizing saliency, brightness, and chrominance. It should be noted that this work represented the first instance of improving underwater images using a fusion method based on the Laplacian pyramid. Adopting a white-balance method specifically designed for underwater images was also subjected to detailed evaluation by Ancuti. Although this method seems to improve the contrast of the produced images, the processing of the images results in non-uniform augmentation and an unnatural appearance, as seen in the results section. Another method, as shown in [82], addresses de-scattering and fusion, focusing on underwater image super-resolution. It's important to note that this approach [82] has limitations when handling inhomogeneous scatterers, making it less effective in such situations.

Besides the methods mentioned above, other linear image modification techniques have been employed, inspired by the approaches for enhancing outdoor scenes. To increase visibility, these techniques involve converting blurry, degraded images from the *RGB* color space into different color spaces, such as *HSV* or international commission on illumination-luminance chrominance . Additionally, methods based on statistical learning and the retinex, as detailed in [99] and [100], enhance the clarity of foggy images across various applications.

2.3 Underwater Image Restoration

Image restoration methods [71], [72] involve the use of multiple images [39], [68], and deep image restoration for scene estimation [103]. Kopf et al. [103] present an image restoration technique employing a deep learning model integrated with georeferenced digital terrain and urban 3D models. However, these approaches might be impractical for average users due to the additional resources, such as hardware they require, which are typically unavailable.

Restoration methods use statistical priors to generating depth maps. The statistical prior-based methods are used to handle ill-posed problem that means it might be trying to reconstruct an image from limited amount of data, without knowing the original image. The prior based method has certain limitations. One of the major limitation is that dehazing becomes challenging when an element within the image imitates the predominant whiteness of the image. Second one, choosing the appropriate number for the atmospheric light can be challenging and essential to the algorithm's success. The third factor that can considerably

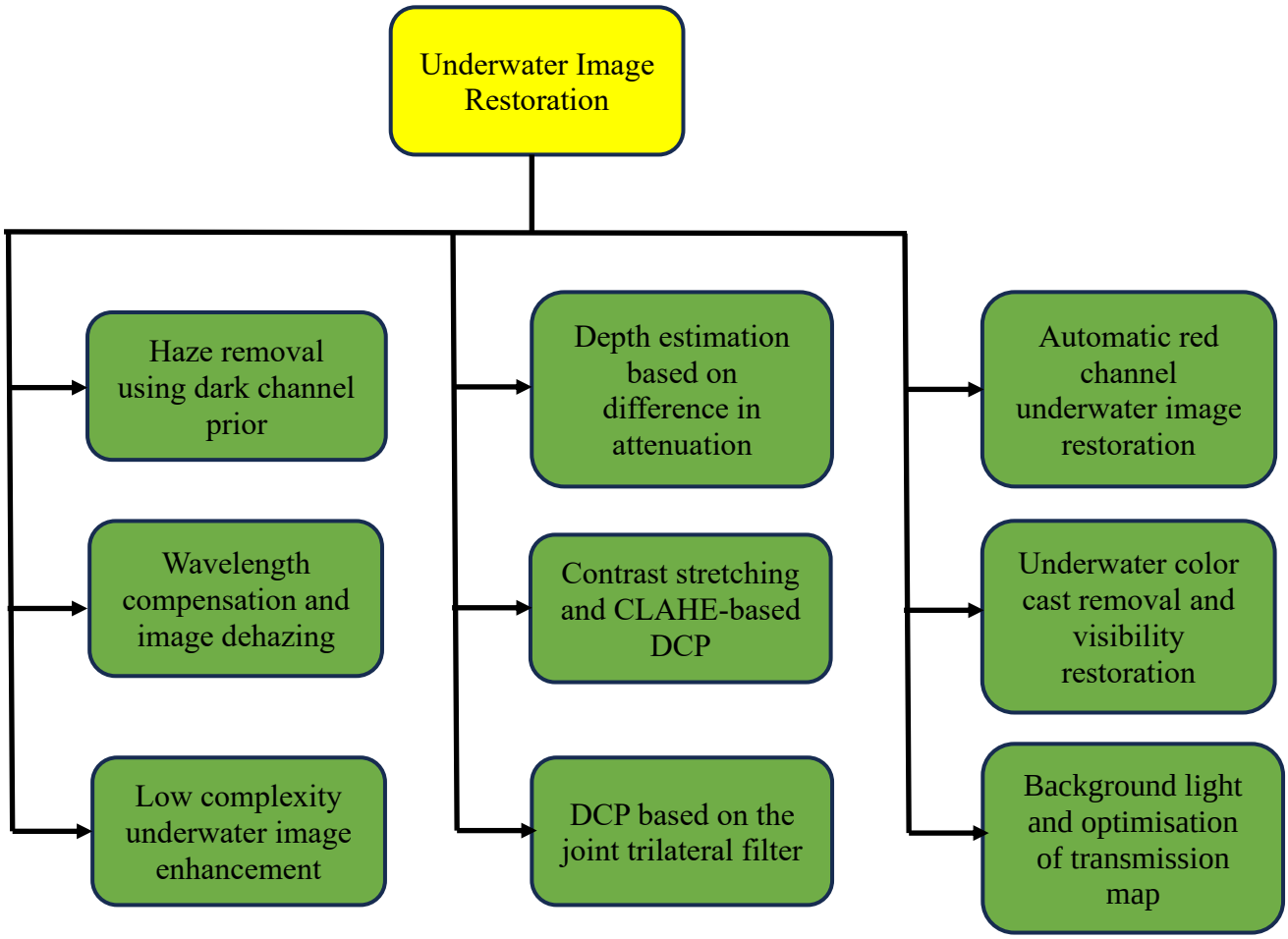

Fig. 2.2 Classification of underwater image restoration.

impact the quality of the dehazed result is the choice of filters for fine-tuning the gearbox map, which frequently involves edge-preserving smoothing filters. In the following discussion, we will examine some cutting-edge prior-based algorithms that aim to address the above issues. The underwater image restoration is divided into different categories as shown in Fig. 2.2.

Haze removal using dark channel prior: To solve haze removal in single input images, He et al. [59] developed the dark channel prior, to restored an underwater image. The statistical findings from haze-free, outdoor images serve as the foundation for the dark channel prior. It is based on a crucial realization such as, in outdoor, haze-free images, most local patches frequently contain some pixels with very low intensity in at least one-color channel. It is now possible to directly assess the haze thickness and recover a haze-free image after adding this dark channel into the haze imaging model. It's important to note that if the hazy imaging model itself is not physically sound, this method may have problems. Alternative strategies must be considered in most other cases where transmission for several color channels may not coordinate. According to [62], [104], [105], and [106], these method have been widely used by researchers in the field of underwater image restoration for a variety of tasks, such as estimating distance maps, addressing blurriness, and enabling adaptive restoration respectively.

Wavelength compensation and image dehazing: The DCP technique, developed initially to remove haze from outdoor images, Chiang and Chen have adapted it for underwater image enhancement, known as wavelength compensation and dehazing [93]. After realizing the differences between air image and underwater images, the authors have adjusted the parameter estimation for luminance in underwater circumstances. In their method, the foreground and background of the image are separated, by applying artificial light. They are used energy ratios and the object-to-camera distance for color loss compensation. Additionally, scattering parameters that are predetermined and unique to the water body are considered. It's crucial to recognize, nevertheless, that these predetermined values can change as a result of things like structural distinctions and temporal fluctuations. These variables limit the method's suitability for general underwater enhancement tasks due to the possibility of only partially removing haze.

Low complexity underwater image restoration: Utilising the dark channel prior, Yang et al. [107] presented a practical and computationally more straightforward method for restoring underwater images. To estimate the depth map of the image, they are used a median filter instead of the soft matting method. They also use a color correction process to enhance color

contrast in underwater images. Experimental findings show that how this introduced method might enhance underwater image quality while speeding up execution time. Furthermore, it is well-suited for real-time applications like surveillance and underwater navigation because it requires fewer processing resources. It's crucial to remember that, like others methods based on the dark channel prior, this method has difficulties in obtaining a precise transmission map. To overcome the limitation of accurate estimation of transmission maps, the [108] and [109] have been introduced based on image blur and light absorption in underwater environment. The above methods offer solutions to the challenges of accurately evaluating the transmission map, especially in underwater environments.

Depth estimation based on difference in attenuation: Bianco et al. [20] addressed the issue of varying attenuation between several color channels in underwater imaging. Light is absorbed and scattered by a medium when it passes through it from a subject to an observer. Scattering can drastically reduce the quality of an image when large suspended particles are present, like in fog or muddy in water. Bianco et al. [20] introduced an algorithm known as dehazing to counteract the effects of light scattering in underwater images. Their main contribution was the suggestion of a prior that uses the significant differences in attenuation across the three-color channels in an image. The difficulty in precisely calculating the depth of substantial solid objects with similar pattern to the hazy veil is a drawback of this approach. In addition to scattering, the authors also presented alternative method for attenuation compensation. It's crucial to remember that in situations of intense haze, this method may still cause image quality degradation.

Contrast stretching and CLAHE-based DCP: Lyu et al. [110] introduced effective method for restoring underwater images and videos stands out for its cheap computational requirements and high-quality outcomes. In this method the authors used color correction to balance the average of each color channel and contrast stretching to enhance visual clarity. An unbalanced color palette is a major problem with underwater images, which frequently produce dominating blue or green tones. However, this color correction step may unintentionally reduce this distinct color without considering the absorption phenomena to underwater environments. The authors introduced a method in which two inputs are used: one representing the contrast-stretched version of the color-corrected underwater image or frame and the other representing the clip-limited adaptive histogram equalization (CLAHE) [111] version. The author also includes a

method to handle cases where underwater images have uneven illumination. The efficiency of their strategy as a whole is increased by this inclusion.

DCP based on the joint trilateral filter: Serikawa et al. [63] introduced a new method based on trigonometric filter to improve and restore underwater images, addressing the challenges of image dehazing, scattering and color distortion. Distortion in underwater imaging is mainly caused by scattering, hazing and color change. Large suspended particles, like marine snow in murky water, cause scattering, and various degrees of light attenuation at different wavelengths cause color distortion, giving underwater surroundings their predominately bluish tone. This technique [63] reduces noise, improves visibility in dark areas, enhances global contrast, and significantly sharpens fine details and edges. It's significant to note that the authors did not address the uneven illumination caused by artificial light, which might be problematic in aquatic environments. They are also highlight the importance of data fusion in this technique [63] for achieving the best results.

Automatic red channel underwater image restoration: Underwater and atmospheric light propagation is similar, but the underwater imaging is more difficult because of increased attenuation caused by scattering and absorption factors [112], [113]. The dark channel prior, which was initially developed for atmospheric haze removal. The extension of dark channel prior method by Galdran et al. [64] for underwater image restoration. Since the red channel of the *RGB* color space is often the most attenuated and contributes the most to the generation of the dark channel image in DCP. The above problem resolve in automatic red channel underwater image restoration method introduced by Galdran. However, the drawback of this algorithm is its initial assumption that the red color channel is predominantly affected by attenuation. However, studies of various underwater images have shown that the blue color wavelength can sometimes experience the most significant attenuation. This mismatch can be viewed as a major flaw in the methodology.

Underwater color cast removal and visibility restoration: Li et al. [114] introduced to determine the global atmospheric light using optical characteristics based on minimizing information loss to restore underwater images. There are several crucial steps of this method [114]. First, an optimization theory is applied to degraded underwater images to reduce color cast. Then, the authors introduced a visibility restoration technique that minimizes information loss in underwater images by considering the relationships between transmission maps across the three-color channels. This technique seeks to increase visibility, boost contrast, and keep

the final image's natural appearance. It's vital to note that while this method has produced encouraging results, it has difficulties being applied to images that lack the background of an underwater environments. The method is also less flexible in practice because it significantly depends on the dark channel prior and predetermined residual energy ratios, which might change depending on the application.

Background light and optimization of transmission map: Song et al. [115] introduced restoration techniques for underwater images using background light estimation and optimization of transmission map. A new dark channel that matches the distribution traits seen in high-definition underwater images creates the red channel's transmission map (TM). This is further improved by including depth map adjustment and improving the red sea model. In underwater circumstances, the transmission maps for the green and blue channels are developed by accounting for the different attenuation rates between the red and combined green-blue channels. Peng et al. [116] introduced a method for the generalization of the dark channel prior to single-image restoration based on adaptive color correction. Wang et al. [117] describe an adaptive attenuation-curve prior that can accurately depict the properties of light attenuation to different underwater environments. Wang divides the transmission estimation into the attenuation factor and the relative transmission to increase the accuracy of the estimation. To increase accuracy, these two factors are calculated independently. In order to prevent oversaturation and lower noise, the authors set the saturation limitations and changed the gearbox. Liang et al. [118] introduced a generalized underwater dark channel prior (GUDCP) technique to estimate the transmission which is based on the fundamental idea that all channels may be attenuated at the most significant rate. Zhang et al. [119] provide a locally adaptable color correction technique based on the least color loss concept and the maximum attenuation map-guided fusion. A new technique based on the color-line model is introduced to address the scattering and absorption issues of light at different wavelengths [120]. Berman et al. [121] introduced a technique that uses a single image as input to recover the distance maps and item colors in underwater and ambient light under lit situations. Peng et al. [122] employ image blurriness and light absorption to estimate depth instead of only using image blurriness alone. While blurriness is a key indicator of depth, it is not the only underwater cue. When the red color is significant, the differential absorption of red light can be used to advantage of the [122] method.

Image enhancement and restoration using deep-learning-based method: Various researchers have recently developed deep-learning-based underwater image enhancement and

restoration methods. Li et al. [123] provide an effective multi-term objective function to correct color cast and improve underwater image's visual quality. Guo et al. [124] introduce a multiscale dense generative adversarial network to enhance the underwater image. Yu et al. [125] presented a methodology for improving underwater images, employing a conditional generative adversarial network (GAN). The model underwent training on a simulated underwater dataset, which was subsequently used to produce an improved image's visual quality directly. In [126], Fabbri et al. employed generative adversarial networks to improve the quality of underwater images. In [127], the authors introduced an unsupervised GAN for underwater image enhancement. This GAN synthesizes paired training data by utilizing air images to correct underwater color cast, thereby enhancing the overall quality of the underwater image. In a recent development, Mei et al. [128] introduced an unsupervised adaptation network to achieve concurrent learning to enhance underwater images. Wang et al. developed a supervised GAN to generate underwater images based on an improved underwater imaging model and then trained a U-net to restore the underwater images [129]. By leveraging ample training data, these learning-based methods directly produce an enhanced image from a degraded underwater image, thereby effectively enhancing the quality of underwater images [130].

The application of convolutional neural networks (CNN) is dominant in various image processing domains, including but not limited to noise reduction [131], enhancement of low-light images [132], [133], and enhancing underwater images [134]–[138]. Zhang et al. [139] incorporated a physical imaging model into a convolutional neural network, creating a transfer learning-based framework to enhance underwater images and achieve superior-quality results. Li et al. [140] combined a visual perception correction model with an updated imaging network model to efficiently convert deteriorated underwater images into improved contrast images. Furthermore, a multi-color space encoder was developed to tackle two challenges: degraded contrast and color distortion [140]. A low-light image enhancement based on CNN was presented to improve illumination and remove darkness, resulting in a 13.84% increase in detection precision for live crabs [141].

To overcome the challenge of lacking ground truth in CNN-based approaches, authors introduce a database for training CNNs and assessing image quality [142], [143], and [144]. Additionally, unsupervised and weakly-supervised learning techniques were developed to tackle the challenge of limited reference images. Yan et al. [145] presented an unsupervised

framework guided by data and physical models to enhance underwater images, leveraging unpaired underwater and outdoor image datasets. A weakly-supervised method has been introduced to train networks in which strictly paired training images are not required [146]. An underwater image and video enhancement technique based on semi-supervised learning has been introduced. Li et al. [147] introduced a cascaded visual attention network technique for single-image low-resolution to enhance the underwater image.

Deep learning frameworks heavily rely on training data, which significantly influences the performance of convolutional neural networks. Yet, obtaining reference images in natural underwater environments poses challenges. Synthetic training data fails to accurately represent the complexities of accurate underwater image distributions, leading to unnatural outcomes in various scenarios.

2.4 Research Gap

The earlier state-of-the-art reveals that there are several shortcomings in the present works, and these are as follows:

- Underwater single image dehazing, underwater image enhancement by dehazing with minimum information loss, histogram distribution prior, and underwater image dehazing using joint trilateral filter method failed to dehaze the attenuated and scattered images.
- In the dark channel method, the computation of depth maps possesses many problems, such as:
    - Scene objects are inherently similar to the color of underwater light.
    - The effect of shadow on an object is due to the fact that organic particles in the water cannot be detected.
- An improved air-light estimation scheme for single haze images using color constancy prior, underwater color constancy enhancement of automatic live fish recognition, Single image haze removal using dark channel prior, and enhancement of underwater images with a statistical model of background light and optimization of transmission map-based method failed to improve colorcast for sand storm images.
- Multiscale retinex color restoration and single underwater image restoration by decomposing attenuation curves, the color-based method did not significantly improve the overall contrast.

- Color balance and fusion for underwater image enhancement, the hybrid framework for underwater image enhancement, a hue preserving-based approach for underwater color image enhancement, and underwater image processing using a hybrid techniques-based method demand underwater variability information. Some methods must adjust the parameters from time to time based on experimental conditions.

- Computation of depth maps based on the dark channel prior without adapting it to the underwater scenario poses many problems.

- The researchers have not fully explored image segmentation based on the non-uniform distribution of haze.

With the growing importance of underwater imaging applications, driven by advancements in technology and underwater cameras, there is a critical need to restore underwater images before using them in decision-making algorithms for computer vision tasks. We need to advance underwater exploration, and science our country is surrounded by water, so we decided to take on this challenging project. In this study, we aim to tackle underwater imaging challenges such as limited visibility, uneven lighting, color reduction, and reduced contrast by developing new image enhancement and restoration techniques to improve the limitations of existing state-of-the-art methods.

2.5 Research Objectives

Underwater optical imaging has many scientific uses, and one of the main goals of the technology is to provide professionals with the most aesthetically pleasing and valuable underwater image representations. The main obstacle in processing underwater images is the lack of ground truth and reference images. We focus on algorithm-based haze removal for single underwater images due to we do not have the flexibility to capture multiple images of the same scene, use gated range lighting, or access polarization cameras for imaging.

This work aims to build hybrid algorithms that combine multimodal fusion and statistical prior-based techniques to restore visibility to underwater images. The following objectives are the focus of the research:

- ✓ To develop an algorithm for underwater image enhancement to overcome the problem of non-uniform illumination and contrast enhancement by addressing the issue of attenuation and scattering of light.

- ✓ To address the problem of transmission map on account of wavelength dependency of color transmission in the underwater scenario.
- ✓ To implement the color restoration technique to deal with the problem of the underwater unwanted color cast.
- ✓ To design an automated method for quantifying the scene depth to restore the dehaze image.

2.6 Underwater Image and Video Dataset

The datasets used in this thesis to implement proposed methods and existing state-of-the-art methods. There is no complete dataset for underwater imaging because collecting underwater images is very difficult. Fig. 2.3 shows examples of a few images taken from underwater image datasets such as underwater image enhancement benchmark, real-world underwater image enhancement, underwater-45, and real-world underwater video of artifacts.

2.6.1 Underwater Image Enhancement Benchmark Dataset

The UIEB dataset, as referenced in [143], comprises 950 real-world underwater images, with 890 accompanied by reference images. A subset of 60 images was kept aside for testing purposes. This dataset is a benchmark for qualitative and quantitative assessments of underwater image enhancement algorithms. It offers diverse resolutions and encompasses various scene and main object categories. These underwater images are likely taken under natural light, artificial light, or a mixture of natural light and artificial light. Moreover, the corresponding reference images for 890 images are provided according to laborious, time-consuming, and well-designed pairwise comparisons. UIEB provides a platform to evaluate, at least to some extent, the performance of different underwater image enhancement algorithms.

2.6.2 Real-World Underwater Image Enhancement Dataset

The real-world underwater image enhancement [144] dataset is a comprehensive collection featuring 4000 underwater images captured from various perspectives. To obtain a Real-world underwater image enhancement dataset, setup a multi-view imaging system under seawater, and construct a large-scale underwater benchmark under natural light, the Real-world Underwater Image Enhancement (RUIE) data set, with over 4, 000 images. This dataset is crucial for evaluating underwater image enhancement and restoration algorithms. It is organized into three distinct subsets: the underwater image quality set (UIQS), the underwater color cast set (UCCS), and the underwater higher-level task-driven set (UHTS). The

underwater image quality set (UIQS) [144] dataset is intended to evaluate UIE algorithms that attempt to improve picture visibility. The UIQS [144] dataset is further categorized into five [A, B, C, D, E] based on the underwater color image quality evaluation (UCIQE) metric score. Each subgroup contains 726 images of 400 × 300 pixels; hence, 3630 images are in the UIQS [144] dataset.

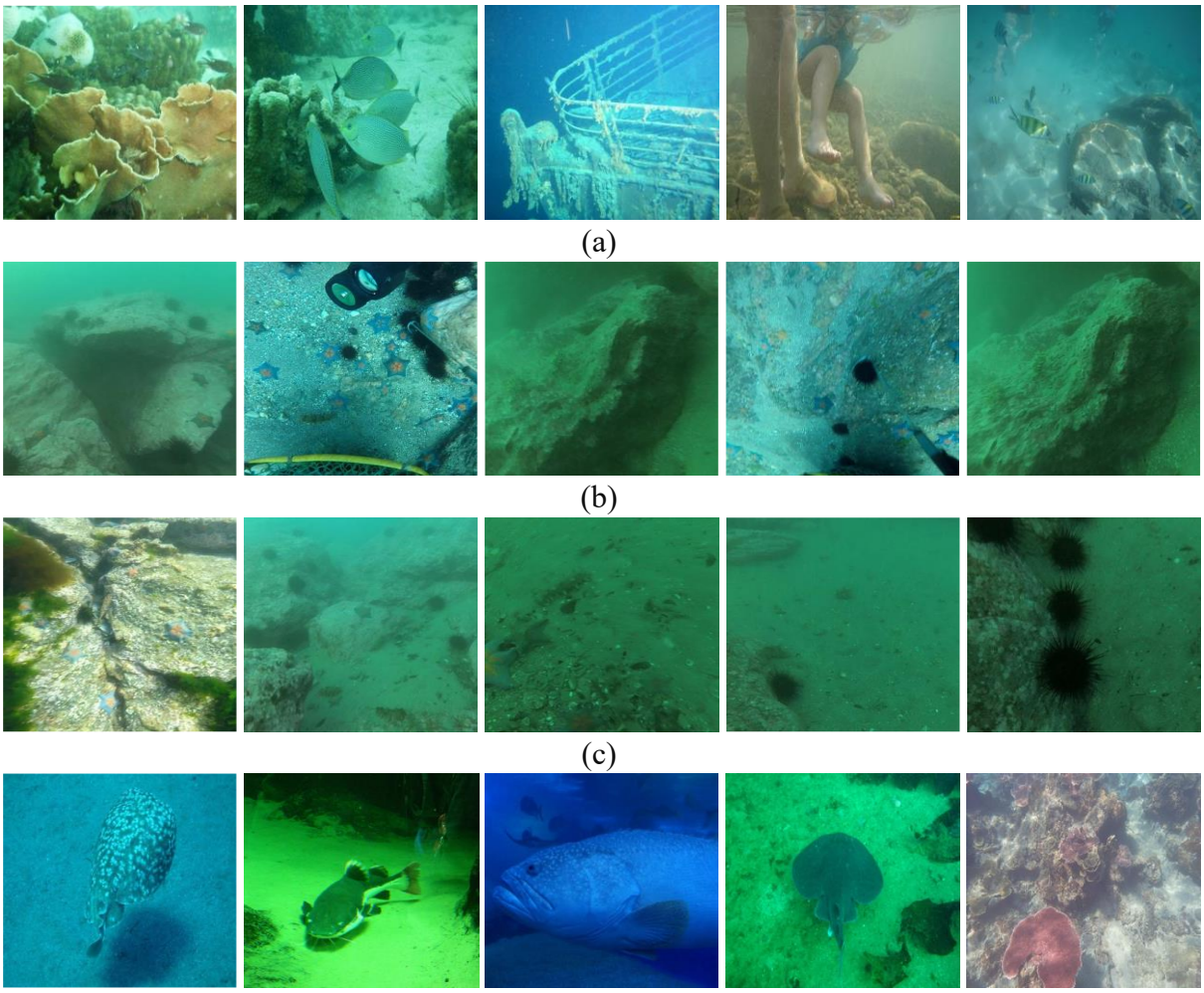

Fig. 2.3 (a) First-row image represents the UIEB dataset, (b) Second-row image is taken from the UCCS dataset, (c) Third-row image is taken from the UIQS dataset, and (d) Fourth-row image is taken from U45 dataset.

This is also part of the real-world underwater image enhancement dataset. The UCCS [144] dataset has three subsets: UCCS Blue, UCCS Blue-Green, and UCCS Green. Each subgroup contains 100 images of 400 × 300 pixels, so the UCCS dataset includes 300 images. These subsets play vital roles in addressing color cast issues, improving visual appeal, and facilitating higher-level computer vision tasks such as detection and classification.

2.6.3 U45 Dataset

In order to evaluate quantitatively different algorithms, we set up an effective and public underwater test dataset (U45) including the color casts, low contrast, and hazelike effects of underwater degradation. The enhanced images on the U45 dataset and videos demonstrate the superiority of the proposed method in both qualitative and quantitative evaluations. The U45 Dataset [148] contains 45 degraded underwater images, of which 15 green, blue, and haze each, respectively. The publicly available dataset U45 includes color casts, low contrast, and haze-like effects of underwater image degradation.

2.6.4 Dataset of Real-world Underwater Video of Artifacts

The proposed methods have been evaluated on the dataset of real-world underwater videos of artifacts (DRUVA) [149] video dataset. The DRUVA comprises 20 (A1.mp4-A20.mp4) videos of different artifacts in shallow waters. The artifacts primarily consist of rocks varying in shape from circular to oblong, with dimensions ranging from 0.5 to 1.5 meters. The duration of the videos is in the range of 28 to 77 seconds, not in a sequence (A1.mp4-A20.mp4). The video was recorded in natural light 3-6 meters below the sea surface using a GoPro Hero 10 black camera at 30 frames per second (fps), 1920×1080 resolution. The camera settings included a variable ISO (ISO refers to the camera sensor's sensitivity to light) range of 100-1600 and auto exposure.

Chapter 3

Underwater Image Enhancement and Restoration Based on Multiscale Decomposition, Brightness Adjustment, and Retinex Algorithm

This chapter presents an effective underwater image enhancement and restoration method using multi-scale decomposition, brightness adjustment, gamma correction, and retinex algorithm. The proposed framework decomposes the degraded underwater image into illumination and reflectance. Further, gamma correction is applied to one of the multi-scale decomposition layers to obtain an enhanced image. The effectiveness of the proposed method is explained and validated through experiments on standard datasets and state-of-the-art comparison of obtained results.

3.1 Underwater Image Enhancement Based on Multiscale Decomposition

3.1.1 Introduction

Underwater research has increased exponentially because of the shortage of land resources, such as manganese, nickel, copper, and cobalt. Acquiring clean underwater images and videos plays a crucial role in finding resources in the ocean. Underwater image processing has also been an essential source of interest in different branches of technology and scientific research, such as detecting underwater objects. Pandey et al. [150] enhancing object detection in aerial images, Hooda et al. [151] estimating the surface roughness for super hydrophobic coating by image processing and machine learning, marine biology research, an inspection of aquatic infrastructure and cable, control of underwater vehicles, and archelogy [152]. The leading cause of quality degradation underwater is the absorption of light energy during propagation. The light exponentially decays with the distance and depth. The red channel of the RGB image is absorbed faster than the green and blue channels since light propagates underwater is wavelength-dependent; that's why images appear bluish and green [78]. Underwater Images and videos are not good because of weak contrast, color distortion, and low illumination. The absorption is caused by reducing light energy and scattering due to the deviation of light from

its original path. Fig. 3.1 shows the optical image formation model (IFM) [153] for the underwater image.

The light received by the camera has three components: a scene irradiance, which is also called a direct component that comes directly from an object; a forward scattering component that deviates its path, i.e., it reaches the camera in another direction; and a back-scattering component reflected by the suspended particle present in the water, the light ray come to the camera before reaches to the object. Finally, the underwater image captured by the camera is a linear combination of these three components. Forward-scattering components are responsible for the blurring of the image, and back-scattering components degrade the details of the picture. Due to these two components, underwater images have lost their visual quality and detailed information. To solve this problem, the researcher gives many techniques like underwater image enhancement, restoration, saliency detection, noise reduction, color constancy and correction, image defogging, and underwater image recovery.

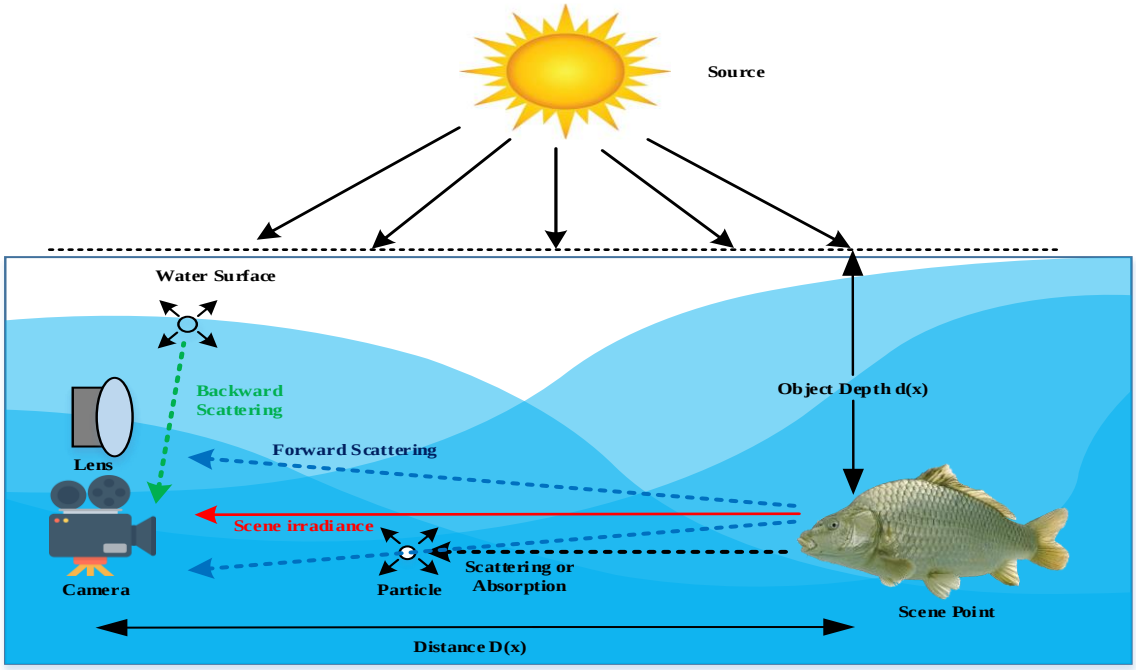

Fig. 3.1 Underwater optical image formation model (IFM) with forward and backward scattering.

There are three primary directions of underwater image enhancement:

1) Based on modifying image pixel values: The modifying image pixel value is also called the IFM-free based model, in which contrast and color of the degraded underwater image are mainly based on pixel intensity re-distribution, without considering the particular underwater

imaging principles. The underwater image enhancement based on modifying image pixels is further categorized into single and multiple color models. Some work has already been done, such as attenuation map guided color correction and detail preserved dehazing [154], Underwater target detection with an attention mechanism and improved scale [155], etc.
2) Based on underwater imaging models: The IFM-based underwater image enhancement method, such as dark channel prior (DCP) [59]; underwater dark channel prior [77]; maximum intensity prior [62]; red channel prior [64]; underwater light attenuation prior [156]; and other.
3) Based on deep learning methods: Finally, texture synthesis guided deep hashing for texture image retrieval [157]; deep learning-based underwater image enhancement methods are Hu et al. [158] use the two-branch deep neural network for underwater image enhancement in 2021; In 2022, Xu et al. [159] use GAN neural network, etc. For example, Cao et al. [160] used a global CNN and refined network to estimate the background light and predict the scene depth map. Kumar et al. [161] use a machine-learning approach for brain tumor detection and segmentation.

The proposed method is based on the retinex algorithm in which the input image is split into the illumination and reflectance parts. Further reflectance is decomposed into the base layer, first detail layer, and second detail layer based on parameters. The reflectance part preserves the edge, whereas the illumination part preserve brightness. Gamma correction is carried out on the base layer, and contrast enhancement in the gradient domain on the first and second layers corresponds. Finally, we multiply these layers with a brightness adjustment component to get the enhanced image. The output image has good visual quality compared to the existing state-of-the-art methods. Also, the parameters of the proposed method for enhancing the image are better than those used in the existing method.

3.1.2 Image Formation Optical Model

McGlamery introduced the optical image formation model; according to this model, the total radiation ($O_c(i,j)$) of the system has three components. These are the following components: (a) Direct component, which is reflected by an object without scattering and is represented by $D_c(i,j)$. (b) The backward-scatter component ($B_c(i,j)$), it is an ambient light scattered by suspended particles. (c) The forward-scatter component is represented by $F_c(i,j)$. This component deviates from its line-of-sight propagation and reaches the camera. The total optical radiation ($O_c(i,j)$) is a linear combination of the above three components.

Mathematically, represented by

$$O_c(i,j) = D_c(i,j) + F_c(i,j) + B_c(i,j) \tag{3.1}$$

where (i,j) is the coordinate of the pixel. We assume the distance between the object and the camera is very close so we can neglect the forward-scattering component [162]. The modified optical radiation

$$\left.\begin{aligned} O_c(i,j) &= D_c(i,j) + B_c(i,j) \\ D_c(i,j) &= Q_c(i,j)\tau_c(i,j) \\ B_c(i,j) &= B_c\big(1 - \tau_c(i,j)\big) \end{aligned}\right\} \tag{3.2}$$

where $Q_c(i,j)$ is scene radiance, $\tau_c(i,j)$ as a transmission whose value lies between zero and one, its value decreases exponentially. B_c denotes the background light. Where c belongs to red, green, and blue channels. The image intensity captured by the camera is represented by

$$I_c(i,j) = Q_c(i,j)\tau_c(i,j) + B_c\big(1 - \tau_c(i,j)\big) \quad c \in \{R,G,B\} \tag{3.3}$$

Based on the Beer-Lambert law, the transmission is commonly written as an exponentially decaying function.

$$\tau_c(i,j) = e^{-\delta_c D(i,j)} \tag{3.4}$$

where δ_c the attenuation coefficient for channel c and $D(i,j)$ is the distance between the imagined device and the scene point.

The proposed method is a novel retinex-based algorithm using gamma correction to enhance underwater images. Firstly, an input image is decomposed into illumination and reflection. Subsequently, brightness adjustment is applied to the illumination part. It shows the display quality of the image. A weighted list square based filter [163] carries on the reflectance part. The reflectance output is the base layer, first detail layer, and second detail layer. Then, gamma correction is applied to the base layer, contrast enhancement is applied to both detail layers, and it is combined with all three layers. Finally, multiply with brightness adjustment to get an enhanced image.

3.1.3 Proposed Method

The author proposed a novel method for single-image real-world underwater image enhancement. In this section, we can also restore the brightness, color, and contrast. In this proposed method, we have split the input underwater image into the illumination and reflectance components. Further reflectance decomposed into multi-scale levels in that way base layer, first detail layer, and second detail layer. The gamma correction is carried out on the base layer, and contrast enhancement in the gradient domain is applied on both detail layers.

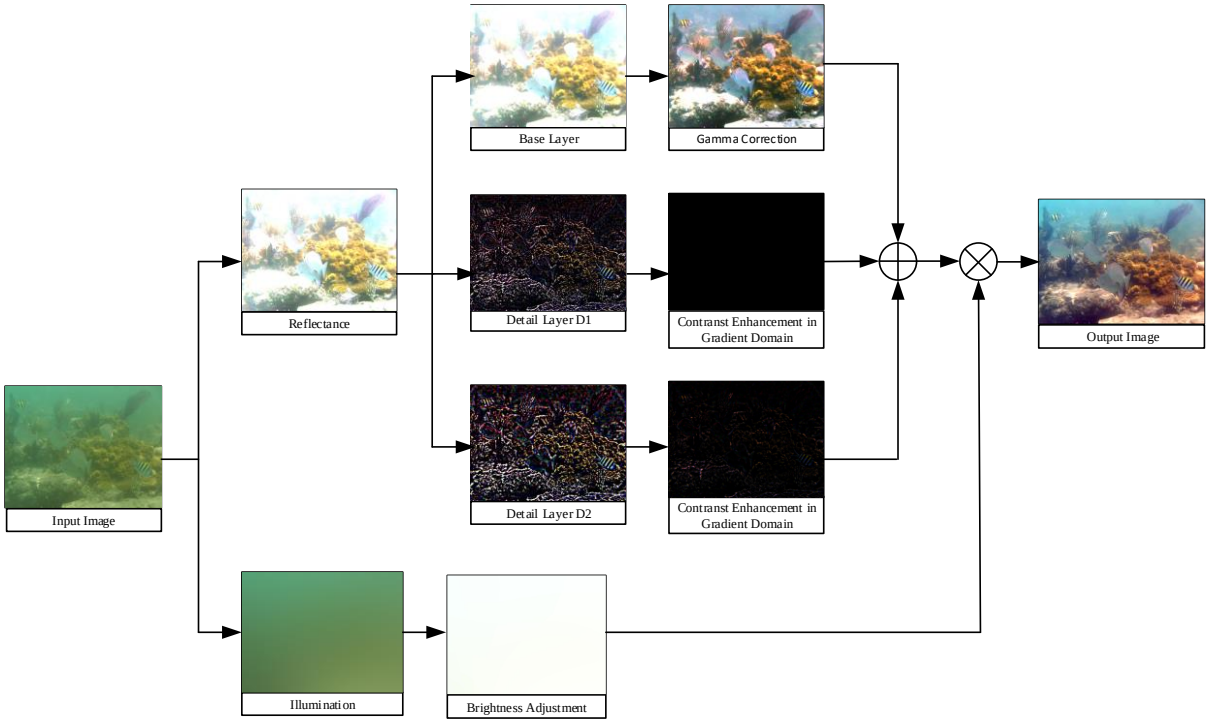

Fig. 3.2 The proposed method based on multi-scale decomposition and brightness adjustment for underwater image enhancement.

These processes are done to restore weak illumination, color cast, and noise. The flow diagram of the proposed method is shown in Fig. 3.2.

3.1.3.1 Evaluation of the Illumination and the Reflectance

Here, retinex model is used to obtain illumination and reflection of the underwater image. According to this model, the underwater capture image has two components, i.e., illumination and reflectance. Mathematically, it is represented as:

$$I_c(i,j) = L_c(i,j) \cdot \mathcal{R}_c(i,j), \qquad c \in \{R, G, B\} \tag{3.5}$$

where $I_c(i,j)$ denote capture image, $L_c(i,j)$ represents illumination, and $\mathcal{R}_c(i,j)$ denote reflectance. Dot '·' represents the multiplication sign. c belongs to the image color space, i.e., red, green, and blue.

The illumination is separated from the input underwater image to improve brightness and contrast. The illumination part is piece-wise smooth and contains illumination variance according to retinex theory. The reflectance preserved color information and details of the underwater input image, while the global incident light of the scenario was captured in the illumination. Further brightness adjustment, gamma correction, and contrast enhancement in

gradient domain strategies are applied to the different image layers to compensate for color, contrast, and illumination separately.

Now we take logarithmic on both sides of Eqn (3.5). The logarithmic function converts multiplication into addition to reduce the algorithm's complexity and make it easy to sense brightness. After taking logarithmic, the Eqn (3.5) is represented as:

$$i\big((i,j)\big) = I(i,j) + r(i,j) \tag{3.6}$$

where, $i(i,j) = \log\left(I_c(i,j)\right)$, $I(i,j) = \log\left(L_c(i,j)\right)$, $r(i,j) = \log\left(\mathcal{R}_c(i,j)\right)$.

From Eqn (3.6), single-scale retinex is defined as:

$$r(i,j) = i(i,j) - I(i,j) \tag{3.7}$$

$$\mathcal{R}_c(i,j) = 10^{r(i,j)} \tag{3.8}$$

$$I(i,j) = \log\big(G(i,j) * I_c(i,j)\big) \tag{3.9}$$

where, $I(i,j)$ represents logarithmic illumination, which is the convolution of the Gaussian function and the underwater input image, $G(i,j)$ is a Gaussian function, $I_c(i,j)$ is the underwater input image, and $\mathcal{R}_c(i,j)$ represents retinex. '$*$' denotes the convolution operator. The Gaussian function is mathematically defined as:

$$G(i,j:\sigma) = \alpha e^{-\frac{i^2+j^2}{2\sigma_n}} \tag{3.10}$$

where α represents a constant, (i,j) denotes the coordinate of the pixel and σ_n is the variance which maintains the shape of the Gaussian function. Eqn (3.10) is a probability density function so according to probability density function properties, the integration of the Gaussian function over the entire range becomes unity. Mathematically,

$$\int_{-\infty}^{+\infty} \int_{-\infty}^{+\infty} G(i,j)\ di\ dj = 1 \tag{3.11}$$

The reflectance and illumination of raw images are shown in Fig. 3.3.

The variational methods that evaluate illumination and reflectance transfer into the logarithmic domain simplify the complex problem. Hence, the dissimilarity of gradient magnitude is typically suppressed in the logarithmic environment, which leads to over-smooth reflectance with edge and texture detail being lost. To overcome the above problem, the weighted variational model proposed by [164] is used to estimate the illumination and reflectance simultaneously. The objective function is defined according to the weighted variational model:

$$F(r,I) = \arg\min_{r,I} \|r + I - i\|_2^2 + \mu_1 \|e^r \cdot \nabla r\|_1 + \mu_2 \left\|e^I \cdot \nabla I\right\|_2^2 \tag{3.12}$$

$$\text{subject to} \quad r \le 0 \text{ and } i \le I$$

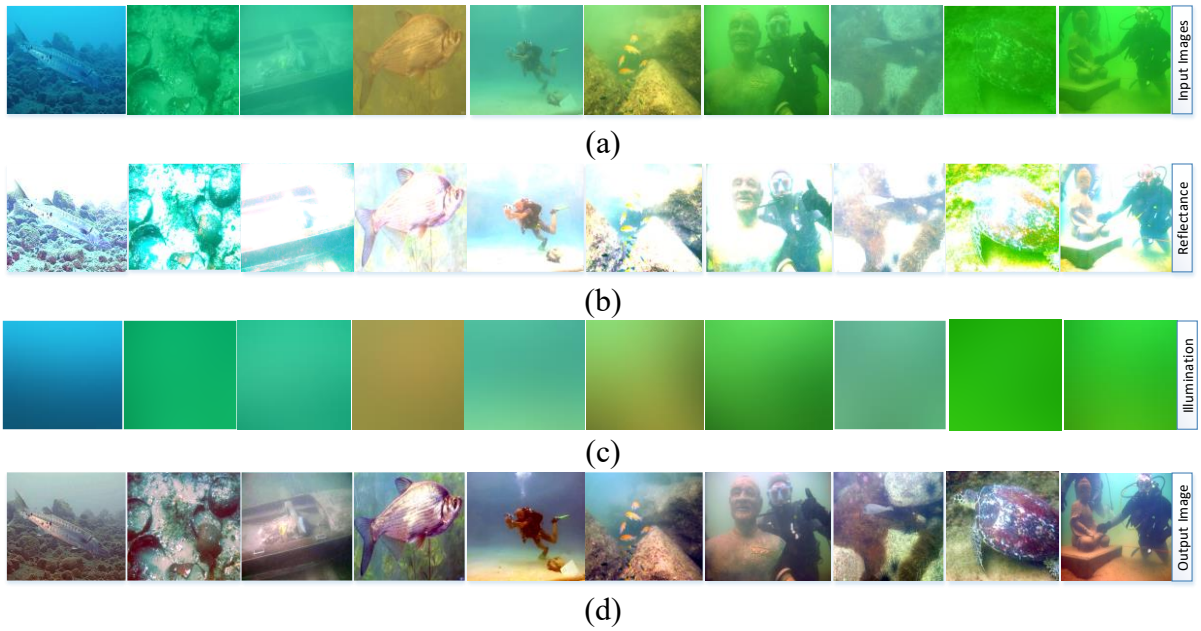

Fig. 3.3 Intermediate process of underwater image enhancement (a) Input image (UIEB dataset), (b) Reflectance of the input image, (c) Illumination of the input image, (d) Output image.

where, $i = \log(I_c(i,j))$, $l = \log(L_c(i,j))$, $r = \log(\mathcal{R}_c(i,j))$. The μ_1 and μ_2 are two positive parameters. ∇ as the mathematical operator gradient and $\|\cdot\|_{\mathrm{P}}$ denote the p-norm operator.

The first term $\|r + l - i\|_2^2$ is used to maintain reliability and minimize the distance between $(r + l)$ and i. This term $\|e^r \cdot \nabla r\|_1$ carry out piece-wise constant on r, and finally, the term $\|e^r \cdot \nabla r\|_2^2$ enforces special smoothness on l. To eradicate the impact of the weights e^r and e^l for the simplification of objective function $F(r,l)$. Now the function can be rewritten as:

$$F(r^k, l^k) = \arg\min_{r^k, l^k} \|r + l - i\|_2^2 + \mu_1 \|R^{k-1} \cdot \nabla r^k\|_1 + \mu_2 \|L^{k-1} \cdot \nabla l^k\|_2^2 \qquad (3.13)$$

$$\text{subject to } r^k \leq 0 \text{ and } i \leq l$$

where k is the k^{th} iteration. To solve the above Eqn (3.13), an alternating direction method of multipliers [165] is used.

3.1.3.2 Multiscale Decomposition of the Reflectance (ℛ)

The derived parameter estimated by the conventional optical image formation-based method relies on precision. It may still present undesired color artifacts after accurately solving the visual image formation model. Even though we have considered the physical characteristics of water, the explicit possibilities and prior are still limited in miscellaneous and composite underwater scenes. However, this article aims to develop a new background for the image

enhancement of composite real-world underwater images. We have taken advantage of both model-based and enhancement-based categories to build a multi-scale gradient-domain contrast enrichment approach stretched into underwater image restoration. In the proposed method, transmission has been calculated by the [166] rather than background light using improved DCP and solving the image formation optical model to indicate the superiority of the observed image.

Further guidance is provided on how to manage enhancement coefficients, which are used in this work. The conventional method has the complexity of restoring the underwater appearance; to overcome this complexity, the author has proposed a plan to fix the underwater image properly. The first step is to decompose the reflectance into a multi-scale layer. To complete this process, we have used a weighted least squares based filter [163], which splits the reflectance into multiple layers. For different values of λ, we obtain corresponding layers. Mathematically, it is represented as:

$$V = F_{\lambda}(\mathcal{R}) = (I + \lambda L_{\mathcal{R}})^{-1}\mathcal{R} \tag{3.14}$$

where V is defined as the smooth version of the $\mathcal{R}$. Here, I is the matrix, which has a unity determinant, $L_{\mathcal{R}} = D_i^T A_i D_i + D_j^T A_j D_j$, where (i, j) represents the spatial coordinate of a pixel, D_i and D_j are discrete differentiation operators, A_i and A_j represent smoothness weights. As we increased the value of λ, we obtained a different, smoother image sequence. V^1, V^2, V^3 ...., V^{k-1}.

In the second step, the progressive image is subtracted from the previous image, and the output after the subtraction is called the multi-scale layers' representation. The V^{k-1} is called the coarsest image, and it is equivalent to base layer $\mathcal{B}$ when the value of k taken as one. This base layer consists of color variation of the reflectance; on the other hand, the detail layer d_i mathematically computed as:

$$d_{\mathrm{i}} = V^{\mathrm{i}-1} - V^{\mathrm{i}}, \qquad where\ \mathrm{i} = 1, \cdots\cdots\cdots k-1 and\ V^0 = \mathcal{R} \tag{3.15}$$

Here, the value of K is set to three. If we increase the value of parameter λ much higher, it will produce a smoother coarsest image. Now, by subtracting this roughest image from reflectance, in this case, the maximum number of the minor textures, like noise and marine snow, can be captured in the output detail layer d_1. Hence, it will lead to noise amplification, so we need to manage the value of parameter λ to compensate for noise amplification. By default, in the weighted least squares base filter, the parameter λ is set to unity. Here, the value of lambda (λ) is set to below unity.

To obtain the color, brightness, and contrast information of different layers corresponding to different lambda values, restoring blurred images and low-light and color distortion problems is applied simultaneously. The flow diagram of the proposed method is shown in Fig. 3.2, in which input underwater images are split into illumination and reflectance. Further reflectance is divided into multi-scale layers, i.e., base and two detail layers. Gamma correction is carried out on the base $\mathcal{B}$ layer of reflectance, and contrast enhancement in the gradient domain is applied on both detail layers d_i. Contrast enhancement is used in the gradient domain to remove artifacts. The second part of the splitter input image, i.e., illumination, applies brightness adjustment.

3.1.3.3 Brightness Adjustment

In the illumination $L_c(i,j)$ part, the variation of light happened. The brightness adjustment is used for low-light problems. In this layer, enhancement of illumination is carried out. We have used the sigmoid function to improve the brightness. The magnitude of the sigmoid function lies between 0 to 1. Mathematically, the brightness adjustment is represented as:

$$£'(i,j) = Sigmoid\big(\beta L_c(i,j)\big) \tag{3.16}$$

where $Sigmoid(\cdot)$ is the sigmoid function and β is the controlling parameter. Here, β is set to:

$$\beta = 10 + \frac{1-£_{mean}}{£_{mean}} \tag{3.17}$$

where $£_{mean}$ denotes the mean of the illumination part. If the value of $£_{mean}$ is low, then the controlling parameter β will increase, enhancing the illumination part. The brightness adjustment example is shown in Fig. 3.4.

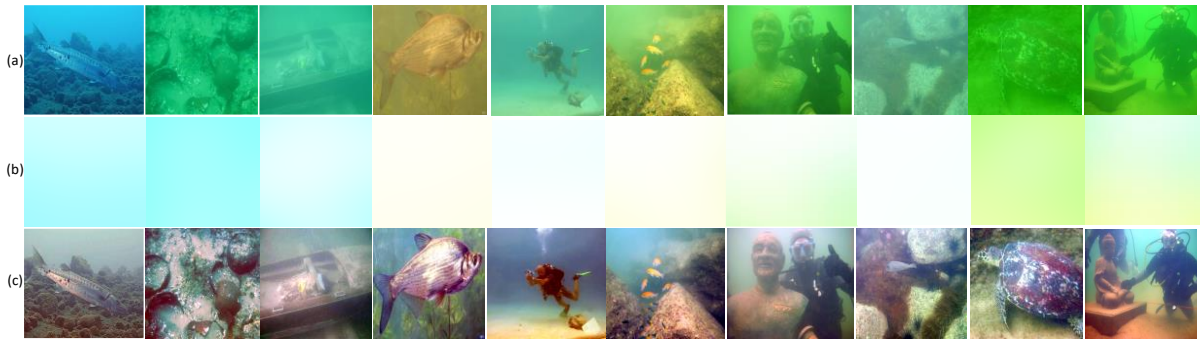

Fig. 3.4 (a) Raw underwater image, (b) Brightness adjustment, and (c) Output of proposed method.

3.1.3.4 Gamma Correction

Most of the underwater images appear blue or green due to the red component of the color channel disappearing first compared to the green and blue channels. The red channel has less energy in frequency or a greater wavelength than the green and blue channels, so it disappears first. According to the retinex model, the input underwater image is split into illumination and Reflectance. After decomposing the reflectance into a subsequent layer, the first layer is the base with a colored variance. The base layer has low color brightness, so we must correct it. So, we have used gamma correction; mathematically, it is represented as:

$$F(i,j) = \alpha(I_c)^{\gamma} \qquad c \in \{R, G, B\} \tag{3.18}$$

where α is constant, in this experiment, its value is set to 0.5, and the value of gamma (γ) is set to 1.6. $Gamma$ (γ) is related to the mean value of the image.

3.1.3.5 Contrast Enhancement

A contrast enhancement in the gradient domain is used to enhance the underwater image by estimating the gradient domain of reflectance instead of solving the image formation model. In this process, the undesired artifacts and noise are suppressed at an efficient level so that texture details enhancement performance is good, as represented in Eqn (3.19).

The contrast of the underwater input image can be estimated by the optical image formation model [78], which is described in Eqn (3.19).

$$\sum_i \|\nabla I(i,j)\| = \tau \sum_i \|\nabla Q_c(i,j)\| = \sum_i \|\nabla Q_c(i,j)\| \tag{3.19}$$

$I(i,j)$ denotes the underwater input image, and $Q_c(i,j)$ is the scene radiance, i is the coordinate of the pixel ∇ as the gradient operator, and $\tau_c(i,j)$ is characterized as a transmission with a value less than or equal to unity, i.e., $\tau_c(i,j) \leq 1$. Its value is estimated using the Fast visibility restoration from a single color or gray-level image, as explained in [72]. The transmission is used as a reciprocal; it works as an enhancement coefficient. If the value of $\tau_c(i,j)$ tends to be zero artifacts and noise is dominant in the enhanced image, the average value of transmission $\tau_c(i,j)$ is used in this experiment to compensate for this effect. Hence, the mathematical expression for the multi-scale detail layer in the gradient domain is expressed as:

$$\nabla D_i' = \frac{\omega_i}{\bar{\tau_c}} \nabla D_i \tag{3.20}$$

where $\bar{\tau_c}$ is the average value of transmission $\tau_c(i,j)$ and ω_i as the non-negative controlling parameters, it shows the enhancement strength. The D_1' component corresponding to ω_1 contains most of the small details and noise. Which desire to reduce enhancement. While the

D_2', part contains a firm edge and significant structure. The D_2' component corresponds to ω_2 need to enhance more strength. So, here, the value of $\omega_1 = 3$ and $\omega_2 = 4$ fixed. By solving the poison equation on modified gradients, two detail-enhanced layers D_1' and D_2' are obtained. Accordingly, better-quality reflectance is given by the summation of both the enhanced details layer and gamma-corrected base layer:

$$\mathcal{R}' = \left.\begin{matrix}\text{Gamma Correction } (B) + \text{Enhance Detail Layer } (D_1')) \\ + \text{Enhance Detail Layer } (D_2')\end{matrix}\right\} \tag{3.21}$$

The different stage output on reflectance is shown in Fig. 3.5.

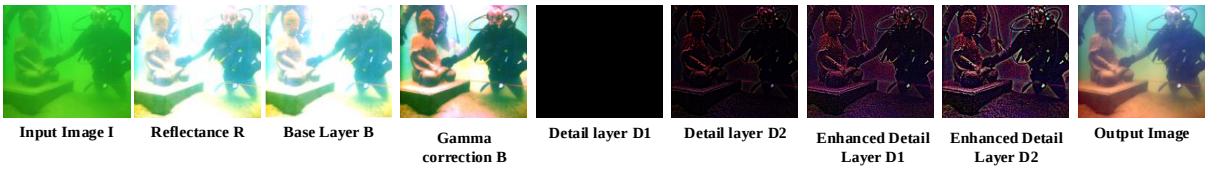

Fig. 3.5 Different stages of underwater image reflectance.

Finally, restored output images are a multiplication of improved reflectance and illumination. Mathematically, it is given as:

$$I' = \mathcal{R}' \cdot £' \tag{3.22}$$

<u>The algorithm steps for underwater image enhancement are summarized as follows:</u>

Step 1: An input raw-underwater image has been processed.

Step 2: Decomposed the input image into two parts, i.e., illumination Eqn (3.9) and reflectance Eqn (3.8).

Step 3: Apply brightness adjustment on the illumination part as shown in Eqn (3.16) and (3.17).

Step 4: Perform a multi-scale decomposition of reflectance in this step by Eqn (3.14).

Step 5: Output of reflectance are base layer, detail layer1, and detail layer2 as given in Eqn (3.15).

Step 6: Apply gamma correction on the base layer Eqn (3.18).

Step 7: Contrast enhancement is carried out on the detail layer1 and detail layer2 as given in Eqn (3.20)

Step 8: Linear combination of the base layer, detail layer1, and detail layer2 as given in Eqn (3.21).

Step 9: Finally, multiply the linear combination of these three layers with the brightness adjustment of the illumination part. It will produce an enhanced output image as given in Eqn (3.22).

3.1.4 Results and Discussion

The proposed method has been implemented on MATLAB software. Firstly, we have applied code to decompose the image into illumination and reflectance. Secondly, using a mathematical equation, we decomposed the reflectance into three layers i.e. base layer, detail layer1, and detail layer2. Thirdly, we enhance these three components such as the base layer, detail layer1, and detail layer2. Finally, all enhanced components i.e. illumination, base layer, detail layer1, and detail layer2 combined to obtain an enhanced image. All these steps have been implemented on MATLAB software. The experimental results of the proposed method have been compared to the existing underwater image enhancement method, which is also implemented on the same software. These methods are minimum information loss (MIL) [153], hybrid techniques for underwater image (HTU) [166] underwater dark channel prior guided image filter (UDCPGIF) [167], underwater dark channel prior guided soft matting (UDCPSM) [168][169], the hybrid framework for underwater image enhancement (HUIE) [170], Color balance and fusion for underwater image (CBFU) [171], hue-preserving for underwater image (HPU) [172], Multiscale retinex with color restoration (MSRCR) [173] and multi-purpose oriented real-world underwater image (MPORU) [174] used to analyze both qualitative and quantitative measure. This experiment used the underwater image enhancement benchmark (UIEB) [143] data set. Here, we have implemented the source code and fairly evaluated the parameters of different methods and their visual quality. For quantitative evaluation, we have used seven metrics which are the measure of enhancement (EME) [27], discrete entropy (DE) [27], peak signal-to-noise ratio (PSNR) [175], structural similarity index (SSIM) [176], underwater image quality measure (UIQM) [27], underwater color image quality evaluation (UCIQE) [177], and patch-based contrast quality index (PCQI) [178]. The value of these metrics used for comparative analysis of the proposed method with other existing state-of-the-art methods is discussed below.

3.1.4.1 Qualitative Analysis

Ten different images are taken, and their enhanced visual quality is checked using different methods. Usually, a specific state-of-the-art process works well for a special image only, and it

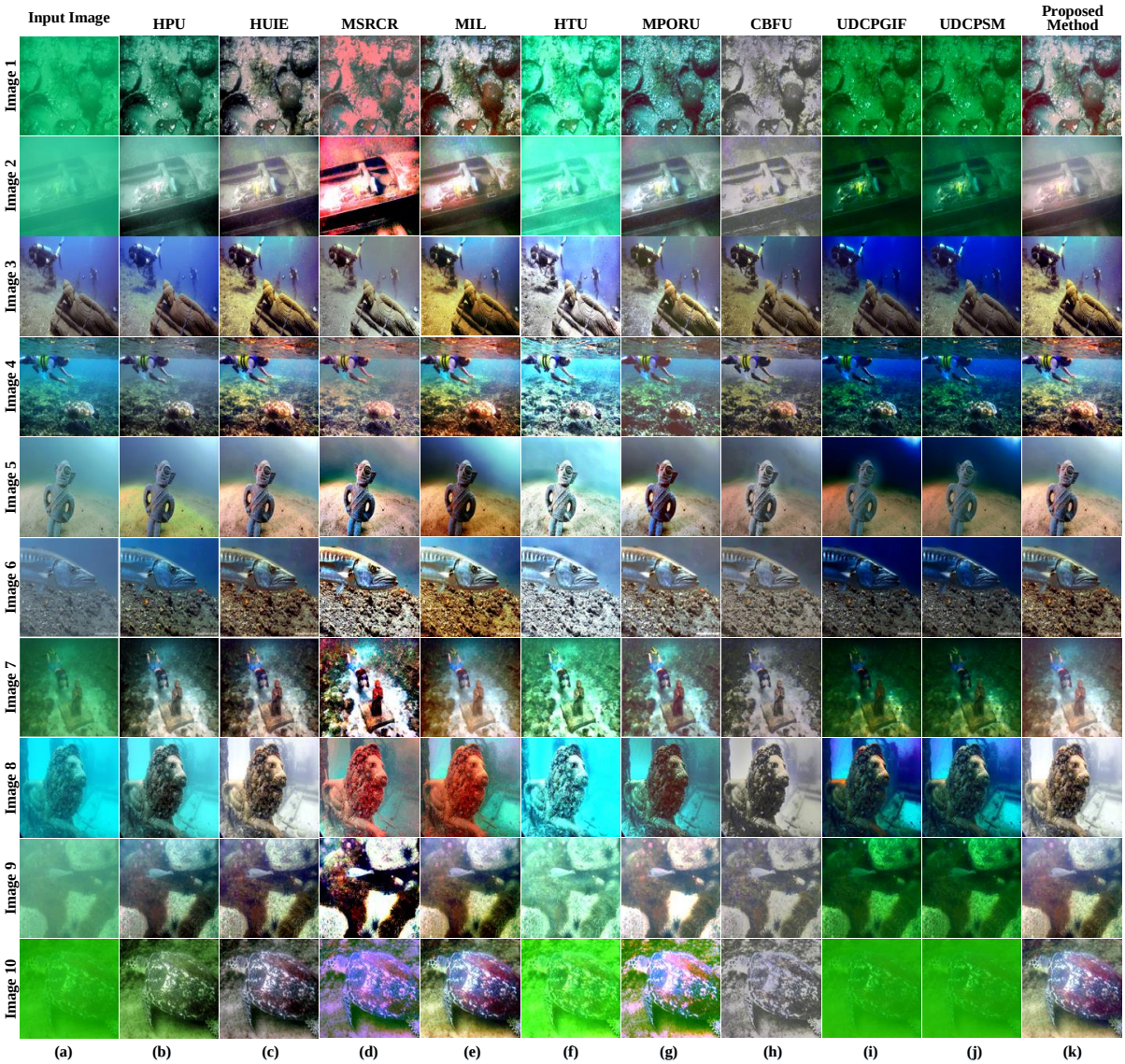

Fig. 3.6 Comparison of proposed method with existing state-of-the-art methods. (a) Input image, (b) Results of HPU, (c) Results of HUIE, (d) Results of MSRCR, (e) Results of MIL, (f) Results of HTU, (g) Results of MPORU, (h) Results of CBFU, (i) Results of UDCPGIF, (j) Results of UDCPSM, (k) Results of the proposed method.

may not be suitable in an extensive logic for another purpose. Fig. 3.6 shows the enhanced visual quality of images of different methods taken from the UIEB [143] database. Image capture in low-light conditions, as shown in Fig. 3.6, because of severe light distortion. The results show that MPORU [174], HUIE [170], MIL [153], CBFU [171], and the proposed proposed methods have good visual quality. On the other hand, HPU [172], UDCPGIF [167], and UDCPSM [168], [169] are inclined to give an abnormal appearance since the result is a little blurred to show the natural response. The methods MSRCR [173] and HTU [166] offer a bright visual quality that does not look natural. Hence, the proposed method illustrates

outstanding performance in the detail enhancement layer in the hazy background region. According to the optical image formation model, light rays get attenuated while traveling underwater because they are wavelength-dependent. Since the red component has less energy than the green and blue parts, i.e., it has the highest wavelength compared to green and blue light. So that the red light disappears first. However, underwater images appear greenish or bluish, as shown in Fig. 3.6 (image 1, image 3, image 4, image 8, image 10). UDCPGIF and UDCPSM methods do not positively affect contrast enhancement for underwater images. The proposed method results are comparable to the HUIE method, but it is superior to preserving more details.

3.1.4.2 Quantitative Analysis

Here, we calculate the parameters of enhanced images. These are the following parameters, EME [27], (DE) [27], PSNR [175], SSIM [176], UIQM [27], UCIQE [177], and PCQI [178].

Table 3.1 Comparison of various parameters of 890 images with proposed method and existing state-of-the-art.

Methods	EME [27]	DE [27]	PSNR [175]	SSIM [176]	UIQM [27]	UCIQE [177]	PCQI [178]
MIL [153]	9.4561	5.2121	32.7311	0.7676	33.3598	6.7876	0.9561
UDCPGIF [167]	10.6999	4.3813	59.9829	0.5188	33.9441	4.8822	0.9887
UDCPSM [168]	10.5716	4.4015	60.5113	0.5461	32.4418	3.1095	0.9896
HUIE [170]	12.2903	5.1761	66.1795	0.7285	32.5351	6.4946	0.7124
CBFU [171]	8.2488	4.8614	**68.1791**	0.8469	35.1462	7.1722	0.9906
HPU [172]	8.3625	5.0032	31.6036	0.8526	32.1707	0.6136	0.8015
HTU [166]	12.2903	5.1761	66.1795	0.7285	32.5351	6.4946	0.7124
MSRCR [173]	11.1108	4.8217	61.8387	0.5873	34.1452	6.2737	0.9911
MPORU [174]	5.4428	4.7332	53.1908	0.4624	35.7365	6.9073	0.1488
Proposed Method	**14.0725**	**5.4564**	67.9461	**0.8544**	**36.7576**	**7.3202**	**0.9997**

**bold value represents the best result

Here, the average value of these parameters is calculated over an underwater image enhancement benchmark [143] data set, which contains 890 raw images and 60 reference images. The evaluated results are shown in Table 3.1.

Furthermore, in order to conduct a quantitative analysis of the proposed method, we categorize the parameters in two ways: full-reference evaluation metrics and non-reference evaluation metrics. We treat the reference images supported by UIEB as the ground truths for full-

reference evaluation and compute the EME, PSNR, SSIM, and PCQI among the restored results and corresponding references. A higher value of the PCQI metric results in better contrast variation for human visual perception. The MSRCR and proposed method have approximately the same PCQI; the proposed method is slightly greater than the MSRCR. Now comes the PSNR metric. A higher value of the peak signal-to-noise ratio means the result is closer to the reference image. The CBFU has a more significant peak signal-to-noise ratio than other methods. The proposed method has comparable PSNR results to CBFU, as shown in Table 3.1.

EME parameters measure the enhancement; the higher the value, the better the result. The proposed method has a higher value compared to another method. Another full-reference metric is SSIM; its value lies between zero and one, and the value is closer to unity; it represents the ideal result in the context of the original image. The non-reference criterion is discrete entropy, UIQM, and UCIQE. Discrete entropy shows the information in an enhanced image; a higher value is better for the image. In our experiment, the proposed method has a higher value than another. MIL, HUIE, HPU, and HTU methods have comparable values but are lower than the proposed method. A higher value of UIQM and UCIQE is favorable. The proposed method gives a higher value than the other nine methods, as shown in Table 3.1. A higher value of UIQM has increased colorfulness, sharpness, and contrast, while a higher value of UCIQE has increased the color cast, blurring, and low contrast.

The experiment shows that the overall performance of the proposed method is better than most existing state-of-the-art methods. Most importantly, the proposed method works on underwater images and accepts any contrast level.

In this chapter, we have proposed two solutions for underwater image enhancement and restoration. In the above section of this chapter, we introduce multiscale decomposition-based image enhancement for underwater images. The second solution proposed is to restore underwater images using the white balance and retinex algorithm.

3.2 Underwater Image Restoration Using White Balance and Retinex Algorithm

Underwater image enhancement and restoration is very difficult due to the physical properties of the underwater environment. The captured underwater image is hazy due to the absorption and dispersion of light. During the capture of an image of an object underwater, the light acquired by a camera in an underwater situation is primarily produced by three components: a backscattering component that replicates light back to the camera before it reaches the objects [26], a forward scattering component that randomly diverges light as it approaches the camera, and the third component is a direct component that reflects light from the objects. The details of the image are hidden due to the scattering component, while the image is blurred due to the forward scattering component. Furthermore, marine snow, such as macroscopical moving elements, introduces undesired clatter and amplifies light scattering. The degraded underwater images pose challenges for marine biology, archaeology [179], and inspecting aquatic robots [21]. We have applied white balance to degrade underwater images and convert them into *YCbCr* color space. The *Y-component* of color space has been decomposed into reflectance and illumination; further restoration processes are carried out on these two components. Finally, concatenate three components of *YCbCr* color space and convert them into *RGB* color space.

The proposed method for image restoration utilizes the retinex algorithm. The main contribution is as follows:

- The white balance has been used before converting *RGB* to *YCbCr* color space to precisely match the degraded underwater image's color cast.
- The retinex algorithm splits the image into reflectance and illumination parts.
- We have applied the restoration process to the reflectance and illumination part. Finally, we concatenate all components of color space and finally, get a high-quality image.
- The proposed method obtained enhanced-quality visual images from raw underwater images with varying light intensities.

3.2.1 Methodology

The proposed method comprises three steps: White balance the underwater input images. Next, RGB color image converted into *YCbCr* color space and decomposed into *Y-component*, *Cb-component*, and *Cr-component*. Then illumination and reflectance are separated from the Y-*component* of *YCbCr* color space. In the second step, restored the illumination and reflectance

component. Finally, the *Y-component*, restored illumination, and restored reflectance are combined, then the *YCbCr* color space is converted into the *RGB* color space. All these steps are shown in Fig. 3.7.

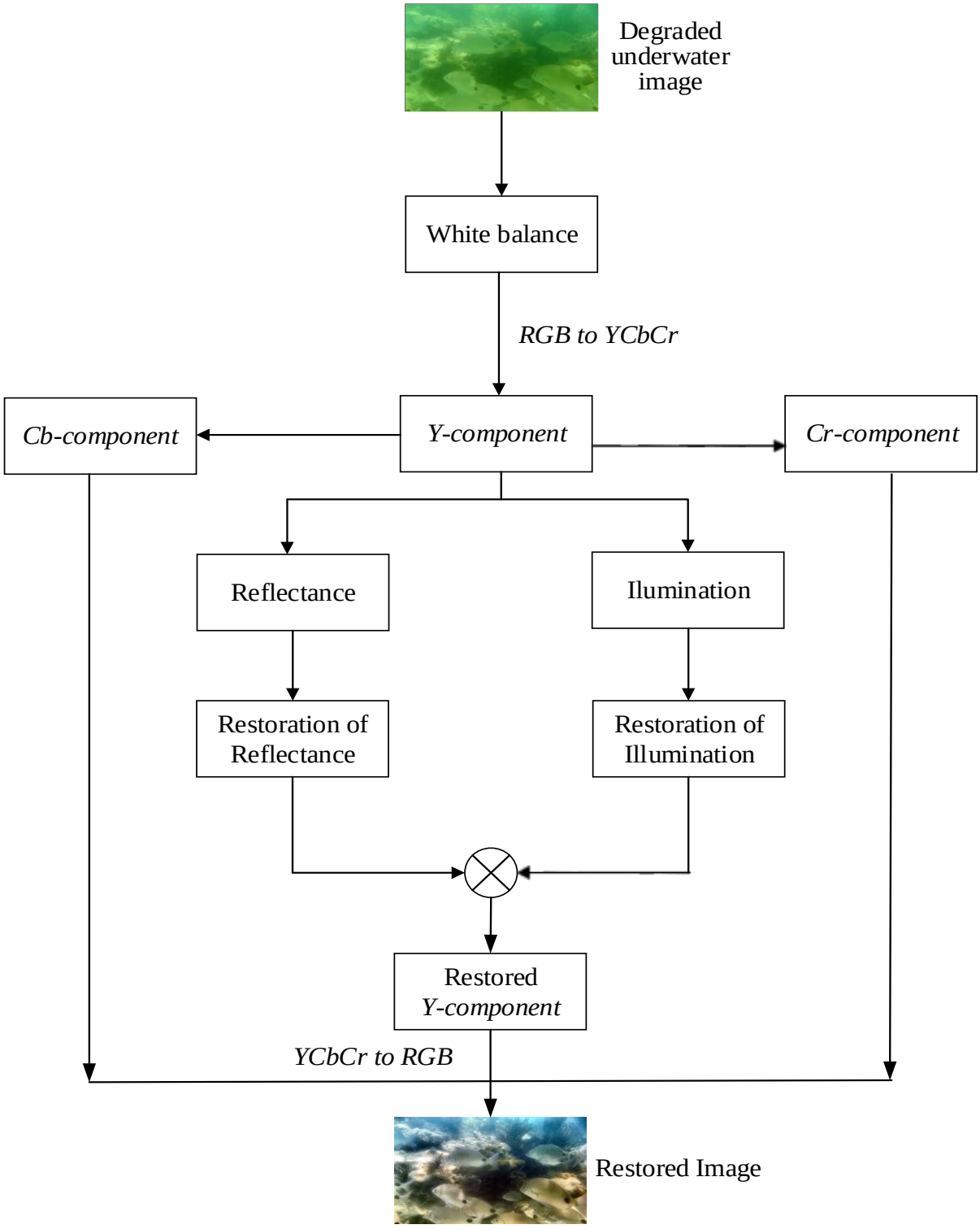

Fig. 3.7 Work flow of the proposed method based on illumination and reflectance restoration for underwater image.

3.2.1.1 The White Balance of the Input

The white balance is a crucial pre-processing step that improves the quality of the image by removing undesirable shade casts brought on by various illuminants. The white balance is impractical in 30 feet deeper water because it is challenging to recover the absorbed hues. Additionally, due to the limited light transmission in this medium, the underwater scene exhibits a considerable lack of contrast. In this method, the white balance of the input image is evaluated using the value (μ_I), which is derived from the scene's reference average (μ_{ref}) and modified by the variable:

$$\mu_I = 0.5 + \lambda\mu_{ref} \tag{3.23}$$

where μ_{ref} represents the mean color used to approximate the illuminant color [180]. The attribute λ assign to use to analyse the concentration and spreading on the color histogram. The value of λ varies from 0 to 0.5; here, it is taken as 0.2.

3.2.1.2 Illumination and Reflectance Assessment

We have applied the retinex model to the underwater picture to obtain illumination and reflectance. According to this paradigm, the underwater capture image comprises two components, i.e., illumination and reflectance. It is evaluated in the section 3.1.3.1 using the Eqn (3.5) to Eqn (3.13).

3.2.1.3 Restoration of Illumination and Reflectance

After computing reflectance and illumination, post-processing has been done on the histogram to address the fuzz and under-exposure issues. The attenuation of reflectance is due to fuzzes caused by suspended particles in water. The reflectance carries the details and edge information. The reflectance is improved by contrast limited adaptive histogram equalization (CLAHE) [54]. While preventing noise amplification, this procedure successfully enhances details and edges of image. The modified histogram definition is being done on the illumination image ($L_c(i,j)$) to address the issue of underexposure (i.e not enough light hitting to the camera's sensor). Precision instruction and genuineness should be maintained while the additional illumination is adequate to enhance acquaintance and lighten dusky areas. The experimental findings show that the form of the arc tangent, $I'(i,j) = arctan\,(L_c(i,j))$ performs well. A weighted histogram is created by using the gray intensity as the weight, based on the Bi-log transformation [181]. This process considers the number of pixels and the

grayscale values to maintain effective naturalness. The cumulative density functions (CDF) of $I'(i,j)$ is as follows, under the explanation of the CDF [62]:

$$C(p) = \frac{\sum_{i=0}^{p}\sum_{j=0}^{p} I'(i,j)\,.\,n(i,j)}{\sum_{i=0}^{\max(p)}\sum_{j=0}^{\max(p)} I'(i,j)\,.\,n(i,j)} \tag{3.24}$$

where $p = p^{th}$ gray level of $L_c(i,j)$, max (p) = maximum gray level of $L_c(i,j)$, *n(i,j)* = number of the p^{th} gray level. We confine the region of the selected histogram in [15, 255] to alleviate dusky areas and keep genuineness to prevent over-enhancing. The specified histogram's CDF is described for reflectance $\mathcal{R}_c(i,j)$ as follows:

$$Cf\big(\mathcal{R}_c(i,j)\big) = \frac{\sum_{i=0}^{q}\sum_{j=0}^{q} m(i,j)}{\sum_{i=0}^{255}\sum_{j=0}^{255} m(i,j)} \tag{3.25}$$

where $m(i) = arctan(q - 232)$, $q \in [0, 255]$. The restore reflectance $\mathcal{R}_{c,restored}(i,j)$ can be obtained by taking the inverse of $Cf^{-1}(\mathcal{R}_c(i,j))$. We combined the improved reflectance and illumination to get an enhanced *Y-component* of *YCbCr* color space. Then, finally, concatenate all components of color space and convert them into *RGB* color space to restore an image.

3.2.2 Results and Discussion

The proposed method has been compared with the existing state-of-the-art methods. These methods are weakly supervised color transfer (WSCT) [182], underwater image blurriness and light absorption (UIBLA) [122], underwater dark channel prior (UDCP) [109], automatic red-channel underwater image restoration (RED) [64], fusion generative adversarial network (FGAN) [148], enhancing underwater images and videos by fusion (FE) [38], and cycle-consistent generative adversarial networks (CycleGAN) [183], used to analyze both qualitative and quantitative analysis. The proposed method has used the underwater image enhancement benchmark dataset. The proposed and existing state-of-the-art methods have been implemented on the same U45 dataset.

3.2.2.1 Qualitative Analysis

Here, we analyze the visual quality of the degraded underwater image. Here, eight images have been taken from the U45 dataset. The output of the existing methods and the proposed method is shown in Fig. 3.8. Compared to the existing state-of-the-art method, the proposed method exhibits good visual quality. Image2, image4, and image7 are green in color. The restored version of the images shows better quality. The existing methods FGAN, FE, and CycleGAN are also producing comparable results. However, the restored image has poor visual quality in

the case of WSCT, UIBLA, and UDCP methods. Image1, image3, image5, image6, and image 8 are hazy underwater images taken as input to the experiment. The UDCP method gives a slightly red output image, which does not provide a visually pleasant result. The proposed method produces better visual quality compared to UDCP. The output of the UIBLA method is brighter than the other method, which does not preserve the image's naturalness. The FE and proposed methods are equivalent to each other in terms of visual quality, the proposed method performed better in terms of UIQM and UCIQE parameters.

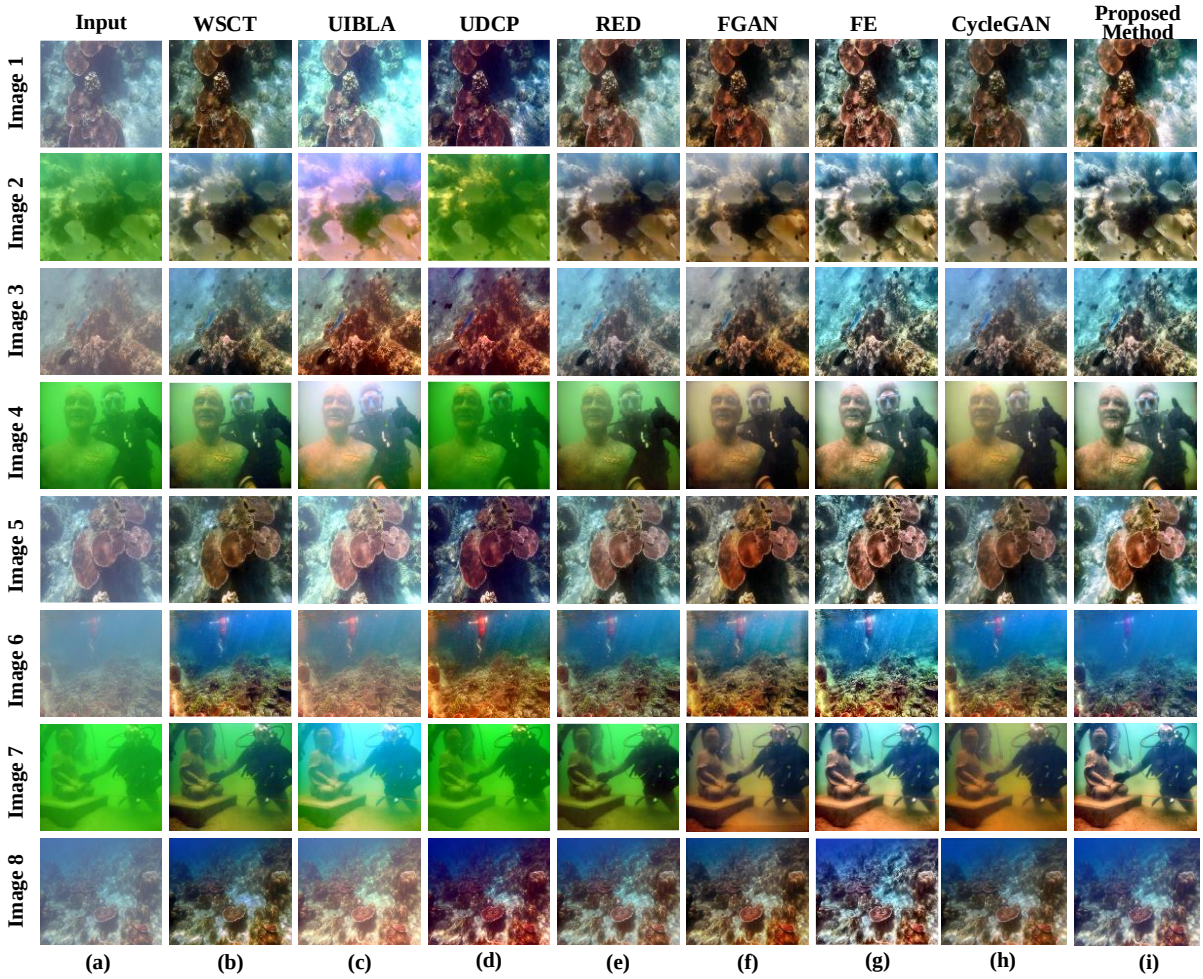

Fig. 3.8 Enhance results of various state-of-the-art and proposed methods, (a) Input image, (b) Result of WSCT, (c) Result of UIBL, (d) Result of UDCP, (e) Result of RED, (f) Result of FGAN, (g) Result of FE, (h) Result of CycleGAN, (i) Result of proposed method respectively.

3.2.2.2 Quantitative Analysis

The quantitative analysis is performed a in this subsection section. The two parameters have been evaluated of the image, i.e., UIQM [184] and UCIQE [177]. These are the non-reference quality evaluation parameters. Three underwater image attribute actions, UISM, UIConM, and

UICM combine to form UIQM. Mathematically defined as $UIQM = c_1 \times UICM + c_2 \times UISM + c_3 \times UIConM$. Higher image quality is represented by a higher UIQM value.

where c_1, c_2, and c_3 are the constant and values are taken as, $c_1 = 0.0271$, $c_2 = 0.2851$, and $c_3 = 3.5642$. The proposed method has greater value for all the images compared to the existing method which is shown in Table 3.2. Also, we compared the proposed method with existing methods by plotting a bar graph which is shown in Fig. 3.9.

Table 3.2 Quantitative evaluation of proposed method and existing methods using UIQM parameter on U45 dataset.

Method	Image1	Image2	Image3	Image4	Image5	Image6	Image7	Image8
WSCT [182]	7.1759	7.1552	7.2081	7.1645	7.1763	7.1552	7.2082	7.1645
UIBLA [122]	7.0359	6.9212	7.0846	7.1019	7.0359	6.9213	7.0846	7.1021
UDCP [109]	7.0521	6.9062	6.9665	7.2835	7.0521	6.9063	6.9665	7.2836
RED [64]	7.2756	7.2966	7.2872	7.2429	7.2756	7.2967	7.2873	7.2429
FGAN [148]	7.0871	7.0717	7.1148	7.0749	7.0872	7.0718	7.1148	7.0750
FE [38]	7.2960	7.2951	7.3640	7.2289	7.2960	7.2951	7.3641	7.2289
CycleGAN [183]	6.9999	6.9659	7.0320	6.9999	6.9993	6.9660	7.0321	6.9999
Proposed method	**7.3021**	**7.2964**	**7.3720**	**7.2941**	**7.3198**	**7.3894**	**7.3741**	**7.2986**

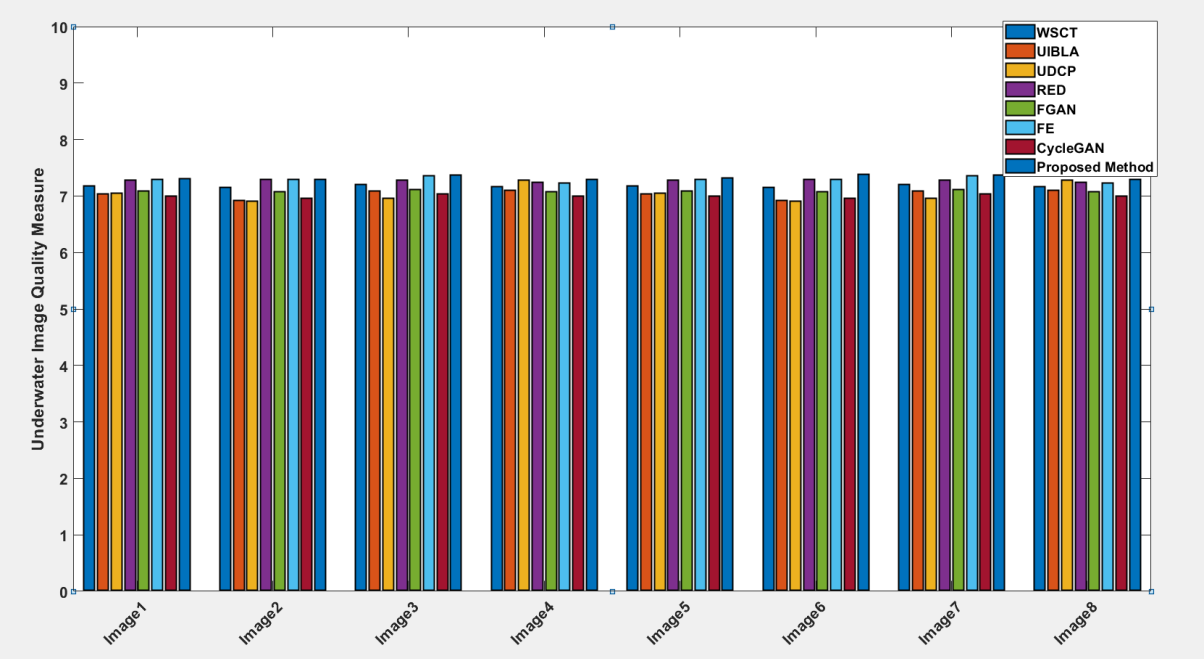

Fig. 3.9 Quantitative comparison of UIQM parameter of the proposed with existing state-of-the-art methods for various images.

UCIQE evaluates image quality by linearly combining luminance contrast, average saturation, and chrominance variation. The more excellent value of UCIQE represents the high quality of the enhanced image. Table 3.3 describes the UCIQE values of the existing and proposed methods. We have also compared it through a bar graph, as shown in Fig. 3.10. The proposed method performed better compared to existing methods for all the images.

Table 3.3 Comparison of UCIQE with proposed method and existing state-of-the-art on U45 dataset.

Method	Image1	Image2	Image3	Image4	Image5	Image6	Image7	Image8
WSCT [182]	0.6023	0.5568	0.4914	0.6184	0.6198	0.5714	0.6032	0.5724
UIBLA [122]	0.5666	0.5862	0.4675	0.6371	0.5310	0.6055	0.5578	0.5371
UDCP [109]	0.4801	0.5801	0.5918	0.6480	0.6284	0.5374	0.4526	0.5306
RED [64]	0.5720	0.5490	0.5245	0.5599	0.6152	0.5443	0.6064	0.5669
FGAN [148]	0.6059	0.5620	0.5336	0.5954	0.6101	0.5800	0.6353	0.5734
FE [38]	0.6337	0.6015	0.6937	0.6343	0.6561	0.5794	0.6862	0.6173
CycleGAN [183]	0.6203	0.5601	0.5068	0.6017	0.6057	0.5729	0.6176	0.5771
Proposed method	**0.6531**	**0.6143**	**0.7014**	**0.6523**	**0.6631**	**0.5915**	**0.7143**	**0.6312**

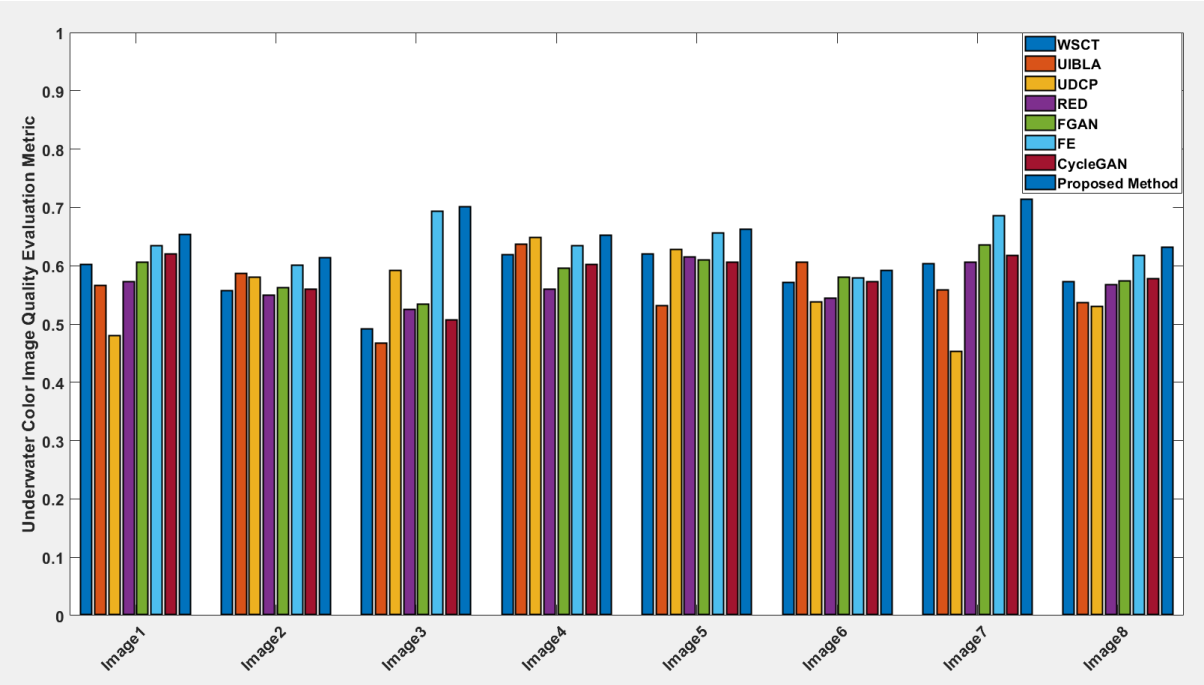

Fig. 3.10 Quantitative comparison of UCIQE parameter of proposed and existing state-of-the-art methods for various images.

It is challenging to compare image enhancement methods using UCIQE, UIQM, or other no-reference metrics since these metrics place differing values on contrast and colorfulness. In contrast to the UCIQE algorithm, the UIQM procedure eliminates 10% of pixels with the degraded quality earlier in calculating the image's color saturation. From Table 3.3, it is concluded that the performance of the proposed method is better than the existing state-of-the-art methods in terms of UCIQE.

3.3 Summary

In this chapter, there are two methods have been proposed for image enhancement and restoration for underwater images. The first novel method effectively applies to almost all real-world underwater images with different contrast-degradation levels, where most existing state-of-the-art methods do not provide satisfactory results. We capture additional information into the corresponding layer to compensate for the brightness, color, and contrast attenuation. Firstly, retinex model is applied a to the input image and decomposed it into illumination and reflectance; illumination represents brightness variation whereas reflectance contains detail information of image. Then, reflectance is decomposed into multi-scale layers. Gamma correction is applied to the smoothest base layer, while contrast enhancement is applied to the gradient domain of detail layers. The output of all reflectance layers are added together and then multiply it with brightness adjustment. Finally, it is observed that, the visually satisfying results with improved brightness, contrast, and color has been obtained. Nine existing state-of-the-art methods were performed over the proposed method to find their strength, and it shows that the proposed method gives a very high quality and enhanced underwater image. The proposed method is not complex because it has straightforward operations like addition, subtraction, multiplication, and convolution.

The second solution proposed an original retinex-based restoration method for underwater images. To solve the fuzziness and underexposure, apply the white balance to degraded underwater images and then obtained images are converted into *YCbCr* color space. Now, reflectance and illumination from a single white balance underwater image are decomposed. After decomposing, a straightforward, efficient post-processing technique improves deteriorated images. Experimental result shows that the proposed scheme produces the highest full-reference quality metric EME, SSIM, PCQI, PSNR, and non-reference quality metric DE, UCIQM, and UIQM. All these metrics show the highest value in the case of the proposed method, except the PSNR values of CBFU, which are slightly more significant than proposed

method. All these parameters are evaluated on the same data set, which are publicly available. Experimental findings show that restored images possess color correction, illumination, and naturalness preservation.

The publication related to this chapter

Amarendra Kumar Mishra, Mahipal Singh Choudhry, and Manjeet Kumar. "Underwater image enhancement using multiscale decomposition and gamma correction." *Multimedia Tools and Applications* 82.10 (2023): 15715-15733, **SCIE, (IF: 3.6)** https://doi.org/10.1007/s11042-022-14008-2

Amarendra Kumar Mishra, Mahipal Singh Choudhry, and Manjeet Kumar. "Underwater image restoration using white balance and retinex algorithm." *2022 IEEE Conference on Interdisciplinary Approaches in Technology and Management for Social Innovation (IATMSI)*. **IEEE, 2022**. **doi:** 10.1109/IATMSI56455.2022.10119294.

Chapter 4

Underwater Image Enhancement and Restoration using White Balance, Contrast Enhancement, Empirical Mode Decomposition and Blending Techniques

This chapter describes an effective underwater image enhancement method using white balance, laplacian contrast weight, saliency weight, saturation weight, weight normalization, and blending techniques. The second method for underwater image restoration has been proposed using color correction and empirical mode decomposition techniques. The proposed method is compared with the existing state-of-the-art methods on publicly available datasets. The effectiveness of the proposed method has been evaluated in terms of the image's visual quality and various parameters.

4.1 Underwater Image Enhancement Based on White Balance and Blending Technique

4.1.1 Introduction

The ecosystem below the water has numerous unique attractions, including fish and marine life, incredible beauty, and mystery shipwrecks. In addition to underwater imaging, underwater photography has generated significant interest in a variety of scientific and technological fields, including the study of marine biology [185] and archaeology [186], the inspection of underwater cables [187], and infrastructure [188] and the detection of man-made objects [189].

Underwater images are distinct from regular images in that they often suffer from poor visibility due to the absorption and scattering of light as it travels through the water. This results in a significant reduction in the amount of available light energy and a change in the direction of light, making distant objects appear blurry or obscured.

In coastal water with abundant phytoplankton, the water often appears green instead of clear. This is because the plant scatters light and absorbs the shorter wavelengths, such as blue and

violet, due to the presence of chlorophyll [190]. The greenish-blue image can result from the complex interaction between light, the transmission medium, and the scene.

In Chapter 3, the underwater image enhancement and restoration techniques have been proposed based on multi-scale decomposition using retinex, gamma correction, contrast enhancement in the gradient domain, and brightness adjustment. In this chapter, we have proposed a method for underwater image enhancement and restoration based on white balance, contrast enhancement, empirical mode decomposition, and blending techniques.

4.1.2 Methodology

Enhancing underwater images is challenging, as it requires correcting colors while simultaneously improving the image details. To tackle this problem, we propose an algorithm based on an image blending technique to enhance the quality of underwater images. The conceptual structure of this method is depicted in Fig. 4.1 Firstly, color correction of the underwater degraded image has been done through white balance and contrast-limited adaptive histogram equalization [191], and we obtain *input1* and *input2*. Secondly, we convert *RGB input1* and *input2* into *YCbCr* color space and decompose them into *Y-component*, *Cb-component*, and *Cr-component*. Thirdly, laplacian, saliency, and saturation filtering are applied to the *Y*-component, and normalization is performed on the obtained image. Finally, we use the blending process to get an enhanced image.

4.1.2.1 Color Correction

In underwater imaging, the color of images is often affected by light absorption at different wavelengths, resulting in a blue or green hue. Color correction can be applied to the input image to address the color distortion present in underwater images. The color-corrected image is shown in Fig. 4.2. A Gaussian distribution-based linear mapping model can be used. The model requires the determination of the maximum and minimum values of the input image in each color channel. These values can be calculated as follows:

$$I_{C,max} = I_{C,mean} + \gamma I_{C,var} \quad (4.1)$$

$$I_{C,min} = I_{C,mean} + \gamma I_{C,var} \quad (4.2)$$

here, $I_{C,mean}$ and $I_{C,var}$ is the mean and standard deviation of the RGB channel. The parameter γ is to control the dynamic range of the image; Here, $\gamma = 2.3$ is taken. The color-corrected image is evaluated as:

$$I_{C,CR} = \left(I_C - I_{C,min}\right)/\left(I_{C,max} + I_{C,min}\right) \quad (4.3)$$

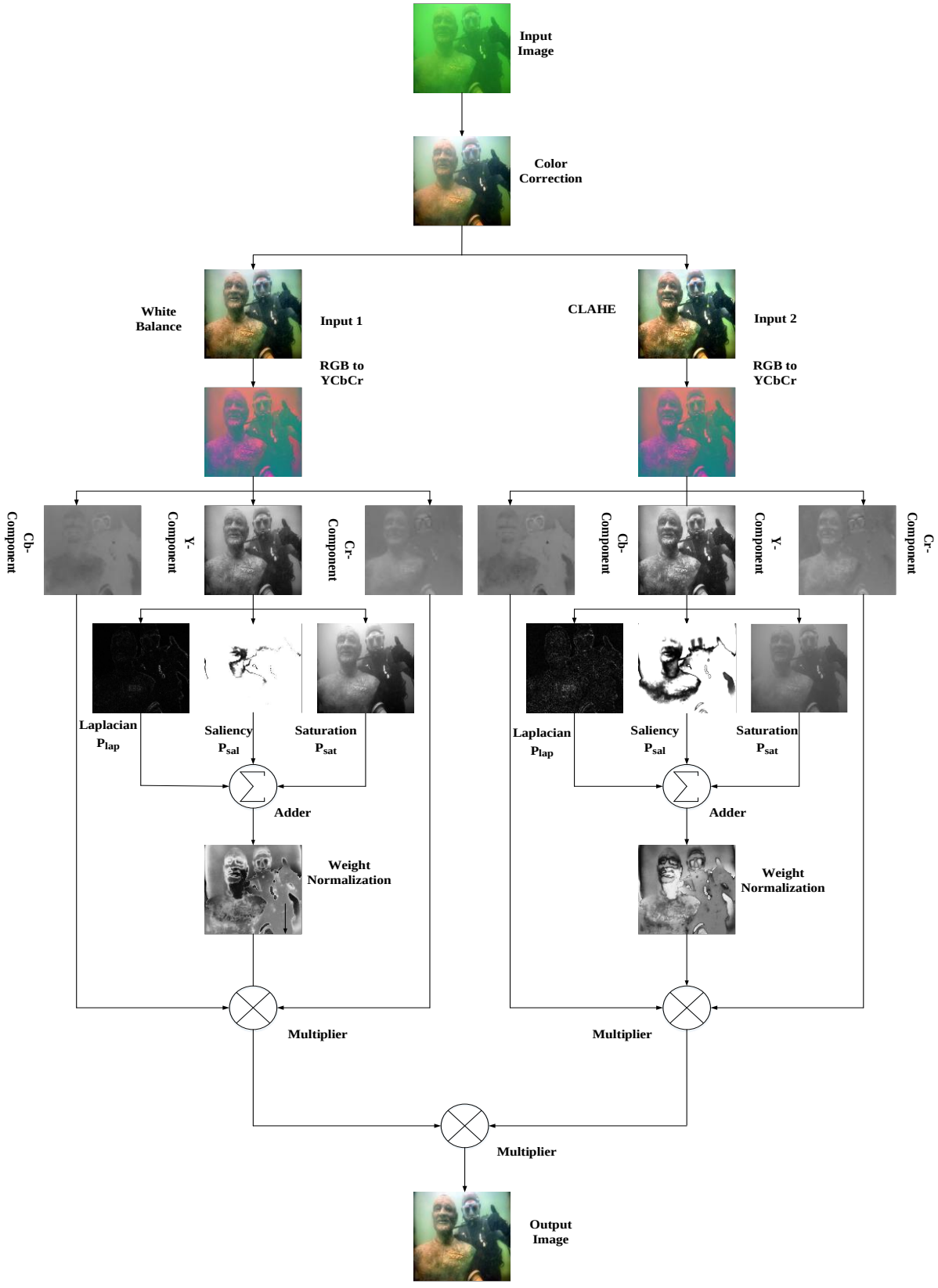

Fig. 4.1 The proposed method involves processing a color-corrected image to produce two additional images: *Input1* and *Input2*. *Input1* is obtained by applying white balance technique, and *Input2* is generated through CLAHE. These two images were input for the blending process to get the final restored image.

Fig. 4.2 (a) Degraded underwater images, (b) Color-corrected images, and (c) Enhanced images of the proposed method.

4.1.2.2 White Balance of the Inputs

The input degraded underwater image has been applied for the color correction through given mathematical Eqn (4.1), Eqn (4.2), and Eqn (4.3), which are based on a white balance technique with optimal gain factor [192], [193].

$$I_1 = \frac{I_{C,CR}}{\varphi_{max} \times \left(\alpha/\alpha_{ref}\right) + \varphi_p} \tag{4.4}$$

$$\alpha_{ref} = \sqrt{(M_r)^2 + \left(M_g\right)^2 + (M_b)^2} \tag{4.5}$$

where I_1 represent a white balance image of degraded underwater image as shown in Eqn (4.4). M_r, M_g, M_b denotes the mean value of each channel of a color-corrected underwater image $I_{C,CR}$ and φ_{max} is evaluated by the maximum value of RGB channels of color-corrected underwater image $I_{C,CR}$. $\alpha = \{M_r, M_g, M_b\}$ represents the sum of each channel of color-corrected underwater image $I_{C,CR}$.

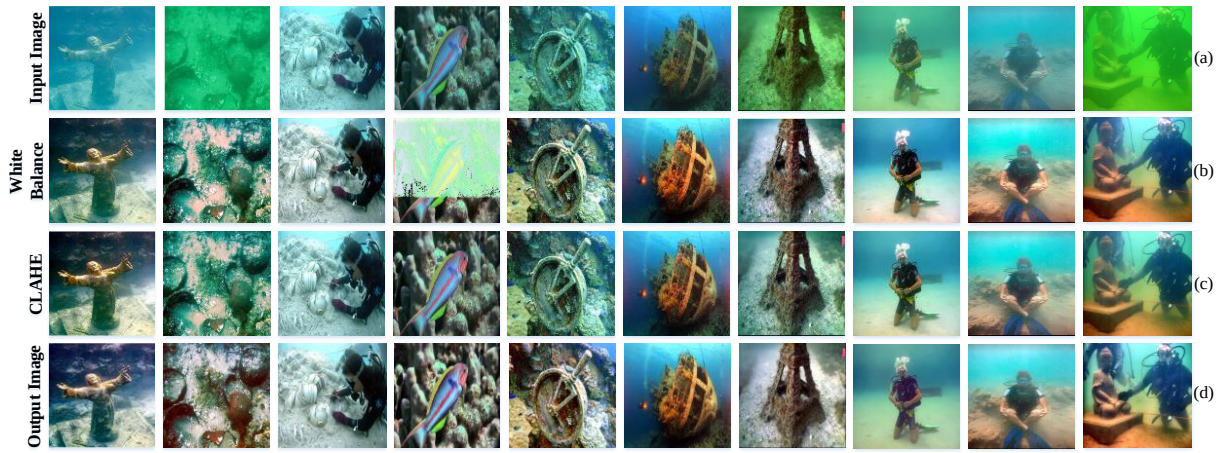

Fig. 4.3 (a) The input image, (b) The white balance image (*input1*), (c) The CLAHE image (*input2*), and (d) Enhanced images of the proposed method.

To obtain the appropriate color of the image $I_{C,CR}$, a value for (φ_p) is chosen in the range of (0, 0.5). The closer value of (φ_p) is to 0, which shows the lowest brightness of the underwater image $I_{C,CR}$. For the higher value of φ_p, i.e., 0.5, the corrected image is brighter. Here, the value of (φ_p) has been taken as 0.28, which preserves the image details and improves the contrast and visual quality of the input image, as shown in Fig. 4.3. The color-corrected image bifurcates, and each part has been converted into *YCbCr* color space.

4.1.2.3 Decomposition of Y-Component

The white balance input image has been bifurcated, and the obtained image has been converted into *YCbCr* color space. The *Y-component* of the image is further split into different components using laplacian, saliency, and saturation techniques, respectively.

4.1.2.3.1 Laplacian Contrast Weight (P_{Lap})

The Laplacian contrast weight is a method used to estimate the overall contrast of an image. It involves applying a laplacian filter to each channel of the image's luminance, which effectively highlights the edges and details present in the image, as shown in Fig. 4.4. The absolute value of the resulting filtered image is then computed, which provides a measure of the image's contrast. This approach is commonly used in image processing and computer vision to analyze and enhance image quality. However, in specific applications, such as underwater dehazing, this weight alone may not fully recover the image's contrast. It cannot effectively distinguish between flat regions and those with a ramp-like intensity distribution. Therefore, to address this limitation, we proposed incorporating an additional contrast assessment metric that complements the laplacian contrast weight [38]. This metric helps to improve the accuracy of contrast recovery in the context of underwater dehazing and other similar applications. Mathematically, it is evaluated as follows:

$$P_{Lap}(i,j) = \left\| Y_k(i,j) - Y_{k,\omega_{hc}}(i,j) \right\| \tag{4.6}$$

Here, $Y_k(i,j)$ denotes the luminance channel of the input to obtain a low-passed version of the luminance channel of the input, denoted by $Y_{k,\omega_{hc}}(i,j)$, a small separable binomial kernel with dimensions of 3×3 and weights $1/16\,[1,4,6,4,1]$ is used. This kernel serves as a good approximation of a Gaussian kernel and allows for more efficient computation. The high-frequency cut-off value used in this process is $\omega_{hc} = \pi/2.75$.

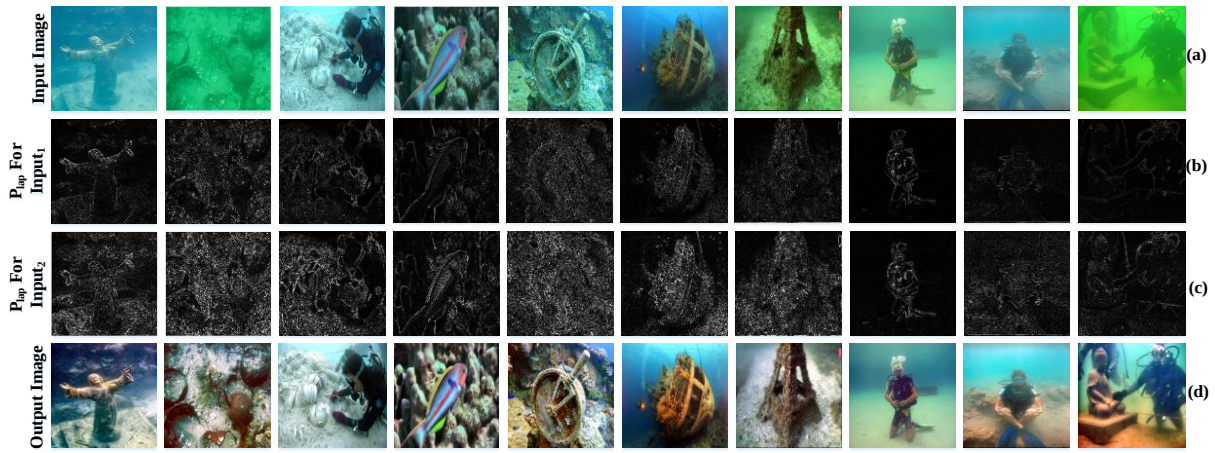

Fig. 4.4 (a) Degraded underwater image, (b) The Laplacian contrast weight for the *input1*, (c) The Laplacian contrast weight for the *input2*, and (d) The enhanced images of the proposed method.

4.1.2.3.2 Saliency Weight (P_{Sal})

The saliency weight enhances the visibility of salient objects that may not be visible in an underwater scene. We adopted the saliency estimator proposed by [204] to determine the saliency level, as shown in Fig. 4.5. This algorithm is based on the center-surround contrast concept, also found in biological systems. However, the saliency map overemphasizes bright areas (i.e., regions with high luminance values).

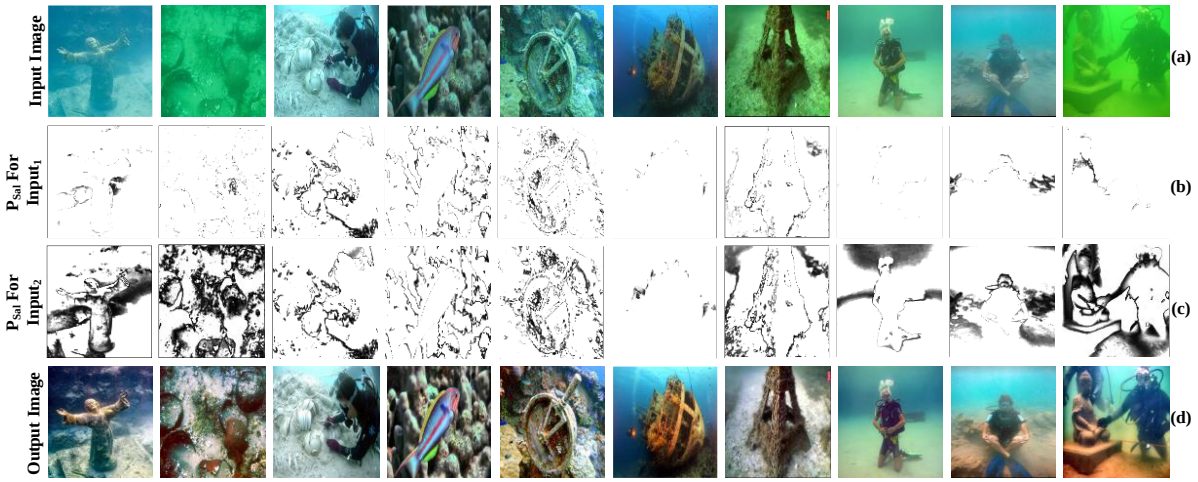

Fig. 4.5 (a) Degraded underwater image, (b) The saliency weight for the *input1*, (c) The saliency weight for the second *input2*, and (d) The enhanced images of the proposed method.

To create a saliency map $P_{Sal}(i,j)$ For an image $I(i,j)$ with dimensions $W \times H$ pixels, we can use the following methods:

$$P_{Sal}(i,j) = \left|I_a(i,j) - I_{\omega_{hc}}(i,j)\right| \tag{4.7}$$

We first compute the average pixel value to generate a saliency map from an image ($I_a(i,j)$). Then, we apply a Gaussian blur to the image, denoted as $I_{\omega_{hc}}(i,j)$, which helps remove small details and noise. We use the norm of pixel-wise differences to measure the differences between the original and blurred images. This efficient approach allows us to generate a saliency map at full resolution.

4.1.2.3.3 Saturation Weight (P_{Sat})

The inclusion of a saturation weight P_{Sat} [60] the blending method helps account for chromatic information by prioritizing highly saturated regions, as shown in Fig. 4.6. To generate this weight map, the difference between the Y_k, Cb_k, and Cr_k color channels and the luminance L_k of each pixel location in the k^{th} input is calculated for every input I_k.

$$P_{Sat} = \sqrt{1/3\,[(Y_k - L_k)^2 + (Cb_k - L_k)^2 + (Cr_k - L_k)^2]} \tag{4.8}$$

In actual use, the three weight maps are combined into one weight map for each input. This is done by adding together the P_{Lap}, P_{Sal}, and P_{Sat} weight maps to create an aggregated weight map, which is denoted as P_k.

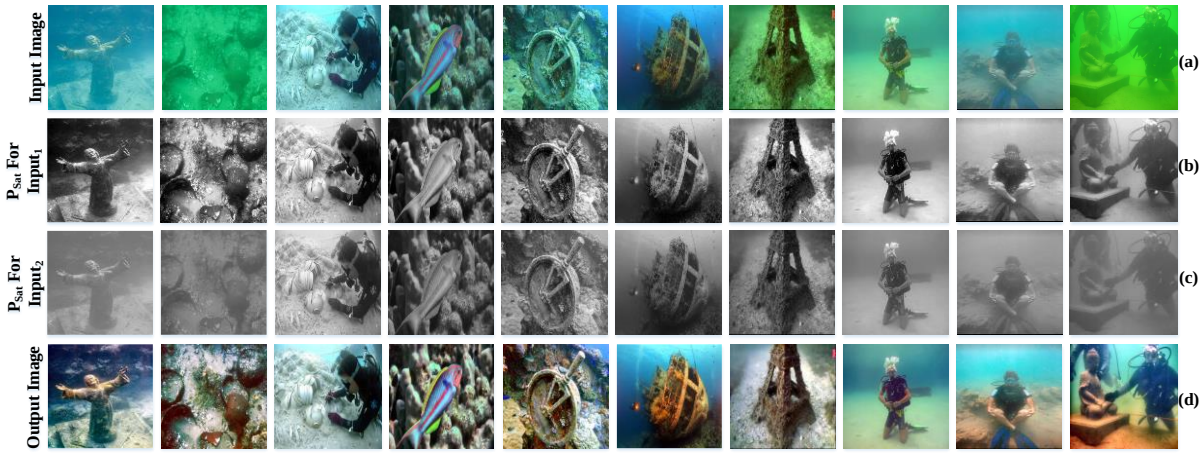

Fig. 4.6 (a) Input images, (b) The saturation weight for the *input1*, (c) The saturation weight for the *input2*, and (d) The enhanced images of the proposed method.

4.1.2.4 Weight Normalisation ($\overline{P_k}$)

The P_k is obtained by summation of all the three weight (i.e, P_{Lap}, P_{Sal}, and P_{Sat}). After obtaining aggregated weight maps for each input is normalized at a pixel level by summing up the three weight maps. This is achieved by dividing the weight of each pixel in each map by the sum of the weights of the same pixel across all the maps. Mathematically, the computation of normalized weight maps, denoted as ($\overline{P_k}$) for each input as shown in Fig. 4.7.

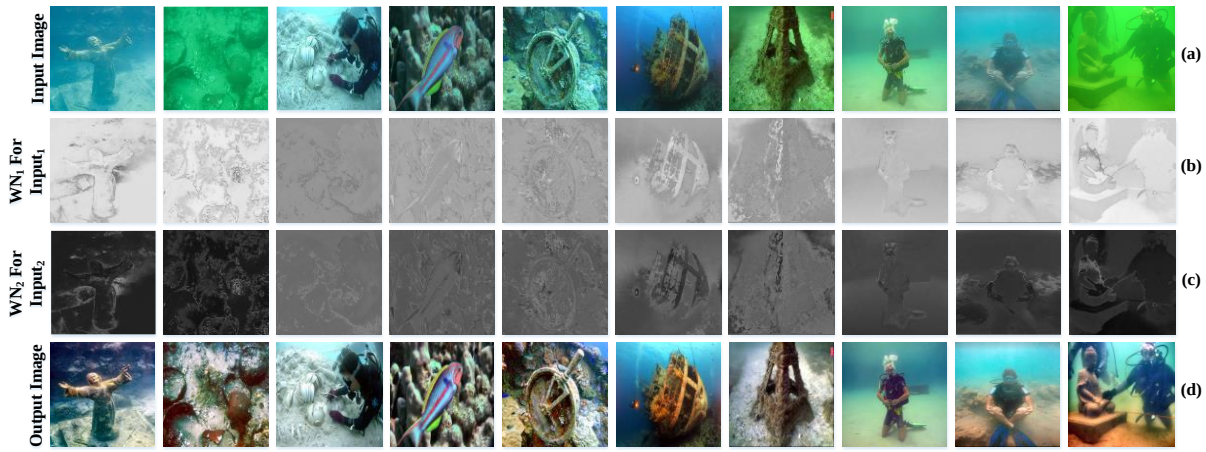

Fig. 4.7 (a) Degraded underwater images, (b) The normalized weight for the *input1*, (c) The normalized weight for the *input2*, and (d) The enhanced images of the proposed method.

$$\overline{P_k} = (P_k + \varepsilon) \Big/ \left(\sum_{k=1}^{K} P_k + K.\varepsilon \right) \tag{4.9}$$

To ensure that each input contributes to the output, a slight regularization term is used and denoted as ε. Throughout this proposed work, ε is assigned a value of 0.1.

4.1.2.5 Blending Process

To obtain the enhanced image $F(i,j)$ from the given normalized weight maps, we combine the input data with the corresponding weight values at each pixel location (i,j). The results of the proposed method are the final image reconstructed based on the weighted contributions of the inputs at each location.

$$F(i,j) = \sum_{k=1}^{K} \overline{P_k}\,(i,j) I_k(i,j) \tag{4.10}$$

The input image is denoted by $I_k(i,j)$, where K represents the index of the inputs, and in this particular case, K equals 2. These inputs are then multiplied by their respective normalized weight maps $\overline{P_k}(i,j)$**.** Which assign weight values to each pixel location based on their importance in the final reconstructed image. This weighting process allows the inputs to be combined to reflect their relative contributions to the final image.

4.1.3 Results and Discussion

Here, we evaluate the performance of the proposed method on three datasets: UIEB [143], RUIE [144], and the U45 [148] dataset. We analyze the overall improvement achieved by the

proposed method. Evaluation of the proposed method has been done through subjective and objective analysis.

4.1.3.1 Subjective Assessment

The subjective assessment is used to evaluate the visual quality of images. We have tested the proposed method on various data sets such as UIEB, UIQS, UCCS, and U45. The obtained results are compared with existing state-of-the-art methods on the same data sets.

4.1.3.1.1 Comparative analysis of the proposed method on the underwater image enhancement benchmark dataset

The proposed method shows the better visual quality of degraded underwater images compared

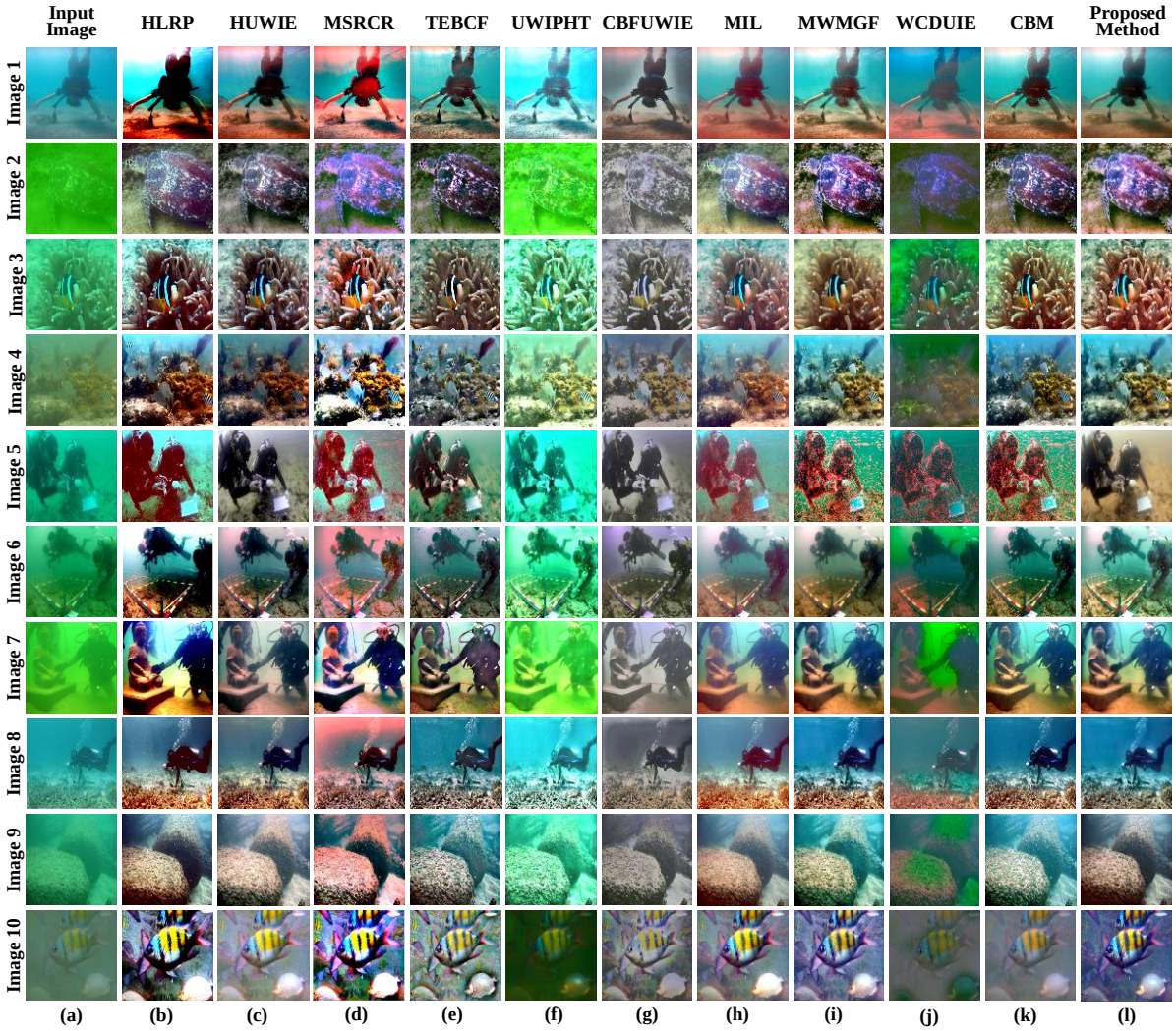

Fig. 4.8 The visual quality of the proposed method compared with the existing state-of-the-art on the UIEB dataset. (a) The degraded image, followed by an enhanced image generated by (b) HLRP, (c) HUWIE, (d) MSRCR, (e) TEBCF, (f) UWIPHT, (g) CBFUWIE, (h) MIL, (i) MWM, (j) WCDUIE, (k) CBM, and (l) The proposed results, respectively.

to existing methods, as shown in Fig. 4.8. These specific input images were chosen from UIEB [143] and displayed a range of underwater color tones and lighting scenarios.

Here, evaluate the effectiveness of the proposed method concerning ten existing state-of-the-art techniques such as hyper-laplacian reflectance prior (HLRP) [194], hue-preserving-based underwater image enhancement (HUWIE) [172], MSRCR [195], texture enhancement blurriness and color fusion (TEBCF) [196], underwater image processing using hybrid technique (UWIPHT) [197], color balance and fusion for underwater image enhancement (CBFUWIE) [60], MIL [198], multi-weight and multi-granularity fusion (MWMGF) [191], wavelength compensation and dehazing for underwater image enhancement (WCDUIE) [93], and contour bougie morphology (CBM) [199] respectively.

4.1.3.1.2 Comparative analysis of the proposed method on the underwater image quality set dataset

The UIQS [144] dataset is intended to evaluate UIE algorithms that attempt to improve picture visibility. Three input images have been taken from each subset, and the corresponding output of all existing methods and the proposed method are shown in Fig. 4.9. We have implemented the proposed method on the UIQS dataset; then, three enhanced images have been randomly chosen from each subset of the UIQS [144] dataset, as shown in Fig. 4.9. we have implemented existing state-of-the-art methods such as HLRP [194], HUWIE [172], MSRCR [195], TEBCF [196], UWIPHT [197], CBFUWIE [60], MIL [198], MWMGF [191], WCDUIE [93], and CBM [199] on the same dataset for the comparison of the proposed method as represented in Fig. 4.9.

4.1.3.1.3 Comparative analysis of the proposed method on the underwater color cast set dataset

Here, the proposed method is implemented on the UCCS dataset. Also, the existing state-of-art methods run on this whole dataset for comparison. The output results of the proposed and existing state-of-the-art methods are shown in Fig. 4.10. Here, four images have been taken randomly from each dataset as input and output for comparison, as shown in Fig. 4.10. The existing state-of-the-art methods are taken here for comparison HLRP [194], HUWIE [172], MSRCR [195], TEBCF [196], UWIPHT [197], CBFUWIE [60], MIL [198], MWMGF [191], WCDUIE [93], and CBM [199].

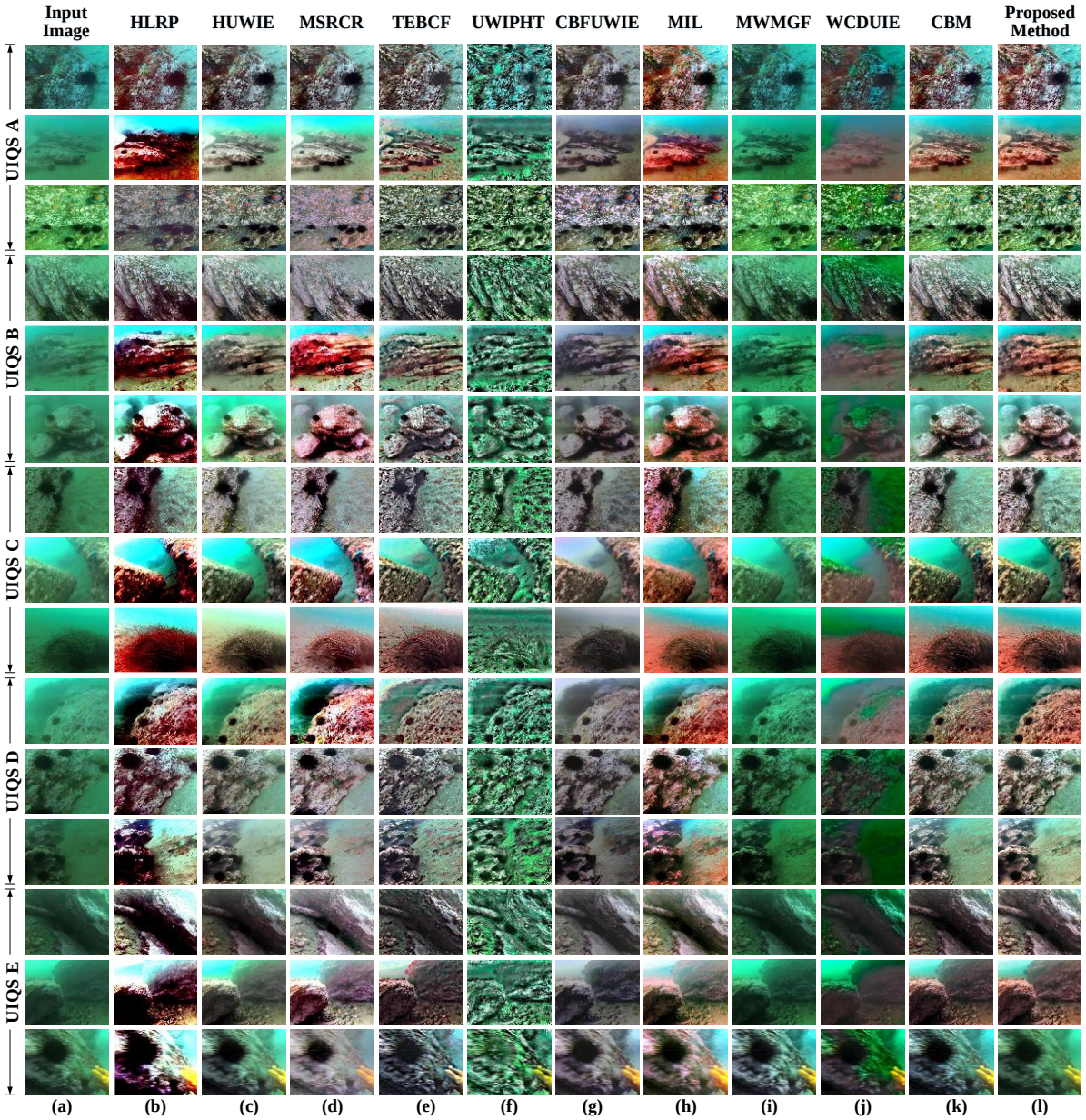

Fig. 4.9 The visual quality of the proposed method compared with existing state-of-the-art on the UIQS dataset. (a) The degraded image, followed by an enhanced image generated by (b) HLRP, (c) HUWIE, (d) MSRCR, (e) TEBCF, (f) UWIPHT, (g) CBFUWIE, (h) MIL, (i) MWMGF, (j) WCDUIE, (k) CBM, and (l) The proposed results, respectively.

4.1.3.1.4 Comparative analysis of the proposed method on the U45 dataset

Apart from the UIEB dataset, UIQS [144] dataset, and UCCS [144] dataset, we have compared the proposed method with existing deep learning base methods on the U45 dataset [148]. We have implemented the proposed method and existing state-of-the-art on the U45 dataset. The existing state-of-the-art methods have been taken for comparison, such as UIBLA [122], under water imagery using generative adversarial networks (UGAN) [126], underwater convolution

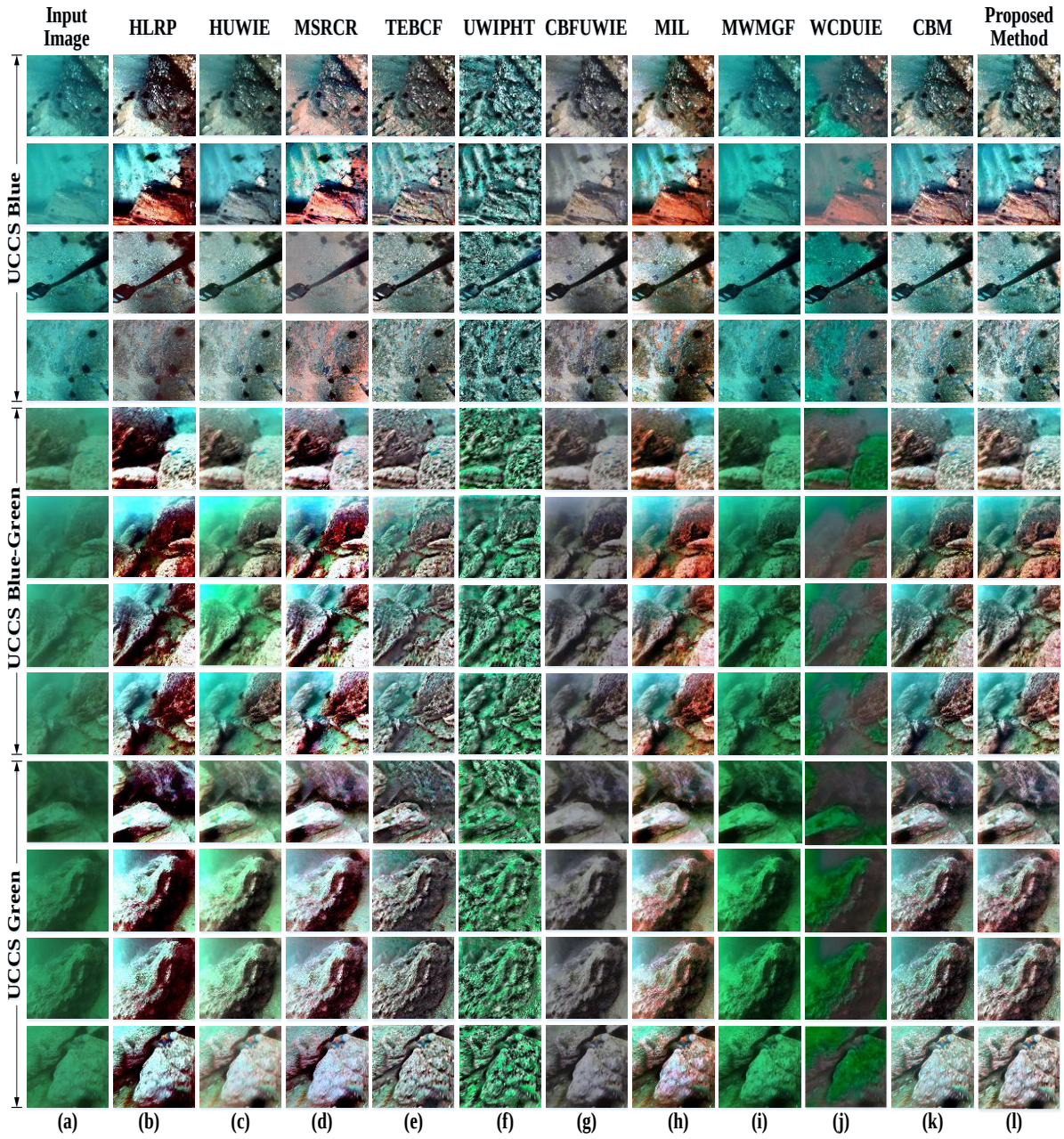

Fig. 4.10 The visual quality of the proposed method compared with existing state-of-the-art on the UCCS dataset. (a) The degraded image is followed by an enhanced image generated by (b) HLRP, (c) HUWIE, (d) MSRCR, (e) TEBCF, (f) UWIPHT, (g) CBFUWIE, (h) MIL, (i) MWMGF, (j) WCDUIE, (k) CBM, and (l) The proposed results, respectively.

neural network structure-decomposition (UWCNN-SD) [200], WSCT [182], CycleGAN [183], and FGAN [201]. Here, eight images have been randomly taken from the U45 dataset as input to the proposed and existing state-of-the-art methods. The input image and corresponding enhanced image are shown in Fig. 4.11.

From Fig. 4.11, It is concluded that the proposed method has a better-enhanced image compared to existing state-of-the-art in terms of visual quality.

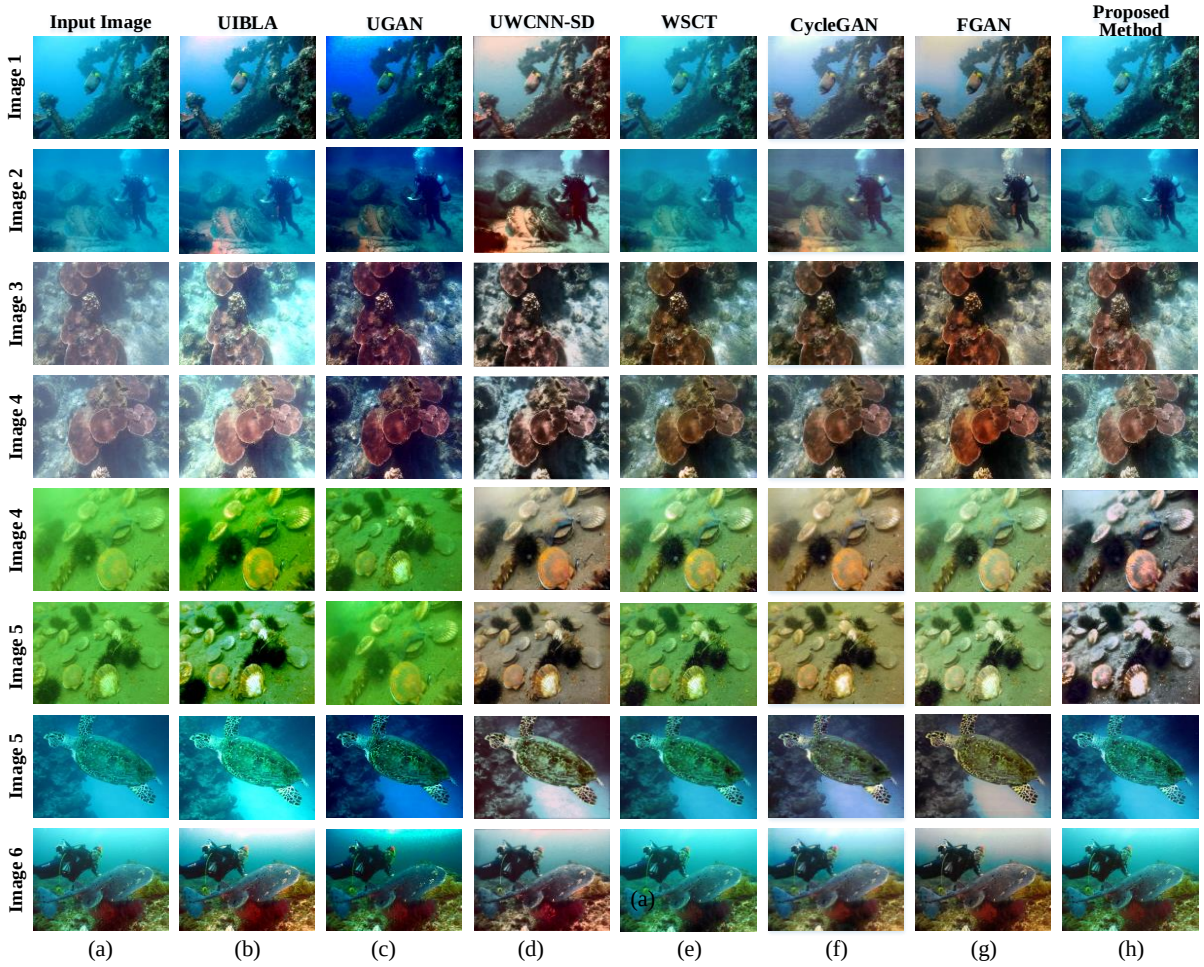

Fig. 4.11 The visual quality of the proposed method compared with the existing state-of-the-art on the U45 dataset. (a) The degraded image followed by the enhanced image generated by (b) UIBLA, (c) UGAN, (d) UWCNN-SD, (e) WSCT, (f) CycleGAN, (g) FGAN, and (h) The method results, respectively.

4.1.4 Discussion

4.1.4.1 Quantitative analysis of the proposed method on the UIEB dataset

The proposed method has been analyzed in two categories: qualitative analysis and quantitative analysis. In the qualitative study, we evaluate the visual quality of an image. Ten images have been taken randomly from the UIEB dataset in this experiment. We conduct a quantitative analysis to confirm the proposed method's effectiveness. In this assessment, the nine parameters have been taken for the evaluation of proposed method.

***Patch-based Contrast Quality Index*:** We evaluate the PCQI of ten images taken from the UIEB dataset, shown in Table 4.1. The proposed method shows better PCQI for all ten images

compared to the existing methods. Table 4.1, shows that the proposed method outperforms existing methods in terms of PCQI parameters.

Table 4.1 Comparison of patch-based contrast quality index of ten Images, taken randomly from the UIEB dataset, with the existing state-of-the-art and proposed methods.

Test Images	PCQI										
	HLRP [194]	HUW IE [172]	MSR CR [195]	TEB CF [196]	UWIP HT [197]	CBFU WIE [60]	MIL [198]	MWM GF [191]	WCD UIE [93]	CBM [199]	Proposed Method
Image1	1.287	0.710	0.993	1.088	0.800	1.192	0.998	1.101	0.972	0.986	**1.322**
Image2	0.896	0.641	0.862	0.992	0.539	0.995	1.166	1.280	0.987	1.099	**1.304**
Image3	0.986	0.797	1.091	0.979	0.854	1.071	1.139	1.259	0.992	0.986	**1.287**
Image4	0.785	0.725	1.191	0.986	0.665	0.989	1.155	1.224	1.016	1.198	**1.401**
Image5	0.475	0.751	0.790	0.788	0.701	0.789	1.055	1.025	0.465	0.491	**1.134**
Image6	0.996	0.594	0.784	0.879	0.403	0.394	1.019	1.086	0.967	0.927	**1.196**
Image7	0.978	0.791	0.987	0.985	0.880	0.987	1.101	1.166	0.924	0.982	**1.258**
Image8	0.987	0.850	0.892	0.791	0.840	0.891	1.096	1.187	0.956	0.389	**1.236**
Image9	0.987	0.687	0.994	0.591	0.764	0.913	0.836	0.681	0.822	0.757	**0.999**
Image10	0.596	0.713	0.494	0.997	0.663	1.095	1.095	1.277	0.798	0.903	**1.301**

**bold value represents the best result

***Underwater Image Quality Measure*:** The value of UIQM [184] is described in Table 4.2. The highest value of UIQM of the image represents good image visual quality. In the case of the proposed method, all ten images have the highest value except image (b). The method

Table 4.2 Comparison of underwater image quality measures of ten images taken randomly from the UIEB dataset with the existing state-of-the-art and proposed methods.

Test Images	UIQM										
	HLRP [194]	HUW IE [172]	MSR CR [195]	TEB CF [196]	UWIP HT [197]	CBFU WIE [60]	MIL [198]	MW MGF [191]	WCD UIE [93]	CBM [199]	Proposed Method
Image1	4.806	3.982	2.237	1.058	0.043	4.845	4.468	3.565	1.782	1.737	**4.896**
Image2	5.007	1.996	4.536	4.086	0.692	**5.483**	5.238	4.164	1.256	5.107	5.453
Image3	4.084	2.256	1.104	4.428	1.264	4.996	4.790	2.320	2.042	1.339	**4.998**
Image4	4.752	1.833	1.335	1.660	2.060	4.988	4.997	4.137	1.524	2.101	**5.847**
Image5	3.767	1.590	4.290	1.037	0.428	4.588	4.799	3.758	1.181	1.803	**5.788**
Image6	4.843	2.196	2.133	1.242	0.212	4.731	4.710	4.483	0.875	2.752	**4.970**
Image7	5.336	2.628	2.825	1.723	0.599	4.872	4.653	3.136	2.183	3.789	**6.476**
Image8	5.473	1.072	1.046	2.501	0.275	5.291	5.076	3.275	1.661	1.723	**5.977**
Image9	3.113	3.548	1.833	3.347	2.562	4.176	5.531	4.729	2.539	4.433	**6.531**
Image10	4.824	4.012	2.386	0.731	0.503	5.141	6.013	4.742	1.012	4.568	**6.913**

**bold value represents the best result

CBFUWIE [60] has greater values of UIQM for image (b) compared to the proposed and other existing state-of-the-art methods. From Table 4.2, it is concluded that the proposed method has a better value of UIQM compared to existing state-of-the-art except for the method [60].

***Underwater Color Image Quality Evaluation*:** The UCIQE [202] is a metric used to evaluate an underwater image's color quality. The UCIQE value of ten images of different methods has been shown in Table 4.3. The proposed method has a better value of UCIQE compared to other methods. From Table 4.3, it is concluded that the proposed method outperforms in terms of UCIQE parameters compared to the existing methods.

Table 4.3 Comparison of underwater color image quality evaluation of ten images taken randomly from the UIEB dataset with existing state-of-the-art and proposed methods.

Test Images	UCIQE										
	HLRP [194]	HUW IE [172]	MSR CR [195]	TEB CF [196]	UWIP HT [197]	CBFU WIE [60]	MIL [198]	MWM GF [191]	WCD UIE [93]	CBM [199]	Proposed Method
Image1	1.818	1.718	2.824	0.368	0.516	1.443	0.718	0.531	3.256	0.911	**3.818**
Image2	0.335	2.071	2.744	1.430	0.375	2.993	1.671	0.938	0.971	2.904	**3.993**
Image3	0.717	0.836	1.739	0.968	0.915	2.060	0.426	1.631	1.962	1.111	**2.960**
Image4	0.424	0.597	2.761	4.136	3.529	2.984	4.679	0.662	3.473	1.887	**5.136**
Image5	2.093	0.926	1.869	3.685	2.523	1.972	3.716	0.599	5.505	3.899	**5.805**
Image6	2.574	0.827	2.104	1.371	0.436	1.875	0.737	3.682	2.543	3.051	**4.132**
Image7	1.451	2.011	1.663	1.948	0.781	1.487	2.691	0.681	1.837	2.041	**3.272**
Image8	4.655	0.902	2.289	0.653	0.474	2.184	0.702	5.637	0.843	4.375	**6.735**
Image9	1.581	1.182	1.474	3.704	0.502	4.137	0.682	0.759	2.815	1.202	**4.197**
Image10	4.915	3.919	3.234	2.398	1.468	2.354	3.669	4.592	3.458	0.995	**5.216**

**bold value represents the best result

***Peak Signal-to-noise Ratio*:** The PSNR is widely used to evaluate enhanced image quality. It measures the ratio between the signal's maximum possible power and the noise's power that affects the image's quality. The proposed method performs better PSNR [73] compared to all the existing methods, as shown in Table 4.4. The proposed method shows better PSNR values for all images compared to the existing state-of-the-art methods. From Table 4.4, it is concluded that the proposed method outperforms existing methods in terms of PSNR parameters.

***Absolute Mean Brightness Enhancement*:** The absolute mean brightness enhancement, as described by [203], refers to the numerical discrepancy between the average brightness levels of an original image and a modified or enhanced version. The AMBE value of ten images of

the proposed method and existing state-of-the-art methods are shown in Table 4.5. The proposed method has a better AMBE value compared to the existing methods, as shown in Table 4.5. This represents that the proposed method has better brightness enhancement compared to existing methods.

Table 4.4 Comparison of peak signal-to-noise ratio of ten images taken randomly from the UIEB dataset using existing state-of-the-art and proposed methods.

Test Images	PSNR										
	HLRP [194]	HUWIE [172]	MSRCR [195]	TEBCF [196]	UWIPHT [197]	CBFUWIE [60]	MIL [198]	MWMGF [191]	WCDUIE [93]	CBM [199]	Proposed Method
Image1	30.67	59.92	55.70	45.19	44.85	61.35	25.27	36.81	51.25	57.72	**68.24**
Image2	30.56	42.92	57.10	58.02	51.23	62.09	20.30	29.80	52.02	59.49	**66.98**
Image3	45.89	61.91	61.82	60.26	33.80	60.34	26.50	38.67	40.12	60.65	**68.83**
Image4	36.57	60.43	58.44	54.85	36.78	58.55	30.62	45.54	44.45	55.02	**68.43**
Image5	25.81	63.02	45.69	51.31	43.46	50.49	38.76	39.12	49.74	57.65	**70.02**
Image6	36.89	49.28	58.47	57.62	42.53	51.59	26.59	43.03	51.17	61.52	**62.89**
Image7	32.98	60.94	50.87	55.91	35.31	48.24	31.01	44.09	45.76	52.74	**61.57**
Image8	37.25	50.15	48.17	45.29	42.68	55.77	27.37	46.35	54.72	50.58	**60.43**
Image9	28.98	41.1	55.96	59.90	42.74	65.00	32.32	25.08	48.29	45.28	**65.94**
Image10	36.85	48.10	48.61	52.75	50.90	40.28	28.56	37.89	47.21	40.21	**58.31**

**bold value represents the best result

Table 4.5 Comparison of absolute mean brightness enhancement of ten images taken randomly from the UIEB dataset using existing state-of-the-art and proposed methods.

Test Images	AMBE										
	HLRP [194]	HUWIE [172]	MSRCR [195]	TEBCF [196]	UWIPHT [197]	CBFUWIE [60]	MIL [198]	MWMGF [191]	WCDUIE [93]	CBM [199]	Proposed Method
Image1	30.60	58.09	54.52	56.10	27.60	34.59	60.79	45.37	34.62	52.63	**60.60**
Image2	10.76	11.18	37.71	40.41	28.01	58.82	54.82	44.89	43.91	16.89	**70.66**
Image3	25.56	92.06	34.22	35.59	41.87	28.67	50.64	51.37	38.43	43.98	**95.01**
Image4	24.98	76.99	32.57	30.56	36.97	33.09	47.11	45.41	35.89	49.98	**85.54**
Image5	21.32	29.28	99.35	28.05	33.21	47.77	39.29	29.06	79.56	45.55	**95.17**
Image6	10.87	39.21	41.17	30.42	75.79	62.89	35.24	45.61	51.43	38.69	**91.76**
Image7	18.31	87.85	29.80	56.28	61.58	35.78	58.12	35.07	38.92	27.46	**90.31**
Image8	16.31	64.45	51.85	28.24	56.52	69.36	3.363	40.61	49.74	20.49	**80.83**
Image9	15.87	36.63	90.11	47.01	67.94	14.87	14.97	28.78	83.68	21.72	**96.90**
Image10	10.87	17.00	86.73	27.60	46.46	25.69	18.34	50.04	78.81	20.90	**97.93**

**bold value represents the best result

***Contrast Per Pixel*:** As introduced in [204], the contrast per pixel metric measures the amount of contrast present in an image. A higher CPP number indicates better contrast. The CPP values of ten images of various methods as shown in Table 4.6. The proposed method has a better value compared to existing state-of-the-art methods as shown in Table 4.6. From Table 4.6, it is concluded that the proposed method outperforms in terms of CPP compared to other methods.

Table 4.6 Comparison of contrast per pixel of ten images taken randomly from the UIEB dataset using existing state-of-the-art and proposed methods.

Test Images	CPP										
	HLRP [194]	HUWIE [172]	MSRCR [195]	TEBCF [196]	UWIPHT [197]	CBFUWIE [60]	MIL [198]	MWMGF [191]	WCDUIE [93]	CBM [199]	Proposed Method
Image1	0.584	1.601	6.411	4.438	2.293	3.840	2.505	5.138	0.411	1.593	**8.310**
Image2	7.145	8.808	6.771	5.589	3.044	7.606	6.512	6.329	3.771	6.055	**11.75**
Image3	5.873	6.297	4.296	5.266	2.096	6.060	3.544	9.167	2.296	4.365	**10.45**
Image4	7.264	8.801	6.438	4.689	3.154	7.222	6.500	6.572	3.438	5.021	**11.36**
Image5	1.985	3.765	2.279	2.689	1.961	5.095	4.515	6.767	1.279	3.430	**9.936**
Image6	8.327	7.351	8.274	5.259	5.134	8.453	7.474	11.169	4.274	5.424	**12.23**
Image7	9.185	7.155	7.250	3.568	5.099	8.524	7.499	10.434	4.950	2.574	**12.89**
Image8	5.186	7.043	4.267	3.730	2.097	6.585	2.472	9.831	2.267	3.935	**10.46**
Image9	6.928	8.779	5.211	2.588	1.838	5.319	7.594	6.890	3.211	3.287	**11.56**
Image10	10.15	9.423	10.94	2.342	6.023	10.56	8.530	12.413	5.946	3.195	**14.68**

**bold value represents the best result

***Discrete Entropy*:** It is a measure used to assess the amount of information contained in an image, as explained in [205]. The entropy value increases with the amount of information present in the image. The DE value of ten images (a) to (j) is shown in Table 4.7. The proposed method has a better value of the DE parameter compared to the existing methods.

***Modified Measure of Enhancement*:** Its value shown in Table 4.8. The proposed method has a better value compared to the existing state-of-the-art methods except [191] for image (g). The existing method MWMGF [191] shows the highest value for image (g) among all the methods. From Table 4.8 it is observed that the proposed method outperforms in terms of MEME parameter.

***Structure Similarity Index Measure*:** The higher the SSIM [206] value between two images, the more similar they are in terms of their structural content. The SSIM values of the proposed method and existing methods are shown in Table 4.9. The proposed method has a better value

Table 4.7 Comparison of discrete entropy of ten images taken randomly from the UIEB dataset with proposed method and existing state-of-the-art.

Test Images	DE										
	HLRP [194]	HUWIE [172]	MSRCR [195]	TEBCF [196]	UWIPHT [197]	CBFUWIE [60]	MIL [198]	MWMGF [191]	WCDUIE [93]	CBM [199]	Proposed Method
Image1	4.884	4.150	5.283	3.499	4.919	2.871	1.043	5.038	4.507	4.209	**6.323**
Image2	5.779	6.145	7.104	4.475	6.483	4.697	6.302	5.206	3.648	5.745	**8.746**
Image3	6.996	7.352	8.280	6.779	5.097	5.917	7.292	6.195	5.659	6.828	**9.387**
Image4	5.519	5.023	6.615	4.548	5.039	3.720	5.240	4.166	4.678	4.601	**7.890**
Image5	4.613	4.296	5.059	5.008	4.116	2.880	3.240	3.150	4.108	3.393	**6.460**
Image6	4.346	3.301	5.001	4.586	4.646	2.690	4.191	3.109	5.246	3.936	**6.591**
Image7	3.989	2.071	4.318	2.682	2.858	1.686	2.172	1.098	3.533	2.898	**5.982**
Image8	6.902	7.262	8.319	6.940	7.994	5.879	7.286	6.179	3.841	6.522	**9.025**
Image9	5.960	6.192	7.277	4.230	6.709	4.884	6.088	5.186	4.680	5.990	**8.793**
Image10	4.173	4.635	4.751	3.661	4.619	2.912	5.199	4.964	4.721	3.810	**6.349**

**bold value represents the best result.

Table 4.8 Comparison of the modified measure of enhancement of ten images taken randomly from the UIEB dataset with the existing state-of-the-art and proposed methods.

Test Images	MEME										
	HLRP [194]	HUWIE [172]	MSRCR [195]	TEBCF [196]	UWIPHT [197]	CBFUWIE [60]	MIL [198]	MWMGF [191]	WCDUIE [93]	CBM [199]	Proposed Method
Image1	50.463	48.88	61.34	25.29	60.57	75.80	57.58	76.28	18.75	25.97	**80.35**
Image2	10.838	10.04	18.25	11.16	30.91	25.10	20.41	20.44	3.563	10.14	**35.48**
Image3	40.561	20.28	20.42	13.06	36.92	38.36	19.76	22.20	14.58	15.32	**44.30**
Image4	8.4556	15.60	15.42	9.462	18.02	20.66	14.81	31.40	10.37	9.109	**32.35**
Image5	6.5697	10.05	20.24	8.761	14.48	14.66	10.09	11.21	8.677	8.340	**25.38**
Image6	60.117	4.618	65.47	30.20	65.22	80.02	70.49	85.24	20.78	35.14	**89.36**
Image7	50.338	50.50	45.42	20.04	63.11	70.49	40.28	**83.31**	13.56	20.28	80.48
Image8	5.7823	7.101	10.22	4.477	10.09	10.68	10.81	21.74	9.473	7.268	**22.86**
Image9	65.459	40.95	57.71	29.40	62.55	65.50	32.84	56.85	15.58	29.74	**79.94**
Image10	4.564	3.930	16.27	11.13	18.13	15.10	14.19	5.821	10.55	12.20	**40.46**

**bold value represents the best result

of SSIM compared to existing methods except for CBFUWIE [60] and CBM [199]. The parameter SSIM has an exceptional value for the image (e) and image (d) of the methods The average value of all the parameters over 890 underwater images is shown in Table 4.10. As we conclude, the proposed method outperforms in terms of all the parameters (i.e., PCQI, UIQM, PSNR, AMBE, CPP, DE, MEME, SSIM) as compared to the existing methods, as shown in Table 4.10.

Table 4.9 Comparison of structure similarity index measure of ten images taken randomly from the UIEB dataset with existing state-of-the-art and proposed methods.

Test Image	SSIM										
	HLRP [194]	HUWIE [172]	MSRCR [195]	TEBCF [196]	UWIPHT [197]	CBFUWIE [60]	MIL [198]	MWMGF [191]	WCDUIE [93]	CBM [199]	Proposed Method
Image1	0.713	0.692	0.463	0.386	0.728	0.858	0.867	0.259	0.561	0.338	**0.881**
Image2	0.515	0.531	0.391	0.893	0.641	0.596	0.414	0.109	0.312	0.686	**0.913**
Image3	0.521	0.633	0.441	0.841	0.695	0.845	0.659	0.149	0.551	0.875	**0.892**
Image4	0.472	0.622	0.316	0.758	0.574	0.791	0.617	0.511	0.419	**0.836**	0.781
Image5	0.804	0.713	0.712	0.788	0.722	**0.924**	0.794	0.507	0.751	0.538	0.851
Image6	0.781	0.656	0.267	0.867	0.808	0.837	0.753	0.213	0.652	0.413	**0.871**
Image7	0.692	0.709	0.604	0.211	0.789	0.885	0.657	0.647	0.459	0.732	**0.921**
Image8	0.526	0.697	0.381	0.658	0.664	0.803	0.627	0.614	0.325	0.732	**0.813**
Image9	0.503	0.668	0.342	0.757	0.813	0.888	0.313	0.113	0.518	0.619	**0.889**
Image10	0.491	0.727	0.359	0.708	0.262	0.779	0.413	0.186	0.612	0.764	**0.831**

**bold value represents the best result

Table 4.10 Average quantitative measurement of existing state-of-the-art and proposed methods on 890 underwater images taken from the UIEB dataset [143]**.**

Methods	PCQI [178]	UIQM [184]	UCIQE [202]	PSNR [73]	AMBE [203]	CPP [204]	DE [205]	MEME [207]	SSIM [206]
HLRP [194]	0.973	4.982	2.015	35.86	91.43	8.495	5.861	27.89	0.542
HUWIE [172]	0.712	2.535	3.494	60.175	46.95	8.978	5.176	12.29	0.728
MSRCR [195]	0.991	4.145	2.373	61.83	52.57	7.895	4.821	11.11	0.587
TEBCF [196]	0.988	3.944	1.882	59.98	31.89	4.869	4.381	10.69	0.518
UWIPHT [197]	0.712	2.535	1.494	66.17	45.79	3.182	5.176	12.29	0.728
CBFUWIE [60]	0.990	5.146	**5.172**	68.17	39.97	7.985	4.861	8.248	0.846
MIL [198]	0.956	3.359	4.787	32.73	30.75	7.828	5.212	9.456	0.767
MWMGF [191]	1.160	3.869	1.879	41.61	40.72	8.619	5.145	28.69	0.289
WCDUIE [93]	0.954	2.169	2.379	50.50	44.79	3.782	4.986	14.67	0.736
CBM [199]	0.989	2.441	3.109	60.51	38.68	4.768	4.401	10.57	0.546
Proposed Method	**1.361**	**5.829**	4.968	**68.24**	**100.5**	**12.68**	**7.683**	**42.58**	**0.898**

**bold value represents the best result

CBFUWIE [60] and CBM [199], respectively, as shown in Table 4.9. From Table 4.9 it is concluded that the proposed method outperforms in terms of SSIM parameters.

A box plot, also known as a box-and-whisker plot, is a graphical representation of data that displays the distribution of the data through their quartiles. The box plot is composed of a box that represents the interquartile range (IQR), which spans from the 25th percentile (Q1) to the

75th percentile (Q3), and a line or "whisker" that extends from each end of the box to the minimum and maximum values that are not considered outliers. Box plots visually identify a data's range, median, distribution, and potential outliers.

Here, Fig. 4.12 illustrates the presence of the patch-based contrast quality index. The proposed method has outperformed the other state-of-the-art methods. The proposed method has shown an average of ten image increments of 38.70% and 33.68% for MIL and MWMGF methods, respectively. This increment shows that the enhanced image of the proposed method has better contrast compared to existing methods.

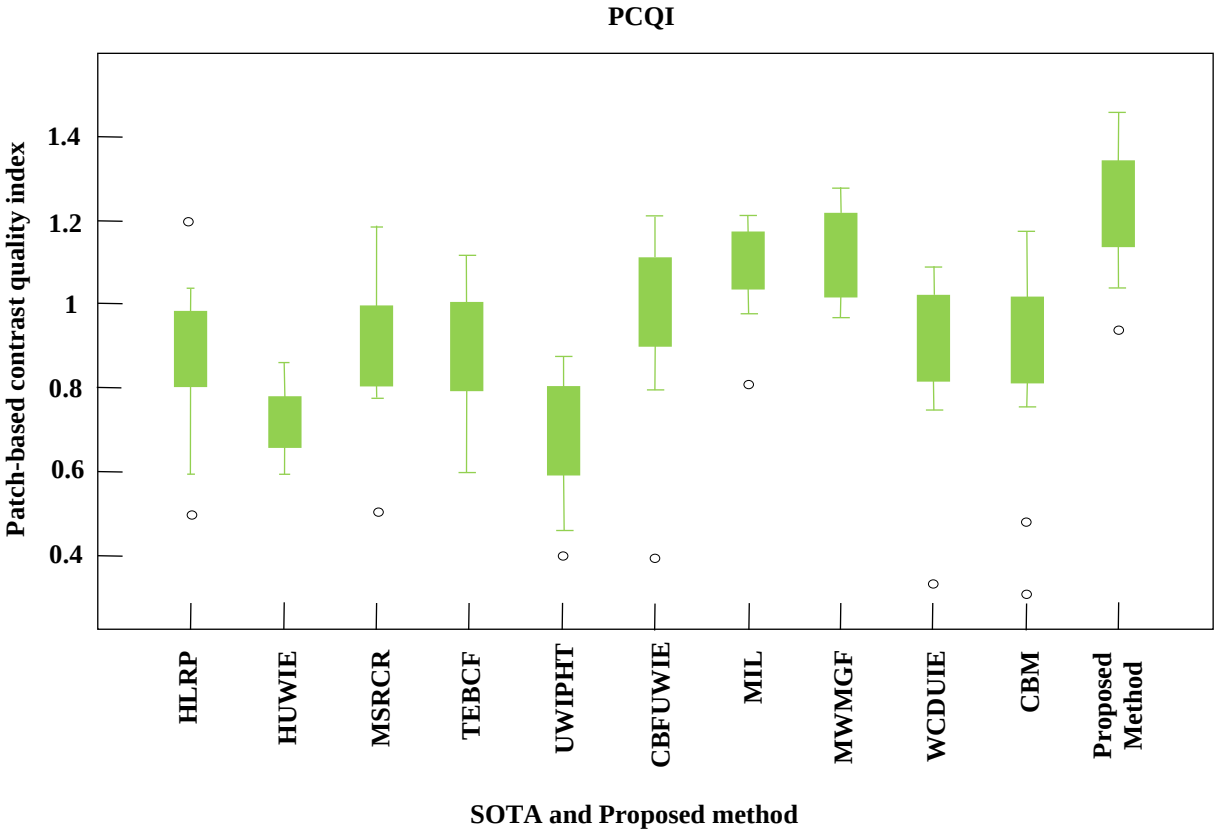

Fig. 4.12 Comparative analysis of patch-based contrast quality index with the proposed method and existing state-of-the-art (SOTA) on the UIEB dataset.

Fig. 4.13 represents the underwater image quality measure value of proposed and existing state-of-the-art methods. The proposed method has outperformed the other state-of-the-art methods as shown in Fig. 4.13. The proposed method has shown an average increment of UIQM of ten images by 15.1%, 20.47%, and 13.09% compared to the CBFUWIE, HLRP, and MIL methods, respectively. The incremental value of UIQM reveals that the output image of the proposed method has better fine details and edges compared to existing state-of-the-art methods.

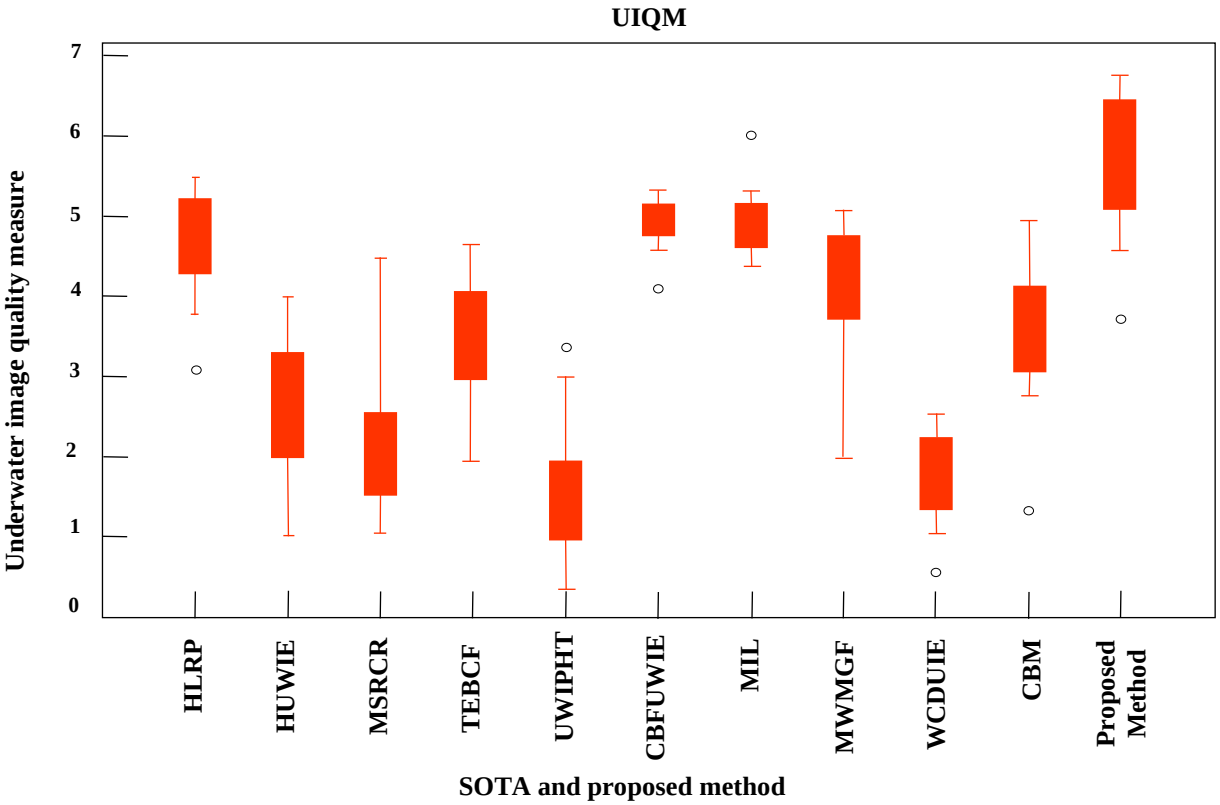

Fig. 4.13 Comparative analysis of underwater image quality measures with the proposed method and existing state-of-the-art (SOTA) on the UIEB dataset.

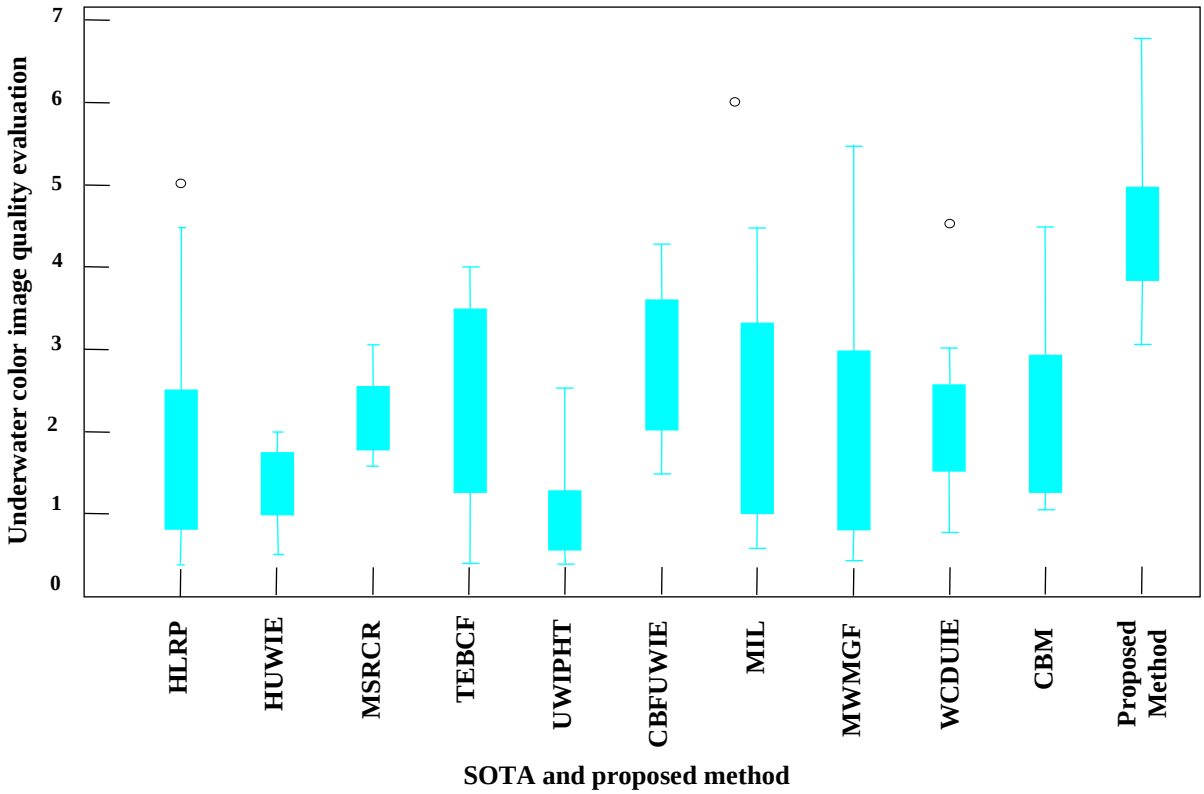

Fig. 4.14 Comparative analysis of underwater color image quality evaluation metrics with the proposed method and existing state-of-the-art (SOTA) on the UIEB dataset.

Fig. 4.14 depicts the presence of underwater color image quality evaluation. The proposed method has shown average increments in UCIQE of ten images 56.44%, 50.56%, and 41.09% for the MWMGF, TEBCF, and WCDUIE methods, respectively. The incremental value of UCIQE shows that the proposed method has a better-enhanced image in terms of contrast and sharpness.

Fig. 4.15 compares SOTA and the proposed method for peak signal-to-noise ratio. The value of PSNR of the proposed method beat 15.02%, 17.45%, 17.04%, 16.96%, and 16.99% for CBFUWIE, HUWIE, MSRCR, TEBCF, and CBM methods respectively. The increase in PSNR value shows that the proposed method has a better-enhanced image compared to existing methods in terms of visual quality.

Fig. 4.16 represents the absolute mean brightness enhancement value of the proposed method and existing state-of-the-art methods. Here, the proposed method shows better results compared to existing methods such as HLRP and MSRCR by 17.97% and 48.02% respectively. The increased value of the AMBE metric shows that the proposed method has better results compared to the existing state-of-the-art in terms of brightness enhancement.

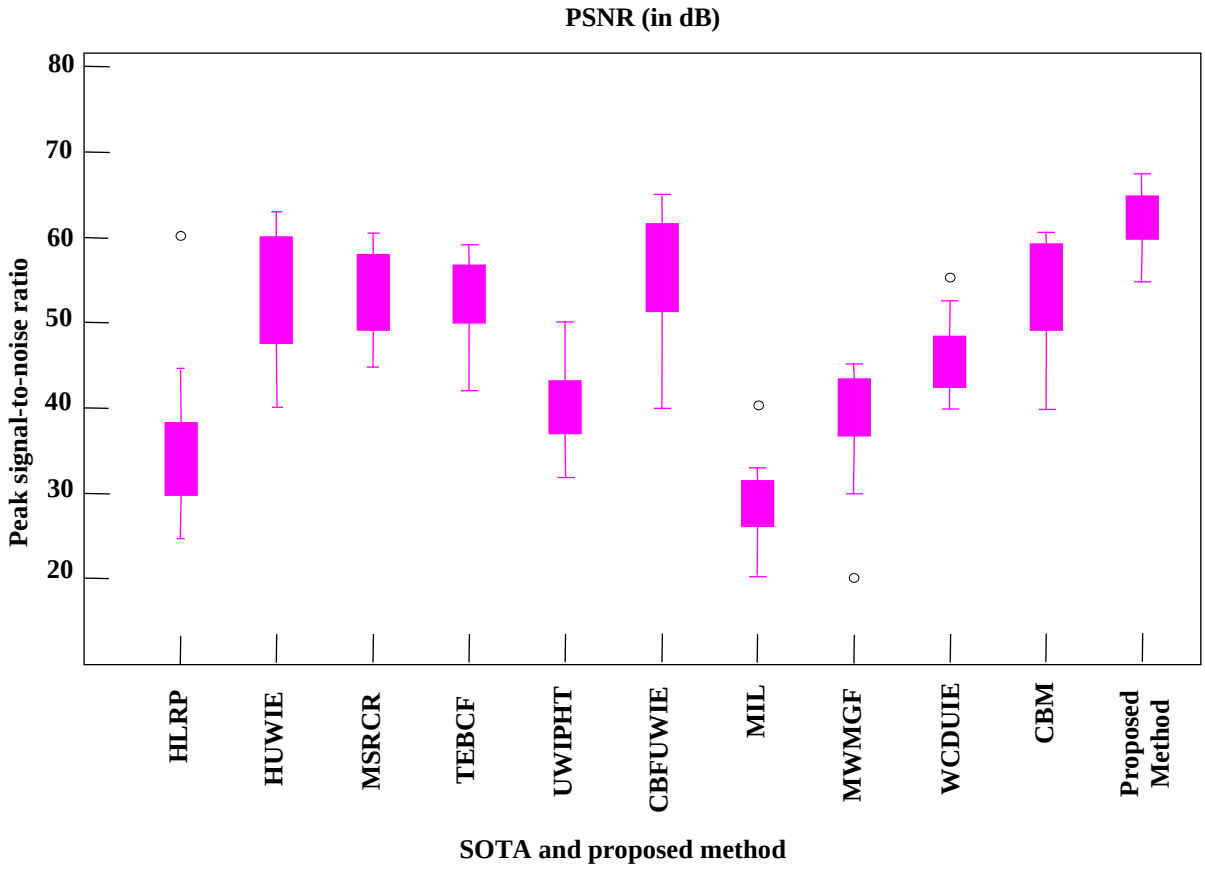

Fig. 4.15 Comparative analysis of peak signal-to-noise ratio metric with the proposed method and existing state-of-the-art (SOTA) on the UIEB dataset.

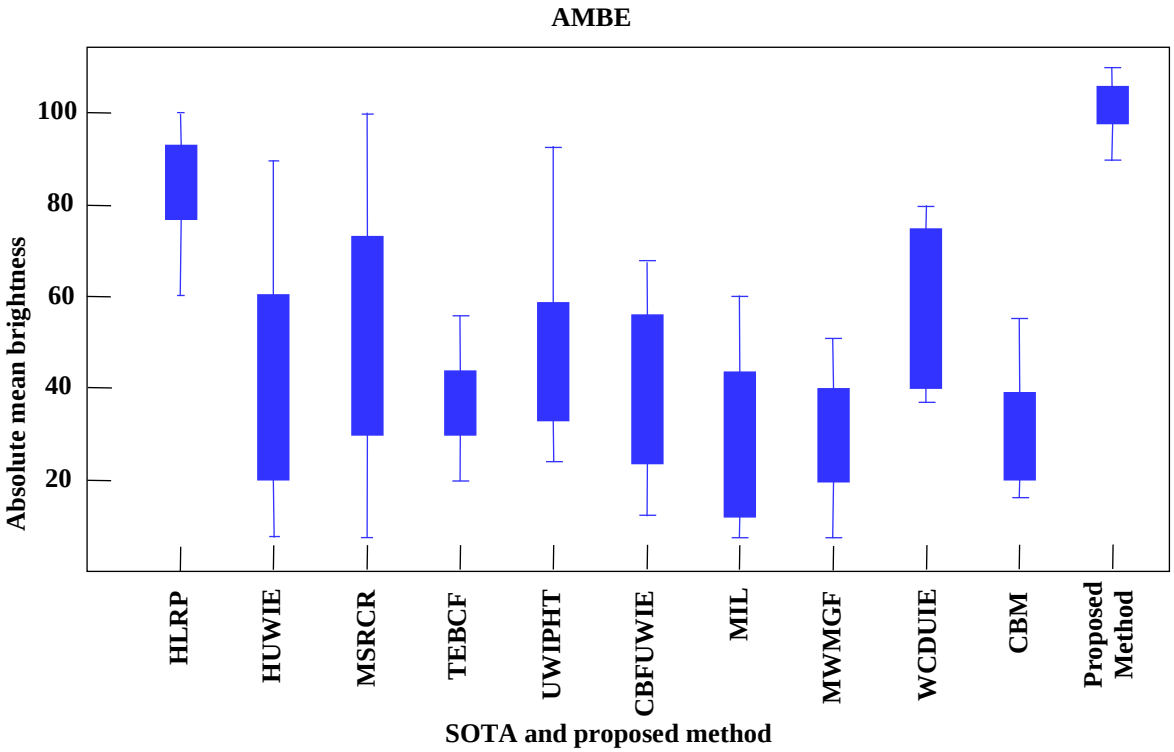

Fig. 4.16 Comparative analysis of absolute mean brightness enhancement metric with the proposed method and existing state-of-the-art (SOTA) on the UIEB dataset.

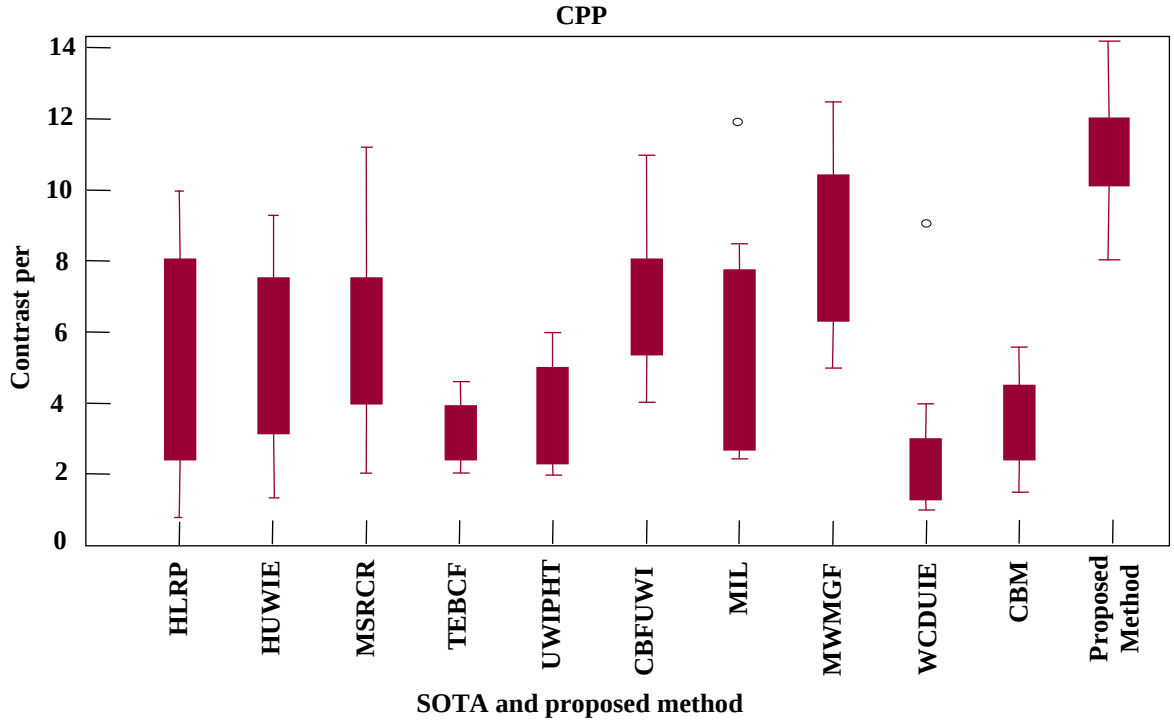

Fig. 4.17 Comparative analysis of contrast per pixel metric with the proposed method and existing state-of-the-art (SOTA) on the UIEB dataset.

Fig. 4.17 demonstrates the contrast per pixel values of the proposed method and existing state-of-the-art methods. Fig. 4.17 shows that the proposed method has the highest value of contrast

per pixel compared to existing methods. From Fig. 4.17, it concludes that the proposed method has a better-enhanced quality image compared to existing methods in terms of contrast per pixel.

Fig. 4.18 illustrates discrete entropy. Among all the existing methods, MWMGF is relatively close to the proposed method in terms of DE parameter, but less than 25.47% of DE value compared to the proposed method. The better value of DE shows that the enhanced image has more information compared to the degraded image.

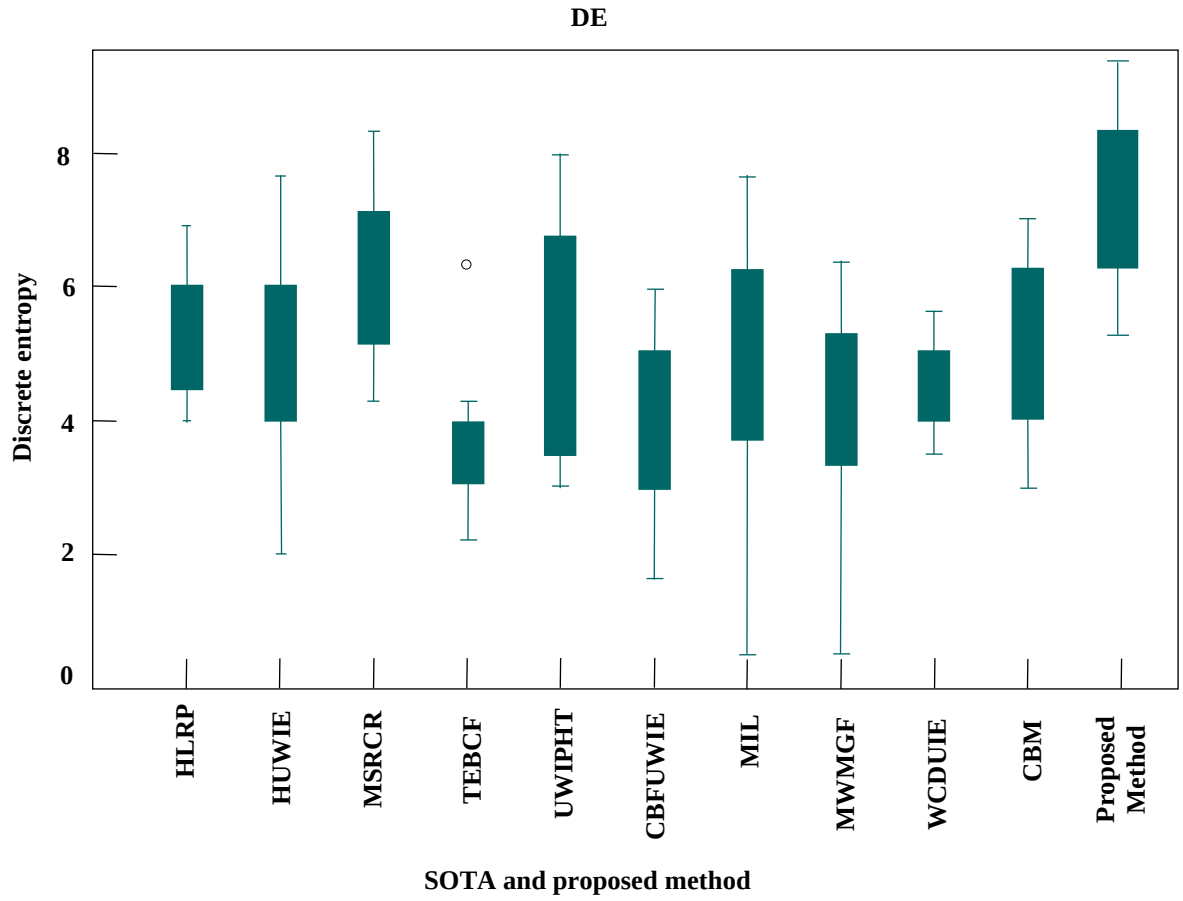

Fig. 4.18 Comparative analysis of discrete entropy metrics with the proposed method and existing state-of-the-art (SOTA) on the UIEB dataset.

Similarly, Fig. 4.19 shows the modified measure of enhancement. The proposed method has a better value of the MEME parameter compared to the existing state-of-the-art methods. The existing methods CBFUWIE, MWMGF, UWIPHT, MIL, and MSRCR are closer to the proposed method, but 21.57%, 21.93%, 28.42%, 36.39%, and 17.92% less than the proposed method, as shown in Fig. 4.19. From Fig. 4.19, it is concluded that the proposed method has a better-enhanced quality image compared to the existing methods in terms of MEME parameters.

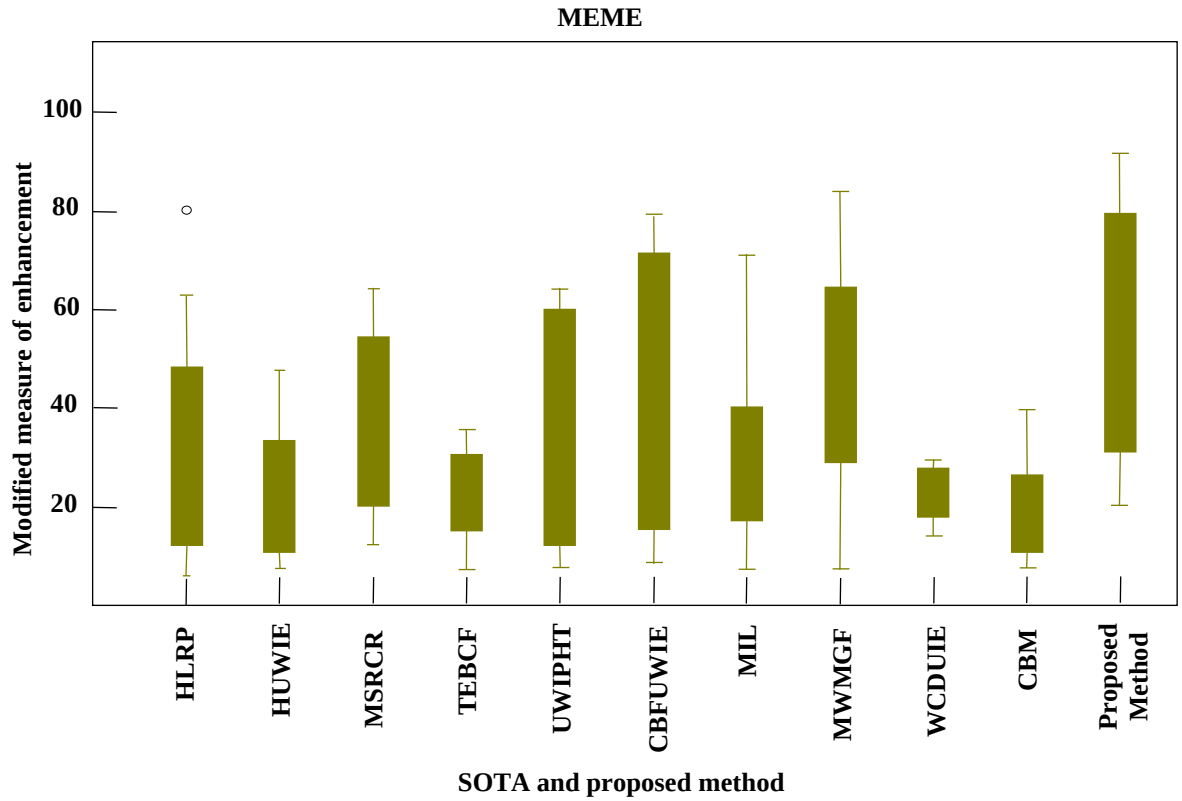

Fig. 4.19 Comparative analysis of modified measures of enhancement metrics with the proposed method and existing state-of-the-art (SOTA) on the UIEB dataset.

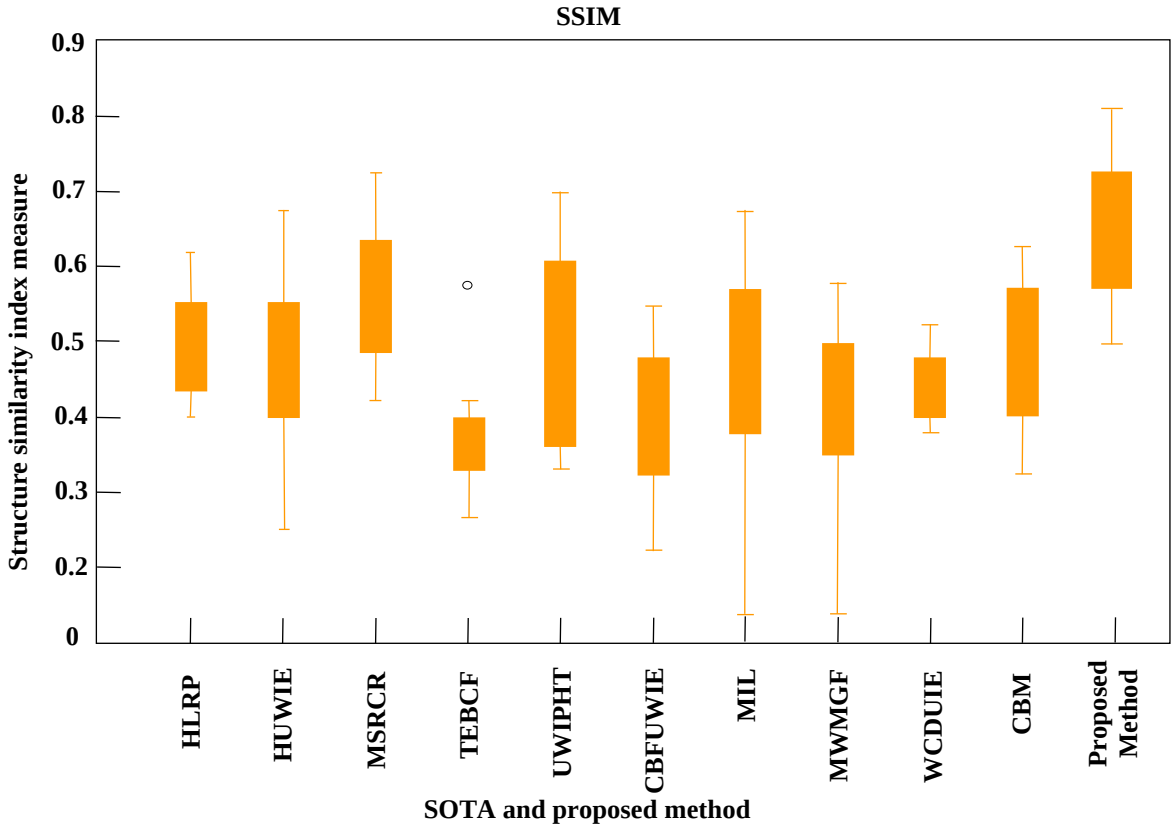

Fig. 4.20 Comparative analysis of structure similarity index measure metric with proposed method and existing state-of-the-art (SOTA) on the UIEB dataset.

Fig. 4.20 denotes the SSIM values of the proposed method and existing state-of-the-art methods. The proposed method has the highest value of structure similarity index compared to existing state-of-the-art as shown in Fig. 4.20. The percentage value of SSIM for the proposed method increased by 20.54% and 5.05% compared to TEBCF and CBFUWIE methods, as shown in Fig. 4.20. The incremental value of SSIM shows that the proposed method has better-enhanced image compared to existing methods in terms of structural information, contrast, brightness, and texture.

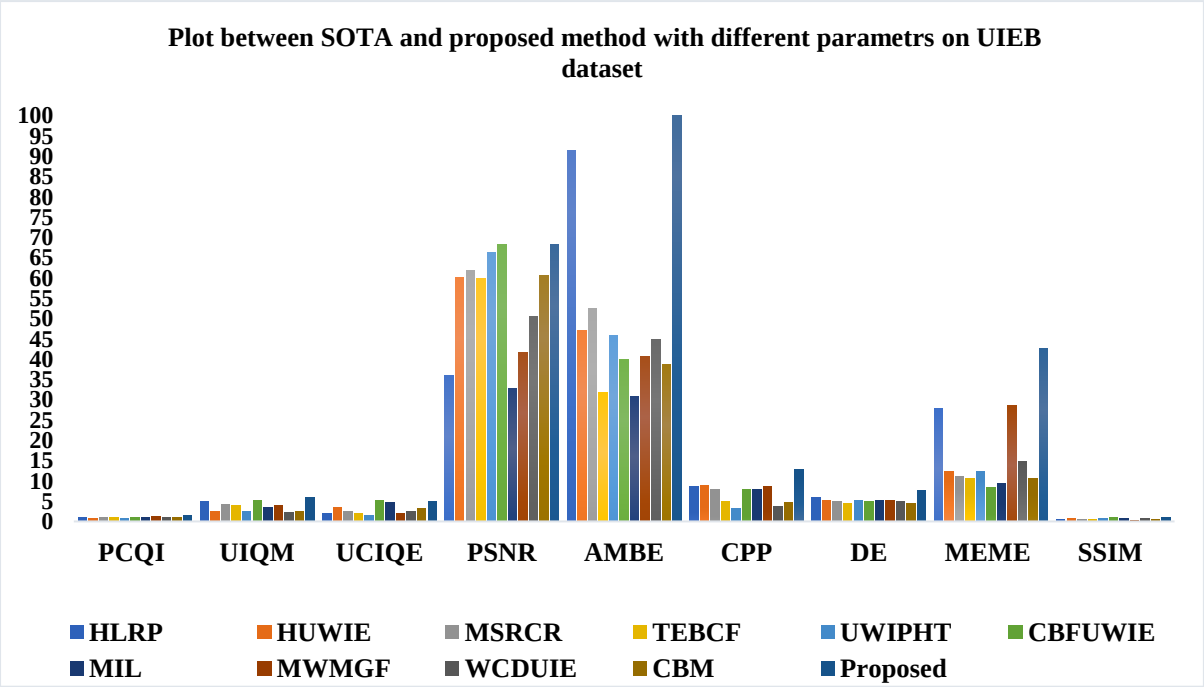

Fig. 4.21 Comparison of different metrics with existing state-of-the-art and proposed method on the UIEB dataset.

It is concluded that the proposed method outperformed the existing state-of-the-art methods in terms of PCQI, UIQM, UCIQE, PSNR, AMBE, CPP, DE, MEME, and SSIM parameters as shown in Fig. 4.21 on the UIEB dataset.

4.1.4.2 Quantitative analysis of the proposed method on UIQS, UCCS, and U45 dataset

Apart from the UIEB dataset, the proposed method has been tested on the UIQS, UCCS, and U45 datasets. Here, two parameters are taken for quantitative comparison, i.e., UIQM [184] and UCIQE [202]. The average values of UIQM and UCIQE are shown in Table 4.11, Table 4.12, and Table 4.13, respectively.

Table 4.11 and Table 4.12 show that the proposed method has a better value of UCIQE and UIQM compared to the existing state-of-the-art except for the method [60] on UIQS and UCCS dataset. The proposed method has a greater value of UCIQE and UIQM compared to existing methods on the U45 dataset as shown in Table 4.13. The greater value of UCIQE and UIQM represents the better visual quality of the enhanced image. It concludes that the proposed method outperforms existing state-of-the-art methods in terms of UCIQE and UIQM parameters.

Table 4.11 The UCIQE and UIQM of images have been compared with the existing and proposed method on the UIQS dataset.

Dataset	Parameters	HLRP [194]	HUWIE [172]	MSRCR [195]	TEBCF [196]	UWIPHT [197]	CBFUWIE [60]	MIL [198]	MWMGF [191]	WCDUIE [93]	CBM [199]	Proposed Method
UIQS A	UCIQE	0.598	0.602	0.653	0.609	0.960	**1.18**	0.669	0.842	0.453	0.630	0.788
	UIQM	3.937	2.881	2.104	4.338	5.101	5.58	4.158	5.534	3.309	3.614	**5.706**
UIQS B	UCIQE	0.598	0.584	0.543	0.607	0.241	0.83	0.680	0.940	0.260	0.617	**0.994**
	UIQM	2.553	2.740	1.131	4.355	5.197	5.31	4.174	5.550	3.284	3.416	**6.029**
UIQS C	UCIQE	0.698	0.604	0.453	0.608	0.695	0.60	0.686	1.107	0.560	0.630	**1.705**
	UIQM	2.503	3.084	1.918	4.327	5.187	4.32	4.041	5.468	4.674	3.322	**6.726**
UIQS D	UCIQE	0.890	0.572	0.813	0.595	0.548	**1.68**	0.685	0.972	0.590	0.614	1.587
	UIQM	5.464	2.853	2.944	4.376	5.216	5.60	4.087	5.603	3.706	3.226	**5.771**
UIQS E	UCIQE	0.790	0.602	0.750	0.609	0.429	0.93	0.647	0.648	0.510	0.624	**0.942**
	UIQM	2.173	2.614	2.729	4.343	5.372	5.27	3.597	1.284	4.679	3.491	**6.212**

**bold value represents the best result

Table 4.12 The UCIQE and UIQM of images have been compared with the proposed method and existing state-of-the-art on the UCCS dataset.

Dataset	Parameters	HLRP [194]	HUWIE [172]	MSRCR [195]	TEBCF [196]	UWIPHT [197]	CBFUWIE [60]	MIL [198]	MWMGF [191]	WCDUIE [93]	CBM [199]	Proposed Method
UCCS Blue	UCIQE	0.58	0.56	0.50	0.60	0.38	**1.93**	0.65	0.77	0.25	0.61	0.60
	UIQM	2.62	3.44	3.16	4.62	5.18	5.77	4.57	5.40	4.22	3.78	**6.17**
UCCS Blue-Green	UCIQE	0.59	0.60	0.51	0.61	0.36	0.76	0.69	0.70	0.49	0.63	**0.82**
	UIQM	3.25	2.27	1.51	4.26	5.39	5.46	3.81	5.57	2.06	3.10	**5.93**
UCCS Green	UCIQE	0.62	0.59	0.42	0.60	0.18	0.51	0.65	0.99	0.31	0.62	**1.15**
	UIQM	3.10	2.28	5.79	4.28	5.32	5.28	3.70	5.70	9.00	3.06	**6.66**

**bold value represents the best result

Table 4.13 The UCIQE and UIQM of images have been compared with the proposed method and existing state-of-the-art on the U45 dataset.

Dataset	Parameters	UIBLA [122]	UGAN [126]	UWCNN-SD [200]	WSCT [182]	CycleGAN [183]	FGAN [201]	Proposed Method
U45 Blue	UCIQE [177]	0.5656	0.6449	0.5896	0.5741	0.5835	0.5934	**0.7193**
	UIQM [27]	7.0359	7.2023	7.29604	7.1759	6.9993	7.0871	**7.3091**
U45 Green	UCIQE [177]	0.5568	0.6568	0.6002	0.5663	0.5748	0.5884	**0.7392**
	UIQM [27]	7.0846	7.2776	7.36406	7.2081	6.9659	7.1148	**7.9245**
U45 Haze	UCIQE [177]	0.5656	0.6449	0.5872	0.5741	0.5835	0.5915	**0.7092**
	UIQM [27]	7.0359	7.2023	7.22892	7.1645	6.9993	7.0872	**7.3214**

**bold value represents the best result

The first part of this chapter represents the enhancement solution for underwater images based on white balance and blending techniques. In the second part, we provide a solution for underwater image restoration using color correction and empirical mode decomposition.

4.2 Underwater Image Restoration Based on Color Correction and Empirical Mode Decomposition

Underwater images are a significant area of research to uncover the underwater for sea bottom exploration and navigation. Due to extensive ocean floor investigation for studying coral reefs, fish recognition, historical heritage site assessment, and other related operations, underwater image processing has received widespread acceptance and interest among scholars [208]. The visual quality of underwater images is fuzzy. This fuzziness is caused by the medium's turbidity, scattered particles, and limited visibility range. Artificial light is used to increase this visibility range, but it also produces forward and backward scattering, along with color attenuation, which leads to low-contrast images. Apart from that, the red color component suffers the most significant attenuation due to the longest wavelength, resulting in poor red composition in underwater images.

In the proposed method, image restoration is done using color correction and empirical mode decomposition. The main contributions are as follows:

- The color correction has been done before changing *RGB* to *HSV* color space to correct the color cast of the degraded underwater image.
- The Empirical mode decomposition algorithm decomposes the image into the intrinsic mode function.

- We have applied the iteration process to the intrinsic mode function (*IMF)*. Finally, concatenate all components of color space to obtain an enhanced image.

4.2.1 Proposed Methodology

Here, a novel method has been proposed for underwater image restoration. The process has created to increase contrast while preserving the brightness of the original image. The degraded image has been taken from the underwater image enhancement benchmark data set. The proposed method depends on the image restoration method, which contains the following key

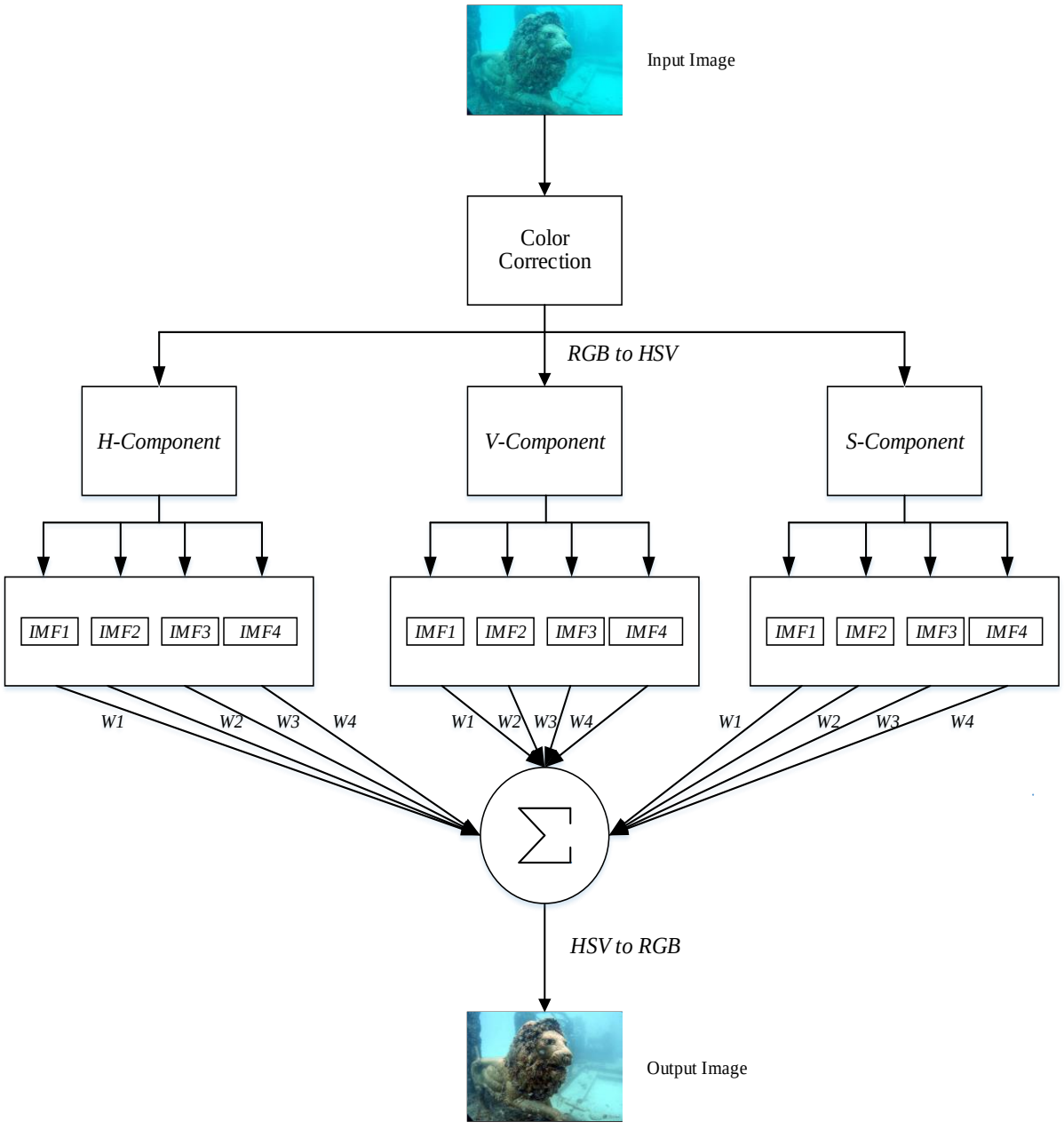

Fig. 4.22 Flow diagram of the proposed work based on color correction and empirical mode decomposition for underwater image.

factors: converting *RGB* to *HSV* color space, color correction, empirical mode decomposition, adding all the *IMF* with assigned weight, and finally, converting *HSV* color space to *RGB* color space as shown in Fig. 4.22.

4.2.1.1 Color Correction

To restore the color distortion of the original image, color correction is applied to the deteriorated input image. A linear mapping model based on a Gaussian distribution is used for color correction. The color-corrected image has been evaluated from Eqn (4.1), Eqn (4.2), and Eqn (4.3) in sub-section 4.1.2.1.

4.2.1.2 Empirical Mode Decomposition (EMD)

Huang et al. [209] introduced an empirical mode decomposition as a flexible time-frequency image data analysis technique. Intrinsic mode functions are generated using the non-parametric data-driven analytic tool. EMD analyses non-linear, non-stationary signals [210]–[212]. This technique decomposes the image (two-dimensional signal) without leaving the time domain into the intrinsic mode function. We also get a residue signal in addition to the *IMFs*. The higher-order *IMFs* capture the slower oscillating signal types. Meanwhile, the lower-order *IMFs* catch faster-oscillating signal patterns [213].
The obtained *IMF* and original signal are orthogonal to each other. The valid *IMFs* must satisfy the following criteria:

- Only one maxima present between zero crossings is permitted for an *IMF*.
- The mean value of the envelope is defined by local maxima, and the local minima must be zero at any point in the envelope created by image pixel data.

IMFs are calculated using a straightforward shifting technique. The original image pixel data is sifted until the subsequent pixel data sequence is fixed. The process is iterative and proceeds as follows:

(a) First, assume that the corrected input image, $I_{m,n}(i,j) = I_{m,cc}(i,j)$ where $I_{m,cc}(i,j)$ represent the color-corrected image. The variable, $m = 1,2,3 \ldots\ldots, M$, means the total intended number of *IMFs*, and $n = 1,2,3,4 \ldots\ldots N$ is the number of iterations required to produce one *IMF*.

(b) Then, all local maxima generated by the 2-D envelope and local minima generated by the 2-D envelope in the input are interpolated using a 2-D cubic spline. Then, generating the upper envelope $E_1(i,j)$ and lower envelope $E_2(i,j)$.

(c) The mean envelope $E(i,j)$ is evaluated by mathematically $E(i,j) = \left(\frac{(E_1(i,j)+E_2(i,j))}{2}\right)$

(d) From the input image, $I_{m,n}(i,j)$, the mean envelope $E(i,j)$ is subtracted. Mathematically, it is defined as, $s_{m,n}(i,j) = I_{m,n}(i,j) - E(i,j)$.

(e) There is a stopping criterion (α), which is required to evaluate and show how many iterations are needed. It is assessed by $\alpha = \frac{\sum_{i=1}^{P}\sum_{j=1}^{Q}|E(i,j)|}{P\times Q}$, where P and Q represent the average envelope's dimensions $E(i,j)$. Now, if the defined condition is less than the specific value, i.e., $\alpha < \gamma$ for a specific $k = K$ where γ is the particular threshold, then $s_{m,n}(i,j)$ is the m^{th} *IMF*, i.e., $IMF_m(i,j) = s_{m,n}(i,j)$. If the condition is not met by the stopping criterion, i.e., $\alpha > \gamma$ then the input $I_{m,n}(i,j)$, used to begin the following loop, and steps (a)-(e) are repeated.

(f) If the m^{th} *IMF* i.e. $IMF_m(i,j)$ is properly obtained, the residual signal is then determined as follows: $\mathcal{R}_m(i,j) = I_{m1}(i,j) - IMF_m(i,j)$.

(g) The residue ($\mathcal{R}_m(i,j)$) is used as an input image to determine the subsequent *IMF*, and steps (a)-(f) are repetitive again. In the above-proposed algorithm, we obtain 'm' $IMF_m(i,j)$ and the final residue ($\mathcal{R}_m(i,j)$). The final image of this algorithm is the summation of all the *IMFs* and residue, and it is represented mathematically as $I(i,j) = \mathcal{R}_m(i,j) + \sum_{m=1}^{M} IMF_m(i,j)$.

(h) The outcome demonstrates that the higher-order *IMF(i,j)* lack spatial properties and have low-frequency characteristics. The lower-order *IMF(i,j)* will provide a more detailed view of the overall spatial structure of the image.

$$S(i,j) = \sum_{m=1}^{M} \mathrm{W}_m \times IMF_m^R(i,j) + \mathrm{W}_m \times IMF_m^G(i,j) + \mathrm{W}_m \times IMF_m^B(i,j) \qquad (4.11)$$

where $S(i,j)$ denotes the restored image, and W_m represent the weight of m^{th} $IMF_m(i,j)$. Here, we took four *IMFs(i,j)* and four corresponding weights, such as W_1, W_2, W_3, and W_4 respectively. The numerical value of weight is taken as 0.15, 0.3, 0.25, and 0.2, respectively.

4.2.2 Results and Discussion

4.2.2.1 Qualitative Analysis

Here, images have been taken of size 900 × 900 pixel value from the U-45 dataset. The output image of existing methods such as MSRCR [173], HUWIE [214], RB [100], RED [64], WSCT [182], and the proposed method has been shown in Fig. 4.23. The proposed method shows better visual results than other methods. The existing method RED [64] does not preserve the naturalness of the image because it produces a brighter image. The red component is dominant in the MSRCR [173] approach, as shown in Fig. 4.23.

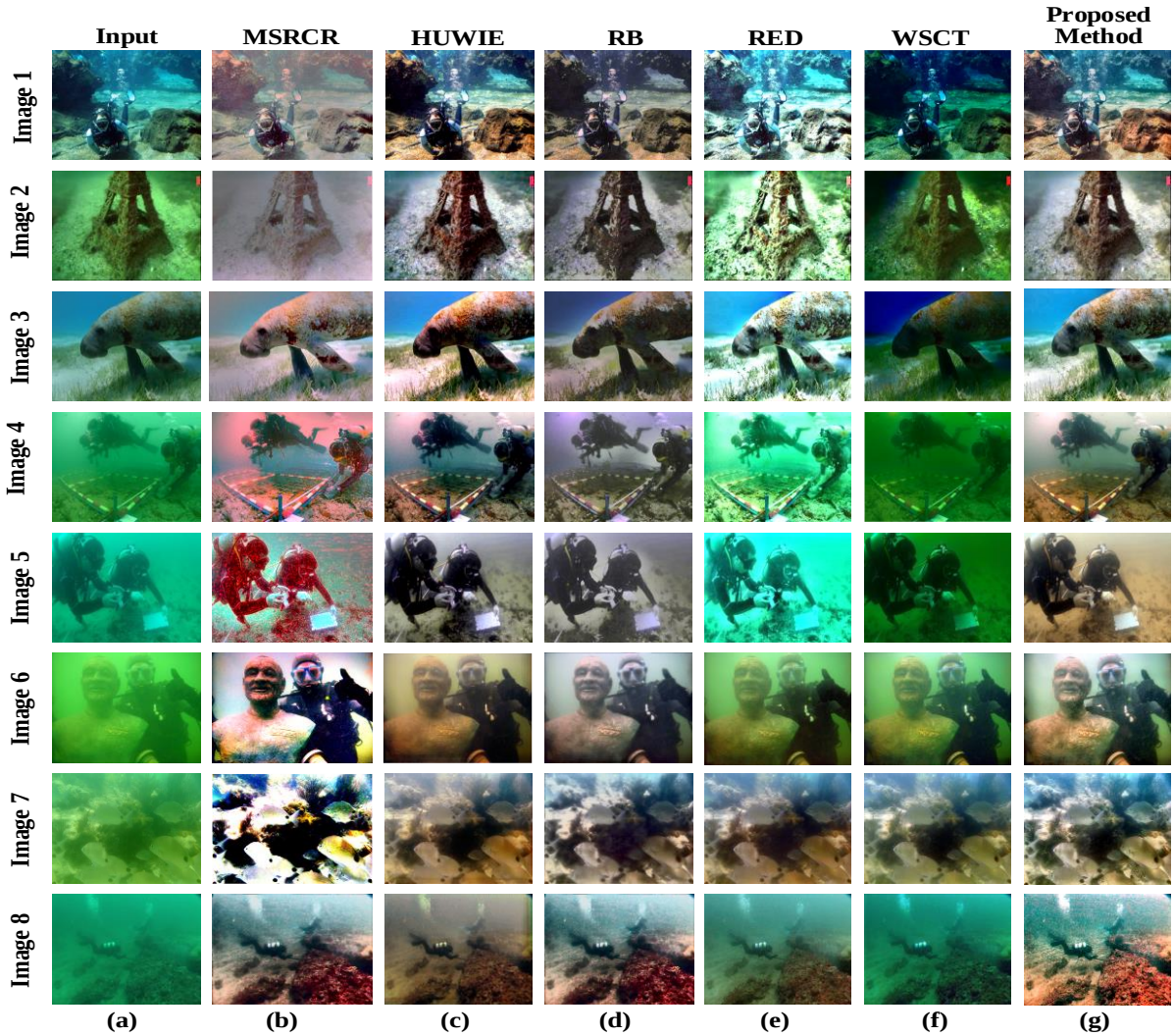

Fig. 4.23 (a) The first column represents the input image; the rest are the output images of (b) MSRCR, (c) HUWIE, (d) RB, (e) RED, (f) WSCT, and (g) the proposed method, respectively.

4.2.2.2 Quantitative Analysis

Apart from qualitative analysis, we have also done a quantitative analysis to assess the superiority of the proposed method. Here, two parameters have been evaluated, i.e., SSIM [207] and PCQI [31], of the five images shown in Table 4.14 and Table 4.15 respectively. The

numerical value of the parameters of five images in the case of the proposed method is better than the existing methods. The SSIM value of five images for the proposed method is better compared to existing state-of-the-art methods as shown in Table 4.14. The better value of SSIM

Table 4.14 Comparative analysis of proposed method with existing state-of-the-art on the U45 dataset for SSIM matric.

Methods	Image1	Image2	Image3	Image4	Image5
MSRCR [173]	0.2056	0.7115	0.2674	0.8096	0.3220
HUWIE [214]	0.7692	0.7475	0.8547	0.6565	0.7964
RB [100]	0.7732	0.8687	0.8654	0.8969	0.8395
RED [64]	0.6211	0.7345	0.6055	0.7660	0.5940
WSCT [182]	0.5605	0.7076	0.7302	0.1263	0.6162
Proposed Method	**0.7783**	**0.8774**	**0.8862**	**0.9075**	**0.8583**

**bold value represents the best result.

is represented by the changes in structural information, brightness, contrast, and texture, which are preserved.

Similarly, the value of PCQI of five images for the proposed method is better compared to the existing methods as shown in Table 4.15. The higher value of PCQI shows the good picture quality of the proposed method compared to existing methods.

Table 4.15 Comparative analysis of proposed method with existing state-of-the-art on the U45 dataset for PCQI matric.

Methods	Image1	Image2	Image3	Image4	Image5
MSRCR [173]	1.588863	1.492424	1.590777	0.991324	0.788415
HUWIE [214]	1.094639	0.801381	0.793299	0.770594	0.545680
RB [100]	1.888685	0.991376	1.492853	0.992954	0.786136
RED [64]	1.759761	0.765160	0.696051	0.578665	0.889791
WSCT [182]	1.684909	1.589482	0.992408	0.989215	0.685477
Proposed Method	**1.989586**	**1.598216**	**1.698654**	**1.396892**	**0.998578**

**bold value represents the best result

The graphical representation of PCQI and SSIM are also represented by a box plot as shown in Fig. 4.24 and Fig. 4.25 respectively. Fig. 4.24 indicates that the numerical value of PCQI for different images does not deviate much more in the case of the proposed method. However, the deviation of PCQI value is greater for MSRCR, RB, and WSCT which affects the visual quality of the enhanced image as shown in Fig. 4.24. Whereas, in Fig. 4.25 the SSIM metric does not

have much variation for the proposed method. The existing methods such as MSRCR and WSCT have more variation of SSIM, which affects the visual quality of the image.

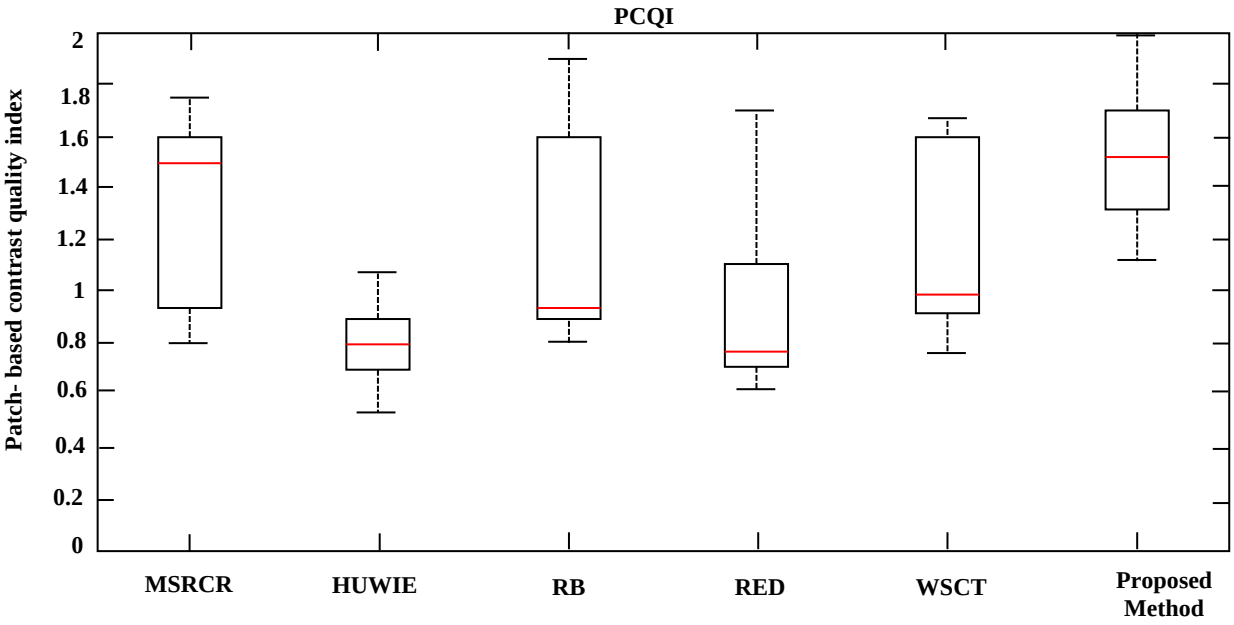

Fig. 4.24 Comparative analysis of proposed method with existing state-of-the-art on U45 dataset for PCQI metric.

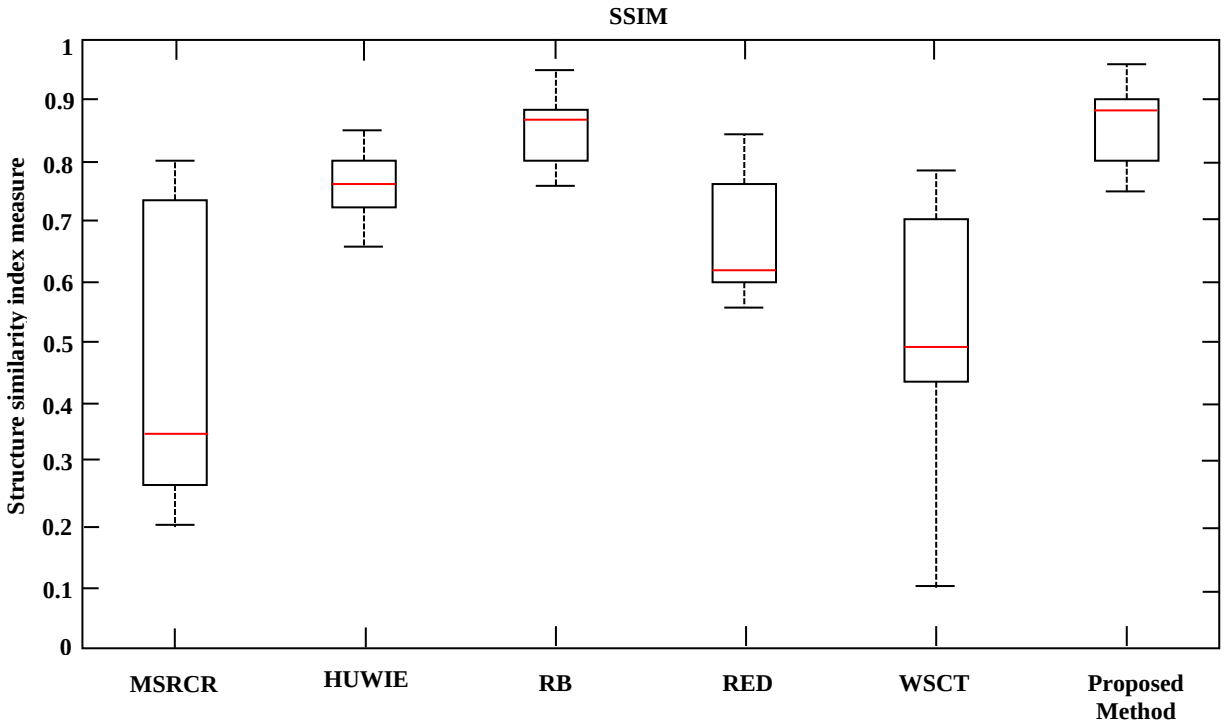

Fig. 4.25 Comparative analysis of the proposed method with existing state-of-the-art on the U45 dataset for SSIM metric.

4.3 Summary

In this chapter, an enhancement method for underwater images that utilizes a multi-weight and blending approach is presented. Unlike traditional methods that rely on information from a single original image, the proposed method directly operates on a degraded image to improve its quality without requiring additional data. The proposed technique enhances underwater images through a three-step process. First, the pre-process the original image to correct its color. Second, the images were decomposed, and a blending process has applied to address the issue of unnaturalness and blurred details. Finally, subjective and objective assessment criteria have evaluated the proposed method's performance. According to the experimental findings, the algorithm consistently enhances image contrast, resolves color shift issues, and accurately captures channel-specific details without compromising the integrity of the original color information. The visual impact of the enhanced image is notably superior to that of the original. The proposed method "underwater image enhancement based on white balance and blending technique" implemented on the UIEB, UIQS, UCCS, and U45 dataset it is observed that the proposed method outperforms existing state-of-the-art methods HLRP, HUWIE, MSRCR, TEBCF, UWIPHT, MIL, MWMGF, WCDUIE, CBM, UIBLA, UGAN, UWCNN-SD, WSCT, CycleGAN, and FGAN in terms of PCQI, UIQM, UCIQE, PSNR, AMBE, CPP, DE, MEME, and SSIM parameters on the.

Here, the second novel method is proposed for restoration of underwater images in this chapter. A color correction is applied to the degraded underwater image. Then, *RGB* color space images is convert into *HSV* color space. The HSV color-corrected image is used as input for the *EMD* algorithm. Here only first four intrinsic mode functions of empirical mode decomposition have been taken of the color-corrected image. Then, take the weighted sum of all the components. Finally, the obtained image is converted into *RGB* color space to obtain a restored image. The proposed method is compared with the existing state-of-the-art methods. It shows superior visual quality compared to other existing state-of-the-art methods. The "underwater image restoration based on color correction and empirical mode decomposition" method is implemented on U45 dataset. It is observed that the proposed method outperforms existing state-of-the-art methods MSRCR, HUWIE, RB, RED, and WSCT in terms of SSIM and PCQI parameters on the U45 dataset.

The publication related to this chapter

Amarendra Kumar Mishra, M S Choudhry, and Manjeet Kumar. "An Effective and Robust Underwater Image Enhancement Approach based on White Balance and Blending Technique " (*Optics and Lasers in Engineering* Journal) **(Under review).**

Amarendra Kumar Mishra, Mahipal Singh Choudhry, and Manjeet Kumar. "Underwater image restoration using color correction and empirical mode decomposition." *2023 10th International Conference on Signal Processing and Integrated Networks (SPIN)*. **IEEE, 2023. doi:** 10.1109/SPIN57001.2023.10116627.

Chapter 5

Underwater Image and Video Enhancement and Restoration based on Fusion

This chapter focuses on the contrast enhancement and visibility restoration of degraded underwater images using principal component analysis based on the fusion of background light and transmission optimisation in detail. The background light is evaluated for degraded underwater images and fused with optimised transmission using principal component analysis. Then, color correction is applied on the fused image. Further, the effectiveness of the proposed framework has been tested on two standard datasets and evaluation of various parameters in brief. An ablation study is also performed on the method. The second proposed method is fusion of multiscale gradient-domain and gamma correction to enhance and restore underwater images and videos in detail. The WLS filter is used for the multiscale decomposition (Base layer and detail layers) of the Y-component of YCbCr color image. Gamma correction is applied to the base layer, and gradient-domain enhancement is carried out on detail layers. The color saturation and restoration are applied to the YCbCr color image's Cb and Cr components. Then, the base layer, details layers, and color-saturated image are fused to obtain an enhanced image. The proposed framework tested for applications like low light and storm images.

5.1 Underwater Image Enhancement Based on Fusion of Background Light and Transmission Optimisation Via Principal Component Analysis

These days, there are two main categories of underwater image enhancement (UIE) techniques: based on physical models and non-physical models. The non-physical models frequently ignore the complexities of underwater imaging, which can lead to problems like over-enhancement, under-enhancement, and fake color. Physical model-based UIE techniques are significantly impacted by background lighting and depth maps. However, there are difficulties in precisely identifying the depth map of underwater images with low contrast and distortion.

Here, the proposed method is based on the physical model. In the physical imaging model, ambient light and transmission are the main causes of underwater image degradation. The

ambient light remains constant throughout the image, while the transmission factor varies significantly based on pixel position, necessitating a distinct transmission value for each pixel. The ambient light is referred to as background light. Then, the optimized transmission maps are fused with background light through principal component analysis. Finally, color correction has been applied to the fused image to obtain an enhanced image.
The main contributions are summarised as follows:

- The proposed method estimates the background light of deteriorated underwater RGB image by DCP. A highly efficient model for estimating the transmission map (TM) in underwater image processing is developed. The TM for the lightness (L) component is determined using an UDCP
- Here, the proposed method of underwater image enhancement by using transmission optimization and background light estimation via principal component analysis fusion (TOBPCA) has a two-step enhancement approach, which is presented for diverse underwater images: (a) Fusing the image using the PCA model with a BL estimator and TM optimizer, and (b) applying an image color correction algorithm on UCCS, UIQS, and UIEB Dataset.
- The proposed method outperforms the state-of-the-art methods in terms of PCQI, UCIQE, SSIM, and DE while maintaining lower computational complexity.

5.1.1 Proposed Methodology

Here, proposes a new method based on a physical model for underwater image enhancement using transmission optimization and background light estimation via principal component analysis (TOBPCA). The proposed method TOBPCA is represented in Fig. 5.1. The block diagram's components are implemented individually based on the proposed methodology (TOBPCA). The background light has been estimated by Eqn (5.1) and Eqn (5.2), and transmission of underwater images is calculated by Eqn (5.5) and Eqn (5.6). Then, the obtained transmission is optimized by Eqn (5.7). The background light and optimized transmission are fused through principal component analysis in Eqn (5.9) and Eqn (5.10). Finally, the underwater enhanced image is obtained after color correction by Eqn (5.11).

5.1.1.1 Background Light Estimation

This subsection presents a mathematical representation of the estimation of background light (BL). The simplest method for estimating background light is to find the single brightest pixel

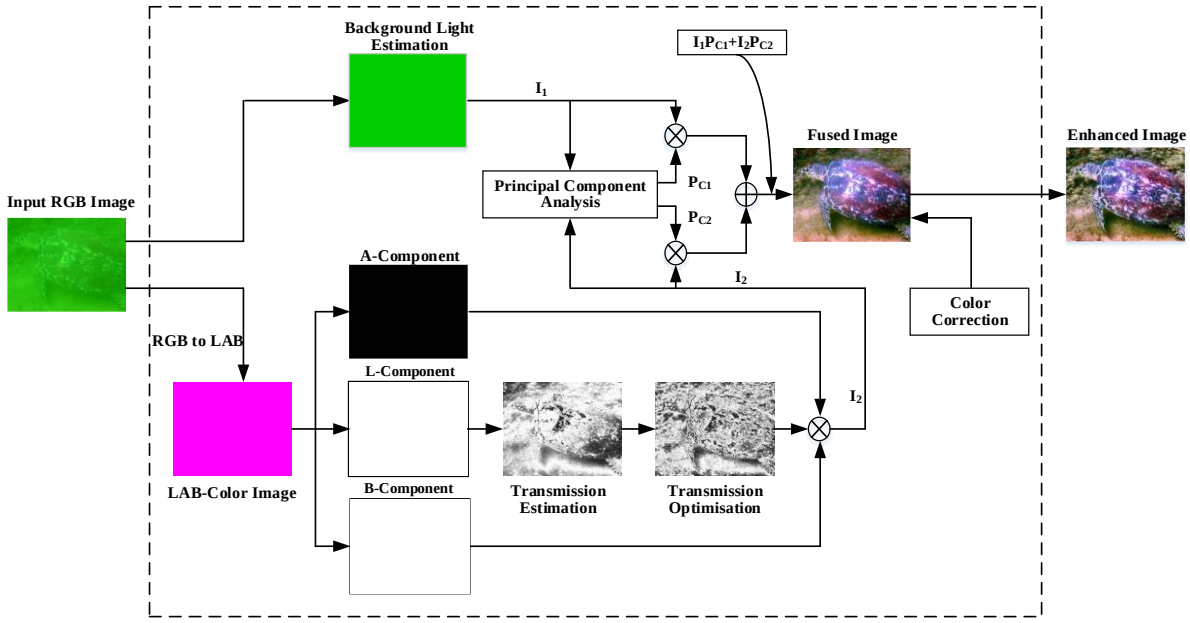

Fig. 5.1 Framework of the proposed methodology (TOBPCA) for image enhancement

in the underwater image. On the other hand, this technique could not work well when there is more light in the foreground than in the background. To mitigate the influence of suspended particles, present in the image, DCP_{rgb} based on the methods detailed in [223], we estimate background light using the pixel located at the darkest point within the image's dark channel. The background light is calculated as:

$$B_c = I_c\left(argmax\left(\min_{(i,j)\,\epsilon\,\omega}\left(\min_{c} I_c(i,j)\right)\right)\right) \tag{5.1}$$

Here, c belongs to the RGB channel and c' denotes a Green-Blue channel. Furthermore, ω, represents a local patch with a dimension of 9×9 pixels. Here, *RGB* color space is equivalent to the *CIE-Lab* color space, i.e., the *R-component* is comparable to the *L-component*, the *G-component* equivalent to the a-component, and the *B-component* of *RGB* color space is equivalent to the *b-component* of *CIE-Lab* color space.

In underwater images, water absorption often affects the red channel. Water absorbs longer wavelengths, such as red, causing a decrease in red tones and making the images appear more blue or green. This can lead to a loss of color accuracy and reduce visibility in underwater photography. To mitigate the effects of the red channel, the DCP_{gb} [62] method chooses background light by selecting the brightest pixel only from the green and blue channels, which is defined as:

$$B_c = I_c\left(argmax\left|\max_{i\,\epsilon\,\omega} I_r(i,j) - \max_{i\,\epsilon\,\omega} I_{u'}(i,j)\right|\right) \tag{5.2}$$

where, $I_r(i,j) = \text{red channel of an input image}$ and $I_{u'}(i,j) = \text{green and blue channel}$ of an input image.

5.1.1.2 Transmission Estimation

The first recapitulation of the dark channel prior introduced by He et al. [59] in most non-sky patches, there is a local patch where one or more *RGB* channel pixels have very low intensity, almost at zero. The abovementioned observation is based on statistical patterns found in clear outside images. Mathematically, it is described as:

$$Q_{dark}^{rgb}(i,j) = \min_{(i,j)\,\epsilon\,\omega^{min}}\left\{\min_{c} Q_c(i,j)\right\} = 0 \tag{5.3}$$

In Eqn (3.3) subsection 3.1.2, apply a minimum filter on both sides and divide with a background light (B_c), the resultant Eqn is as follows:

$$\min_{(i,j)\,\epsilon\,\omega}\left\{\min_{c}\frac{I_c(i,j)}{B_c}\right\} = \min_{(i,j)\,\epsilon\,\omega}\left\{\min_{c} Q_c(i,j)\right\} + \left(1 - \tau_{DCP}(i,j)\right) \tag{5.4}$$

From Eqn (5.19) and (5.20) the transmission coefficient $\tau_{DCP}(i,j)$ as:

$$\tau_{DCP}(i,j) = 1 - \min_{(i,j)\,\epsilon\,\omega}\left\{\min_{c}\frac{I_c(i,j)}{B_c}\right\} \tag{5.5}$$

Because the red channel in underwater photography is significantly attenuated, a version of the dark channel prior, known as DCP_{gb}, was devised to only look at the green (*G*) and blue (*B*) channels. To formulate $\tau_{UDCP}(i,j)$, $I_c(i,j)$ is replaced with $I_{u'}(i,j)$ in Eqn (5.5). Hence

$$\tau_{UDCP}(i,j) = 1 - \min_{(i,j)\,\epsilon\,\omega}\left\{\min_{c}\frac{I_{u'}(i,j)}{B_c}\right\} \tag{5.6}$$

5.1.1.3 Transmission Optimization

The red channel transmission given by Eqn (5.5) can be optimized by Eqn (5.7) [127]

$$\tau_{NUDCP}^{r}(i,j) = \left(1 - \min_{c}\left\{\frac{\min_{x\,\epsilon\,\omega}\left(I_c(i,j)\right)}{B_c}\right\}\right)\Big/\left(1 - \frac{0.1}{B_{max}}\right) \tag{5.7}$$

Here, $B_{max} = \max_{c} B_c$- To improve the red channel's transmission map in the Eqn (5.5), $\tau_r(i,j)$ is stretched to produce a more seamless representation within a given range ($\varkappa_{min}$, $\varkappa_{max}$).

$$\tau_{out} = (\tau_{in} - \tau_{min})\left(\frac{\varkappa_{max} - \varkappa_{min}}{\tau_{max} - \tau_{min}}\right) + \varkappa_{min} \tag{5.8}$$

To reduce the possibility of problems caused by under and overstretching, the transmission map's input and output pixels are designated as τ_{in} and τ_{out}, respectively. The transmission map's lower and upper bounds, denoted by the parameters τ_{min} and τ_{max}, are precisely adjusted to 0.2% of the respective values in the TM histograms. Furthermore, the range for the stretched gearbox map, denoted by ($\varkappa_{min}$, $\varkappa_{max}$), is set at (0.1, 0.9) to reduce the effect of stretching.

5.1.1.4 Fusion of Background Light and Optimized Transmission

The proposed method demonstrates that two images (Background light and Transmission map) are fused by principal component analysis (PCA). This method is crucial in creating a composite image that preserves essential details from the merged input image. This model uses PCA fusion by combining a TM optimization processed image with background light from an input image. The incoming images, I_1 (BL) and I_2(TM optimized), are arranged in this fusion procedure to produce a resultant matrix M_n, which is made up of two column vectors that are $2 \times n$ in size. The empirical mean vector, μ_n, is calculated using each 1×2 column vector. Each column vector has its mean (μ_n) Which are subtracted from each column to create a matrix N. Next, the covariance matrix C_n For M is calculated. Then eigen, vector Z, and Eigenvalue K are computed from a covariance matrix (C_n) and arranged them into decreasing order of eigenvalue. The dimensions of both the eigenvector and eigenvalue are 2×2 matrix. The feature vectors $Z(1)$ and $Z(2)$ linked to higher eigenvalues are identified using Eqn (5.9) to provide the principal values (P_{c_1}) and (P_{c_2}). In the end, a fused image is produced using Eqn (5.18).

$$P_{c_1} = \frac{Z(1)}{\sum Z} \text{ , and } P_{c_2} = \frac{Z(2)}{\sum Z} \tag{5.9}$$

$$Fused = P_{c_1} I_1 + P_{c_2} I_2 \tag{5.10}$$

5.1.1.5 Color Correction of Fused Image

Underwater images can be improved by the image enhancement method using the restoration parameters of the transmission maps and brightness levels. However, the fused images obtained from principal component analysis often have poor contrast and brightness, making it hard to visualize essential details. The color correction algorithm with an ideal gain factor is

the foundation of the recommended color-correcting method [192]. The color correction of the fused image is evaluated as follows:

$$\left.\begin{aligned} I_{OC} &= (I_c)/(P_{max} \times (\alpha/\alpha_{ref}) + \eta_\rho) \\ \alpha_{ref} &= \left((M_r)^2 + (M_g)^2 + (M_b)^2\right)^{1/2} \end{aligned}\right\} \quad (5.11)$$

The color-corrected image and the original underwater image are denoted by I_{OC} and I_c, respectively. M_r, M_g, and M_b represent the average values for each RGB channel in the input underwater image (I_c). The maximum value found in the RGB channels of the input underwater image I_c serves as the basis for P_{max} estimation. The parameter (η_ρ) is meticulously selected to attain the intended color augmentation for the final image. The parameter (η_ρ) lies within the given range of (0, 0.5). The brightness of the rectified image tends to decrease as η_ρ approaches 0.

After doing tests on many underwater images, it has found that (η_ρ) at 0.2 yielded a corrected image that was marginally brighter, whereas (η_ρ) at 0.3 created a significantly brighter image. Thus, 0.25 is the best value for (η_ρ) in this investigation.

5.1.2 Results and Discussion

Here, the proposed (TOBPCA) image enhancement method and existing methods are implemented on the same dataset for validation. The proposed TOBPCA method is evaluated with three datasets, namely UIEB [143], UCCS [224], and UIQS [224]. The UCCS, UIQS dataset contains 3630 images. In this study, the proposed method (TOBPCA) has implemented on these three datasets, considering their visual quality and parameter configuration. Six parameters have been used for the quantitative assessment such as PCQI [178], UCIQE [202], UIQM [184], SSIM [206], PSNR [73], and DE [205].

The proposed method is compared with ten existing state-of-the-art methods. The existing state-of-the-art method such as HLRP [194], MPORU [174], MSRCR [195], underwater hybrid technique (UHT) [197], MIL [153], HUWIE [172], TEBCF [196], CBFUWIE [60], MWMGF [191], and WCDUIE [93] were among the comparative approaches that used for qualitative and quantitative analysis. The parameter values used for the comparative examination of the proposed method versus other existing state-of-the-art methods described in the discussion as shown in Table 5.1. It is observed from Table 5.1 that the proposed method outperforms existing methods in terms of PCQI, UCIQE SSIM, and DE parameters.

Table 5.1 Comparative analysis of the proposed method in terms of PCQI, UCIQE, UIQM, SSIM, PSNR, and DE with existing state-of-the-art on the UIEB dataset.

Methods	PCQI [178]	UCIQE [202]	UIQM [184]	SSIM [206]	PSNR [73]	DE [205]
HLRP [194]	0.9978	1.3092	3.5615	*0.8725*	30.687	0.2333
MPORU [174]	*1.8263*	1.2979	2.1050	0.4871	53.488	4.9705
MSRCR [195]	0.9924	1.0956	**18.052**	0.7115	62.241	5.0824
UHT [197]	0.7651	0.5360	0.8362	0.7345	37.087	4.9293
MIL [153]	1.0911	0.6591	5.1627	0.6663	27.104	5.2384
HUWIE [172]	1.2983	0.9834	*15.060*	0.7475	*64.963*	*5.2911*
TEBCF [196]	1.1466	0.6662	3.2077	0.7843	37.090	5.1190
CBFUWIE [60]	0.9876	*1.7928*	5.1176	0.8601	**67.493**	4.3828
MWMGF [191]	1.1665	0.6813	3.1369	0.6470	30.742	4.9986
WCDUIE [93]	1.2742	0.3652	4.8135	0.3847	48.287	4.4183
Proposed Method	**2.0913**	**1.9283**	5.6921	**0.8957**	29.816	**5.8682**

**The bold value represents the most optimal results, and the Italic value represents the second highest.

5.1.2.1 Qualitative Analysis

Here, the proposed and the existing state-of-the-art methods have been implemented on the three datasets: UIEB, UCCS, and UIQS. The five degraded underwater images have been taken from the underwater image enhancement benchmark dataset, and their enhanced version, using different methods, is shown in Fig. 5.2. The first column, from the left to the right side, represents the input image, and the second to last column represents enhanced images of

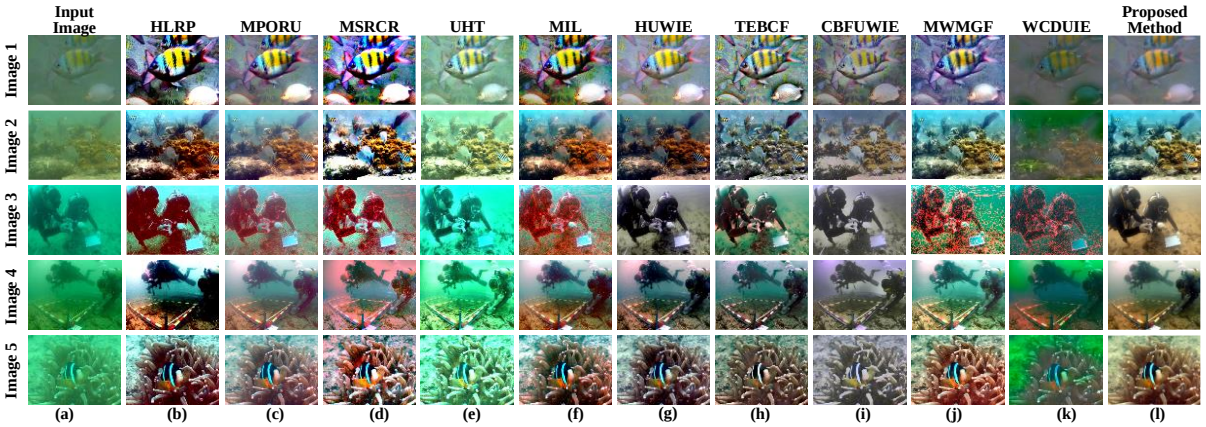

Fig. 5.2 Visual comparison of the proposed method with existing state-of-the-art methods such as (a) Degraded image, (b) Enhanced image of HLRP, (c) Enhanced image of MPORU, (d) Enhanced image of MSRCR, (e) Enhanced image of UHT, (f) Enhanced image of MIL, (g) Enhanced image of HUWIE, (h) Enhanced image of TEBCF, (i) Enhanced image of CBFUWIE, (j) Enhanced image of MWMGF, (k) Enhanced image of WCDUIE, and (l) Enhanced image of the proposed method over the UIEB dataset.

existing methods HLRP, MPORU, MSRCR, UHT, MIL, HUWIE, TEBCF, CBFUWIE, MWMGF, WCDUIE, and the proposed method, respectively.

The result shows that the proposed approach gives better visual images compared to HLRP [194], MPORU [174], MIL [153], CBFUWIE [60], TEBCF [196], and MWMGF [191] for input images such as image (2), image (3), and image (4), the HLRP, MPORU, MSRCR, and MIL methods show the more reddish color in their enhanced images, which looks like an unnatural color, as shown in Fig. 5.2. Meanwhile, the proposed method has a balanced color in the enhanced image. The enhanced image (5) of the MWMGF method shows better visual quality compared to the proposed method, as shown in Fig. 5.2. On the other hand, HUWIE and WCDUIE typically lack a natural response and have an aberrant appearance with a slightly blurred output. The results from MSRCR and UHT are optically dazzling, but they don't seem natural. The proposed method produces good visual quality among all the methods, as shown in Fig. 5.2.

5.1.2.2 Quantitative Analysis

In this subsection, the proposed method is evaluated through various parameters, including the PCQI [178], UCIQE [202], UIQM [184], SSIM [206], PSNR [73], and DE [205]. The evaluation is conducted on UIEB, UCCS, and UIQS datasets. Table 5.1 lists the average values of parameters such as PCQI, UCIQE, UIQM, SSIM, PSNR, and DE for UIEB datasets. The proposed method with the UIEB dataset provides PCQI, UCIQE, UIQM, SSIM, PSNR, and DE of 2.0913, 1.9283, 5.6921, 0.8957, 29.816, and 5.8682 respectively.

The box plot of various parameters is depicted in Fig. 5.3. The box plot represents the variation of parameter values. The box plot shows that the tweaking performance leverages the proposed method over existing state-of-the-art methods.

The variation of DE parameters of the proposed method is significant compared to TEBCF, UHT, WCDUIE, MSRCR, and HLRP but the average value is higher than that of these methods. In the case of PSNR, The MIL method has the lowest value compared to the other methods and the proposed method. The CBFUWIE, HUWIE, and MSRCR methods have almost the same PSNR value as shown in Fig. 5.3 (e). The proposed method has less variation than existing state-of-the-art methods and has the highest average value, as shown in Fig. 5.3 (e). The structural similarity index of the proposed method varies between 7.5 and 9.8, which

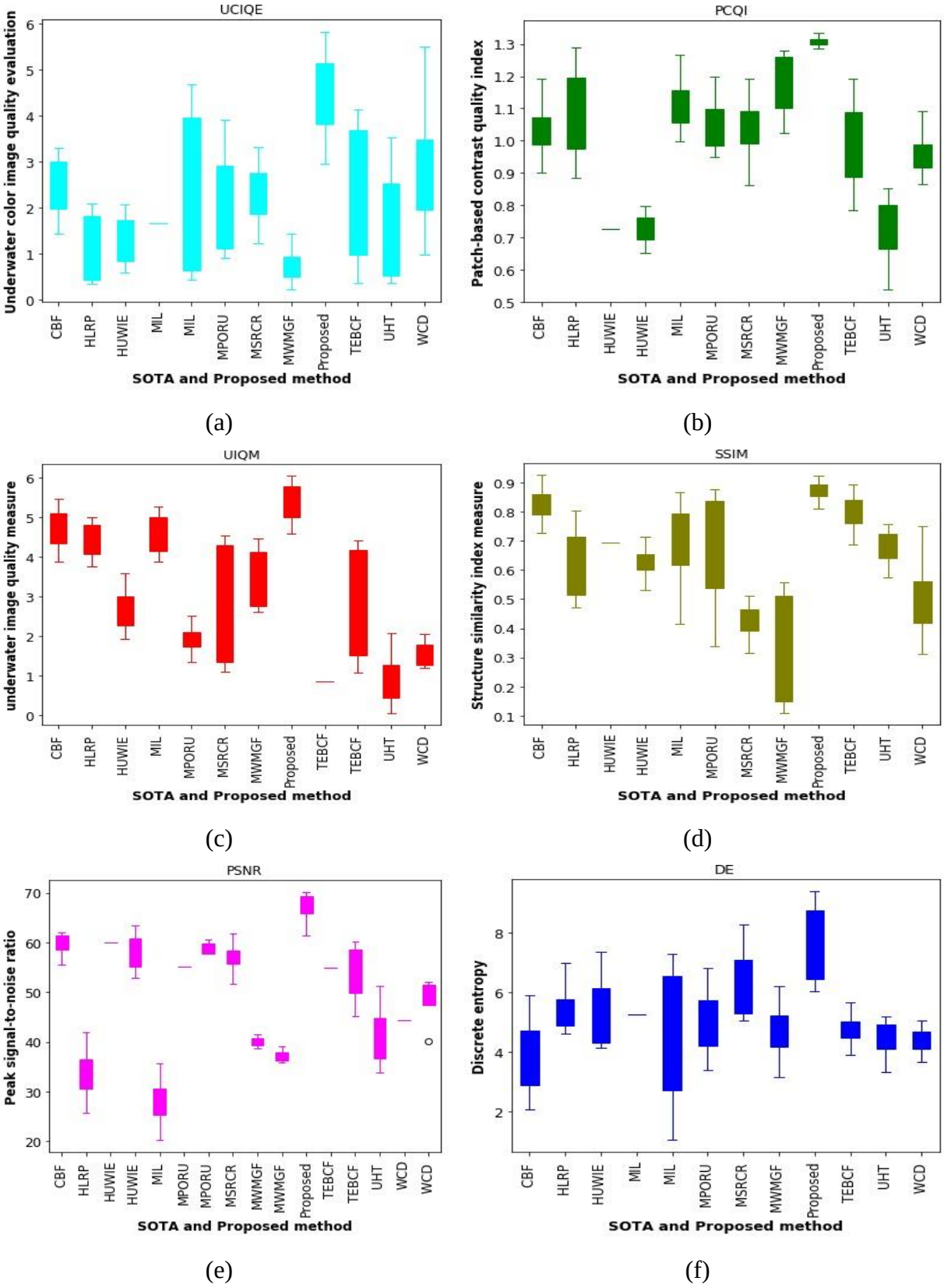

Fig. 5.3 Box plot of the performance metrics such as (a) UCIQE (b) PCQI (c) UIQM (d) SSIM (e) PSNR and (f) DE of the proposed method and existing state-of-the-art (SOTA) methods over UIEB datasets.

shows less variation compared to the existing method, as shown in Fig. 5.3 (d), where the average value is greater than that of the existing methods. The variation of the proposed method's underwater image quality measure parameter lies between 4.5 to 6, which shows less variation compared to other methods except for MPORU and WCDUIE. Still, the average value of the proposed method is the highest among all different methods, as shown in Fig. 5.3 (c). The value of PCQI varies from 1.25 to 1.35 in the proposed method, which shows less variation than in the existing method, whereas the average value is higher than that of other methods. It is concluded from Fig. 5.3 that the proposed method shows superior results compared to most existing methods.

5.1.2.3 Ablation Study

In this subsection, the ablation test has been conducted on UCCS [224], UIQS [224], and UIEB [143] datasets. The ablation test of each important step in the proposed TOBPCA method separately shows how each contributes positively to its effectiveness. Categorically, the different stages of ablation study are defined as follows: (1) the proposed method (OTBPCA) without Transmission optimization (-w/o TO), (2) the proposed method (TOBPCA) without

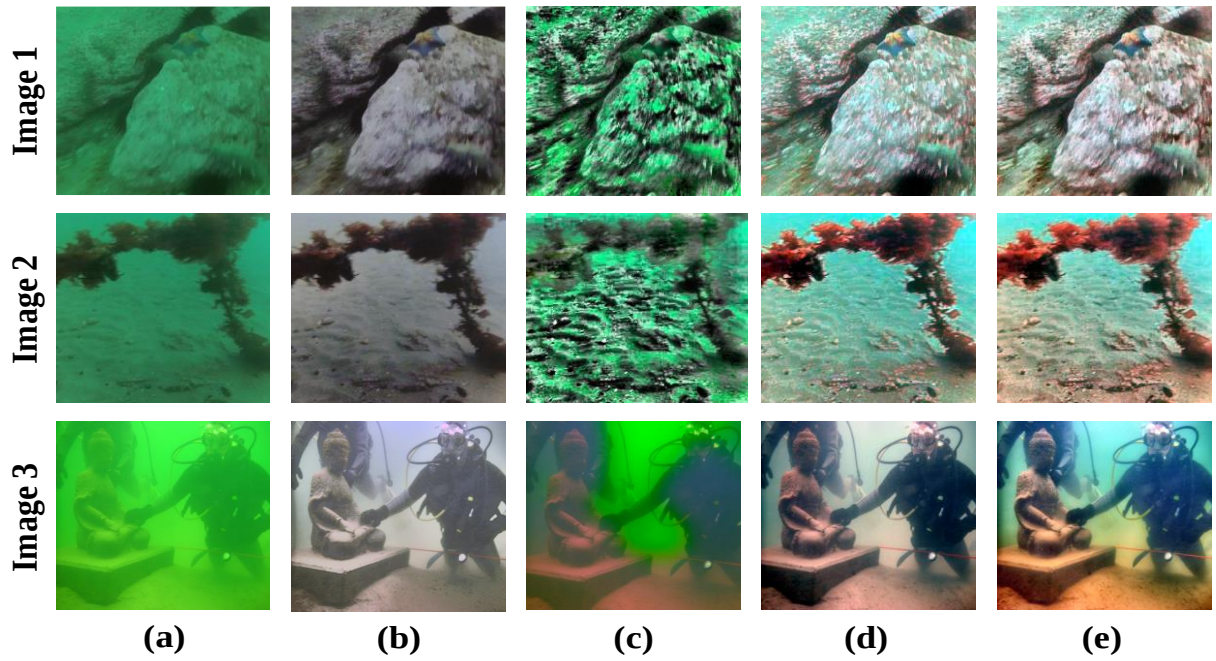

Fig. 5.4 Ablated results of each core component of the proposed method on UCCS, UIQS, and UIEB datasets. From top to bottom, the raw images (a) are derived from UCCS, UIQS, and UIEB datasets. The ablated results using (b) -w/o TO, (c) -w/o PCA, (d) -w/o CC, and (e) TOBPCA (full model).

principal component analysis (-w/o PCA) (3) the proposed method (TOBPCA) without color correction (-w/o CC). From Fig. 5.4, it is observed that the visual results that in -w/o TO model the color distortion is not present but fails to improve image contrast. Whereas, in -w/o PCA model fails to remove color cast. The -w/o CC model does not significantly enhance the texture structure of images. When performed on a fully integrated model, the proposed method (TOBPCA) yields better visual results compared to existing state-of-the-art methods. The average scores of the ablated models are given in Table 5.2, which represents the full model that provides the higher value of PCQI, UCIQE, UIQM, SSIM, PSNR, and DE parameters. It is observed from Table 5.2 that each core module contributes to increasing the effectiveness of the proposed method (TOBPCA).

Table 5.2 Summarises the quantitative findings from the ablation study of the proposed method conducted on the UCCS, UIQS, and UIEB datasets.

Ablated Models	PCQI [178]	UCIQE [202]	UIQM [184]	SSIM [206]	PSNR [73]	DE [205]
TOBPCA -w/o TO	1.13	0.74	4.26	0.73	26.31	5.62
TOBPCA -w/o PCA	0.98	0.46	3.62	0.64	59.58	4.73
TOBPCA -w/o CC	1.34	1.09	4.84	0.79	25.85	5.71
TOBPCA (Full Model)	**2.09**	**1.92**	**5.69**	**0.89**	**29.81**	**5.86**

**The bold value represents the most optimal results

This chapter provides underwater image and video enhancement based on the fusion technique. In the above part, we proposed a novel method for underwater image enhancement using principal component analysis based on background light and transmission optimization. The second method provides both enhancement and restoration of underwater image and video based on multiscale gradient-domain enhancement and gamma correction.

5.2 Underwater Image/Video Enhancement and Restoration Based on Fusion of Gradient Domain Enhancement and Gamma Correction

5.2.1 Introduction

The undersea surface is an excellent habitat for living organisms such as fish, invertebrates, marine mammals, reptiles, plankton, coral seabirds, and many more. The undersea surface has a lot of characteristics such as topography and bathymetry, sediment composition, geological structure, biological communities, mineral resources, hydrothermal vent system, and many more that make it more interesting than a terrestrial surface [38]. The undersea surface has a reach of resources like fisheries, oil and gas, marine organisms, and many more. The underwater images frequently exhibit blurring, low contrast, and grayed-out hues due to the absorption and scattering [182] effects as light travels through water. Light absorption in the aquatic medium is due to water molecules, suspended particles, and other impurities present in the water.

On the other hand, scattering loss occurs due to multiple reflections and deflection of light when it is incident on objects and before reaching the camera. The blurriness in the image occurs due to forward scattering, and the image appears hazy because of backward scattering. Hence, the viewer cannot find detailed information from images [119], [215]. In this case, several standard procedures are used initially, followed by an enhancement process. Distance or depth is also an important component in underwater photography since when depth exceeds 10 meters, image capture diminishes due to poor degradation and visibility [93].

In chapter 4, we have proposed a method for underwater image enhancement and restoration based on white balance, contrast enhancement, empirical mode decomposition, and blending techniques. In this chapter, we have proposed a method for image as well as video enhancement and restoration. There are two solutions provided: the first one is image as well as video enhancement and restoration based on the fusion of multiscale gradient-domain enhancement and gamma correction. The second solution is based on the fusion of background light and transmission optimization via principal component analysis for image enhancement.

The detailed procedure involving color correction and image enhancement is applied to an underwater image for improved visual quality. The process includes transforming the original

color-corrected RGB image into the *YCbCr* color space. The *YCbCr* color space image is divided into luma (*Y*) and chroma (*Cb* and *Cr*) components. The proposed method subsequently uses a WLS filter on the *Y-component*, which plays a role in determining the overall brightness and illumination of the image. The gamma correction is applied to the *Y-component*'s base layer, and gradient-domain enhancement is used to its detail layers. The enhanced *Y-component* is then combined with the *Cb* and *Cr*-components before being converted back into the *RGB* color space, resulting in an improved version of the underwater image.

The main contributions are as follows:

- The proposed method examined the causes of the decline in underwater image and video quality. Color correction, gamma correction, gradient-domain enhancement, and color saturation have enhanced and restored degraded underwater images and video.
- The color correction is performed before converting *RGB* to the *YCbCr* color space. A WLS filter was applied to decompose the *Y-component* into the base and detail layers. The gamma correction enhances the base layer, while the *S*-shape function is utilized to improve detail layers within the gradient domain.
- The PSNR, SSIM, EME, DE, UIQM, and UCIQE have been evaluated on the UIEB and U45 datasets to validate the proposed method. Finally, the proposed and existing state-of-the-art methods are tested on a DRUVA dataset.

5.2.2 Methodology

The proposed method improves degraded underwater image's color cast and visual quality. This method undergoes underwater image enhancement involving color correction, subsequently transforming it into the *YCbCr* color space. There are three components of a *YCbCr* image, i.e., I_Y, $I_{Cb}, and\ I_{Cr}$. Here, the WLS filter [216] is applied to decompose I_Y-components in to base layer and detail layer (d_1, d_2). The Gamma correction is applied to the base layer, while gradient enhancement by using S-shape function is implemented on the corresponding detailed (d_1, d_2) layers. Finally, the enhanced base layer and details layers are fused and combined with *Cb* and *Cr*-components. The pictorial flow diagrams of the proposed method are shown in Fig. 5.5.

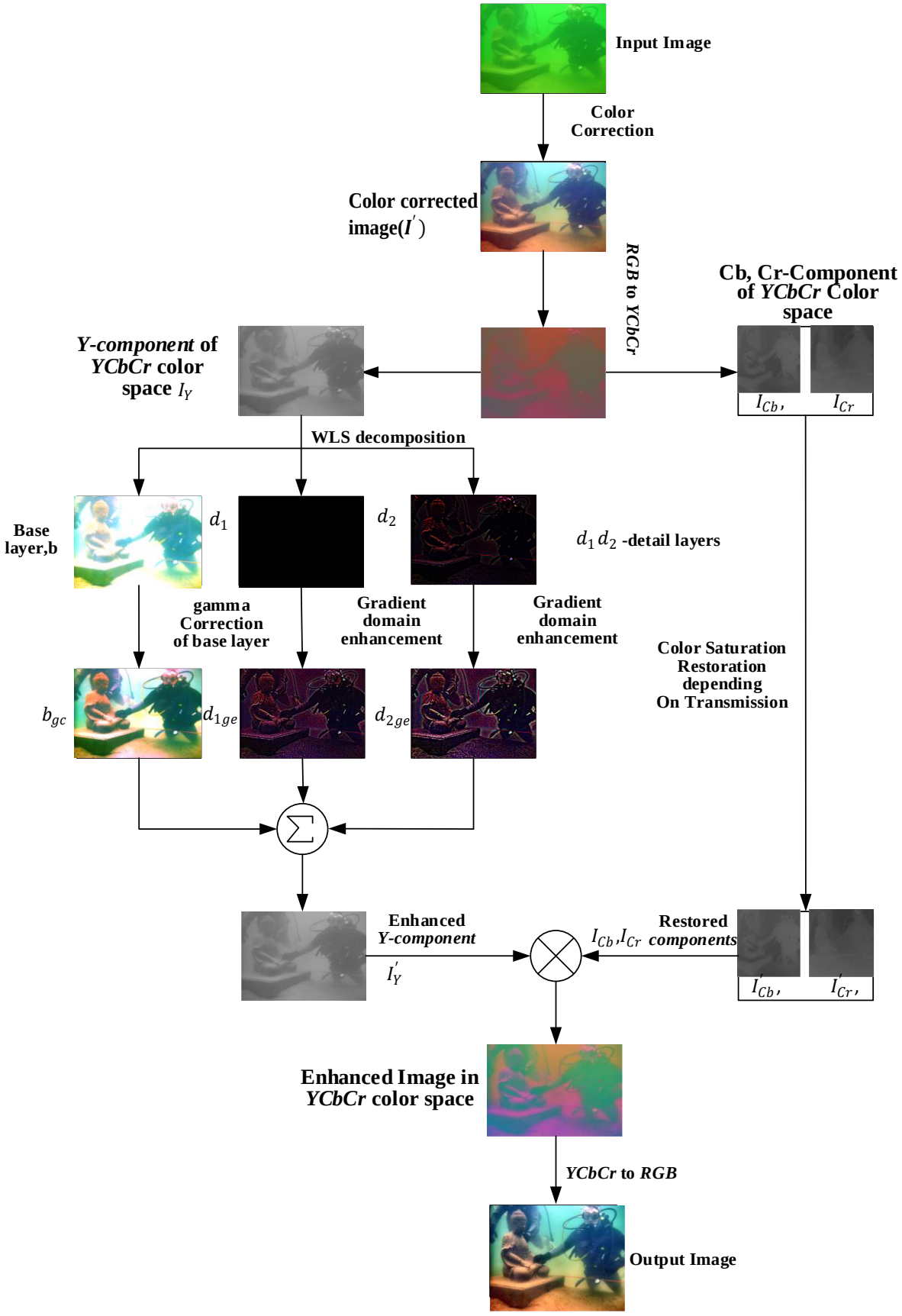

Fig. 5.5 The proposed method is based on the fusion of gradient-domain enhancement and gamma correction.

5.2.2.1 Color Correction

The white balance technique is presented in prior work to adjust the color casts, which is used as the mean illumination value. Instead of utilizing the mean amount, the illumination is approximated using the Minkowski *p*-norm. Mathematically evaluated as:

$$I' = \alpha_1 \frac{\theta_I}{\theta_{ref}} + \alpha_2 \tag{5.12}$$

where, $\theta_I = (\theta_R, \theta_G, \theta_B)$ represent the combination of pixel values of three channels of image *I (i, j)*. $\alpha_1 = \left(\alpha_{R,}\, \alpha_G,\ \alpha_B\right)$ represent the RGB gain factor, which can be obtained by evaluating the maximum pixel value of each channel. The range of α_2 varies in [0, 0.5]. The value of α_2 is closer to zero, which gives a higher brightness result. In other words, one can say that if the value of α_2 is increased, the image gets less bright, and $\theta_{ref} = ((\theta_R)^2 + (\theta_G)^2 + (\theta_B)^2)^{1/2}$.

5.2.2.2 Decomposition of I_Y-Component using Weighted Least Squares Algorithm

The color-corrected image converts into *YCbCr* color space, which has three components $(I_Y), (I_{cb}),$ and (I_{cr}). Although the physical characteristics (such as polarity, high specific heat capacity, density anomalies, surface tension, and universal solvent) of water have been taken into account, there are still certain limitations on different composite underwater environments (such as coral reefs, kelp forest, estuaries, mangrove forest, and seagrass meadow). According to Eqn. (3.14) and Eqn. (3.15), for different values of λ, one can obtain the respective layer from section 3.1.3.2 in Chapter 3. The pictorial block diagram of the proposed method to obtain detailed layers is shown in Fig. 5.5.

5.2.2.3 Contrast Enhancement of Base Layer Using Gamma Correction.

Here, contrast enhancement of the base layer using gamma correction is performed. The predominant hues in underwater images tend to be blue and green because the red color channel diminishes earlier than the green and blue channels [60]. The red channel vanishes first because it has less energy due to less frequency or a longer wavelength than the green and blue channels. During the decomposition of $I_{Y-component}$ using a weighted least square filter, the first component obtained in this process is called the base layer, which has a color variance. Gamma correction has been applied to fix the poor color variance of the base layer. Mathematically, it is represented by:

$$F(i,j) = \alpha(I_c(i,j))^{\gamma} \tag{5.13}$$

Here, α represents a constant term, and its value has been taken to 0.5. The gamma ($\gamma = 1.6$) is also constant. It is connected to the image's mean value. $I_c(i,j)$ represents the decomposed base layer.

5.2.2.4 Contrast Enhancement

According to the atmospheric scattering model, scene depth and attenuation coefficient are considered to be constant in a small local patch centered at the location *x;* thus, transmission $\tau_c(i,j)$ is uniform and conforms to $\tau_c(i,j) \leq 1$, and the contrast of the input image is assessed as the sum of the gradient [59]:

$$\sum_{i.j} \|\nabla I(i,j)\| = \sum_{i,j} \|\tau \nabla Q_c(i,j) + (1-\tau(i,j))\nabla A\| = \tau \sum_{i,j} \|\nabla Q_c(i,j)\| \leq \sum_{i,j} \|\nabla \tau(i,j)\| \quad (5.14)$$

Here, $I(i,j)$ represents the input image, $\tau_c(i,j)$ denote a transmission, which has a value less than 1; A represents the atmospheric light, and $Q_c(i,j)$ represent the scene's radiance.

5.2.2.4.1 Transmission Calculation

The transmission described by Tarel [72] is estimated in this article. When the observed image is known, the physical qualities underwater are subjected to two constraints: the transmission $\tau_c(i,j)$, which is positive ($\tau_c(i,j) \geq 0$) and pure white pixel. Each pixel value cannot be higher than the minimum pixel value of the image $I_c(i,j)$. Thus, the minimum pixel value of an image is evaluated as $\omega(i,j) = min\,(I_c(i,j))$ defined as the image of the minimal component of $I_c(i,j)$ for each pixel. ω is the image of the whiteness within the observed image $I_c(i,j)$. It concludes that $\omega \geq \tau_c(i,j)$. The local average of ω is thus computed as $A(i,j) = median_{s_v}(\omega(i,j))$ where (s_v) is the square or disc window size used in the median filter. The last step consists of multiplying $B(i,j) = A - median_{s_v}(|\omega - A|)$ by factor p in [0,1] to control the visibility strength. The summary of an algorithm for the calculation of transmission is:

$$\tau_c(i,j) = max\big(min\big(pB(i,j), \omega(i,j)\big), 0\big) \quad (5.15)$$

with $B(i,j) = A(i,j) - median_{s_v}(|\omega - A|)(i,j)$, and $A(i,j) = median_{s_v}\big(\omega(i,j)\big)$. Here, the value of p is taken as 0.90, and the size of the median filter, $s_v = 41$ is taken.

5.2.2.4.2 Contrast Enhancement in the Gradient Domain

Instead of evaluating the additional degradation model parameters, the underwater image transforms by modifying its gradient field via contrast enhancement. This approach is simple

in concept but can effectively increase details without introducing halo artifacts. The gradient operator is defined as follows in Eqn (5.16):

$$\nabla d_{ige} = \frac{\omega_i}{\bar{\tau}} \nabla d_i \tag{5.16}$$

where, $\bar{\tau}$ denotes the mean of the transmission $\tau(i,j)$ calculated from the image. The symbol indicates the non-negative parameters governing each layer's strength of gradient enhancement (ω_i). The d_{1ge} component corresponding to ω_1 which includes mainly the noises and minor details. While d_{2ge} has a strong edge and substantial structure. The d_{2ge} component corresponds to the ω_2 requirement to increase strength. In the proposed method, the value of $\omega_1 = 3$ and $\omega_2 = 4$ are fixed. Evaluating the gradient from Eqn. (5.16) only for two layers, i.e., $d_{1ge}\ and\ d_{2ge}$. The resultant improved image is represented as:

$$I'_R = b_{gc} + S(\delta_1, d_{1ge}) + S(\delta_2, d_{2ge}) \tag{5.17}$$

where S is a sigmoid function defined mathematically as, $S(a,i) = 1/(1+e^{-ai})$. δ is the controlling factor that controls the shape of the sigmoid function, and the function $S(\delta, d_{ige})$ control the boosting contrast of detail layers. In this way, one can improve the visibility of the image without over-sharpening.

5.2.2.5 Color Saturation and Restoration

The scattering model [217] of light claims that color distortion also happens during atmospheric transmission. Similarly, in the case of underwater images, color distortion occurs, and the mathematical equation compensates for the color distortion:

$$I'_{Cb} = e^{a(1-\tau)} I_{Cb} \tag{5.18}$$

$$I'_{Cr} = e^{a(1-\tau)} I_{Cr} \tag{5.19}$$

where a is the constant, and its value is taken as 2, it gives a good result for the most degraded images. The τ is a transmission, and its value is estimated using the method Fast visibility restoration from a single color or gray-level image, as explained in [72]. The components (I_{Cb}) and (I_{Cr}) are the color components of *YCbCr* color space.

5.2.3 Results and Discussion

Here, the performance of the proposed method is analyzed qualitatively and quantitatively. The visual quality of the enhanced underwater image of the proposed method is compared to the existing state-of-the-art methods using qualitative analysis. This work categorizes the existing

state-of-the-art methods into two groups for comparison. The first group uses comparison methods based on physical and non-physical models, while the second relies on deep learning-based methods. The existing state-of-the-art methods for the comparisons within the first group are HPU [172], underwater dark channel prior using guided filter (UDCPGF) [92], MSRCR [195], WCDUIE [93], UWIPHT [197], MPORU [218], HLRP [194], CBM [199], MIL [198], and CBFUWIE [60]. The existing state-of-the-art methods have been implemented on a publicly available UIEB [143] dataset. The second group is based on deep learning methods for the comparison such as simultaneous enhancement and super-resolution (SESR) [219], UWCNN-SD [200], UGAN [126], WSCT [182], CycleGAN [183], and FGAN [148]. The deep learning-based existing method is implemented on the U45 dataset. The proposed method and the existing methods are also tested on the DRUVA video dataset. The quantitative analysis of the proposed method has been evaluated in terms of parameters such as PSNR, SSIM, EME, DE, UIQM, and UCIQE on the UIEB and U45 datasets.

5.2.3.1 Visual Assessment

5.2.3.1.1 Qualitative analysis of the proposed method with existing state-of-the-art methods on the UIEB dataset

The proposed underwater image enhancement and restoration method achieves visual superiority by qualitative analysis. Fig. 5.6 shows the enhanced results of the proposed method and existing state-of-the-art methods.

It is observed that the MSRCR [195] and UWIPHT [197] methods give more brightness but do not preserve the naturalness of the image. In Fig. 5.6, image-10 exhibits a predominantly red color when processed using the MSRCR [195] method. Despite red color dominance, the MSRCR [195] method yields superior results compared to the WCDU [93], UDCPGF [92], and UWIPHT [197] methods. However, it falls short of restoring the green component. For image10, the proposed method produces better visual quality than other existing methods. Wavelength compensation and dehazing of the underwater method do not provide visually good results. It provided color distortion in all the images except image3, image8, and image9. Due to color distortion artifacts of WCDU [93] in Fig. 5.6, image8 is green and gray, and the details of the image frame are blurred, which extremely changes the visual appearance of the original image. The underwater image enhancement results provided by the WCDU [93] in Fig. 5.6 image10 have unsuppressed noise in the whole image. The underwater dark channel prior to a guided filter cannot remove the blue and green color of the enhanced result.

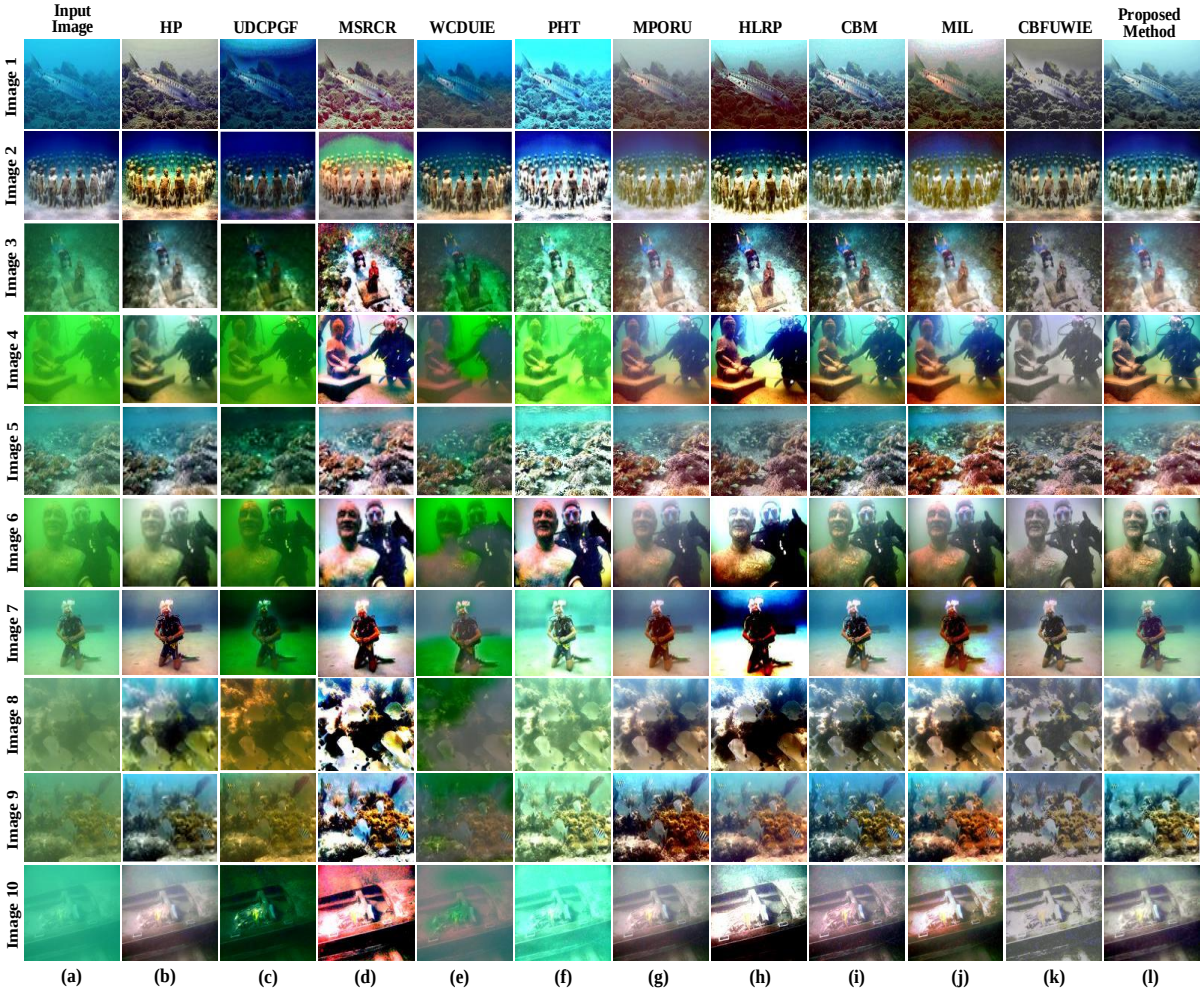

Fig. 5.6 Enhanced results of the proposed method and existing state-of-the-art methods on the UIEB dataset. From left to right (a) Degraded underwater images, (b) Enhanced image of HPU, (c) Enhanced image of UDCPGF, (d) Enhanced image of MSRCR, (e) Enhanced image of WCDUIE, (f) Enhanced image of UWIPHT, (g) Enhanced the image of MPORU, (h) Enhanced image of HLRP, (i) Enhanced image of CBM, (j) Enhanced image of MIL, (k) Enhance the image of CBFUWIE, and (l) Enhanced image of proposed method.

In Fig. 5.6, images4, image6, and image7 are almost the same color as the input image for UDCPGF [92], thus failing to enhance the degraded image. Image1 is saturated with a blue color, which is more blueish compared to the input underwater image for the UDCPGF method. However, for image-1, the proposed method provides a pleasant visual color compared to existing state-of-the-art methods. The hue-preserving-based underwater color image enhancement approach offers an excellent visual appearance compared to UDCPGF [92], MSRCR [195], and WCDU [93]. The output image of method UWIPHT [197] has good brightness compared to other methods. Because of brightness, the edge information of the enhanced image is not clear in the UWIPHT [197] method. HLRP [194] and the proposed method have almost similar visual quality of enhanced images except for a few images in Fig.

5.6 such as image1, image7, and image9. The overall performance of the proposed method compared to existing state-of-the-art methods HPU, UDCPGF, MSRCR, WCDUIE, UWIPHT, MPORU, HLRP, CBM, MIL, and CBFUWIE gives better results in terms of visual appearance as well as texture and color information as shown in Fig. 5.6.

5.2.3.1.2 Qualitative comparison of the proposed method with existing deep learning-based methods on the U45 dataset

Deep learning-based methods are used for comparisons such as SESR [219], UWCNN-SD [200], UGAN [126], WSCT [182], CycleGAN [183], and FGAN [148]. Fifteen images were taken from the U45 dataset for enhancement. These images are categorized into green, blue, and haze. The enhanced results of the proposed and existing state-of-the-art methods are shown in Fig. 5.7, Fig. 5.8, and Fig. 5.9. It is concluded that the proposed method outperforms the existing state-of-the-art in terms of visual quality as shown in Fig. 5.7, Fig. 5.8, and Fig. 5.9.

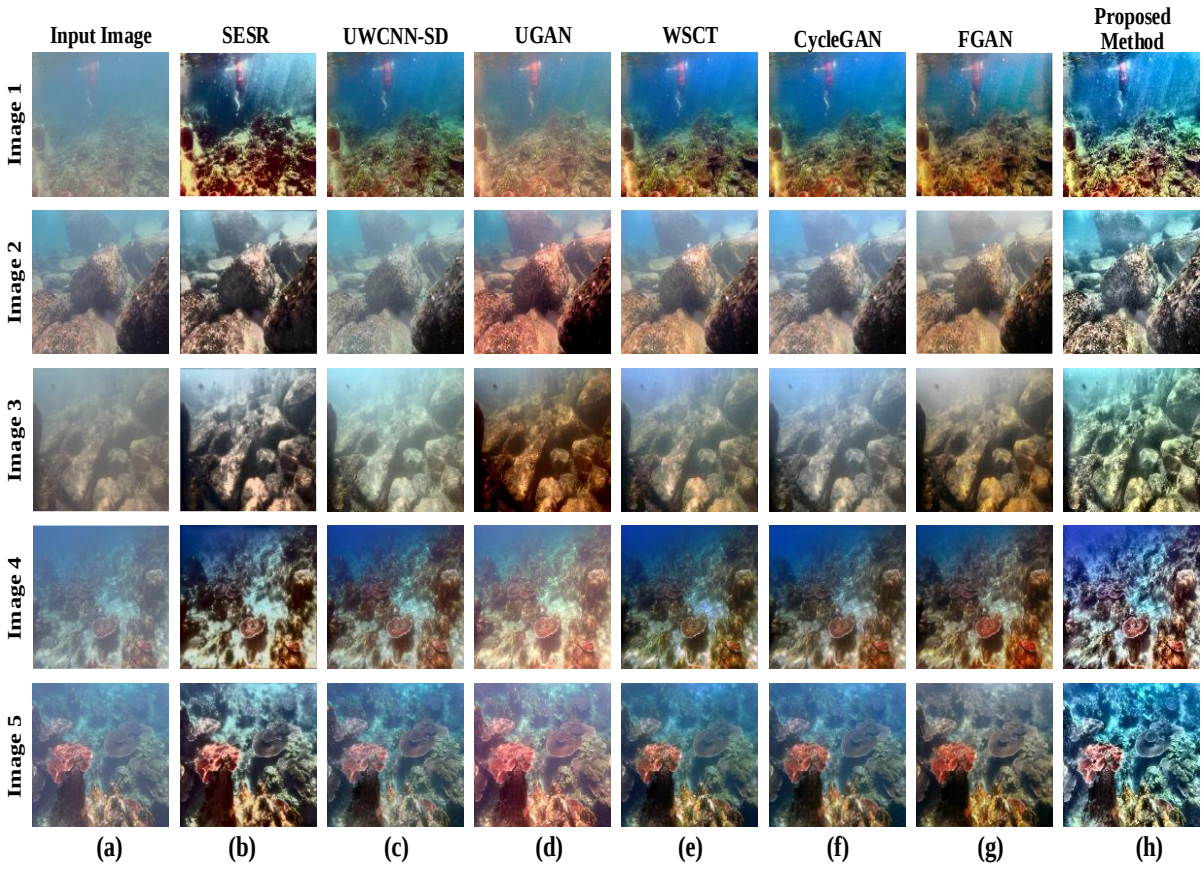

Fig. 5.7 From left to right (a) Degraded haze underwater images, and enhanced results of (b) SESR, (c) UWCNN-SD, (d) UGAN, (e) WSCT, (f) CycleGAN, (g) FGAN, and (h) The proposed method respectively on the U45 dataset.

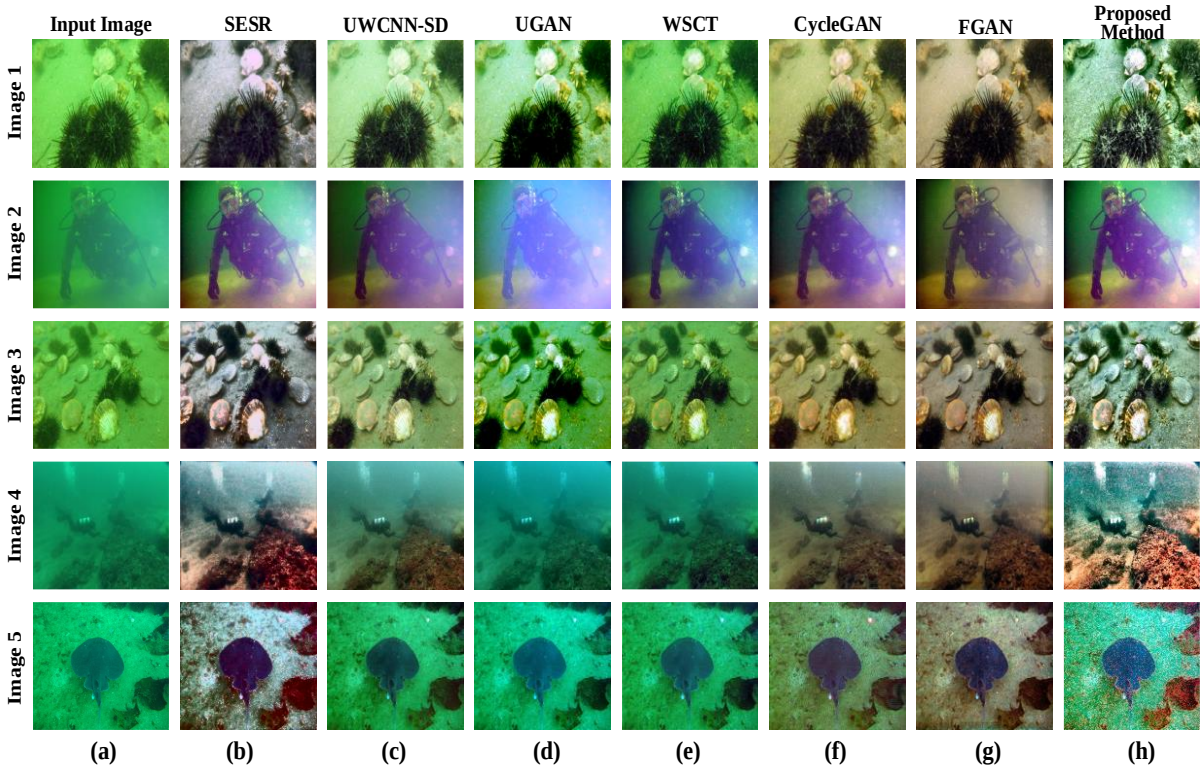

Fig. 5.8 From left to right (a) Degraded green underwater images, and enhanced results of (b) SESR, (c) UWCNN-SD, (d) UGAN, (e) WSCT, (f) CycleGAN, (g) FGAN, and (h) The proposed method respectively on the U45 dataset.

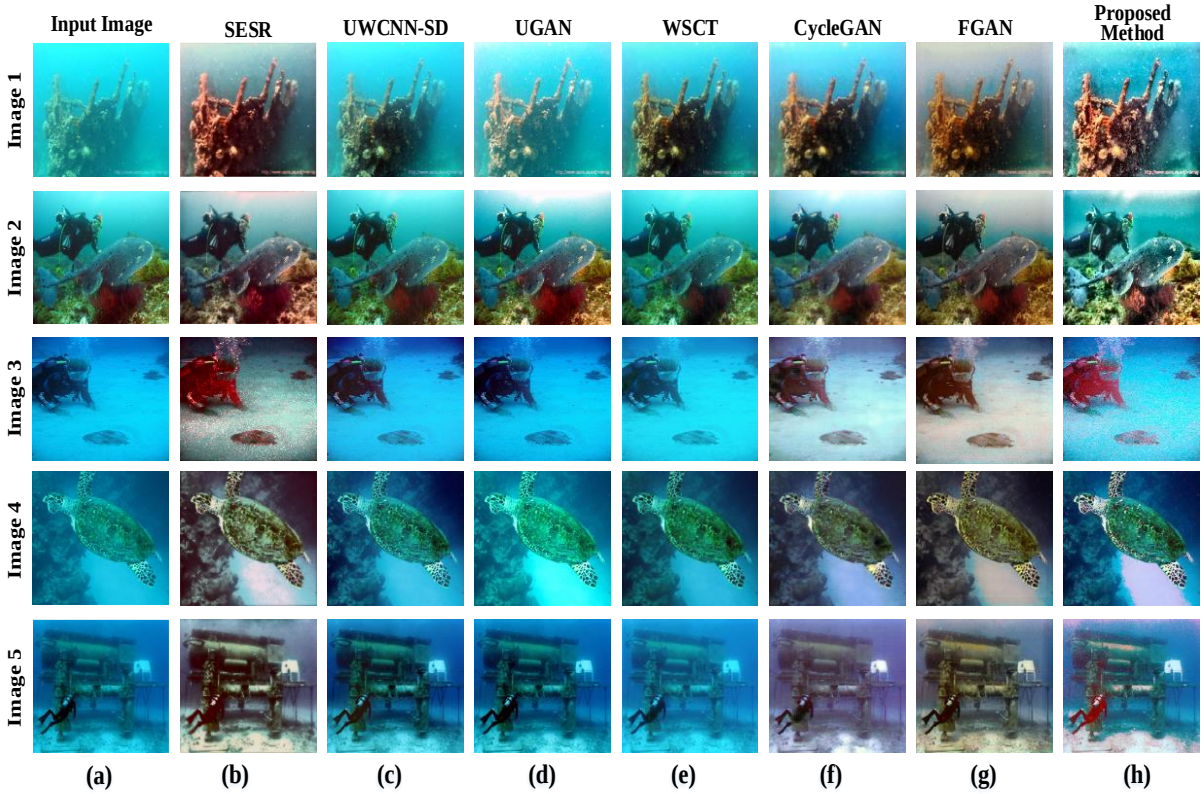

Fig. 5.9 From left to right (a) Degraded blue underwater images, and enhanced results of (b) SESR, (c) UWCNN-SD, (d) UGAN, (e) WSCT, (f) CycleGAN, (g) FGAN, and (h) The proposed method respectively on the U45 dataset.

5.2.3.2 Quantitative Result

In addition to qualitative analysis, quantitative evaluation using six different image quality measures such as PSNR [220], SSIM [221], EME [222], DE [222], UIQM [184], and UCIQE [202] is considered the fidelity of the proposed method with the existing state-of-the-art methods.

Peak signal-to-noise ratio: The PSNR measures the noise present in the enhanced image. An improved image with a higher PSNR represents less noise in the enhanced image. Table 5.3 describes the PSNR of the proposed method and existing state-of-the-art methods. Ten images have been taken from the UIEB data set, and their PSNR value is shown in Table 5.3. Fig. 5.10 shows the variation of PSNR for the proposed and existing methods in terms of PSNR. Table 5.3 shows that the proposed method provides the best result in terms of average PSNR value compared to the existing methods. The UWIPHT method gives the lowest average PSNR compared to all the methods.

Table 5.3 Comparison of PSNR (in dB) value with the proposed method and existing state-of-the-art on the UIEB dataset.

Images	HUWIE [172]	UDCPGF [92]	MSRCR [195]	WCDUIE [93]	UWPHT [197]	MPORU [218]	HLRP [194]	CBM [199]	MIL [198]	CBFUWIE [60]	Proposed Method
Image 1	29.61	53.67	51.90	31.51	30.63	35.45	48.37	45.73	53.56	50.87	57.39
Image 2	26.53	53.54	24.15	26.83	21.49	38.59	51.67	29.58	48.69	47.79	55.95
Image 3	27.15	53.43	24.97	29.65	23.65	31.57	50.46	35.59	52.38	36.58	56.68
Image 4	26.17	53.57	24.07	26.59	24.79	40.38	52.98	42.49	47.98	52.98	54.41
Image 5	25.73	53.53	24.44	26.34	25.38	42.71	53.72	51.39	39.46	51.42	55.06
Image 6	28.08	53.42	24.10	26.49	20.30	39.93	49.38	48.29	28.49	50.81	54.85
Image 7	28.15	53.44	24.17	26.44	23.49	41.65	52.87	43.83	56.85	51.09	55.18
Image 8	27.25	53.46	24.06	26.73	24.83	51.43	50.74	52.58	51.59	28.09	55.01
Image 9	27.00	53.54	24.06	27.61	27.08	43.65	48.45	39.94	55.48	31.58	54.56
Image 10	29.46	53.42	24.61	28.19	23.49	49.38	51.82	28.87	52.84	46.91	54.50
Average	27.51	53.50	27.05	27.64	24.51	41.47	51.04	41.82	47.13	44.81	**55.36**

**The bold value represents the most optimal results.

Fig. 5.10 shows the variation of PSNR on the UIEB dataset of the proposed method with the existing state-of-the-art methods. The thin blue line in Fig. 5.10 represents the average trend line. The bold highlighted value of the proposed method in Table 5.3 shows better PSNR among all the existing methods. The second highest value of PSNR is represented by blue color. It is concluded that the overall performance of the proposed method outperforms the existing state-of-the-art methods in terms of PSNR parameters.

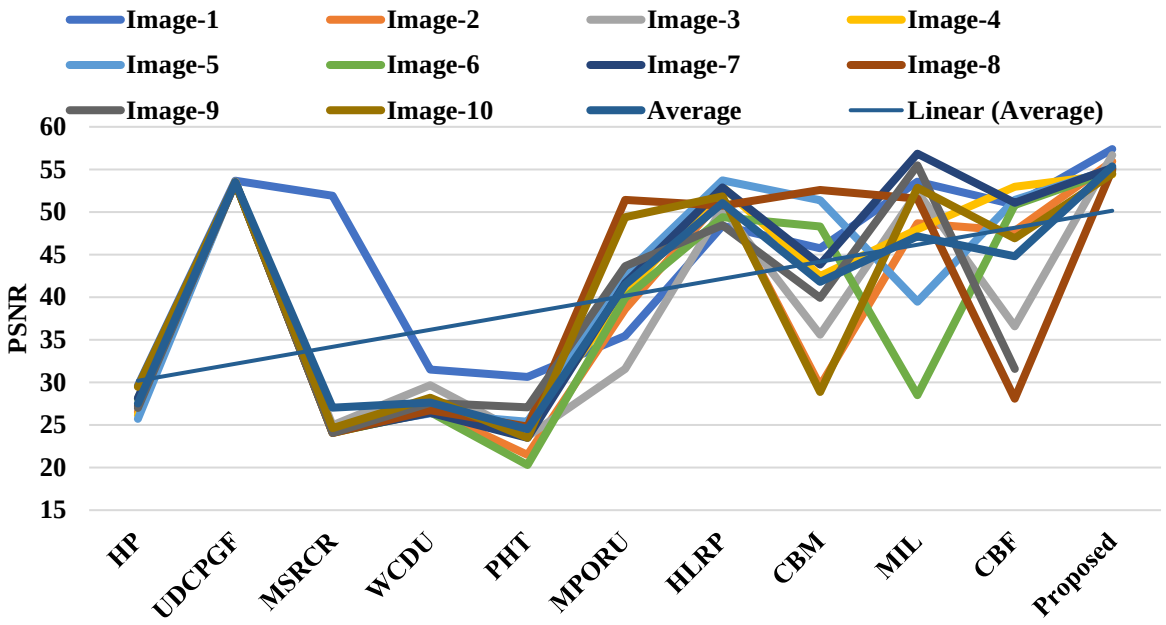

Fig. 5.10 Quantitative comparison of the proposed method with existing state-of-the-art on the UIEB dataset for PSNR parameter.

Structure similarity index measure: The SSIM is the popular metric for comparing the structural similarity between reference and enhanced image. It compares the value of an enhanced image's illuminance, contrast, and structural information with the original image. Table 5.4 represents the SSIM value of 10 different images and its average value which is taken from the UIEB dataset. The variation of SSIM on the UIEB dataset of the proposed method with the existing state-of-the-art methods is shown in Fig. 5.11.

Table 5.4 Comparison of SSIM value with the proposed method and existing state-of-the-art on the UIEB dataset.

Images	HUWIE [172]	UDCPGF [92]	MSRCR [195]	WCDUIE [93]	UWPHT [197]	MPORU [218]	HLRP [194]	CBM [199]	MIL [198]	CBFUWIE [60]	Proposed Method
Image 1	0.660	0.443	0.702	0.728	0.691	0.729	0.749	0.753	0.687	0.753	0.776
Image 2	0.761	0.804	0.858	0.870	0.718	0.494	0.832	0.793	0.769	0.809	0.890
Image 3	0.787	0.570	0.795	0.050	0.136	0.539	0.693	0.832	0.597	0.795	0.818
Image 4	0.839	0.857	0.787	0.810	0.719	0.738	0.857	0.829	0.719	0.815	0.839
Image 5	0.847	0.492	0.851	0.883	0.581	0.683	0.784	0.798	0.841	0.783	0.884
Image 6	0.869	0.865	0.721	0.882	0.801	0.802	0.815	0.846	0.864	0.803	0.855
Image 7	0.872	0.708	0.878	0.860	0.732	0.695	0.798	0.869	0.882	0.816	0.884
Image 8	0.808	0.707	0.750	0.846	0.692	0.709	0.842	0.783	0.759	0.851	0.899
Image 9	0.784	0.760	0.736	0.724	0.592	0.584	0.805	0.763	0.728	0.768	0.795
Image 10	0.804	0.458	0.831	0.886	0.791	0.809	0.863	0.895	0.838	0.839	0.917
Average	0.803	0.666	0.791	0.754	0.645	0.678	0.803	0.816	0.768	0.803	**0.856**

**The bold value represents the most optimal results.

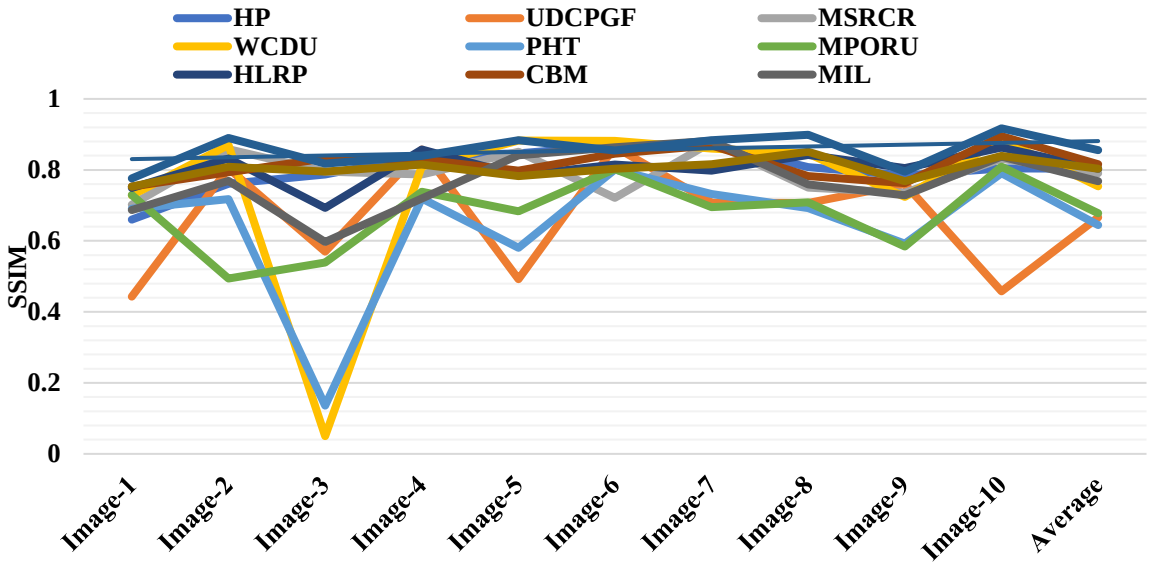

Fig. 5.11 Quantitative comparison of the proposed method with existing state-of-the-art on the UIEB dataset for SSIM parameter.

Its range lies between zero to one. Its value should be close to unity, which represents better enhancement. The SSIM value for image-6 for the WCDUIE method is more excellent than all methods, as shown in Table 5.4, which is represented in blue. However, the visual quality of that image is not good, as shown in Fig. 5.6. Similarly, Image-4 and Image-9 have the highest value for the HLRP method; the visual quality of these two images contains more reddish color. The overall average value of 10 images of the proposed method is greater than that of all the existing state-of-the-art methods, as shown in Table 5.4. From Fig. 5.11, it is concluded that the SSIM value of the proposed method is higher than that of the existing method. It is concluded from Table 5.4 that the overall performance of the proposed method outperforms the existing state-of-the-art methods in terms of SSIM parameters.

Discrete entropy: It measures how much information is contained in the image. Table 5.5 reports the DE value of 10 images from the UIEB data set of the proposed method and state-of-the-art methods. The proposed method has the second-highest average value compared to the existing methods. The variation of discrete entropy of the proposed method and existing state-of-the-art methods is represented in Fig. 5.12. Image5 has the highest value of discrete entropy for WCDUIE among all the methods, as shown in Table 5.5. The HLRP method has the highest value for image1 among all the methods, represented by blue in Table 5.5. The average value of discrete entropy of the proposed method is the second highest (First for CBFUWIE) among all the existing state-of-the-art methods, which is summarised in Table 5.5.

The overall performance of the proposed method outperformed the state-of-the-art methods such as HPU, UDCPGF, MSRCR, WCDUIE, UWIPHT, MPORU, HLRP, CBM, and MIL in terms of DE parameters.

Table 5.5 Comparison of DE value with the proposed and existing state-of-the-art methods on the UIEB dataset.

Images	HUWIE [172]	UDCPGF [92]	MSRCR [195]	WCDUIE [93]	UWPHT [197]	MPORU [218]	HLRP [194]	CBM [199]	MIL [198]	CBFUWIE [60]	Proposed Method
Image 1	5.005	3.044	3.478	2.816	2.283	4.759	6.125	4.832	5.097	5.869	5.279
Image 2	5.314	4.305	4.003	2.930	3.729	3.948	4.935	5.327	5.487	5.964	5.864
Image 3	5.247	4.678	3.907	6.575	5.629	4.793	5.839	5.631	5.168	6.931	6.881
Image 4	5.156	4.390	4.219	2.264	4.937	3.593	4.592	3.842	6.256	6.248	6.073
Image 5	4.957	4.383	4.425	7.454	3.581	5.261	5.152	4.283	5.468	6.098	5.902
Image 6	5.319	4.433	4.154	3.309	4.639	4.391	4.983	5.429	4.986	5.867	5.778
Image 7	5.239	3.947	4.049	2.938	3.519	4.526	4.809	4.592	5.974	6.186	5.913
Image 8	5.132	4.571	4.044	3.080	2.847	3.792	5.418	3.832	4.896	5.946	5.863
Image 9	5.121	4.541	3.970	5.635	3.592	4.869	5.208	6.752	5.869	6.056	5.946
Image 10	5.283	4.212	3.614	5.437	2.849	5.021	4.692	5.382	5.963	5.875	5.648
Average	5.177	4.250	3.986	4.244	3.760	4.495	5.175	4.990	5.516	**6.104**	**5.915**

**The bold value represents the most optimal results.

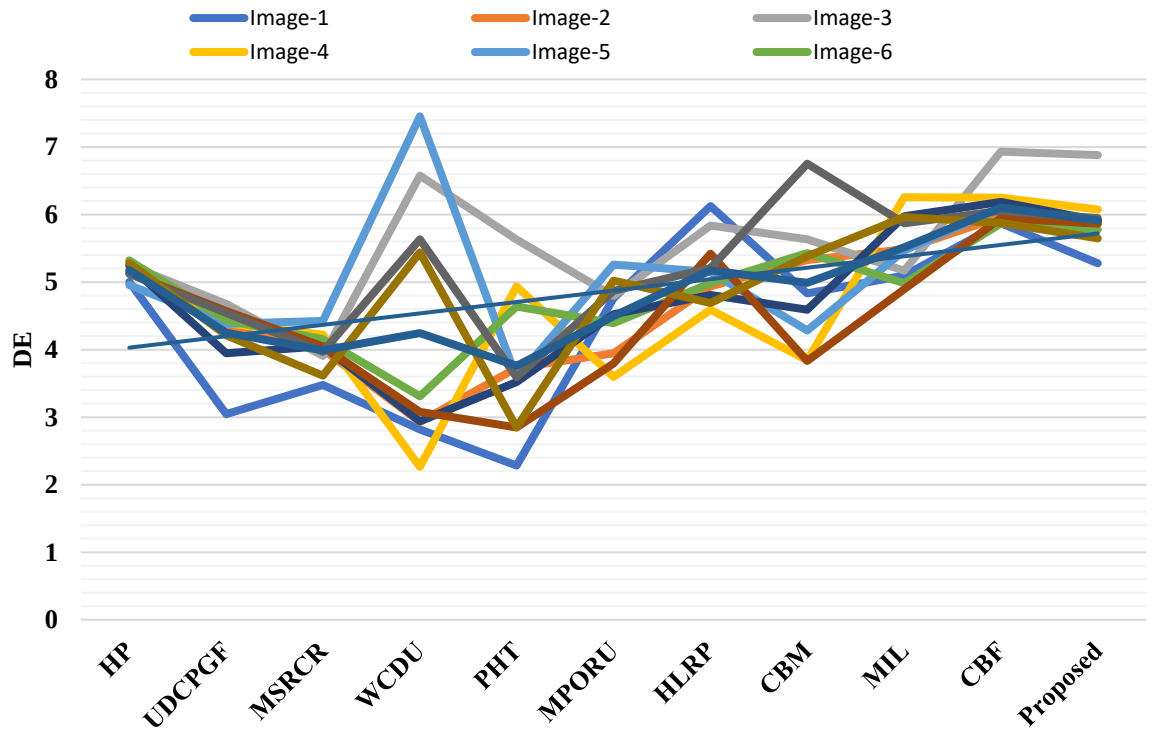

Fig. 5.12 Quantitative comparison of the proposed method with existing state-of-the-art on the UIEB dataset for DE parameter.

Underwater image quality measure: Underwater image quality measure (UIQM) [184] is a metric used to evaluate the visual quality of underwater images. The UIQM algorithm analyses several key factors to determine the image quality, such as *colorfulness, contrast, sharpness,* and *noise*. Higher UIQM scores indicate better image quality, while lower scores suggest decreased visual fidelity. Table 5.6 shows the value of UIQM of the proposed method and existing deep learning methods on the U45 dataset. The proposed method has the highest average value of UIQM compared to all existing state-of-the-art methods for each case, i.e., haze, blue, and green color images.

Some images have the highest UIQM value compared to the proposed method, such as I_1, I_3, and I_4 haze images for UGAN [126], FGAN [148], and UWCNN-SD [200] respectively. Similarly, I_2, I_3, I_4 and I_5 blue images have highest value of UIQM for UGAN [126], FGAN [148], UWCNN-SD [200], and UGAN [126] respectively. Overall, the average value of UIQM of the proposed method is better than the existing methods, as reported in Table 5.6.

Table 5.6 Comparison of UIQM value with existing deep learning and proposed method on the U45 Dataset.

Color	Images	SESR [219]	UWCNN-SD [200]	UGAN [126]	WSCT [182]	CycleGAN [183]	FGAN [148]	Proposed Method
HAZE	I_1	3.274	2.829	4.109	3.537	2.316	3.156	3.754
	I_2	3.978	4.139	3.519	2.452	3.529	2.438	4.203
	I_3	2.968	2.739	2.971	2.835	3.741	4.021	3.814
	I_4	4.639	5.141	4.192	3.582	2.829	3.924	5.024
	I_5	3.859	2.893	3.618	4.021	3.854	2.892	4.186
	Average	3.743	3.548	3.681	3.285	3.253	3.286	**4.196**
BLUE	I_1	1.592	2.018	1.879	2.009	1.396	1.957	2.178
	I_2	1.948	2.182	3.165	1.869	2.018	2.158	2.478
	I_3	1.835	2.582	2.592	1.973	2.148	3.196	2.975
	I_4	2.519	3.842	2.859	2.793	1.968	2.802	3.045
	I_5	2.832	2.849	4.023	3.163	2.097	2.458	3.249
	Average	2.1452	2.694	**2.903**	2.361	1.925	2.512	2.785
GREEN	I_1	2.926	3.093	3.108	2.831	2.435	3.132	3.362
	I_2	3.193	2.792	3.093	3.518	2.829	3.547	3.735
	I_3	3.091	3.132	2.821	2.863	2.638	3.254	3.312
	I_4	3.326	2.841	3.245	3.218	3.183	3.093	3.460
	I_5	2.289	2.189	1.846	2.429	2.109	1.935	2.597
	Average	2.965	2.8094	2.822	2.971	2.638	2.992	**3.293**

**The bold value represents the most optimal results.

It is concluded from Table 5.6 that the overall performance of the proposed method compared to existing state-of-the-art methods outperforms in terms of UIQM parameters.

Underwater color image quality evaluation: Underwater color image quality evaluation [202] refers to the process of assessing and quantifying the visual quality of color images captured underwater.

The evaluation of underwater color image quality typically involves the following terms: image acquisition, pre-processing, quality assessment metrics, *benchmark datasets,* and *evaluation and analysis.* Overall, underwater color image quality evaluation plays a vital role in improving the visual fidelity of underwater images, enabling better analysis and interpretation of underwater scenes, and advancing research in underwater imaging technologies.

Table 5.7 Comparison of UCIQE parameter with existing deep learning methods and proposed method on fifteen images of different colors such as haze, blue, and green taken from U45 Dataset.

Color	Images	SESR [219]	UWCNN-SD [200]	UGAN [126]	WSCT [182]	CycleGAN [183]	FGAN [148]	Proposed Method
HAZE	I_1	0.583	0.617	0.643	0.548	0.597	0.504	0.6525
	I_2	0.596	0.528	0.659	0.509	0.516	0.562	0.6005
	I_3	0.498	0.548	0.512	0.412	0.491	0.482	0.5701
	I_4	0.609	0.603	0.582	0.591	0.584	0.563	0.6101
	I_5	0.589	0.597	0.591	0.579	0.537	0.601	0.6142
	Average	0.575	0.578	0.597	0.527	0.545	0.542	**0.6094**
BLUE	I_1	0.529	0.642	0.596	0.609	0.593	0.629	0.6378
	I_2	0.621	0.613	0.653	0.593	0.619	0.618	0.6601
	I_3	0.583	0.583	0.649	0.572	0.582	0.526	0.5961
	I_4	0.572	0.528	0.548	0.538	0.509	0.572	0.5864
	I_5	0.537	0.543	0.574	0.532	0.511	0.583	0.5881
	Average	0.568	0.581	0.604	0.568	0.562	0.585	**0.6137**
GREEN	I_1	0.509	0.518	0.585	0.531	0.612	0.537	0.5534
	I_2	0.542	0.586	0.572	0.572	0.519	0.524	0.5875
	I_3	0.516	0.628	0.512	0.541	0.542	0.498	0.5585
	I_4	0.589	0.573	0.583	0.502	0.633	0.584	0.6405
	I_5	0.618	0.594	0.621	0.592	0.609	0.614	0.6393
	Average	0.554	0.579	0.574	0.547	0.583	0.551	**0.5958**

**The bold value represents the most optimal results.

Table 5.7 summarizes the UCIQE value of the proposed method and existing deep learning methods images of different colors, such as haze, blue, and green, taken from the U45 Dataset.

The average value of the proposed method is the greatest among all the existing techniques, shown in bold. Some of the images have the highest value of UCIQE, such as I_2 haze image has the highest value for UGAN [126] compared to all the methods, represented by blue color in Table 5.7. Similarly, I_1 and I_3 blue images have highest value of UCIQE for methods UWCNN-SD [200] and UGAN [126]. The green images I_1, and I_3 have greater value of UCIQE for UGAN [126], CycleGAN [183], and UWCNN-SD [200], respectively. The average value of UCIQ for the proposed method is greater than that of all the existing state-of-the-art methods. It is concluded from Table 5.7 that the overall performance of the proposed method is better compared to existing state-of-the-art methods in terms of UCIQE parameters.

5.2.3.3 Evaluation of the Proposed Method on the Underwater DRUVA Video Dataset

To assess the effectiveness of the proposed method in enhancing underwater video A12.mp4, the proposed method carried out the simulation specifically on captured underwater video footage. The duration of the video is 50 seconds, with a frame rate of 30fps and a size of 41.4MB. The video A12.mp4 comprises a total of 1520 frames. In this article, the frame size has been taken to 256×256. Here, ten frames such as frame_0001, frame_0100, frame_0200, frame_0300, frame_0400 frame_0500 frame_0600 frame_0700 frame_0900, frame_1520, are taken from A12.mp4 video frame, shown in Fig. 5.13. The execution time of the proposed method and existing state-of-the-art methods are listed in Table 5.8. The average execution time of the HPU, CBFUWIE, and UDCPGF for the video is much slower and only about less than one frame per second. Although the UWIPHT has less execution time, the enhancement quality is not good. The mean execution time of the proposed method is 185.67ms for a single frame, and the average execution speed is about five fps. The execution time of the proposed method can also satisfy the requirement of the underwater survey in real time with better enhancement quality. As illustrated in Fig. 5.13, the proposed method successfully eliminates the color cast and enhances the contrast in underwater videos. Additionally, the proposed results

Table 5.8 The comparative analysis of underwater video A12.mp4 with the proposed method and existing state-of-the-art underwater DRUVA video dataset in terms of execution time.

Methods	HUWIE [172]	UDCPGF [92]	MSRCR [195]	WCDUIE [93]	UWPHT [197]	MPORU [218]	HLRP [194]	CBM [199]	MIL [198]	CBFUWIE [60]	Proposed Method
Time (s)	8527.2	1583.84	1348.24	816.24	**121.9**	846.8	340.48	524.4	942.4	2812	282.21
TPF (ms)	5610.4	1042.6	887.3	537.5	**80.20**	557.10	224.4	345.8	620.1	1856.7	185.67
FPS	0.27	0.96	1.12	1.86	**12.46**	1.79	4.46	2.89	1.61	0.53	5.386

**TPF* Time per frame, *FPS* Frame per second, the bold value represents the best result

maintain consistency across different frames, free from flickering artifacts.

Fig. 5.13 Enhanced results of the proposed method and existing state-of-the-art on the underwater video A12.mp4. (a) Raw underwater video A12.mp4 (from top to bottom are frame_0001, frame_0100, frame_0200, frame_0300, frame_0400, frame_0500, frame_0600, frame_0700, frame_0900, frame_1520 in this video). (b) Results of HPU, (c) Results of UDCPGF, (d) Results of MSRCR, (e) Results of WCDUIE, (f) Results of UWIPHT, (g) Results of MPORU, (h) Results of HLRP, (i) Results of CBM, (j) Results of MIL, (k) Results of CBFUWIE, (l) Results of the proposed method. Zoom in all images for better visibility.

In contrast, the existing state-of-the-art methods produce inconsistent enhancement between different frames, which decreases visual quality. For example, for frame_0400, the MSRCR, HLRP, and MIL methods produce a visually pleasant result; however, this method introduces a reddish color cast in frame_0600, frame_0700, frame_0900, and frame_1520. The other methods also have similar inconsistent enhancement performance, as shown in Fig. 5.13.

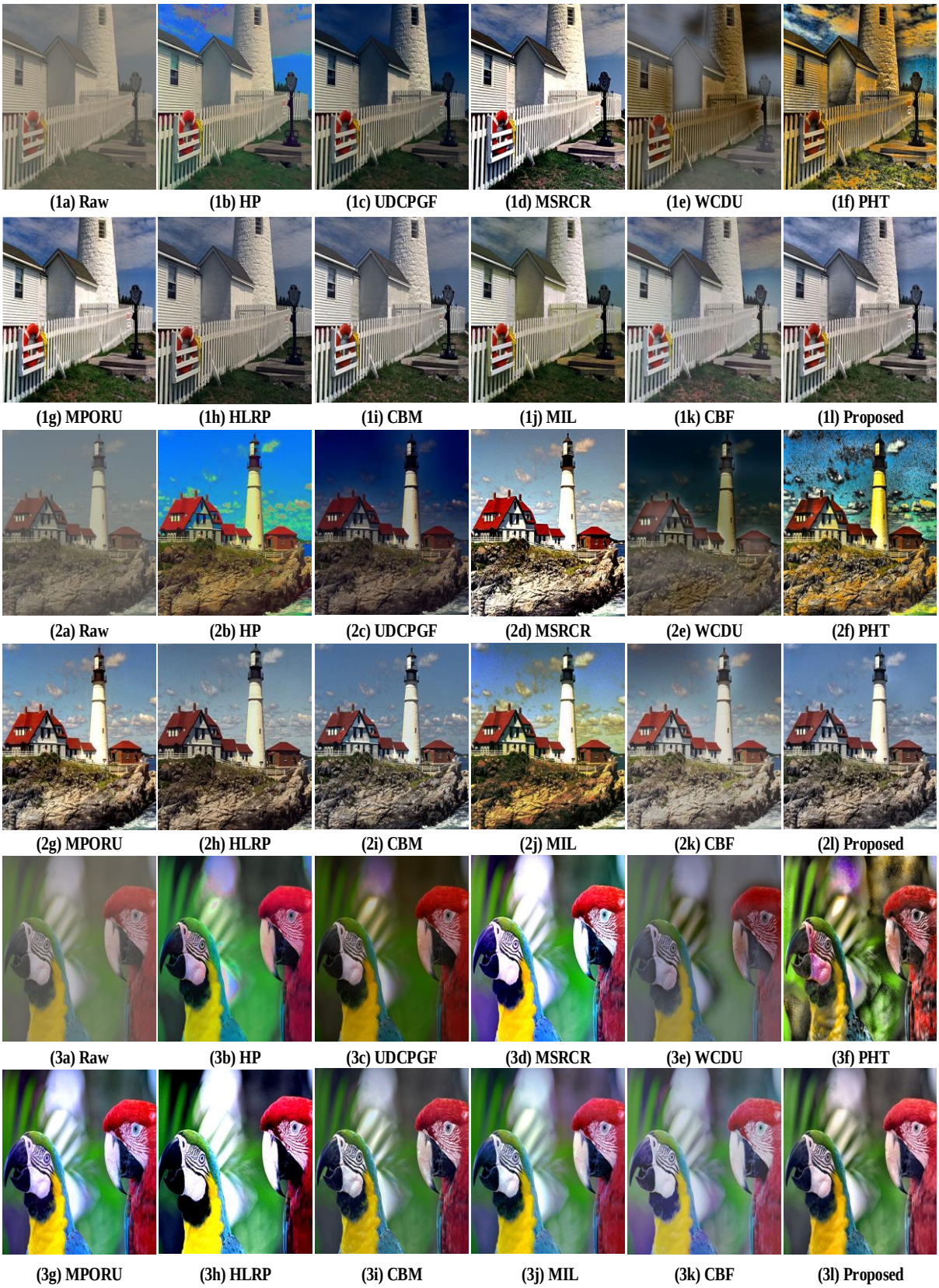

Fig. 5.14 Comparative analysis of the proposed method with existing state-of-the-art on the TID 2013 dataset.

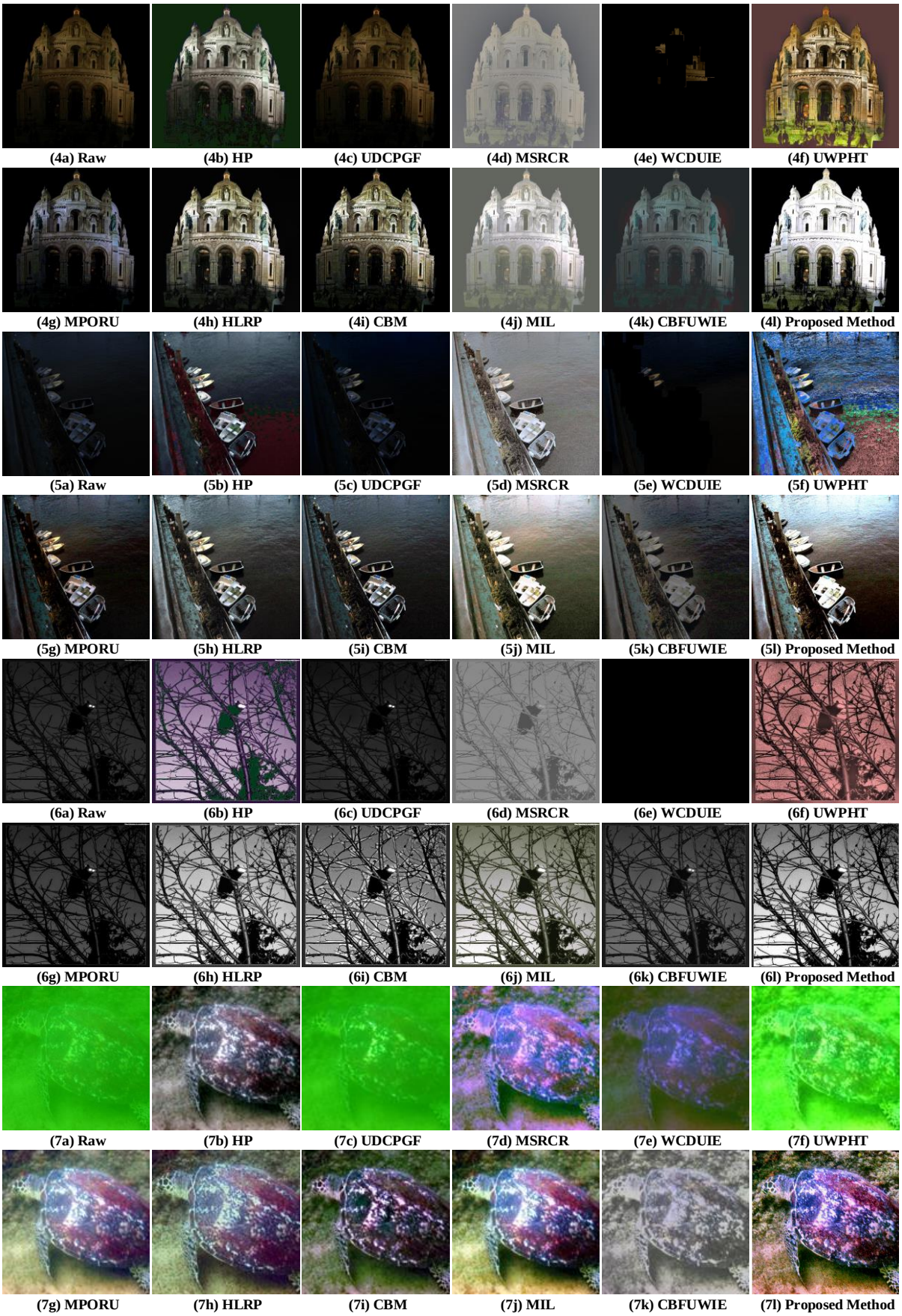

Fig. 5.15 Comparative analysis of the proposed method with existing state-of-the-art on low illumination images and underwater images.

5.2.3.4 Other Applications Test

The proposed method also tested for the low light image dataset and storm image dataset to validate its effectiveness. These particles lead to light absorption and diffusion, resulting in color distortion and reduced contrast. Fig. 5.14 shows the enhanced results of existing state-of-the-art and proposed methods. One can observe that the MSRCR method in Fig. 5.14 (1d), (2d), and (3d) shows a brighter image which does not look natural. Whereas UWIPHT produces color casts as shown in Fig. 5.14 (1f), (2f), and (3f)). The Fig. 5.14 (1c), (2c), and (3c), are relatively low light after enhancement compared to the input image for the UDCPGF method. The WCDUIE method is not able to enhance the input image, as shown in Fig. 5.14 (1e), (2e), and (3e). The MPOUR, HLRP, CBM, and MIL have almost the same visual quality, but MIL has some yellowish color, as shown in Fig. 5.14 (1j), (2j), and (3j). The proposed method is shown in Fig. 5.14 (1l), (2l), and (3l) not only enhances structures effectively and suppresses noise but also demonstrates promising outcomes in terms of color correction and preservation of naturalness.

Furthermore, low-illumination images are enhanced in Fig. 5.15 to showcase the effectiveness of the proposed method. One can see that the HPU, UDCPGF, WCDUIE, UWIPHT, and MPOUR cannot enhance the low-illumination images, as shown in Fig. 5.15. However, the proposed method consistently demonstrates superior enhanced quality compared to existing state-of-the-art techniques, as shown in Fig. 5.15 (4l), (5l), and (6l). The above results demonstrate the extensive application capability of the proposed method.

It is concluded that the proposed method outperforms in terms of PSNR, SSIM, EME, UIQM, and UCIQE compared to existing state-of-the-art methods under different light intensities. Furthermore, the method's efficiency has been tested on fog and low-illumination images.

5.3 Summary

In this chapter, a new image enhancement method based on the fusion of transmission optimization and background light estimation via principal component analysis (TOBPCA) is proposed. The proposed method does not depend on prior information about the underwater environment. The proposed method is executed on the underwater color cast set, underwater image quality set, and underwater image enhancement benchmark dataset to evaluate the PCQI, UCIQE, UIQM, SSIM, PSNR, and DE parameters. The proposed method with the UIEB dataset provides PCQI, UCIQE, SSIM, and DE of 2.0913, 1.9283, 0.8957, and 5.8682,

respectively. The simulation results show that the proposed method outperforms other methods in terms of PCQI, UCIQE, SSIM, and DE parameters. The ablation study contributes to the effectiveness of the proposed method. It is reported that the proposed method not only enhances the degraded image but also does not disturb the naturalness of the image.

Next, a new method underwater image and video enhancement and restoration based on fusion of gradient domain enhancement and gamma correction is proposed. Gamma correction is used to increase the brightness of the image and video by applying non-linear operations to the pixel value of the image. The contrast between underwater images and video is increased by applying gradient-domain enhancement and adjusting the saturation to better visual quality. The proposed method is evaluated on the underwater image enhancement benchmark dataset and U45 dataset based on parameters PSNR, SSIM, EME, DE, UIQM, and UCIQE. The proposed method with the UIEB dataset provides PSNR, SSIM, and EME of 55.36, 0.856, and 5.828, respectively, and the U45 dataset provides UIQM and UCIQE of 3.7445 and 0.6063, respectively. The simulation results show that the proposed method outperforms existing state-of-the-art methods in terms of PSNR, SSIM, EME, UIQM, and UCIQE parameters. The proposed method's execution time for the DRUVA video dataset outperforms existing state-of-the-art methods such as HPU, UDCPGF, MSRCR, WCDUIE, MPOUR, HLRP, CMB, MIL, and CBFUWIE. Additionally, the proposed method is beneficial in enhancing and restoring fog and low-illumination images. It is reported that the proposed method enhances the degraded image and video and does not disturb their naturalness.

The publication related to this chapter

Amarendra Kumar Mishra, Manjeet Kumar, and Mahipal Singh Choudhry. "Underwater image enhancement by using transmission optimization and background light estimation via principal component analysis fusion." *Signal, Image and Video Processing* (2024): 1-11, **SCIE, (IF: 2.3)** https://doi.org/10.1007/s11760-024-03047-x

Amarendra Kumar Mishra, Manjeet Kumar, and Mahipal Singh Choudhry. "Fusion of multiscale gradient domain enhancement and gamma correction for underwater image/video enhancement and restoration." *Optics and Lasers in Engineering* 178 (2024): 108154, **SCIE, (IF: 4.6)** https://doi.org/10.1016/j.optlaseng.2024.108154.

Chapter 6

Conclusion and Future Scope

6.1 Conclusion

In this thesis, we have developed following methods to deal with the practical problems of underwater image enhancement and restoration. The methods are summarized as follows:

Firstly, we have developed three methods independently such as underwater image enhancement using multi scale decomposition and gamma correction, underwater image enhancement based on white balance and blending technique, and underwater image enhancement using transmission optimization and background light estimation via principal component analysis (TOBPCA) for underwater image enhancement to overcome the problem of non-uniform illumination, contrast enhancement, and transmission map by addressing the issue of attenuation and scattering of light.

The method "underwater image enhancement using multi scale decomposition and gamma correction" outperforms existing state-of-the-art methods MIL, UDCPGIF, UDCPSM, HUIE, HPU, HTU, MSRCR, MPORU in terms of EME, DE, SSIM, UIQM, UCIQE, PCQI parameters on the UIEB dataset. The proposed method "underwater image enhancement based on white balance and blending technique" implemented on the UIEB, UIQS, UCCS, and U45 dataset it is observed that the proposed method outperforms existing state-of-the-art methods HLRP, HUWIE, MSRCR, TEBCF, UWIPHT, MIL, MWMGF, WCDUIE, CBM, UIBLA, UGAN, UWCNN-SD, WSCT, CycleGAN, and FGAN in terms of PCQI, UIQM, UCIQE, PSNR, AMBE, CPP, DE, MEME, and SSIM parameters on the. The "underwater image enhancement using transmission optimization and background light estimation via principal component analysis (TOBPCA)" method outperform existing state-of-the-art methods HLRP, MPORU, UHT, MIL, HUWIE, TEBCF, MWMGF, and WCDUIE in terms of PCQI, UCIQE, SSIM, and DE parameters on the UIEB, UIQS, and UCCS dataset. The ablation study contributes to the effectiveness of the proposed method. It is reported that the proposed method not only enhances the degraded image but also does not disturb the naturalness of the images.

Secondly, two methods have been developed for underwater image restoration i.e., underwater image restoration using white balance and retinex algorithm and underwater image restoration

based on color correction and empirical mode decomposition to solve the problem of noise removal, blurring of image, artifacts removal, structural preservation, and color restoration underwater unwanted color cast, and quantifying the scene depth.

The proposed method “underwater image restoration using white balance and retinex algorithm” outperforms existing state-of-the-art methods WSCT, UIBLA, UDCP, RED, FGAN, FE, and CycleGAN in terms of UIQM and UCIQE parameters on the U45 dataset. The “underwater image restoration based on color correction and empirical mode decomposition” method is implemented on U45 dataset. It is observed that the proposed method outperforms existing state-of-the-art methods MSRCR, HUWIE, RB, RED, and WSCT in terms of SSIM and PCQI parameters on the U45 dataset.

A novel method “underwater image and video enhancement and restoration based on fusion of gradient domain enhancement and gamma correction” is proposed for both enhancement and restoration of underwater images and videos. The method is evaluated on the UIEB, U45, and DRUVA video dataset. The proposed method outperforms existing state-of-the-art methods HUWIE, UDCPGF, MSRCR, WCDUIE, UWIPHT, MPORU, HLRP, CBM, MIL, SESR, UWCNN-SD, UGAN, WSCT, CycleGAN, and FGAN in terms of PSNR, SSIM, DE, UIQM, and UCIQE parameters. Further, we have evaluated our method on the TID 2013 dataset and exclusive dark image dataset for other application, which shows effectiveness of the proposed method.

6.2 Future direction

We have endeavoured to tackle the challenges surrounding the enhancement and restoration of underwater vision. The field of underwater image processing remains relatively emerging, with many accesses yet to be explored. In terms of future directions, numerous challenges exist that could have a substantial impact on the field of ocean engineering science.

Understanding the characteristics of turbidity remains a significant challenge. Developing an underwater image formation model that accounts for the effects of turbidity is a complex and complicated task. Also, a drawback of the proposed methods is the amplification of some noise during the enhancement and restoration process. This issue will be addressed by using different filtering techniques and executing through GPU programming so that the proposed method’s efficiency can be further improved.

In recent years, significant progress has been made in developing algorithms for enhancing underwater images. However, no algorithm has yet been created to effectively enhance the underwater images captured in diverse underwater environments and at varying depths. The Enhancement algorithms can be improved by strategically integrating image enhancement and restoration techniques.

REFERENCES

[1] O. Pizarro and H. Singh, "Toward large-area mosaicing for underwater scientific applications," *IEEE Journal of Oceanic Engineering*, vol. 28, no. 4, pp. 651–672, 2003, doi:10.1109/JOE.2003.819154..

[2] R. M. Eustice, H. Singh, J. J. Leonard, and M. R. Walter, "Visually mapping the RMS Titanic: Conservative covariance estimates for SLAM information filters," *International Journal of Robotic Research*, vol. 25, no. 12, pp. 1223–1242, 2006, doi:10.1177/0278364906072512.

[3] J. Escartín *et al.*, "Globally aligned photomosaic of the Lucky Strike hydrothermal vent field (Mid-Atlantic Ridge, 37 18.5′ N): Release of georeferenced data, mosaic construction, and viewing software," *Geochemistry, Geophys. Geosystems*, vol. 9, no. 12, 2008, doi.org/10.1029/2008GC002204.

[4] A. C. R. Gleason *et al.*, "Documenting hurricane impacts on coral reefs using two-dimensional video-mosaic technology," *Marin Ecology*, vol. 28, no. 2, pp. 254–258, 2007, doi.org/10.1111/j.1439-0485.2006.00140.x.

[5] Z. Zhu, E. M. Riseman, A. R. Hanson, and H. Schultz, "An efficient method for geo-referenced video mosaicing for environmental monitoring," *Machine Vision and Application*, vol. 16, pp. 203–216, 2005, doi.org/10.1007/s00138-005-0173-x.

[6] P. Drap, "Underwater photogrammetry for archaeology," *Special Application of Photogrammetric*, vol. 114, 2012, doi: 10.1109/48.338398.

[7] K. Vyas and A. Sanghi, "Design and Modelling of Underwater Image Enhancement using Improved Computing Techniques," *Acta Energetica*, no. 03, pp. 53–62, 2022, actaenergetica.org/index.php/journal/article/view/478.

[8] P. Cervenka and C. de Moustier, "Postprocessing and corrections of bathymetry derived from sidescan sonar systems: Application with SeaMARC II," *IEEE Journal of Oceanic Engineering*, vol. 19, no. 4, pp. 619–629, 1994, doi: 10.1109/48.338398.

[9] D. R. Yoerger, M. Jakuba, A. M. Bradley, and B. Bingham, "Techniques for deep sea near bottom survey using an autonomous underwater vehicle," in *Robotics Research:*

Results of the 12th International Symposium ISRR, pp. 416–429, 2007, doi.org/10.1007/978-3-540-48113-3_36.

[10] N. Nagarajan, G. Nivetha, and S. Jothiraj, "Robust and Real-Time Detection of Underwater Sonar Image Representations by Using Fast Transferred Design Learning Method," in *Industry Applications of Thrust Manufacturing: Convergence with Real-Time Data and AI*, IGI Global, pp. 248–279, 2024, doi: 10.4018/979-8-3693-4276-3.ch011.

[11] D. M. Kocak, F. R. Dalgleish, F. M. Caimi, and Y. Y. Schechner, "A focus on recent developments and trends in underwater imaging," *Marine Technology Socity Journal*, vol. 42, no. 1, p. 52, 2008.

[12] Z. Li, G. Li, B. Niu, and F. Peng, "Sea cucumber image dehazing method by fusion of retinex and dark channel," *IFAC-PapersOnLine*, vol. 51, no. 17, pp. 796–801, 2018, doi.org/10.1016/j.ifacol.2018.08.098.

[13] J. Ahn, S. Yasukawa, T. Sonoda, T. Ura, and K. Ishii, "Enhancement of deep-sea floor images obtained by an underwater vehicle and its evaluation by crab recognition," *Journal of Marine Science Technology*, vol. 22, pp. 758–770, 2017, doi.org/10.1007/s00773-017-0442-1.

[14] J. R. V Zaneveld and W. S. Pegau, "Robust underwater visibility parameter," *Optics Express*, vol. 11, no. 23, pp. 2997–3009, 2003, doi.org/10.1364/OE.11.002997.

[15] R. Schettini and S. Corchs, "Underwater image processing: state of the art of restoration and image enhancement methods," *EURASIP Journal on Advances in Signal Processing*, vol. 2010, pp. 1–14, 2010, doi:10.1155/2010/746052.

[16] E. Trucco and A. T. Olmos-Antillon, "Self-tuning underwater image restoration," *IEEE Journal of Oceanic Engineering*, *Eng.*, vol. 31, no. 2, pp. 511–519, 2006, doi: 10.1109/JOE.2004.836395.

[17] J. S. Jaffe, "Computer modeling and the design of optimal underwater imaging systems," *IEEE Journal of Oceanic Engineering*, vol. 15, no. 2, pp. 101–111, 1990, doi: 10.1109/48.50695.

[18] A. T. Çelebi and S. Ertürk, "Visual enhancement of underwater images using empirical mode decomposition," *Expert System with Application*, vol. 39, no. 1, pp. 800–805, 2012, doi.org/10.1016/j.eswa.2011.07.077.

[19] D. Akkaynak, T. Treibitz, T. Shlesinger, Y. Loya, R. Tamir, and D. Iluz, "What is the space of attenuation coefficients in underwater computer vision?," in *Proceedings of the IEEE conference on computer vision and pattern recognition*, pp. 4931–4940, 2017.

[20] G. Bianco, M. Muzzupappa, F. Bruno, R. Garcia, and L. Neumann, "A new color correction method for underwater imaging," *International Archives of the Photogrammetry Remote Sensing Spatial Information Science*, vol. 40, pp. 25–32, 2015, doi.org/10.5194/isprsarchives-XL-5-W5-25-2015.

[21] L. A. Torres-Méndez and G. Dudek, "Color correction of underwater images for aquatic robot inspection," in *International Workshop on Energy Minimization Methods in Computer Vision and Pattern Recognition*, pp. 60–73, 2005, doi.org/10.1007/11585.

[22] E. O. Hulburt, "Optics of distilled and natural water," *Journal of the Optical Society of America*, vol. 35, no. 11, pp. 698–705, 1945, doi.org/10.1364/jOSA.35.000698.

[23] E. J. McCartney, "Optics of the atmosphere: scattering by molecules and particles," *New York*, 1976.

[24] Y. Wang, W. Song, G. Fortino, L.-Z. Qi, W. Zhang, and A. Liotta, "An experimental-based review of image enhancement and image restoration methods for underwater imaging," *IEEE access*, vol. 7, pp. 140233–140251, 2019, doi:10.1109/ACCESS.2019.2932130.

[25] S. Anwar and C. Li, "Diving deeper into underwater image enhancement: A survey," *Signal Processing Image Communication*, vol. 89, p. 115978, 2020, doi.org/10.1016/j.image.2020.115978.

[26] B. L. McGlamery, "A computer model for underwater camera systems," in *Ocean Optics VI*, vol. 208, pp. 221–231, 1980, doi.org/10.1117/12.958279.

[27] A. K. Bhandari, "A logarithmic law based histogram modification scheme for naturalness image contrast enhancement," *Journal of Ambient Intellegence and*

Humanized Computing, vol. 11, no. 4, pp. 1605–1627, 2020, doi: 10.1007/s12652-019-01258-6.

[28] J. Bednar and T. Watt, "Alpha-trimmed means and their relationship to median filters," *IEEE Transaction on Acoustic*, vol. 32, no. 1, pp. 145–153, 1984, doi: 10.1109/TASSP.1984.1164279.

[29] K. Panetta, A. Samani, and S. Agaian, "Choosing the optimal spatial domain measure of enhancement for mammogram images," *Journal of Biomedical Imaging*, vol. 2014, p. 3, 2014, doi.org/10.1155/2014/937849.

[30] K. Panetta, S. Agaian, Y. Zhou, and E. J. Wharton, "Parameterized logarithmic framework for image enhancement," *IEEE Transaction on System, Man,and Cybernetics, Part B*, vol. 41, no. 2, pp. 460–473, 2010, doi: 10.1109/TSMCB.2010.2058847.

[31] S. Wang, K. Ma, H. Yeganeh, Z. Wang, and W. Lin, "A patch-structure representation method for quality assessment of contrast changed images," *IEEE Signal Processing Letters*, vol. 22, no. 12, pp. 2387–2390, 2015, doi: 10.1109/LSP.2015.2487369.

[32] K. Gu, W. Lin, G. Zhai, X. Yang, W. Zhang, and C. W. Chen, "No-reference quality metric of contrast-distorted images based on information maximization," *IEEE Transaction on Cybernetics*, vol. 47, no. 12, pp. 4559–4565, 2016, doi: 10.1109/TCYB.2016.2575544.

[33] A. Mittal, A. K. Moorthy, and A. C. Bovik, "No-reference image quality assessment in the spatial domain," *IEEE Transaction on Image Processing*, vol. 21, no. 12, pp. 4695–4708, 2012.

[34] C. Wang and Z. Ye, "Brightness preserving histogram equalization with maximum entropy: a variational perspective," *IEEE Transaction on Consumer Electronics*, vol. 51, no. 4, pp. 1326–1334, 2005, doi: 10.1109/TIP.2012.2214050.

[35] S. Q. Duntley, "Light in the sea," *Journal of the Optical Society of America*, vol. 53, no. 2, pp. 214–233, 1963.

[36] W. W. Hou, "A simple underwater imaging model," *Optics Letters*, vol. 34, no. 17, pp.

2688–2690, 2009, doi.org/10.1364/OL.34.002688.

[37] H. Lu, Y. Li, Y. Zhang, M. Chen, S. Serikawa, and H. Kim, “Underwater optical image processing: a comprehensive review,” *Mobile networks and Application*, vol. 22, pp. 1204–1211, 2017, doi.org/10.1007/s11036-017-0863-4.

[38] C. Ancuti, C. O. Ancuti, T. Haber, and P. Bekaert, “Enhancing underwater images and videos by fusion,” in *2012 IEEE conference on computer vision and pattern recognition*, pp. 81–88, 2012, doi: 10.1109/CVPR.2012.6247661.

[39] S. G. Narasimhan and S. K. Nayar, “Contrast restoration of weather degraded images,” *IEEE Transaction on Pattern Analalysis Machine Intelligence*, vol. 25, no. 6, pp. 713–724, 2003, doi: 10.1109/TPAMI.2003.1201821.

[40] Y. Y. Schechner and Y. Averbuch, “Regularized image recovery in scattering media,” *IEEE Transaction on Pattern Analalysis and Machine Intelligence.*, vol. 29, no. 9, pp. 1655–1660, 2007, doi: 10.1109/TPAMI.2007.1141.

[41] D.-M. He and G. G. L. Seet, “Divergent-beam lidar imaging in turbid water,” *Optic and Lasers in Engineering*, vol. 41, no. 1, pp. 217–231, 2004, doi.org/10.1016/S0143-8166(02)00138-0.

[42] R. Garcia, T. Nicosevici, and X. Cufí, “On the way to solve lighting problems in underwater imaging,” in *OCEANS’02 MTS/IEEE*, vol. 2, pp. 1018–1024, 2002, doi: 10.1109/OCEANS.2002.1192107.

[43] A. Rizzi, C. Gatta, and D. Marini, “A new algorithm for unsupervised global and local color correction,” *Pattern Recognition Letter*, vol. 24, no. 11, pp. 1663–1677, 2003, doi.org/10.1016/S0167-8655(02)00323-9.

[44] M. Chambah, D. Semani, A. Renouf, P. Courtellemont, and A. Rizzi, “Underwater color constancy: enhancement of automatic live fish recognition,” in *Color Imaging IX: processing, hardcopy, and applications*, vol. 5293, pp. 157–168, 2003, doi.org/10.1117/12.524540.

[45] M. S. Hitam, E. A. Awalludin, W. N. Jawahir Hj Wan Yussof, and Z. Bachok, “Mixture contrast limited adaptive histogram equalization for underwater image enhancement,”

International Conference on Computer Application and Technology, ICCAT 2013, pp. 0–4, 2013, doi: 10.1109/ICCAT.2013.6522017.

[46] G. Deng, "A generalized unsharp masking algorithm," *IEEE Transaction on Image Processing*, vol. 20, no. 5, pp. 1249–1261, 2011, doi: 10.1109/TIP.2010.2092441.

[47] X. Fu, Y. Liao, D. Zeng, Y. Huang, X. P. Zhang, and X. Ding, "A Probabilistic Method for Image Enhancement with Simultaneous Illumination and Reflectance Estimation," *IEEE Transaction on Image Processing*, vol. 24, no. 12, pp. 4965–4977, 2015, doi: 10.1109/TIP.2015.2474701.

[48] K. Iqbal, M. Odetayo, A. James, R. A. Salam, and A. Z. H. Talib, "Enhancing the low quality images using unsupervised colour correction method," in *2010 IEEE International Conference on Systems, Man and Cybernetics*, pp. 1703–1709, 2010, doi: 10.1109/ICSMC.2010.5642311.

[49] X. Fu, Z. Fan, M. Ling, Y. Huang, and X. Ding, "Two-step approach for single underwater image enhancement," in *2017 international symposium on intelligent signal processing and communication systems (ISPACS)*, pp. 789–794, 2017, 10.1109/ISPACS.2017.8266583.

[50] C. O. Ancuti, C. Ancuti, C. De Vleeschouwer, and M. Sbert, "Color channel compensation (3C): A fundamental pre-processing step for image enhancement," *IEEE Transaction on Image Processing*, vol. 29, pp. 2653–2665, 2019, doi: 10.1109/TIP.2019.2951304.

[51] S. Zhang, T. Wang, J. Dong, and H. Yu, "Underwater image enhancement via extended multi-scale Retinex," *Neurocomputing*, vol. 245, pp. 1–9, 2017, doi.org/10.1016/j.neucom.2017.03.029.

[52] X. Fu, Y. Huang, D. Zeng, X.-P. Zhang, and X. Ding, "A fusion-based enhancing approach for single sandstorm image," in *2014 IEEE 16th international workshop on multimedia signal processing (MMSP)*, pp. 1–5, 2014, doi: 10.1109/MMSP.2014.6958791.

[53] C. Dai, M. Lin, J. Wang, and X. Hu, "Dual-purpose method for underwater and low-light image enhancement via image layer separation," *IEEE Access*, vol. 7, pp. 178685–

178698, 2019, doi: 10.1109/ACCESS.2019.2958078.

[54] K. Zuiderveld, “Contrast limited adaptive histogram equalization,” *Graph gems*, pp. 474–485, 1994.

[55] G. Deng, “A generalized unsharp masking algorithm,” *IEEE Transaction on Image Processing*, vol. 20, no. 5, pp. 1249–1261, 2010, doi: 10.1109/TIP.2010.2092441.

[56] X. Fu, Y. Liao, D. Zeng, Y. Huang, X.-P. Zhang, and X. Ding, “A probabilistic method for image enhancement with simultaneous illumination and reflectance estimation,” *IEEE Transaction on Image Processing*, vol. 24, no. 12, pp. 4965–4977, 2015, doi: 10.1109/TIP.2015.2474701.

[57] R. T. Tan, “Visibility in bad weather from a single image,” in *2008 IEEE conference on computer vision and pattern recognition*, pp. 1–8, 2008, 10.1109/CVPR.2008.4587643.

[58] S. Salazar-Colores, E. Cabal-Yepez, J. M. Ramos-Arreguin, G. Botella, L. M. Ledesma-Carrillo, and S. Ledesma, “A fast image dehazing algorithm using morphological reconstruction,” *IEEE Transaction on Image Processing*, vol. 28, no. 5, pp. 2357–2366, 2018, doi: 10.1109/TIP.2018.2885490.

[59] K. He, J. Sun, and X. Tang, “Single image haze removal using dark channel prior,” *IEEE Transaction on Pattern Analysis and Machine Intelligence*, vol. 33, no. 12, pp. 2341–2353, 2010, doi: 10.1109/TPAMI.2010.168.

[60] C. O. Ancuti, C. Ancuti, C. De Vleeschouwer, and P. Bekaert, “Color balance and fusion for underwater image enhancement,” *IEEE Transaction on image Processing*, vol. 27, no. 1, pp. 379–393, 2017, doi: 10.1109/TIP.2017.2759252.

[61] P. Sahu, N. Gupta, and N. Sharma, “A survey on underwater image enhancement techniques,” *International Journal of Computer and Application*, vol. 87, no. 13, 2014.

[62] N. Carlevaris-Bianco, A. Mohan, and R. M. Eustice, “Initial results in underwater single image dehazing,” in *Oceans 2010 Mts/IEEE Seattle*, pp. 1–8, 2010, doi: 10.1109/OCEANS.2010.5664428.

[63] S. Serikawa and H. Lu, “Underwater image dehazing using joint trilateral filter,” *Computer and Electrical Engineering*, vol. 40, no. 1, pp. 41–50, 2014,

doi.org/10.1016/j.compeleceng.2013.10.016.

[64] A. Galdran, D. Pardo, A. Picón, and A. Alvarez-Gila, "Automatic red-channel underwater image restoration," *Journal of Visual Communication and Image Represent.*, vol. 26, pp. 132–145, 2015, doi.org/10.1016/j.jvcir.2014.11.006.

[65] X. Zhao, T. Jin, and S. Qu, "Deriving inherent optical properties from background color and underwater image enhancement," Journal of *Ocean Engineering*, vol. 94, pp. 163–172, 2015, doi.org/10.1016/j.oceaneng.2014.11.036.

[66] B. Ouyang, F. Dalgleish, A. Vuorenkoski, W. Britton, B. Ramos, and B. Metzger, "Visualization and image enhancement for multistatic underwater laser line scan system using image-based rendering," *IEEE Journal of Ocean Engineering*, vol. 38, no. 3, pp. 566–580, 2013, doi: 10.1109/JOE.2012.2229066.

[67] M. Levoy, B. Chen, V. Vaish, M. Horowitz, I. McDowall, and M. Bolas, "Synthetic aperture confocal imaging", *ACM Transactions on Graphics (ToG)* 23.3, 825-834, (2004), doi.org/10.1145/1015706.1015806.

[68] Q. Zhu, J. Mai, and L. Shao, "A fast single image haze removal algorithm using color attenuation prior," *IEEE Transaction on image Processing*, vol. 24, no. 11, pp. 3522–3533, 2015, doi: 10.1109/TIP.2015.2446191.

[69] J.-P. Tarel and N. Hautiere, "Fast visibility restoration from a single color or gray level image," in *2009 IEEE 12th international conference on computer vision*, pp. 2201–2208, 2009, doi: 10.1109/ICCV.2009.5459251.

[70] L. Kratz and K. Nishino, "Factorizing scene albedo and depth from a single foggy image," in *2009 IEEE 12th International Conference on Computer Vision*, pp. 1701–1708, 2009.

[71] A. Latif *et al.*, "Content-based image retrieval and feature extraction: A comprehensive review," *Mathematical Problem in Engineering*, vol. 2019, 2019, doi: 10.1155/2019/9658350.

[72] J. P. Tarel and N. Hautière, "Fast visibility restoration from a single color or gray level image," *Proc. IEEE International Conference on Computer Vision*, vol. 2009-Janua, no.

Iccv, pp. 2201–2208, 2009, doi: 10.1109/ICCV.2009.5459251.

[73] A. K. Mishra, M. S. Choudhry, and M. Kumar, “Underwater image enhancement using multiscale decomposition and gamma correction,” *Multimedia Tools and Application.*, vol. 82, no. 10, pp. 15715–15733, 2023, doi.org/10.1007/s11042-022-14008-2.

[74] C. Ancuti, C. O. Ancuti, C. De Vleeschouwer, and A. C. Bovik, “Night-time dehazing by fusion,” in *2016 IEEE International Conference on Image Processing (ICIP)*, 2016, pp. 2256–2260, doi: 10.1109/ICIP.2016.7532760.

[75] K. A. Skinner and M. Johnson-Roberson, “Underwater Image Dehazing with a Light Field Camera,” *IEEE Computer Socitey Conference on Computer Vision and Pattern Recognition Work*, vol. 2017-July, pp. 1775–1782, 2017, doi: 10.1109/CVPRW.2017.224.

[76] S. Gautam, T. K. Gandhi, and B. K. Panigrahi, “An Improved Air-Light Estimation Scheme for Single Haze Images Using Color Constancy Prior,” *IEEE Signal Processing Letter*, vol. 27, pp. 1695–1699, 2020, doi: 10.1109/CVPRW.2017.224.

[77] P. Drews, E. Nascimento, F. Moraes, S. Botelho, and M. Campos, “Transmission estimation in underwater single images,” in *Proceedings of the IEEE international conference on computer vision workshops*, pp. 825–830, 2013.

[78] J. Y. Chiang and Y. C. Chen, “Underwater image enhancement by wavelength compensation and dehazing,” *IEEE Transaction on Image Processing*, vol. 21, no. 4, pp. 1756–1769, 2012, doi: 10.1109/TIP.2011.2179666.

[79] H. Lu, Y. Li, L. Zhang, and S. Serikawa, “Contrast enhancement for images in turbid water,” *Journal of Optical Society of America*, vol. 32, no. 5, pp. 886–893, 2015.

[80] R. Fattal, “Dehazing using color-lines,” *ACM Transaction on Graphics*, vol. 34, no. 1, pp. 1–14, 2014, doi: 10.1145/2651362.

[81] H. Lu, Y. Li, S. Nakashima, H. Kim, and S. Serikawa, “Underwater image super-resolution by descattering and fusion,” *IEEE Access*, vol. 5, pp. 670–679, 2017, doi.org/10.1364/JOSSA.32.000886.

[82] H. Lu, Y. Li, S. Nakashima, H. Kim, and S. Serikawa, “Underwater image super-

resolution by descattering and fusion," *IEEE Access*, vol. 5, pp. 670–679, 2017, doi: 10.1109/ACCESS.2017.2648845.

[83] S. Bazeille, I. Quidu, L. Jaulin, and J.-P. Malkasse, "Automatic underwater image pre-processing," in *CMM'06*, p. xx, 2006.

[84] A. Arnold-Bos, J.-P. Malkasse, and G. Kervern, "Towards a model-free denoising of underwater optical images," in *Europe Oceans 2005*, vol. 1, pp. 527–532, 2005.

[85] F. Petit, A.-S. Capelle-Laizé, and P. Carré, "Underwater image enhancement by attenuation inversionwith quaternions," in *2009 IEEE International Conference on Acoustics, Speech and Signal Processing*, pp. 1177–1180, 2009, 10.1109/ICASSP.2009.4959799.

[86] W. Zhang, S. Jin, P. Zhuang, Z. Liang, and C. Li, "Underwater image enhancement via piecewise color correction and dual prior optimized contrast enhancement," *IEEE Signal Processing Letter*, vol. 30, pp. 229–233, 2023, doi: 10.1109/LSP.2023.3255005.

[87] C. J. Prabhakar and P. U. Kumar, "An image based technique for enhancement of underwater images," *arXiv Prepr. arXiv1212.0291*, 2012, doi.org/10.48550/arXiv.121.0291.

[88] M. S. Hitam, E. A. Awalludin, W. N. J. H. W. Yussof, and Z. Bachok, "Mixture contrast limited adaptive histogram equalization for underwater image enhancement," in *2013 International conference on computer applications technology (ICCAT)*, pp. 1–5, 2013, doi: 10.1109/ICCAT.2013.6522017.

[89] Y. Y. Schechner, S. G. Narasimhan, and S. K. Nayar, "Instant dehazing of images using polarization," in *Proceedings of the 2001 IEEE Computer Society Conference on Computer Vision and Pattern Recognition. CVPR 2001*, vol. 1, pp. I–I, 2001, doi: 10.1109/CVPR.2001.990493.

[90] S. G. Narasimhan and S. K. Nayar, "Interactive (de) weathering of an image using physical models," in *IEEE Workshop on color and photometric Methods in computer Vision*, vol. 6, no. 6.4, p. 1, 2003.

[91] R. Fattal, "Single image dehazing," *ACM Transaction on Graphics*, vol. 27, no. 3, pp.

1–9, 2008, doi.org/10.1145/1360612.1360671.

[92] K. He, J. Sun, and X. Tang, "Guided image filtering," *IEEE Transaction Pattern Analysis and Machine Intelligence.*, vol. 35, no. 6, pp. 1397–1409, 2012, doi: 10.1109/TPAMI.2012.213.

[93] J. Y. Chiang and Y.-C. Chen, "Underwater image enhancement by wavelength compensation and dehazing," *IEEE Transaction on image Processing*, vol. 21, no. 4, pp. 1756–1769, 2011, doi: 10.1109/TIP.2011.2179666.

[94] G. Meng, Y. Wang, J. Duan, S. Xiang, and C. Pan, "Efficient image dehazing with boundary constraint and contextual regularization," in *Proceedings of the IEEE international conference on computer vision*, pp. 617–624, 2013.

[95] K. Iqbal, R. A. Salam, A. Osman, and A. Z. Talib, "Underwater Image Enhancement Using an Integrated Colour Model.," *IAENG International Journal of Computer Science*, vol. 34, no. 2, 2007.

[96] A. S. A. Ghani and N. A. M. Isa, "Underwater image quality enhancement through integrated color model with Rayleigh distribution," *Applied Soft Computing*, vol. 27, pp. 219–230, 2015, doi.org/10.1016/j.asoc.2014.11.020.

[97] N. A. M. Isa, "Pixel distribution shifting color correction for digital color images," *Applied Soft Computing*, vol. 12, no. 9, pp. 2948–2962, 2012, doi.org/10.1016/j.asoc.2012.04.028.

[98] A. S. Abdul Ghani and N. A. Mat Isa, "Underwater image quality enhancement through composition of dual-intensity images and Rayleigh-stretching," *Springerplus*, vol. 3, pp. 1–14, 2014, doi.org/10.1186/2193-1801-3-757.

[99] A.-N. Ponce-Hinestroza, L. A. Torres-Méndez, and P. Drews, "A statistical learning approach for underwater color restoration with adaptive training based on visual attention," in *OCEANS 2016 MTS/IEEE Monterey*, pp. 1–6, 2016, doi: 10.1109/OCEANS.2016.7761187.

[100] X. Fu, P. Zhuang, Y. Huang, Y. Liao, X.-P. Zhang, and X. Ding, "A retinex-based enhancing approach for single underwater image," in *2014 IEEE International*

Conference on Image Processing (ICIP), pp. 4572–4576, 2014.

[101] A. K. Mishra, M. S. Choudhry, and M. Kumar, "Underwater Image Restoration Using Color Correction and Empirical Mode Decomposition," in *2023 10th International Conference on Signal Processing and Integrated Networks (SPIN)*, pp. 522–525, 2023, doi: 10.1109/SPIN57001.2023.10116627.

[102] A. K. Mishra, M. S. Choudhry, and M. Kumar, "Underwater Image Restoration Using White Balance and Retinex Algorithm," in *2022 IEEE Conference on Interdisciplinary Approaches in Technology and Management for Social Innovation (IATMSI)*, pp. 1–5, 2022, doi: 10.1109/IATMSI56455.2022.10119294.

[103] J. Kopf *et al.*, "Deep photo: Model-based photograph enhancement and viewing," *ACM Transaction on Graphics*, vol. 27, no. 5, pp. 1–10, 2008, doi.org/10.1145/1409060.1409069.

[104] Y.-T. Peng, X. Zhao, and P. C. Cosman, "Single underwater image enhancement using depth estimation based on blurriness," in *2015 IEEE International Conference on Image Processing (ICIP)*, pp. 4952–4956, 2015, doi: 10.1109/ICIP.2015.7351749.

[105] J.-K. Guo, C.-C. Sung, and H.-H. Chang, "Improving visibility and fidelity of underwater images using an adaptive restoration algorithm," in *OCEANS 2014-TAIPEI*, pp. 1–6, 2014, doi: 10.1109/OCEANS-TAIPEI.2014.6964546.

[106] S.-J. Horng, P. J. Liu, and J.-S. Lin, "Improving the contrast enhancement of oceanic images using modified dark channel prior," in *2016 International Symposium on Computer, Consumer and Control (IS3C)*, pp. 801–804, 2016, doi: 10.1109/IS3C.2016.204.

[107] H.-Y. Yang, P.-Y. Chen, C.-C. Huang, Y.-Z. Zhuang, and Y.-H. Shiau, "Low complexity underwater image enhancement based on dark channel prior," in *2011 Second International Conference on Innovations in Bio-inspired Computing and Applications*, pp. 17–20, 2011, doi: 10.1109/IBICA.2011.9.

[108] L. Chao and M. Wang, "Removal of water scattering," in *2010 2nd international conference on computer engineering and technology*, vol. 2, pp. V2-35, 2010.

[109] P. L. J. Drews, E. R. Nascimento, S. S. C. Botelho, and M. F. M. Campos, "Underwater depth estimation and image restoration based on single images," *IEEE Computer Graphics and Application*, vol. 36, no. 2, pp. 24–35, 2016.

[110] Z. Lyu, A. Peng, Q. Wang, and D. Ding, "An efficient learning-based method for underwater image enhancement," *Displays*, vol. 74, p. 102174, 2022.

[111] D. Garg, N. K. Garg, and M. Kumar, "Underwater image enhancement using blending of CLAHE and percentile methodologies," *Multimedia Tools and Application*, vol. 77, pp. 26545–26561, 2018, doi: 10.1109/ICCET.2010.5485339.

[112] M. Boffety, F. Galland, and A.-G. Allais, "Influence of polarization filtering on image registration precision in underwater conditions," *Optics and Letter*, vol. 37, no. 15, pp. 3273–3275, 2012, doi.org/10.1364/OL.37.003273.

[113] G. Wang, B. Zheng, and F. F. Sun, "Estimation-based approach for underwater image restoration," *Optics and Letter*, vol. 36, no. 13, pp. 2384–2386, 2011, doi.org/10.1364/OL.36.002384.

[114] C. Li, J. Guo, B. Wang, R. Cong, Y. Zhang, and J. Wang, "Single underwater image enhancement based on color cast removal and visibility restoration," *Journal of Electronic Imaging*, vol. 25, no. 3, p. 33012, 2016, doi.org/10.1117/1.JEI.25.3.033012.

[115] W. Song, Y. Wang, D. Huang, A. Liotta, and C. Perra, "Enhancement of underwater images with statistical model of background light and optimization of transmission map," *IEEE Transaction on Broadcast*, vol. 66, no. 1, pp. 153–169, 2020, doi: 10.1109/TBC.2019.2960942.

[116] Y.-T. Peng, K. Cao, and P. C. Cosman, "Generalization of the dark channel prior for single image restoration," *IEEE Transaction on Image Processing*, vol. 27, no. 6, pp. 2856–2868, 2018, doi: 10.1109/TIP.2018.2813092.

[117] Y. Wang, H. Liu, and L.-P. Chau, "Single underwater image restoration using adaptive attenuation-curve prior," *IEEE Transaction on Circuits and System. I Regular Paper*, vol. 65, no. 3, pp. 992–1002, 2017, doi: 10.1109/TCSI.2017.2751671.

[118] Z. Liang, X. Ding, Y. Wang, X. Yan, and X. Fu, "GUDCP: Generalization of underwater

dark channel prior for underwater image restoration," *IEEE Transaction on circuits System for video Technology*, vol. 32, no. 7, pp. 4879–4884, 2021, doi: 10.1109/TCSVT.2021.3114230.

[119] W. Zhang, P. Zhuang, H.-H. Sun, G. Li, S. Kwong, and C. Li, "Underwater image enhancement via minimal color loss and locally adaptive contrast enhancement," *IEEE Transaction on Image Processing*, vol. 31, pp. 3997–4010, 2022, doi: 10.1109/TIP.2022.3177129.

[120] Y. Zhou, Q. Wu, K. Yan, L. Feng, and W. Xiang, "Underwater image restoration using color-line model," *IEEE Transaction on Circuits System for Video Technology*, vol. 29, no. 3, pp. 907–911, 2018, doi: 10.1109/TCSVT.2018.2884615.

[121] D. Berman, D. Levy, S. Avidan, and T. Treibitz, "Underwater single image color restoration using haze-lines and a new quantitative dataset," *IEEE Transaction on Pattern Analalysis and Machine Intelligence*, vol. 43, no. 8, pp. 2822–2837, 2020, doi: 10.1109/TPAMI.2020.2977624.

[122] Y.-T. Peng and P. C. Cosman, "Underwater image restoration based on image blurriness and light absorption," *IEEE Transaction on image Processing*, vol. 26, no. 4, pp. 1579–1594, 2017, doi: 10.1109/TIP.2017.2663846.

[123] H. Li and P. Zhuang, "DewaterNet: A fusion adversarial real underwater image enhancement network," *Signal Processing and Image Communication*, vol. 95, p. 116248, 2021, doi.org/10.1016/j.image.2021.116248.

[124] Y. Guo, H. Li, and P. Zhuang, "Underwater image enhancement using a multiscale dense generative adversarial network," *IEEE Journal of Oceanic Engineering*, vol. 45, no. 3, pp. 862–870, 2019, doi: 10.1109/JOE.2019.2911447.

[125] X. Yu, Y. Qu, and M. Hong, "Underwater-GAN: Underwater image restoration via conditional generative adversarial network," in *Pattern Recognition and Information Forensics: ICPR 2018 International Workshops, CVAUI, IWCF, and MIPPSNA, Beijing, China, August 20-24, 2018, Revised Selected Papers 24*, pp. 66–75, 2019, doi.org/10.1007/978-3-030-05792-3_7.

[126] C. Fabbri, M. J. Islam, and J. Sattar, "Enhancing underwater imagery using generative

adversarial networks," in *2018 IEEE international conference on robotics and automation (ICRA)*, pp. 7159–7165, 2018, doi: 10.1109/ICRA.2018.8460552.

[127] J. Li, K. A. Skinner, R. M. Eustice, and M. Johnson-Roberson, "WaterGAN: Unsupervised generative network to enable real-time color correction of monocular underwater images," *IEEE Robotics and Automation Letter*, vol. 3, no. 1, pp. 387–394, 2017, doi: 10.1109/LRA.2017.2730363.

[128] X. Mei *et al.*, "Uir-net: a simple and effective baseline for underwater image restoration and enhancement," *Remote Sensing.*, vol. 15, no. 1, p. 39, 2022, doi.org/10.3390/rs15010039.

[129] N. Wang, Y. Zhou, F. Han, H. Zhu, and J. Yao, "UWGAN: underwater GAN for real-world underwater color restoration and dehazing," *arXiv Prepr. arXiv1912.10269*, 2019, doi.org/10.48550/arXiv.1912.10269.

[130] W. Zhang *et al.*, "CVANet: Cascaded visual attention network for single image super-resolution," *Neural Networks*, vol. 170, pp. 622–634, 2024, doi.org/10.1016/j.neunet.2023.11.049.

[131] P. Duan, Z. W. Wang, X. Zhou, Y. Ma, and B. Shi, "EventZoom: Learning to denoise and super resolve neuromorphic events," in *Proceedings of the IEEE/CVF Conference on Computer Vision and Pattern Recognition*, pp. 12824–12833, 2021.

[132] C. Dai, Z. Guan, and M. Lin, "Single low-light image enhancer using Taylor expansion and fully dynamic convolution," *Signal Processing*, vol. 189, p. 108280, 2021.

[133] C. Dai and M. Lin, "Adjustable enhancer for low-light image enhancement using multi-expressions fusion and convolutional kernel calibration," *Multimedia Tools and Application*, vol. 83, no. 5, pp. 14609–14636, 2024, doi.org/10.1016/j.sigpro.2021.108280.

[134] N. Kumar, J. Manzar, Shivani, and S. Garg, "Underwater Image Enhancement using deep learning," *Multimedia Tools and Application*, vol. 82, no. 30, pp. 46789–46809, 2023, doi.org/10.1007/s11042-023-15525-4.

[135] Q. Liu, Q. Zhang, W. Liu, W. Chen, X. Liu, and X. Wang, "WSDS-GAN: A weak-

strong dual supervised learning method for underwater image enhancement," *Pattern Recognition*, vol. 143, p. 109774, 2023.

[136] R. Liu, Z. Jiang, S. Yang, and X. Fan, "Twin adversarial contrastive learning for underwater image enhancement and beyond," *IEEE Transaction on Image Processing*, vol. 31, pp. 4922–4936, 2022, doi.org/10.1016/j.patcog.2023.109774.

[137] J. Moran and H. Qing, "MTNet: a multi-task cascaded network for underwater image enhancement," *Multimedia Tools and Application*, vol. 83, no. 6, pp. 17629–17643, 2024, doi.org/10.1007/s11042-023-16967-6.

[138] M. Ummar, F. A. Dharejo, B. Alawode, T. Mahbub, M. J. Piran, and S. Javed, "Window-based transformer generative adversarial network for autonomous underwater image enhancement," *Engineering Application of Artificial Intelligence*, vol. 126, p. 107069, 2023, doi.org/10.1016/j.engappai.2023.107069.

[139] Y. Zhang, Q. Jiang, P. Liu, S. Gao, X. Pan, and C. Zhang, "Underwater image enhancement using deep transfer learning based on a color restoration model," *IEEE Journal of Oceanic Engineering*, vol. 48, no. 2, pp. 489–514, 2023, doi: 10.1109/JOE.2022.3227393.

[140] C. Li, S. Anwar, J. Hou, R. Cong, C. Guo, and W. Ren, "Underwater image enhancement via medium transmission-guided multi-color space embedding," *IEEE Transaction on Image Processing*, vol. 30, pp. 4985–5000, 2021, doi: 10.1109/TIP.2021.3076367.

[141] S. Cao, D. Zhao, Y. Sun, and C. Ruan, "Learning-based low-illumination image enhancer for underwater live crab detection," *ICES Journal of Marine Science*, vol. 78, no. 3, pp. 979–993, 2021, doi.org/10.1093/icesjms/fsaa250.

[142] G. Hou, Y. Li, H. Yang, K. Li, and Z. Pan, "UID2021: an underwater image dataset for evaluation of no-reference quality assessment metrics," *ACM Transaction on Multimedia Computing Communication and Application*, vol. 19, no. 4, pp. 1–24, 2023, doi.org/10.1145/3578584.

[143] C. Li *et al.*, "An underwater image enhancement benchmark dataset and beyond," *IEEE Transaction on Image Processing*, vol. 29, pp. 4376–4389, 2019, doi: 10.1109/TIP.2019.2955241.

[144] R. Liu, X. Fan, M. Zhu, M. Hou, and Z. Luo, "Real-world underwater enhancement: Challenges, benchmarks, and solutions under natural light," *IEEE Transaction on circuits and System for video Technology*, vol. 30, no. 12, pp. 4861–4875, 2020, doi: 10.1109/TCSVT.2019.2963772.

[145] S. Yan, X. Chen, Z. Wu, M. Tan, and J. Yu, "Hybrur: A hybrid physical-neural solution for unsupervised underwater image restoration," *IEEE Transaction on Image Processing*, 2023, doi: 10.1109/TIP.2023.3309408.

[146] C. Li, S. Anwar, and F. Porikli, "Underwater scene prior inspired deep underwater image and video enhancement," *Pattern Recognition*, vol. 98, p. 107038, 2020, doi.org/10.1016/j.patcog.2019.107038.

[147] K. Li *et al.*, "Beyond single reference for training: underwater image enhancement via comparative learning," *IEEE Transacion on Circuits System for Video Technology*, 2022, doi: 10.1109/TCSVT.2022.3225376.

[148] H. Li, J. Li, and W. Wang, "A fusion adversarial underwater image enhancement network with a public test dataset," *arXiv Prepr. arXiv1906.06819*, 2019, doi.org/10.48550/arXiv.1906.06819.

[149] N. Varghese, A. Kumar, and A. N. Rajagopalan, "Self-supervised Monocular Underwater Depth Recovery, Image Restoration, and a Real-sea Video Dataset," in *Proceedings of the IEEE/CVF International Conference on Computer Vision*, pp. 12248–12258, 2023.

[150] V. Pandey, K. Anand, A. Kalra, A. Gupta, P. P. Roy, and B.-G. Kim, "Enhancing object detection in aerial images," *Mathematical. Bioscience Engineering*, vol. 19, no. 8, pp. 7920–7932, 2022, doi:10.3934/mbe.2022370.

[151] A. Hooda, A. Kumar, M. S. Goyat, and R. Gupta, "Estimation of surface roughness for transparent superhydrophobic coating through image processing and machine learning," *Molecular Crystal and Liquid Crystals*, vol. 726, no. 1, pp. 90–104, 2022, doi.org/10.1080/15421406.2021.1935162.

[152] G. N. Bailey and N. C. Flemming, "Archaeology of the continental shelf: Marine resources, submerged landscapes and underwater archaeology," *Quarterly Science*

Reviews, vol. 27, no. 23–24, pp. 2153–2165, 2008, doi: 10.1016/j.quascirev.2008.08.012.

[153] C. Y. Li, J. C. Guo, R. M. Cong, Y. W. Pang, and B. Wang, "Underwater image enhancement by Dehazing with minimum information loss and histogram distribution prior," *IEEE Transaction on Image Processing*, vol. 25, no. 12, pp. 5664–5677, 2016, doi: 10.1109/TIP.2016.2612882.

[154] Z. Liang, Y. Wang, X. Ding, Z. Mi, and X. Fu, "Single underwater image enhancement by attenuation map guided color correction and detail preserved dehazing," *Neurocomputing*, vol. 425, pp. 160–172, 2021, doi.org/10.1016/j.neucom.2020.03.091.

[155] X. Wei, L. Yu, S. Tian, P. Feng, and X. Ning, "Underwater target detection with an attention mechanism and improved scale," *Multimedia Tools and Application*, vol. 80, no. 25, pp. 33747–33761, 2021.

[156] W. Song, Y. Wang, D. Huang, and D. Tjondronegoro, "A rapid scene depth estimation model based on underwater light attenuation prior for underwater image restoration," in *Pacific Rim Conference on Multimedia*, pp. 678–688, 2018, doi.org/10.1007/s11042-021-11230-2.

[157] A. K. Bhunia, S. R. K. Perla, P. Mukherjee, A. Das, and P. P. Roy, "Texture synthesis guided deep hashing for texture image retrieval," in *2019 IEEE Winter Conference on Applications of Computer Vision (WACV)*, pp. 609–618, 2019, doi: 10.1109/WACV.2019.00070.

[158] J. Hu, Q. Jiang, R. Cong, W. Gao, and F. Shao, "Two-branch deep neural network for underwater image enhancement in hsv color space," *IEEE Signal Processing Letter*, vol. 28, pp. 2152–2156, 2021.

[159] B. Xu, D. Zhou, and W. Li, "Image Enhancement Algorithm Based on GAN Neural Network," *IEEE Access*, vol. 10, pp. 36766–36777, 2022, doi: 10.1109/LSP.2021.3099746.

[160] K. Cao, Y.-T. Peng, and P. C. Cosman, "Underwater image restoration using deep networks to estimate background light and scene depth," in *2018 IEEE Southwest Symposium on Image Analysis and Interpretation (SSIAI)*, pp. 1–4, 2018, doi:

10.1109/SSIAI.2018.8470347.

[161] A. Kumar, P. Chauda, and A. Devrari, “Machine Learning Approach for Brain Tumor Detection and Segmentation,” *International Journal of Organizational Collectivism and Intelligence*, vol. 11, no. 3, pp. 68–84, 2021, doi: 10.4018/IJOCI.2021070105.

[162] Y. Wang, W. Song, G. Fortino, L. Z. Qi, W. Zhang, and A. Liotta, “An Experimental-Based Review of Image Enhancement and Image Restoration Methods for Underwater Imaging,” *IEEE Access*, vol. 7, pp. 140233–140251, 2019, doi: 10.1109/ACCESS.2019.2932130.

[163] Z. Farbman, R. Fattal, D. Lischinski, and R. Szeliski, “Edge-preserving decompositions for multi-scale tone and detail manipulation,” *SIGGRAPH’08 The International Conference on Computer Graphics and Interactive Techniques ACM SIGGRAPH 2008 Pap. 2008*, 2008, doi: 10.1145/1399504.1360666.

[164] X. Fu, D. Zeng, Y. Huang, X. P. Zhang, and X. Ding, “A Weighted Variational Model for Simultaneous Reflectance and Illumination Estimation,” *Proceedings of the IEEE Computer Society Conference on Computer Vision and Pattern Recognition*, vol. 2016-Decem, pp. 2782–2790, 2016, doi: 10.1109/CVPR.2016.304.

[165] T. Goldstein and S. Osher, “The split Bregman method for L1-regularized problems,” *SIAM Journal on Imaging Sciences*, vol. 2, no. 2, pp. 323–343, 2009, doi: 10.1137/080725891.

[166] T. S. Krishnapriya and N. Kunju, “Underwater Image Processing using Hybrid Techniques,” *Proceedings of the 1st International Conference on Innovative Information and Communication Technology (ICIICT) 2019*, no. 1, pp. 13–16, 2019, doi: 10.1109/ICIICT1.2019.8741468.

[167] K. He, J. Sun, and X. Tang, “Guided image filtering,” *IEEE Transaction on Pattern Analysis and Machine Intelligence*, vol. 35, no. 6, pp. 1397–1409, 2013, doi: 10.1109/TPAMI.2012.213.

[168] A. Levin, D. Lischinski, and Y. Weiss, “A closed-form solution to natural image matting,” *IEEE Transaction on Pattern Analysis and Machine Intelligence*, vol. 30, no. 2, pp. 228–242, 2008, doi: 10.1109/TPAMI.2007.1177.

[169] S. Image and H. Removalusing, "(12) United States Patent," vol. 2, no. 12, 2012, doi.org/10.1007/s11042-022-14008-2.

[170] X. Li, G. Hou, L. Tan, and W. Liu, "A hybrid framework for underwater image enhancement," *IEEE Access*, vol. 8, pp. 197448–197462, 2020, doi: 10.1109/ACCESS.2020.3034275.

[171] C. O. Ancuti, C. Ancuti, C. De Vleeschouwer, and P. Bekaert, "Color Balance and Fusion for Underwater Image Enhancement," *IEEE Transaction on Image Processing*, vol. 27, no. 1, pp. 379–393, 2018, doi: 10.1109/TIP.2017.2759252.

[172] G. Hou, Z. Pan, B. Huang, G. Wang, and X. Luan, "Hue preserving-based approach for underwater colour image enhancement," *IET Image Processing*, vol. 12, no. 2. pp. 292–298, 2018, doi: 10.1049/iet-ipr.2017.0359.

[173] S. Parthasarathy and P. Sankaran, "An automated multi scale Retinex with color restoration for image enhancement," *2012 Natl. Conf. Commun. NCC 2012*, 2012, doi: 10.1109/NCC.2012.6176791.

[174] Z. Mi, Y. Li, Y. Wang, and X. Fu, "Multi-Purpose Oriented Real-World Underwater Image Enhancement," 2020, doi: 10.1109/ACCESS.2020.3002883.

[175] A. K. Bhandari, V. K. Singh, A. Kumar, and G. K. Singh, "Cuckoo search algorithm and wind driven optimization based study of satellite image segmentation for multilevel thresholding using Kapur's entropy," *Expert Systems with Applications*, vol. 41, no. 7. pp. 3538–3560, 2014, doi: 10.1016/j.eswa.2013.10.059.

[176] Z. Wang, A. C. Bovik, H. R. Sheikh, and E. P. Simoncelli, "Image quality assessment: From error visibility to structural similarity," *IEEE Transaction on Image Processing*, vol. 13, no. 4, pp. 600–612, 2004, doi: 10.1109/TIP.2003.819861.

[177] M. Yang and A. Sowmya, "An Underwater Color Image Quality Evaluation Metric," *IEEE Transaction on Image Processing*, vol. 24, no. 12, pp. 6062–6071, 2015, doi: 10.1109/TIP.2015.2491020.

[178] S. Wang, K. Ma, H. Yeganeh, Z. Wang, and W. Lin, "A Patch-Structure Representation Method for Quality Assessment of Contrast Changed Images," *IEEE Signal Processing.*

Lett., vol. 22, no. 12, pp. 2387–2390, 2015, doi: 10.1109/LSP.2015.2487369.

[179] M. Ludvigsen, B. Sortland, G. Johnsen, and H. Singh, "Applications of geo-referenced underwater photo mosaics in marine biology and archaeology," *Oceanography*, vol. 20, no. 4, pp. 140–149, 2007.

[180] M. Ebner, "Color constancy," in *Computer Vision: A Reference Guide*, Springer, 2021, pp. 168–175, doi.org/10.1007/978-3-030-63416-2_454.

[181] S. Wang, J. Zheng, H.-M. Hu, and B. Li, "Naturalness preserved enhancement algorithm for non-uniform illumination images," *IEEE Transaction on image Processing*, vol. 22, no. 9, pp. 3538–3548, 2013, doi: 10.1109/TIP.2013.2261309.

[182] C. Li, J. Guo, and C. Guo, "Emerging from water: Underwater image color correction based on weakly supervised color transfer," *IEEE Signal Processing Letter*, vol. 25, no. 3, pp. 323–327, 2018, doi: 10.1109/LSP.2018.2792050.

[183] J.-Y. Zhu, T. Park, P. Isola, and A. A. Efros, "Unpaired image-to-image translation using cycle-consistent adversarial networks," in *Proceedings of the IEEE international conference on computer vision*, pp. 2223–2232, 2017.

[184] K. Panetta, C. Gao, and S. Agaian, "Human-visual-system-inspired underwater image quality measures," *IEEE Journal of Oceanic Engineering*, vol. 41, no. 3, pp. 541–551, 2015, doi: 10.1109/JOE.2015.2469915.

[185] B. A. Levedahl and L. Silverberg, "Control of underwater vehicles in full unsteady flow," *IEEE Journal of Oceanic Engineering*, vol. 34, no. 4, pp. 656–668, 2009, doi: 10.1109/JOE.2009.2027798.

[186] C. H. Mazel, "In situ measurement of reflectance and fluorescence spectra to support hyperspectral remote sensing and marine biology research," in *OCEANS 2006*, pp. 1–4, 2006, doi: 10.1109/OCEANS.2006.307001.

[187] A. Ortiz, M. Simó, and G. Oliver, "A vision system for an underwater cable tracker," *Machine and Visual Application*, vol. 13, pp. 129–140, 2002, doi.org/10.1007/s001380100065.

[188] G. L. Foresti, "Visual inspection of sea bottom structures by an autonomous underwater

vehicle," *IEEE Transaction on Systems, Man, and Cybernetic Part B*, vol. 31, no. 5, pp. 691–705, 2001, doi: 10.1109/3477.956031.

[189] A. Olmos and E. Trucco, "Detecting man-made objects in unconstrained subsea videos.," in *British Machine Vision Conference*, pp. 1–10, 2002.

[190] C. D. Mobley, "Radiative transfer in the ocean," *Encyclopaedia of Ocean Sciences*, vol. 4, pp. 2321–2330, 2001, doi:10.1006/rwos.2001.0469.

[191] S. Wang, Z. Chen, and H. Wang, "Multi-weight and multi-granularity fusion of underwater image enhancement," *Earth Science Informatics*, vol. 15, no. 3, pp. 1647–1657, 2022, doi.org/10.1007/s12145-022-00804-9.

[192] X. Ding, Y. Wang, J. Zhang, and X. Fu, "Underwater image dehaze using scene depth estimation with adaptive color correction," in *OCEANS 2017-Aberdeen*, pp. 1–5, 2017, doi: 10.1109/OCEANSE.2017.8084665.

[193] S. D. Hordley and G. D. Finlayson, "Re-evaluating colour constancy algorithms," in *Proceedings of the 17th International Conference on Pattern Recognition, 2004. ICPR 2004.*, vol. 1, pp. 76–79, 2004, doi: 10.1109/ICPR.2004.1334009.

[194] P. Zhuang, J. Wu, F. Porikli, and C. Li, "Underwater image enhancement with hyper-laplacian reflectance priors," *IEEE Transaction on Image Processing*, vol. 31, pp. 5442–5455, 2022, doi: 10.1109/TIP.2022.3196546.

[195] S. Parthasarathy and P. Sankaran, "An automated multi scale retinex with color restoration for image enhancement," in *2012 National Conference on Communications (NCC)*, pp. 1–5, 2012, doi: 10.1109/NCC.2012.6176791.

[196] J. Yuan, Z. Cai, and W. Cao, "TEBCF: Real-world underwater image texture enhancement model based on blurriness and color fusion," *IEEE Transactions on Geoscience and Remote Sensing*, vol. 60, pp. 1–15, 2021, doi: 10.1109/TGRS.2021.3110575.

[197] T. S. Krishnapriya and N. Kunju, "Underwater image processing using hybrid techniques," in *2019 1st International Conference on Innovations in Information and Communication Technology (ICIICT)*, pp. 1–4, 2019, doi:

10.1109/ICIICT1.2019.8741468.

[198] C.-Y. Li, J.-C. Guo, R.-M. Cong, Y.-W. Pang, and B. Wang, "Underwater image enhancement by dehazing with minimum information loss and histogram distribution prior," *IEEE Transaction on Image Processing.*, vol. 25, no. 12, pp. 5664–5677, 2016, doi: 10.1109/TIP.2016.2612882.

[199] J. Yuan, W. Cao, Z. Cai, and B. Su, "An underwater image vision enhancement algorithm based on contour bougie morphology," *IEEE Transactions on Geoscience and Remote Sensing*, vol. 59, no. 10, pp. 8117–8128, 2020, doi: 10.1109/TGRS.2020.3033407.

[200] S. Wu *et al.*, "A two-stage underwater enhancement network based on structure decomposition and characteristics of underwater imaging," *IEEE Journal of Oceanic Engineering*, vol. 46, no. 4, pp. 1213–1227, 2021, doi: 10.1109/JOE.2021.3064093.

[201] M. J. Islam, Y. Xia, and J. Sattar, "Fast underwater image enhancement for improved visual perception," *IEEE Robotics and Automation Letter*, vol. 5, no. 2, pp. 3227–3234, 2020, doi: 10.1109/LRA.2020.2974710.

[202] M. Yang and A. Sowmya, "An underwater color image quality evaluation metric," *IEEE Transaction on Image Processing*, vol. 24, no. 12, pp. 6062–6071, 2015, doi: 10.1109/TIP.2015.2491020.

[203] S.-C. Huang and C.-H. Yeh, "Image contrast enhancement for preserving mean brightness without losing image features," *Engineering Application of Artificial. Intelligence*, vol. 26, no. 5–6, pp. 1487–1492, 2013, doi.org/10.1016/j.engappai.2012.11.011.

[204] M. Eramian and D. Mould, "Histogram equalization using neighborhood metrics," in *The 2nd Canadian Conference on Computer and Robot Vision (CRV'05)*, 2005, pp. 397–404.

[205] C. Thum, "Measurement of the entropy of an image with application to image focusing," *International Journal of Optics*, vol. 31, no. 2, pp. 203–211, 1984, doi.org/10.1080/713821475.

[206] X. Wang and L. Chen, “An effective histogram modification scheme for image contrast enhancement,” *Signal Processing Image Communication*, vol. 58, pp. 187–198, 2017, doi.org/10.1016/j.image.2017.07.009.

[207] Z. Wang, A. C. Bovik, H. R. Sheikh, and E. P. Simoncelli, “Image quality assessment: from error visibility to structural similarity,” *IEEE Transaction on image Processing*, vol. 13, no. 4, pp. 600–612, 2004, doi: 10.1109/TIP.2003.819861.

[208] A. K. Mishra, M. S. Choudhry, and M. Kumar, “Underwater image enhancement using multiscale decomposition and gamma correction,” *Multimedia Tools and Application.*, pp. 1–19, 2022, doi.org/10.1007/s11042-022-14008-2.

[209] N. E. Huang *et al.*, “The empirical mode decomposition and the Hilbert spectrum for nonlinear and non-stationary time series analysis,” *Proceedings of the Royal Society A: Mathematical, Physical and Engineering Sciences*, vol. 454, no. 1971, pp. 903–995, 1998, doi.org/10.1098/rspa.1998.0193.

[210] R. Fontugne, J. Ortiz, D. Culler, and H. Esaki, “Empirical mode decomposition for intrinsic-relationship extraction in large sensor deployments,” in *Workshop on Internet of Things Applications, IoT-App*, vol. 12, 2012.

[211] D. M. Klionski, N. I. Oreshko, V. V Geppener, and A. V Vasiljev, “Applications of empirical mode decomposition for processing nonstationary signals,” *Pattern Recognition and image Analysis*, vol. 18, no. 3, pp. 390–399, 2008, doi.org/10.1134/S105466180803005X.

[212] S. Majumdar and A. K. Mishra, “Empirical mode decomposition with wavelet transform based analytic signal for power quality assessment,” *International Journal of Electronic Communication Engineering*, vol. 12, no. 4, pp. 329–334, 2018, doi.org/10.5281/zenodo.1316708.

[213] H. Hariharan, A. Gribok, M. A. Abidi, and A. Koschan, “Image fusion and enhancement via empirical mode decomposition,” *Journal of Pattern Recognition Research*, vol. 1, no. 1, pp. 16–32, 2006, doi:10.13176/11.4.

[214] X. Li, G. Hou, L. Tan, and W. Liu, “A hybrid framework for underwater image enhancement,” *IEEE Access*, vol. 8, pp. 197448–197462, 2020, doi,

10.1109/ACCESS.2020.3034275.

[215] P. Zhuang and X. Ding, “Underwater image enhancement using an edge-preserving filtering retinex algorithm,” *Multimedia Tools and Application*, vol. 79, pp. 17257–17277, 2020, doi.org/10.1007/s11042-019-08404-4.

[216] Z. Farbman, R. Fattal, D. Lischinski, and R. Szeliski, “Edge-preserving decompositions for multi-scale tone and detail manipulation,” *ACM Transaction on Graphics*, vol. 27, no. 3, pp. 1–10, 2008, doi.org/10.1145/1360612.1360666.

[217] H. Koschmieder, “Theorie der horizontalen Sichtweite,” *Beitrage zur Phys. der freien Atmosphare*, pp. 33–53, 1924.

[218] Z. Mi, Y. Li, Y. Wang, and X. Fu, “Multi-Purpose Oriented Real-World Underwater Image Enhancement,” *IEEE Access*, vol. 8, pp. 112957–112968, 2020, doi: 10.1109/ACCESS.2020.3002883.

[219] M. J. Islam, P. Luo, and J. Sattar, “Simultaneous enhancement and super-resolution of underwater imagery for improved visual perception,” *arXiv Prepr. arXiv2002.01155*, 2020, doi.org/10.38550/arXiv.2002.01155.

[220] A. K. Bhandari, V. K. Singh, A. Kumar, and G. K. Singh, “Cuckoo search algorithm and wind driven optimization based study of satellite image segmentation for multilevel thresholding using Kapur’s entropy,” *Expert Systems and Application*, vol. 41, no. 7, pp. 3538–3560, 2014, doi.org/10.1016/j.eswa.2013.10.059.

[221] Z. Wang, A. C. Bovik, H. R. Sheikh, and E. P. Simoncelli, “Image quality assessment: from error measurement to structural similarity,” *IEEE Transaction on image Processing*, vol. 13, no. 1, 2004.

[222] A. K. Bhandari, “A logarithmic law based histogram modification scheme for naturalness image contrast enhancement,” *Journal of Ambient Intelligence and Humanized Computing*, vol. 11, no. 4, pp. 1605–1627, 2020, doi.org/10.1007/s12652-019-01258-6.

[223] Q. Guo, H. Wang, and J. Yang, “Adaptive dark channel prior enhancement algorithm for different source night vision halation images,” *IEEE Access*, vol. 10, pp. 92726–

92739, 2022, doi: 10.1109/ACCESS.2022.3203183.

[224] R. Liu, X. Fan, M. Zhu, M. Hou, and Z. Luo, “Real-World Underwater Enhancement: Challenges, Benchmarks, and Solutions under Natural Light,” *IEEE Transaction on Circuits and System for Video Technology*, vol. 30, no. 12, pp. 4861–4875, 2020, doi: 10.1109/TCSVT.2019.2963772.

Author Biography

Amarendra Kumar Mishra
(Roll No.: 2k18/PHDEC/502)
Department of Electronics and Communication Engineering.
Delhi Technological University

Amarendra Kumar Mishra received a B.Tech. degree in Electronics and Communication Engineering from Uttar Pradesh Technical University Lucknow, India, and M.Tech. degree in Electronics and Communication Engineering from Delhi Technological University, New Delhi, India. He has completed his PhD degree in the department of Electronics and Communication Engineering, Delhi Technological University, New Delhi, India. His current research interests include signal processing, image processing, computer vision, pattern recognition, machine learning, and deep learning. He has won the gold medal in chess tournament at college level. He is finisher of 10k running challenge at DTU.